The copyright of this thesis vests in the author. No quotation from it or information derived from it is to be published without full acknowledgement of the source. The thesis is to be used for private study or non-commercial research purposes only.

Published by the University of Cape Town (UCT) in terms of the non-exclusive license granted to UCT by the author.

University of Cape Town

CHARACTERISATION OF THE FLAVIN ADENINE DINUCLEOTIDE BINDING REGION IN *MYXOCOCCUS XANTHUS* PROTOPORPHYRINOGEN OXIDASE

MAVIS O BOATENG

University of Cape Town

A DISSERTATION SUBMITTED TO THE UNIVERSITY OF CAPE TOWN IN FULFILLMENT OF THE REQUIREMENTS OF THE DEGREE MSc.

ACKNOWLEDGEMENTS

I have had a wonderful learning experience at the Porphyria Unit and Liver Centre. I would like to thank my supervisors Professor Peter Meissner and Doctor Anne Corrigall who over the years have always believed, encouraged and spurred me on. You have taught me science in a larger spectrum, one that can be applied anywhere, any time. Thank you for your mentorship, friendship and help over the years. To Brandon, Maglona, Helen, Maggie and Amiena, thank you for your encouraging words, support, friendship and laughter over the years. To everyone at the Liver Centre, and particularly Prof. Wendy Spearman, Dr Henry Hairwadzi and Prof. Michael Kew; thank you for your words of encouragement and support over the years. To Prof. Edward Sturrock thank you for the many insightful and helpful discussions over the years.

Thank you to my funders: UCT, MRC and Guy Eliot Scholarship.

To my family - "M*e da muo sɛ. Ye Njami ye krong krong*", I will for ever be in debt to you all. A special thank you to my dearest sister Lydia simply because you know what goes on in a dark room and for the overuse of the word inoculate! To my friends, "behind us lays fertile footsteps of a journey well lived and fondly remembered and before us a journey laced with mischief, laughter, heart-embers and endless freedom."

To my Creator - "...all the days ordained for me were written in Your book before one of them came to be" (Psalm 139:16). Thank you for the adventures so far!

University of Cape Town

ABSTRACT

This dissertation focuses on protoporphyrinogen oxidase (PPOX), the penultimate enzyme in the haem biosynthetic pathway. Partial defects in PPOX result in variegate porphyria, an autosomal dominant disorder. PPOX catalyzes the six electron oxidation of protoporphyrinogen IX to protoporphyrin IX, in the presence of flavin adenine dinucleotide (FAD) and oxygen. FAD is a cofactor, functioning as an intermediate electron acceptor in the catalytic function of PPOX. In this study the FAD binding region in *Myxococcus xanthus* PPOX was analysed by engineering and characterising a selection of relevant mutants.

Following assessment of the available *Myxococcus xanthus* PPOX protein crystal structure we focused on amino acid residues that should interact with FAD via their side chains, as opposed to possible backbone interactions. Thus residues serine 20, glutamate 39, tryptophan 408 and asparagine 441 were analysed. All mutants were engineered by site-directed mutagenesis of the relevant residues. Mutants were characterised and compared with wild type protein. Characterisation included FAD quantitation and analysis of FAD spectra of wild type and mutant protein. Kinetic activity of proteins was also assessed. Results revealed that serine 20 mutants could bind FAD, but polarity in this position is important for the integrity of FAD binding. Glutamate 39 mutants suggest that a negative charge at position 39 is critical as all non-conservative replacements could not bind sufficient FAD. Tryptophan 408 appears to play a role in orientating or stabilizing the bound substrate during catalysis, and a polar aromatic group in this position is favoured with regards to the amount of FAD bound. Asparagine 441 is involved in stabilizing the FAD once it is bound and polarity in this position appears vital.

Sulfite reactivity, which is a characteristic of some flavoprotein oxidases, was assessed in both *Myxococcus xanthus* and human PPOXs. Results showed that *Myxococcus xanthus* PPOX had no reactivity with sulfite while human PPOX reacted slowly with sulfite. We conclude that this difference may be attributable to the differences in water-mediated polarity around the bound FAD in the two forms of the protein. Lastly, the consumption of O_2 during the reaction was assessed and the reactivity of *Myxococcus xanthus* PPOX with oxygen analysed. *Myxococcus xanthus* PPOX had a high affinity (K_M = 0.9 μM) for oxygen and we confirmed that 3 moles of oxygen are consumed for every mole of protoporphyrin formed.

Overall this study sheds further light on how the FAD binding region achieves optimum binding, orientation and alignment of FAD to allow for an efficiently working enzyme.

University of Cape Town

TABLE OF CONTENTS

ACKNOWLEDGEMENTS **2**

ABSTRACT **3**

TABLE OF CONTENTS **4**

List of Figures **9**

List of Tables **14**

Abbreviations **15**

CHAPTER 1 ..... **19**

Proteins of the haem biosynthetic pathway **19**

Introduction 20

The Porphyrias 22

Enzymes of the haem biosynthetic pathway 23

5-Aminolevulinic acid synthase 25

5-Aminolevulinic acid dehydratase 28

Porphobilinogen deaminase 31

Uroporphobilinogen III synthase 34

Uroporphyrinogen decarboxylase 37

Coproporphyrinogen oxidase 40

Protoporphyrinogen oxidase 41

Ferrochelatase 42

CHAPTER 2 ..... **46**

Protoporphyrinogen oxidase **46**

Introduction 47

Function 47

Structure 48

Functional characterisation 49

University of Cape Town

Classification 49
Flavin adenine dinucleotide 50
Catalytic reaction 53
Reactivity with Sulfite 56
Structural characterisation 56
Expression and purification properties 56
Structural properties 57
The PPOX FAD conserved binding sequence 58
FAD binding features 59
FAD binding in other PPOX structures 63
The role of water molecules in FAD binding 70
Structure function studies 73
Arginine 59 73
GlyXGlyXXGly 73
VP mutations 74
Flavin binding studies in Monoamine oxidase 74

CHAPTER 3 76

Development of this thesis 76

Introduction 77
Previous studies on PPOX and FAD 77
This Study 79
Primary Aim 81
Secondary aims: 81

CHAPTER 4 82

Selection of *M. xanthus* PPOX mutant proteins for further study 82

Introduction 83
Objectives 83
Method 84
Mutant selection 84
Results 85
Sequence alignment 85
LigPlot analysis 85
PyMol analysis 86
Discussion 91

University of Cape Town

Conclusions 94

CHAPTER 5 95

Engineering, expression, and purification of *M. xanthus* PPOX mutant proteins 95

Introduction 96
Objectives 96
Method 97
Site-directed mutagenesis 97
QuickChange® Site Directed Mutagenesis kit system 98
Principle 98
Procedure 98
Screening clones 99
Sequence confirmation 99
Expression of wild type and mutant mxPPOX protein 100
Purification of wild type and mutant mxPPOX protein 100
Results 101
Mutational analysis 101
Sequence confirmation 106
Expression and purification 109
SDS-PAGE 110
Purification of human PPOX 113
Discussion 114
Conclusions 115

CHAPTER 6 116

Spectral analysis of the FAD cofactor of *M. xanthus* PPOX 116

Introduction 117
Objectives 117
Method 118
Results 119
Human PPOX FAD analysis 122
Discussion 123
Conclusions 125

University of Cape Town

CHAPTER 7 ..... **127**

Kinetic characterisation of *M. xanthus* PPOX **127**

Introduction 128
Experimental difficulties in assaying protogen oxidase activity 128
Objectives 129
Method 130
Results 131
Discussion 133
Conclusions 135

CHAPTER 8 ..... **137**

FAD-N(5) sulfite reactivity and the effect of substrate oxidation on oxygen consumption in *M. xanthus* PPOX **137**

FAD-N(5) sulfite reactivity 138
Introduction 138
Objectives 138
Method 139
Reactivity with sulfite 139
Results 139
Discussion 143
Effect of substrate oxidation on oxygen consumption 145
Introduction 145
Objectives 145
Method 146
Clarke Electrode 146
Results 148
Discussion 150
Conclusions 151

CHAPTER 9 ..... **152**

Final Conclusions, Overview and Future directions **152**

Overview, and Final Conclusions 153
Future Work 157

University of Cape Town

References **158**

Appendices **171**

Appendix 1 - M. xanthus PPOX sequences (GeneBank ID: 4106756) 171
Appendix 2 - Sequence of designed fragments of M. xanthus PPOX cDNA..... 173
Appendix 3 - Media 175
Appendix 4 - Generation and Storage of M. xanthus PPOX stocks (Dailey & Dailey, 1996a)..... 177
Appendix 5 - Plasmid DNA extraction 178
Appendix 6 - DNA Quantitation 180
Appendix 7 - Oligonucleotides design and preparation for use 181
Appendix 8 - Polymerase Chain Reaction 183
Appendix 9 - DNA separation and visualization 185
Appendix 10 - GeneEditor Site Directed Mutagenesis 188
Appendix 11 - QuickChange Site directed mutagenesis 195
Appendix 12 - Restriction analysis 201
Appendix 13 - Direct Sequencing 203
Appendix 14 - Protein Purification 205
Appendix 15 - Protein separation and visualisation 209
Appendix 16 - BSA microassay protein quantitation 213
Appendix 17 - Protoporphyrinogen oxidase assay (Meissner et al., 1986) 214
Appendix 18 - Flavin Cofactor Analysis 220
Appendix 19 - OxyGraph: Oxygen consumption 221
Oxygraph Electrode preparation 221
Chamber preparation 222
Liquid phase Calibration with H_2O 222
PPOX readings 222
Degassing 223
Appendix - 20 LigPlot analysis (Dym et al., 2001) 224
Appendix - 21 Sequence alignment 225
Alignment 1 - Prokaryote PPOX sequence blast 225
Alignment 2 - Alignment of PPOX protein with resolved protein structure 231

University of Cape Town

List of Figures

Figure 1.1: Schematic representation of the haem biosynthetic pathway showing the various cofactors involved in the pathway. In brackets are the respective enzymes responsible for catalysis. 21

Figure 1.2: A) A chemical schematic view of the biosynthesis of ALA. B) Self-constructed LigPlot, of ALAS_PLP binding site in monomer A of *Rhodobacter capsulatus* (Astner *et al*., 2005). Black = carbon; blue = nitrogen; red = oxygen; purple = phosphate. PLP is bound to conserved Lys-248, hence complex referred to as Llp248 (highlighted in green). Polar interactions are shown as dotted lines and hydrophobic interactions are shown as “eye-lashes”. 27

Figure 1.3: A) Chemical schematic of the biosynthesis of PBG from ALA, catalysed by ALAD (Davids, 2003). B) Self-constructed PyMol (Mills-Davies, 2000) image showing the schematic representation of the catalytic Zn binding region in human ALAD protein structure (PDB: 1E51), highlighting the importance of the 3 Cys residues. PBG and cysteine residues are shown in stick format; the Zn ion is shown as a purple sphere; neighbouring protein residues are shown as lines. Blue - nitrogen; red - oxygen; grey - carbon; yellow - sulphur..... 30

Figure 1.4: A) A chemical schematic view of the biosynthesis of hydroxymethylbilane. B) Image showing the dipyrromethane (DPM) binding region in PBGD. Hydrogen bond interactions are show as dotted lines. Interacting residues and DPM are shown in stick format while surrounding protein is shown as a cartoon (secondary structure) (Gill *et al*., 2009). In the stick structures red = oxygen; yellow = sulphur; blue = nitrogen; grey = carbon. 33

Figure 1.5: A chemical schematic view of the biosynthesis of uroporphyrinogen. Both the non-enzymatic as well as enzymatic (UROIIIS) reaction is shown (Davids, 2003). P = propionate (-CH_2CH_2COOH), and A = acetate (-CH_2COOH). 36

Figure 1.6: A) A chemical schematic view of the decarboxylation of uroporphyrinogen III to form corproporphyrinogen III. Reaction catalysed by uroporphyrinogen decarboxylase (UROD) releasing carbon dioxide (CO_2) as by-product. B) Interaction of asparagine 86 with the porphyrinogen macrocycle (Ajioka *et al*., 2006). Red = oxygen, blue = nitrogen, and green = carbon. 39

Figure 1.7: A chemical schematic view of the decarboxylation of coproporphyrinogen III to form protogen. Reaction catalysed by coproporphyrinogen oxidase (CPOX) releasing carbon dioxide (CO_2) as by product. P = propionate (-CH_2CH_2COOH), M = methyl (-CH_3), V = vinyl (-$CH=CH_2$)..... 41

Figure 1.8: A) A chemical schematic view of the insertion of iron (Fe^{2+}) into proto to form haem. Reaction catalysed by ferrochelatase (FECH) (Dailey *et al*., 2000). B) Self-constructed LigPlot showing the hydrogen bond network around His-263 in wild type FECH. Image drawn using subunit A. Black = carbon; blue = nitrogen; red = oxygen; purple = phosphate; yellow = sulphur. Polar interactions are shown as dotted lines and hydrophobic interactions are shown as “eye-lashes”..... 44

Figure 1.9: Self-constructed LigPlot showing the hydrogen bond network of residue 263. A) His-263 was mutated to a cysteine residue (PDB: 2PO5); no water molecules are seen interacting with the Cys-263. B) The structure of His341Cys (PDB: 2PO7 showing the hydrogen bond network around His-263; one water molecule is seen interacting with

University of Cape Town

His-263. Both images drawn using subunit A. Black = carbon; blue = nitrogen; red = oxygen; purple = phosphate; yellow = sulphur. Polar interactions are shown as dotted lines and hydrophobic interactions are shown as “eye-lashes”. 45

Figure 2.1: A chemical schematic view of the oxidation of protogen. Protogen is oxidised in the presence of O_2 and flavin adenine dinucleotide (FAD) to generate proto and H_2O_2. The reaction is catalysed by protoporphyrinogen oxidase (PPOX). 47

Figure 2.2: Secondary structural images of the four crystallised PPOX proteins as published (Koch *et al*., 2004; Corradi *et al*., 2006; Qin *et al*., 2010; Qin *et al*., 2011). ... 48

Figure 2.3: An example of sulfite (SO_3) reactivity with FAD-N(5). R denotes the remaining FAD molecule. 50

Figure 2.4: A schematic view of flavin adenine dinucleotide (FAD) structural formula in its oxidized state. 51

Figure 2.5: Redox states of the flavin adenine dinucleotide (FAD). R denotes the rest of the FAD molecule. 52

Figure 2.6: Constructed LigPlot of the isoalloxazine ring of FAD (highlighted in green) and the FAD-N(5) conserved water molecule (pink arrow). A) mxPPOX showing four water molecules interacting with the FAD isoalloxazine. B) hPPOX showing ten water molecules interacting with the FAD isoalloxazine. Black – carbon, blue – nitrogen, red – oxygen, cyan – water, dotted line – hydrogen bond, “eye-lashes” – hydrophobic interaction. 54

Figure 2.7: Self-constructed LigPLot, representation of the FAD (highlighted in green), binding site in subunit A of mxPPOX (PDB: 2IVE) (Corradi *et al*., 2006). Black = carbon; blue = nitrogen; red = oxygen; purple = phosphate; Cyan = water molecule. Polar interactions are shown as dotted lines and hydrophobic interactions are shown as “eye-lashes”. 60

Figure 2.8: Self-constructed LigPlot representation of the FAD (highlighted in green), binding site in an occupied active site, subunit A of mxPPOX with an occupied active site (acifluorfen; PDB: 2IVD) (Corradi *et al*., 2006). Black = carbon; blue = nitrogen; red = oxygen; purple = phosphate; Cyan = water molecule. Polar interactions are shown as dotted lines and hydrophobic interactions are shown as “eye-lashes”. 62

Figure 2.9: Self-constructed LigPlot representation of the FAD binding site in subunit A of mtPPOX (PDB:1SEZ). Black = carbon; blue = nitrogen; red = oxygen; purple = phosphate; Cyan = water molecule. Polar interactions are shown as dotted lines and hydrophobic interactions are shown as “eye-lashes”. 64

Figure 2.10: Self-constructed LigPlot representation of bsPPOX FAD (highlighted in green) binding region in subunit A. Black = carbon; blue = nitrogen; red = oxygen; purple = phosphate Acj = acifluorfen (AF). Polar interactions are shown as dotted lines and hydrophobic interactions are shown as”eye-lashes”. 66

Figure 2.11: Self-constructed LigPlot image of the FAD (highlighted in green) binding region in hPPOX, subunit A. Black = carbon; blue = nitrogen; red = oxygen; purple = phosphate; yellow = sulphur. Polar interactions are shown as dotted lines and hydrophobic interactions are shown as “eye-lashes”. 68

University of Cape Town

Figure 2.12: Schematic hydrogen bond pattern of conserved water molecule's interaction with the phosphate group of FAD. Dotted line denotes hydrogen bonds (Bottoms *et al*., 2002). 70

Figure 2.13: Self-constructed LigPlot of the hydrogen bonding pattern of conserved water molecules in PPOX. A) A schematic view of the stereochemical hydrogen bond interaction of the structurally conserved water molecule (HOH145) with conserved residues (Gly-18 and Gly-21) in mxPPOX-AF (PDF: 2IVD). B) A schematic view of the stereochemical hydrogen bond interaction of the structurally conserved water molecule (HOH480) in hPPOX (PDF: 3NKS). Black = carbon; blue = nitrogen; red = oxygen; purple = phosphate; cyan = water molecule. Polar interactions are shown as dotted lines. 72

Figure 4.1: A PyMol image of the possible interaction of Ser-20 mutants (shown in stick format within an alpha-helix - grey), with pyrophosphate section of the FAD cofactor (shown in stick format). Red stars - represent surrounding water molecules. A) Wild type Ser-20 interaction with FAD-pyrophosphate. B) Mutants (Ser20Thr and Ser20Ala) possible interaction with FAD. In all cases red - oxygen; blue - nitrogen; grey - carbon, orange - phosphate and red stars - water molecules. Polar interactions are shown as dotted lines. 87

Figure 4.2: A PyMol image showing the possible interaction of Glu-39 mutants with the adenine ring of the FAD cofactor. Glu-39 is shown in stick format at the end of a beta-sheet (grey). A) Wild type Glu39 interaction with FAD-adenine. B) Mutants (Glu39Asp, Glu39Lys, Glu39Gln and Glu39Ala) possible interaction with FAD. In all cases red - oxygen; blue - nitrogen; grey – carbon, and orange - phosphate. Polar interactions are shown as dotted lines. 88

Figure 4.3: A PyMol image showing the possible interaction of Trp-408 mutants with isoalloxazine ring of the FAD cofactor. Trp-408 is shown in stick format at the end of a beta-sheet. A) Wild type Trp-408 interaction with FAD-isoalloxazine. B) Mutants (Trp408Tyr and Trp408Leu) possible interaction with FAD. In all cases red - oxygen; blue - nitrogen; grey - carbon and red stars - water molecules. Polar interactions are shown as dotted lines. 89

Figure 4.4: PyMol image showing the possible interaction of Asn-441 mutants with both ribityl and pyrophosphate section of the FAD cofactor. Asn-441 is shown in stick format within a turning loop (grey). A) Wild type Asn-441 interaction with FAD. B) Mutants (Asn441Gln and Asn441Ile) possible interaction with FAD. In all cases red - oxygen; blue - nitrogen; grey - carbon, orange - phosphate and red stars - water molecules. Polar interactions are shown as dotted lines. 90

Figure 5.1: 6 % SDS PAGE showing *HinfI* restriction digest analysis of the PCR product of fragment 1 of three Glu-39 mutants. The wild type fragment has three cutting sites whilst the incorporation of the single base change results in the abolishment of a cutting site, hence two cutting sites in the mutant. A) Glu39Gln restriction analysis. Lanes 1 = pre-digest; 2-5 =positive clones; lanes 6, 7 wild type negative controls and lane 8 - bp marker. B) Glu39Lys restriction analysis using *HinfI*. Lane 1 - pre-digest; lanes 2-4: positive clones; lanes 5, 6 = wild type, negative controls; lane 7 – bp marker. C) Glu39Ala restriction analysis. Lanes 1 = pre-digest; lane 2-3 = wild type; lanes 4-6 = positive clone; lane 7 =bp marker. 103

Figure 5.2: 6 % SDS PAGE showing *TfiI* restriction digest analysis of the PCR product of fragment 1 of the Glu39Asp mutant. Lane 1 = pre-digest; lanes 2- 4 = positive clones; lanes 5 = wild type; lane 6 = bp marker. **Note** the 115 and 118 bp fragments are not

University of Cape Town

resolved hence only 2 bands are clearly visible, the lower one being thicker in lanes 2, 3, and 4. 104

Figure 5.3: 6 % SDS PAGE showing *ItaI* restriction digest analysis of the PCR product of fragment 4 (using the MxF4R oligo) of the Trp408Leu mutant. Lane 1 = pre-digest; lanes 2-4, 6-8, 10-11 = positive clones; lanes 5, 9 = negative clones; lanes 12-13 = wild type; lane 14 = bp maker. 104

Figure 5.4: 6 % SDS PAGE showing *Hpy188III* restriction digest analysis of the PCR product of fragment 4 (using the vMxF4R oligo) of the Asn441Gln mutant. Lane 1 - pre-digest; lanes 2-4: positive clones; lanes 5, 6 = wild type negative controls; lane 7 - bp marker. 104

Figure 5.5: 6 % SDS PAGE showing *BsmI* restriction digest analysis of the PCR product of fragment 4 (using the MxF4R oligo) of the Asn441Ile mutant. Lane 1= pre-digest; 2, 3, 5 = positive clones; lane 4 = incomplete digestion; lane 6 = wild type; lane 7 = bp marker. 105

Figure 5.6: Partial direct sequencing of fragment 1 of the Ser-20 mutants: A) Ser20Thr using the reverse primer mxF1R. B) Ser20Ala sequenced using primer mxF1F. The altered bp is encircled. 106

Figure 5.7: Partial direct sequencing of fragment 1 of the Glu-39 mutants: A) Glu39Ala using the forward primer mxF1F; B) Glu39Asp mutant using the reverse primer mxF1R; C) Glu39Lys using primer mxF1F; D) Glu39Gln mutant using primer mxF1R. The altered bp is encircled. 107

Figure 5.8: Partial direct sequencing of fragment 4 of the Trp-408 mutants: A) Trp408Leu using reverse primer vMxF4R; B) Trp408Tyr using reverse primer, vMxF4R. The altered bps are encircled. 108

Figure 5.9: Partial direct sequencing of fragment 4 of the Asparagine 441 mutants: A) Asn441Ile mutant using primer vMxF4F; B) Asn441Ile using primer vMxF4R. The altered bps are encircled. 109

Figure 5.10: 7.5-17 % denaturing SDS-PAGE of the purification of wild type and mutant mxPPOX proteins. Lane 1 – load (5 µl protein) was loaded; lane 2 –void (5 µl) was loaded; lane 3 – wash (50 µl) was loaded; lane 4 – eluate protein (5 µl was loaded except in Glu39Gln and Glu39Ala where 50 µl was loaded); lane 5 – molecular weight marker (6 µl was loaded). 110

Figure 5.11: 7.5-17.5 % denaturing SDS-PAGE of purified wild type hPPOX protein. Lane 1 – load (5 µl loaded); lane 2 –void (5 µl loaded); lane 3 – wash (50 µl loaded); lane 4 – purified protein (5 µl loaded); lane 5 - molecular weight marker (7 µl loaded). 113

Figure 6.1: FAD quantitation in mxPPOX protein; FAD absorbance at 450 nm was expressed as OD_{450nm}/mg of protein/ml. Data=mean ± SD, n=3. 119

Figure 6.2: UV/VIS spectra (300 - 550 nm) of wild type mxPPOX (solid line), Ser20Thr (dashed lines) and Ser20Ala (dotted lines). Enzymes (~10 µM) were recorded in 50 mM $NaPO_4$ buffer pH 7.0, 0.5 % Tween 20. 120

Figure 6.3: UV/VIS spectra (300 – 550 nm) of wild type (solid line), Glu39Asp (dashed line), Glu39Lys (dotted line), Glu39Ala (dotted and dashed line) and Glu39Gln (dotted

University of Cape Town

maze line). Enzymes (~10 μM) were recorded in 50 mM $NaPO_4$ buffer pH 7.0, 0.5 % Tween 20.....120

Figure 6.4: UV/VIS spectra (300 - 530 nm) of wild type (solid line), Trp408Tyr (dashed lines) and Trp408Leu (dotted lines). Enzymes (~10 μM) were recorded in 50 mM $NaPO_4$ buffer pH 7.0, 0.5 % Tween 20.....121

Figure 6.5: UV/VIS spectra (300 - 550 nm) of wild type (solid line), Asn441Gln (dashed lines) and Asn441Ile (dotted lines). Enzymes (~10 μM) were recorded in 50 mM $NaPO_4$ buffer pH 7.0, 0.5 % Tween 20.....121

Figure 6.6: A) Bar graph showing FAD quantitation in hPPOX and mxPPOX. Plots are of mean ± S.D (n=3). B) Spectral analysis of hPPOX showing peaks at 450 nm and 375 nm. hPPOX spectrum (~10 μM) was recorded in 50 mM $NaPO_4$ buffer pH 7.0, in 0.5 % n-octyl-β-D-glucopyranoside. 122

Figure 7.1: A pH versus percentage of activity plot showing the pH optimisation of wild type (solid line), Ser20Ala (dotted line), Ser20Thr (dashed line). Arrows indicate the pH optimum.....132

Figure 8.1: A) The spectral measurement of sulfite [50 mM] reactivity with commercial FAD (~10 μM). Absorbance (OD_{450nm}) versus time plot. B) FAD spectra showing a normal (solid line) and two bleached spectra upon addition of 50 mM (dash line) and 300 mM (dotted line) [sulfite]. 140

Figure 8.2: Spectral measurement of mxPPOX reactivity with sulfite (300 mM). A final concentration of 10 μM protein was used. Absorbance (OD_{450nm}) versus time plot, showing no increase in absorbance. Insert: FAD spectra showing an “unbleached” (normal) spectrum. 141

Figure 8.3: Spectral measurement of Na_2SO_3 reactivity with human PPOX (~10 μM). A) Time vs absorbance plot showing an increase in absorbance at OD_{450nm} observed in 300 mM [sulfite]. B) FAD spectra of human PPOX showing a normal spectrum (solid line); 50 mM [sulfite] incubation reaction spectrum (dotted) and a 300 mM [sulfite] reaction (dashed line).....142

Figure 8.4: Reaction chamber and water jacket the Oxygraph. A) Lugs B) Top plate; C) Water jacket; D) glass reaction vessel; E) Electrode disc; F) Standard plunger (used in this study) G) Non-gas tight plunger assembly; H) Base ring; I) Water jacket. 147

Figure 8.5: Graph showing the continuous measurement of O_2 consumption during the consumption of protogen. Approximately 25 μM substrate was used and 0.04 μM protein. 149

Figure 8.6: Double reciprocal plot, showing O_2 consumption in mxPPOX. V_{max} and K_M were extrapolated from the graph. Graph plotted using Microsoft-Excel. 149

University of Cape Town

List of Tables

Table 1.1: Clinical features of the genetic porphyrias and the partially defective haem enzyme involved. 23

Table 2.1: A summary of FAD - protein interactions in PPOX structures obtained from LigPlots. In the case of mxPPOX and mtPPOX subunit A was analyzed. 69

Table 5.1: Restriction analysis and details of fragments produced by restriction enzyme 102

Table 5.2: Purification table showing yield, activity and recovery % of WT and mutant mxPPOX protein. Where result = 0, no activity was detected. 111

Table 5.3: Purification table showing yield, activity and recovery WT hPPOX protein. 113

Table 7.1: Specific activity of PPOX WT and mutant proteins 131

Table 7.2: Kinetic parameters of wild type and mutant mxPPOX proteins. ND – not determined. Results determined as mean ± SD (n=3) 132

Table 8.1: The stoichiometry of O_2 consumed per product (proto) formed in mxPPOX catalytic reaction for different protein concentrations. 150

University of Cape Town

Abbreviations

General

µg	microgram
µl	microlitre
µM	micromolar
AF	acifluorfen
bp	base pair
BSA	bovine serum albumin
°C	degrees centigrade
cDNA	complementary deoxyribonucleic acid
cm	centimetre
Da	Dalton
dH_2O	distilled water
DNA	deoxyribonucleic acid
dNTPs	deoxynucleotide triphosphates
DTT	1,4-dithiol - DL - threitol
EDTA	ethylenediamine-tetra-acetic acid
g	centrifugal force/gram
hr	hour(s)
IMAC	immobilized metal affinity chromatography
kb	kilobase(s)
k_{cat}	catalytic constant
kDa	kiloDalton
K_M	Michaelis constant
L	Litre
LB	Luria-Bertani
M	Molar
mg	milligram
min	minute(s)
ml	millilitre
mM	millimolar
mm	millimetre
MOPS	3-N-Morpholinol propanesulfonic acid
N	normal
n	sample number
ng	nanogram
nm	nanometer
nmol	nanomole
O/N	over night
PAGE	polyacrylamide gel electrophoresis
PCR	polymerase chain reaction
PDB	protein data bank
pmol	picomole

University of Cape Town

PMSF	phenylmethylsulfonyl fluoride
RFU	relative fluorescent unit
rpm	revolutions per minute
RT	room temperature
S	substrate
SD	Standard deviation
SDS	sodium dodecyl sulphate
sec	second(s)
SOC	super optimal broth
TBE	Tris/borate/EDTA
TEMED	N, N, N', N' - tetramethyl-ethylenediamine
Tris	Tris(hydroxymethyl)methylamine
u	unit(s)
V	volts
V_{max}	maximal velocity
vs	versus
WT	wild type

DNA nucleotide bases

A	adenine
C	cytosine
G	guanine
T	thymine

Amino acids

A	Ala	alanine
C	Cys	cysteine
D	Asp	aspartate
E	Glu	glutamate
F	Phe	phenylalanine
G	Gly	glycine
H	His	histidine
I	Ile	isoleucine
K	Lys	lysine
L	Leu	leucine
M	Met	methionine
N	Asn	asparagine
P	Pro	proline
Q	Gln	glutamine
R	Arg	arginine
S	Ser	serine
T	Thr	threonine

University of Cape Town

V	Val	valine
W	Trp	tryptophan
Y	Tyr	tyrosine

Enzymes

ALAD	5-Aminolevulinic acid dehydratase
ALAS	5-Aminolevulinic acid synthase
CPOX	Coproporphyrinogen oxidase
FECH	Ferrochelatase
MAO	Monoamine oxidase
PAO	Polyamine oxidase
PBGD	Porphobilinogen deaminase
PPOX	Protoporphyrinogen oxidase
UROIIIS	Uroporphobilinogen III synthase
UROD	Uroporphyrinogen decarboxylase

Cofactors

DPM	Dipyrromethane
FAD	Flavin adenine dinucleotide
NAD	Nicotinamide adenine dinucleotide
PLP	Pyridoxal 5'-phosphate
Zn	Zinc

Haem precursors

ALA	5-aminolevulinic acid
CPO	coproporphyrinogen
HMB	hydroxymethylbilane
PBG	porphobilinogen
proto	protoporphyrin IX
protogen	protoporphyrinogen IX
UROIII	uroporphyrinogen III

Porphyrias

AIP	Acute Intermittent Porphyria
ALADP	Delta-aminolevulinate dehydratase porphyria
CEP	Congenital Erythropoietic porphyria

University of Cape Town

EPP	Erythropoietic protoporphyria
HCP	Hereditary Coproporphyria
PCT	Porphyria Cutanea Tarda
VP	Variegate Porphyria
XLDP	X-linked dominant protoporphyria

CHAPTER 1

Proteins of the haem biosynthetic pathway

University of Cape Town

Introduction

Haem is a protoporphyrin IX (proto) molecule with ferrous iron inserted in its centre, functioning in a wide range of activities. Indeed, haem is a critical component of several hundred proteins found throughout nature, its diverse functionality due to the redox activity of the iron. In humans, such functions include the well known oxygen (O_2) transportation in haemoglobin where, as a cofactor, haem binds O_2 and transports atmospheric O_2 from lungs to cells. Besides its role in haemoglobin, haem is also able to store O_2 in myoglobin, and can participate in detoxification (e.g. cytochrome P450s), oxidative metabolism (e.g. cytochrome c oxidase), gas sensing (e.g. guanylate cyclase) and thyroid hormone synthesis (thyroid peroxidase) (Rivera & Walker, 1995; Hofacker & Schulten, 1998; Ajioka *et al*., 2006; Harvey & Ziegler, 2006; Tsiftsoglou *et al*., 2006; Davydov *et al*., 2008).

Haem cannot be obtained through the diet in humans. Rather, it is biosynthesized intracellularly, the pathway being conserved and ubiquitous in every human cell. The biosynthesis of haem involves eight enzymes starting in the mitochondria. The synthesis then moves into the cytoplasm and finally back into the mitochondria (fig. 1.1). In short, glycine and succinyl CoA condense (enzyme: 5-aminolevulinic acid synthase, ALAS) to form 5-aminolevulinic acid (ALA). ALA then moves into the cytoplasm where the condensation of two molecules of ALA occurs to form porphobilinogen (enzyme: 5-aminolevulinic acid dehydratase, ALAD). Four porphobilinogen molecules are then joined forming hydroxymethylbilane (enzyme: porphobilinogen deaminase, PBGD). This then cyclizes to uroporphyrinogen III (enzyme: uroporphyrinogen III synthase, UROIIIS); followed by decarboxylation to form coproporphyrinogen (enzyme: uroporphyrinogen decarboxylase, UROD). Coproporphyrinogen is transported into the mitochondria and decarboxylated further forming protoporphyrinogen IX (protogen; enzyme: coproporphyrinogen oxidase, CPOX). Finally, six electrons are removed from protogen followed by the insertion of iron into the porphyrin ring (enzymes: protoporphyrinogen oxidase, PPOX, and ferrochelatase, FECH, respectively) (Jordan, 1990; Muhammad Akhtar, 1991; Dailey, 2002; Ajioka *et al*., 2006).

University of Cape Town

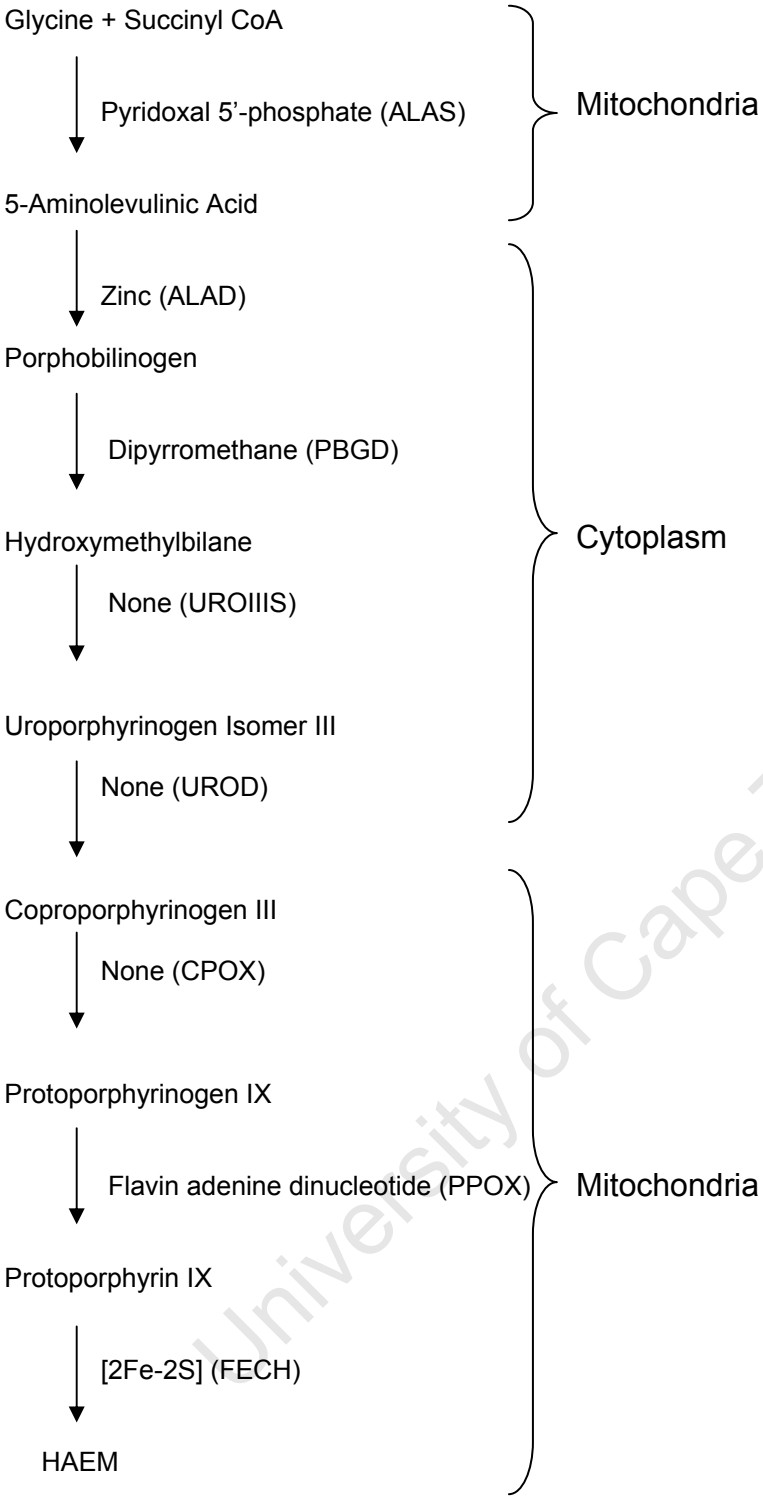

Figure 1.1: Schematic representation of the haem biosynthetic pathway showing the various cofactors involved in the pathway. In brackets are the respective enzymes responsible for catalysis.

University of Cape Town

While haem may be biosynthesized by all cells, the majority of haem is either generated in the erythroid (for haemoglobin) or liver (for haemoproteins, cytochromes, etc) (Ajioka *et al*., 2006). The biosynthesis of ALA by ALAS is the rate limiting step in the haem biosynthetic pathway and regulation is different in these two tissues. The enzyme ALAS, is encoded by two genes namely: ALAS1 (ubiquitous) and is ALAS2 (erythroid). In the liver, ALAS1 is regulated by negative feedback by the intracellular uncommitted haem

pool mechanisms. In erythroid tissue, regulation occurs during erythroid differentiation in response to erythropoietin ensuring that ALAS2 synthesis is only induced during active haem synthesis. Iron availability also plays a role in its regulation and unlike ALAS1, haem does not play a direct inhibitory role (Fraser *et al*., 2002; Thunell, 2006; Tsiftsoglou *et al*., 2006). Factors that disrupt the homeostatic balance of haem production may lead to the so called porphyrias.

The Porphyrias

Genetic factors, as well as environmental influences, may lead to abnormal function of the haem biosynthetic pathway. This abnormal functioning may result in accumulation and excretion of intermediates of the haem pathway – the porphyrins (James & Hift, 2000). While environmental causes, such as lead (an inhibitor of ALA dehydratase), are important (Jaffe *et al*., 2001a), it is primarily genetic mutations in the various haem biosynthetic enzymes that are considered the main drivers of the so-called "porphyrias" (other than in the acquired form of porphyria cutanea tarda) (Jaffe *et al*., 2001b; Puy *et al*., 2010). Indeed, the potential consequence of genetic mutations in all eight haem biosynthetic enzymes is porphyria. Thus, the porphyrias are generally defined as inherited metabolic disorders of haem biosynthesis and are characterized by the partial defect of an enzyme in the pathway, which then leads to the accumulation of haem intermediates. These intermediates include either the early precursors of the pathway (ALA and porphobilinogen), or the later occurring porphyrin intermediates, or both.

The excess accumulation of intermediates is responsible for the clinical presentations of the disease, which are neurovisceral acute attacks and/or photosensitivity (see table 1.1) (Brenner & Bloomer, 1980; Meissner *et al*., 1986; James & Hift, 2000; Thunell, 2006; Whatley *et al*., 2008). Literature reveals that the early occurring haem precursors are invariably associated with the neurovisceral acute clinical presentation (through yet to be elucidated, direct and indirect neurotoxic effects); while photosensitivity, is due to the photoreactive (porphyrins are fluorescent) properties of the later occurring porphyrins (Puy *et al*., 2010). Porphyria can either be classified according to the site of precursor accumulation (liver or red blood cells) or, a more practically useful classification, by the dominant clinical feature: acute and/or cutaneous porphyria (Ajioka *et al*., 2006).

University of Cape Town

Table 1.1: Clinical features of the genetic porphyrias and the partially defective haem enzyme involved.

Clinical features of Porphyria	Defective enzyme
PHOTOSENSITIVITY ONLY	
Congenital Erythropoietic Porphyria (CEP)	UROIIIS
Porphyria Cutanea Tarda (PCT)	UROD
Erythropoietic Protoporphyria (EPP)	FECH
NEUROVISCERAL ATTACKS ONLY	
Acute Intermittent Porphyria (AIP)	PBGD
ALAD Porphyria (ALADP)	ALAD
NEUROVISCERAL ATTACKS AND PHOTOSENSITIVITY	
Hereditary Coproporphyria (HCP)	CPOX
Variegate Porphyria (VP)	PPOX
NEW PHOTOSENSITIVE PORPHYRIA	
X-linked Dominant Protoporphyria	ALAS (gain of function)

University of Cape Town

Enzymes of the haem biosynthetic pathway

Enzymes of the haem biosynthetic pathway have been extensively studied. The structure for all eight human enzymes has been resolved except for ALAS whose structure has only been resolved in the *Rhodobacter capsulatus* (Whitby *et al*., 1998; Mills-Davies, 2000; Mathews *et al*., 2001; Wu *et al*., 2001; Astner *et al*., 2005; Lee *et al*., 2005; Gill *et al*., 2009; Qin *et al*., 2011). In terms of the development of this project, and the work described in this dissertation, it is important to note that at the commencement of this study, the human structure of PPOX had not yet been resolved. As will become apparent, this study is thus based on an investigation of PPOX in *Myxoccocus xanthus* (*M. xanthus*) (Corradi *et al*., 2006).

Of the eight haem biosynthetic enzymes, five require the presence of a cofactor to function (Mills-Davies, 2000; Astner *et al*., 2005; Corradi *et al*., 2006; Gill *et al*., 2009; Song *et al*., 2009). These cofactors are optimally positioned in the protein to aid

catalysis. Thus, the binding regions of these cofactors are of particular interest and importance since enzyme-cofactor interactions are vital for the enzymes activity (Edmondson & Newton-Vinson, 2001; Neeli *et al*., 2005; Heuts *et al*., 2007; Brenner *et al*., 2008; Fitzpatrick, 2011). The remaining four enzymes in this pathway function in the absence of a cofactor (fig. 1.1).

Below follows a more detailed review of the enzymes of the haem biosynthetic pathway. In accordance with the topic of this project (cofactor binding in PPOX), we pay particular attention to the structure, function and cofactor interactions where applicable. In all cases the human structure is discussed, other than where other forms are specifically mentioned. This chapter is followed by a detailed look at PPOX focusing on its cofactor, FAD. In this case the structure of *M. xanthus,* the latest available structure at the start of this project, with an FAD bound cofactor is analysed. We will also compare the structure of *M. xanthus* PPOX to the now released human PPOX structure.

University of Cape Town

5-Aminolevulinic acid synthase

The first enzyme in the haem biosynthetic pathway is the mitochondrially located, ALAS (EC 2.3.1.37). It catalyzes the formation of ALA from glycine and succinyl CoA with the aid of cofactor, pyridoxal 5'-phosphate (PLP, fig. 1.2) (Shemin & Kikuchi, 1958; Jordan, 1990). ALAS thus belongs to the PLP-dependent group of enzymes, the aminotransferases. Enzymes of this group catalyse the decarboxylative condensation of a carboxylic acid CoA thioester, and an amino acid. In the case of ALAS, the carboxylic acid CoA is succinyl CoA and the amino acid is glycine (fig. 1.2) (Shemin & Kikuchi, 1958; Jordan, 1990; Mehta, *et al*., 1993).

The biosynthesis of ALA in humans, takes place via the so-called 'Shemin' pathway (Shemin & Kikuchi, 1958). The Shemin pathway involves a series of reactions namely: deprotonation, condensation, decarboxylation, and reprotonation (Hunter & Ferreira, 1999a). In the "open" conformation of ALAS, the first substrate, glycine, binds to PLP via a Schiff-base bond forming an external aldimine. Once bound glycine deprotonates forming a stable carbanion at the glycine-α-carbon atom. The second substrate, succinyl CoA, binds - inducing the "closed" ALAS conformation. In the active site, succinyl CoA, having an electrophilic carbonyl group, reacts with the nucleophilic glycine in a condensation reaction (loosing CoA in the process). This forms an enzyme–PLP-2-amino-3-ketoadipic complex, which decarboxylates to form the product, ALA. ALA is released and ALAS returns to its "open" conformation with PLP bound to a conserved lysine residue via a Schiff base (internal aldimine).

University of Cape Town

The human ALAS structure has not yet been resolved. The structure from *R. capsulatus* [Protein data bank code (PDB): 2BWN] is the latest (and only) structure of ALAS (Astner *et al*., 2005). Human and *R. capsulatus* both synthesize ALA via the Shemin pathway and have a high sequence homology (70 % - similar residues considered) and could be predicted to have a similar structure. $ALAS_{(RS)}$, is a homodimer with each monomer consisting of three domains namely N-terminal, catalytic and C-terminal. In the absence of substrate, PLP is covalently bound in a symmetrical manner via a conserved lysine residue in the N-terminal domain (fig. 1.2).

An alignment study has shown that only few amino acids in the aminotransferase sequence are invariant in aminotransferases; namely lysine, aspartate/glutamate, arginine and GlyXGlyXXGly, where Gly and X denotes glycine and any residue,

respectively (Mehta *et al*., 1993). Lysine is responsible for the internal aldimine formation (PLP covalent interaction) before substrate binds and once product is released. The mutation of this residue results in the noncovalent binding of PLP to ALAS and an enzyme with dramatically reduced activity (Hunter & Ferreira, 1999b). The negatively charged carboxylate group of aspartate/glutamate is responsible for stabilizing the pyrrole ring of PLP during catalysis. The conserved arginine is said to interact with the phosphate group of PLP and is positioned by the conserved, GlyXGlyXXGly which is generally found in a nucleotide binding motif (Danishefsky *et al*., 1991; Gong *et al*, 1996; Gong *et al*., 1998; Tan *et al*., 1998).

Gong and colleagues (1996) studied the functional role of the first two glycine residues in the conserved GlyXGlyXXGly motif in human ALAS, in order to understand the role of this consensus sequence located in a loop. The first glycine was mutated to a cysteine. Glycine is structurally favourable in loops while cysteine is bulkier than glycine and hence this alteration would theoretically introduce steric hindrance (Petsko & Ringe, 2004). Indeed, results showed that the conformation of the enzyme was altered in this mutant. In addition, although the binding of PLP was not affected, the orientation of the cofactor, PLP, was altered. These alterations resulted in a less efficient enzyme. The second conserved glycine residue was mutated to an alanine (nonpolar, neutral residue); a serine and threonine (both polar neutral residues). All mutants bound PLP poorly and had decreased activity. As mentioned, glycine is a small structured residue and is often found in loop turns. Thus, alteration of glycine to cysteine, alanine, serine, or threonine (much bulkier residues) could introduce steric hindrance in the turning of the loop. Also the conserved arginine located a few residues after this consensus sequence could be optimally positioned by the GlyXGlyXXGly sequence (Gong *et al*., 1996). The arginine is believed to interact with the phosphate group of the PLP and alteration of the conserved glycine could alter the position of the arginine, thus interfering with the phosphate interaction and ultimately affecting the orientation of PLP.

From this study it is clear that steric factors, for example amino acid size, and orientation of the amino acid side chain, play vital roles in the binding of cofactor in the case of ALAS, as one would expect.

University of Cape Town

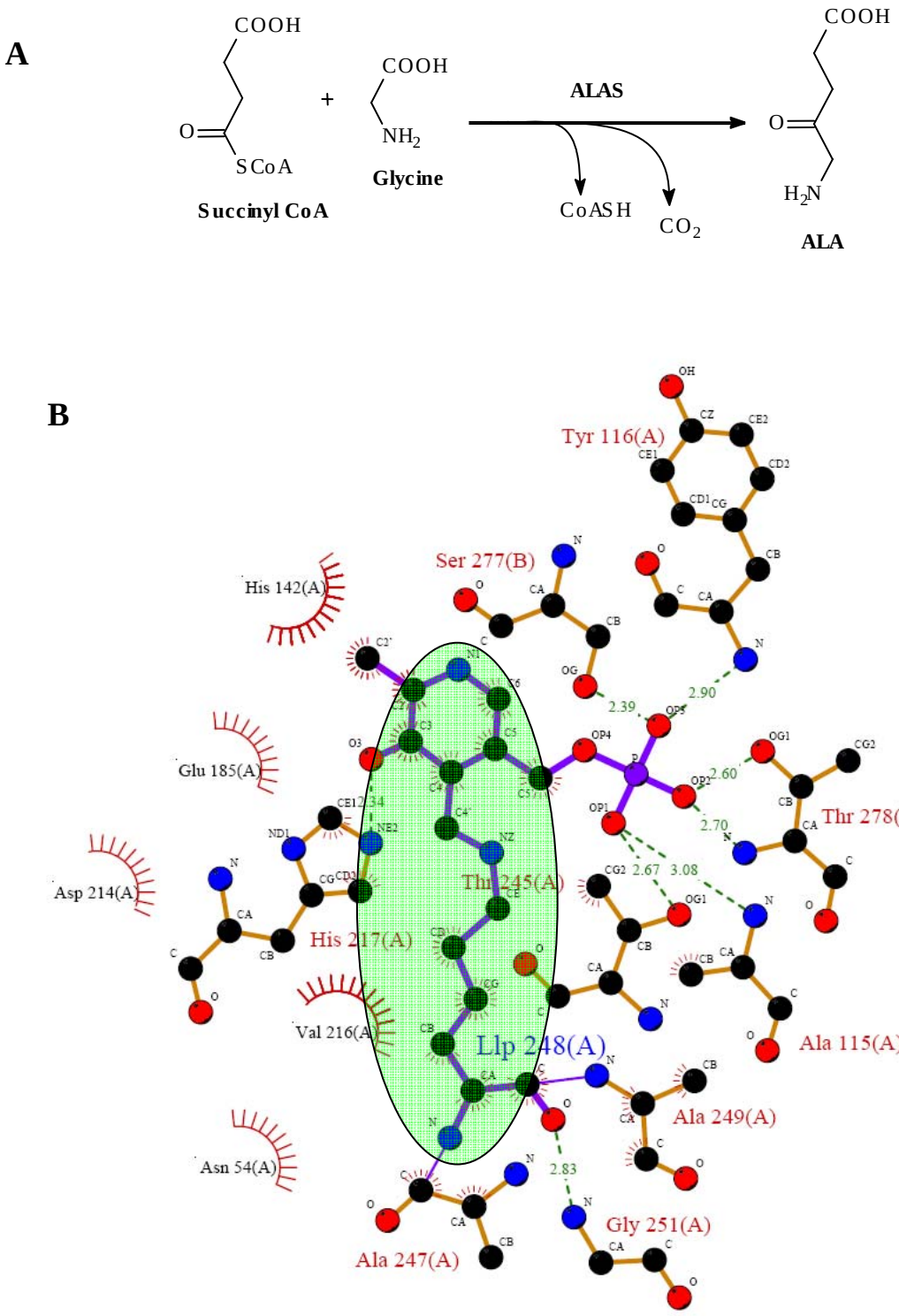

Figure 1.2: A) A chemical schematic view of the biosynthesis of ALA. B) Self-constructed LigPlot, of ALAS_PLP binding site in monomer A of *Rhodobacter capsulatus* (Astner *et al*., 2005). Black = carbon; blue = nitrogen; red = oxygen; purple = phosphate. PLP is bound to conserved Lys-248, hence complex referred to as Llp248 (highlighted in green). Polar interactions are shown as dotted lines and hydrophobic interactions are shown as "eye-lashes".

5-Aminolevulinic acid dehydratase

The second enzyme in the haem biosynthetic pathway is ALAD (E.C. 4.2.1.24) also known as porphobilinogen synthase (PBGS). It catalyzes the condensation of two molecules of ALA to form porphobilinogen (PBG), with two water molecules as by-product (fig. 1.3). In humans, zinc II (Zn) is the cofactor in this reaction; interestingly in plants this Zn is replaced with magnesium while in prokaryotes it can either be Zn or magnesium (Jaffe & Hanesg, 1986; Erskine *et al*., 1999; Jaffe, 2004).

By virtue of its cofactor, ALAD belongs to the Zn metalloenzyme family whereby Zn can have one of three roles in a protein namely, catalytic, cocatalytic or structural (McCall *et al*., 2000). Catalytic Zn is directly involved in catalysis (i.e. in the forming or breaking of bonds); cocatalytic Zn proteins have several Zn ions in close proximity with each other participating in catalysis or enhancing catalytic activity. The structural Zn function in metalloenzymes involves stabilising the tertiary structure of the enzyme in a manner analogous to disulphide bonds. In ALAD, Zn plays both structural (ZnA) and catalytic (ZnB) roles.

As mentioned above, ALAD catalyzes the condensation of two ALA molecules, which are transported from the mitochondria into the cytoplasm, to produce a monopyrrole product, PBG. The overall reaction requires the forming/breaking of at least eight bonds. The enzyme requires a maximum of eight Zn ions but can function with four; which are bound to the enzyme by conserved cysteine residues (Jaffe & Hanesg, 1986). The first step of the PBG formation is the binding of ALA which structurally, is divided into an A and P-side. One ALA molecule binds the Propionyl (P)-side while the other ALA binds the Acetyl (A)-side of ALAD (Jaffe & Hanesg, 1986; Jaffe, 2004). The P-side ALA binds first, forming a Schiff base with a conserved active site lysine residue. The closing of the active site is said to occur before the Schiff base formation. This is followed by the A-side ALA binding which triggers the closing of the active site "lid". The A-side carboxyl group forms hydrogen bonds to residues in the active site lid thus stabilizing the closed lid configuration. These hydrogen bonds also allow the A-side chain is necessary motion to allow for "gating" of the active site. This is followed by a series of bond formation and breaking to generate an 'almost-pyrrole' intermediate. Next, the A side looses a proton and forms a bond with the P-side. This leads to the P-side binding to the adjacent active site of the octamer. The gate of the active site is then "opened" to release PBG (Breinig *et al*., 2003; Jaffe, 2004; Zappa *et al*., 2010).

University of Cape Town

ALAD has a conserved structure between most species. The human structure (PDB: 1ES1) is a homooctameric oligomer, having all eight active sites on the surface (with bound Zn molecules). It is structurally referred to as a morpheein which is an isoform wherein parts of a monomer can structurally co-ordinate different aspects of an oligomer (Tang *et al*., 2006). The entrance to the active site is gated, protecting the active site from solvent. Although the human PBGD has Zn molecules, in various other species magnesium has been reported as well as species with both magnesium and Zn. As ALAD presents a high variability with regards to the need of Zn for catalysis, the active site is highly conserved except those residues involved in Zn binding (PDB: 1E51) (Breinig *et al*., 2003). A dimer will have at least two Zn ions - a distal Zn ion (ZnA) which is coordinated by two residues (histidine and cysteine) at an orifice of the active centre in one subunit, and a proximal Zn ion (ZnB), which is coordinated by 3 cysteine residues near the catalytic site (fig. 1.3) (Jaffe & Hanesg, 1986; Erskine *et al*., 1999; Jaffe *et al*., 2001a; Sawada *et al*., 2010). Mutagenesis of these three cysteine residues in human ALAD shows that these residues are critical for the binding of Zn and affects the activity of the enzyme when altered to nonpolar residue, alanine. Another interesting mutation is Cys132Arg, which is a naturally occurring mutation giving rise to ALAD porphyria (Jaffe & Stith, 2007). Cys-132 has a vital interaction with the catalytic Zn (fig. 1.3). Characterisation of this mutant revealed that the quaternary morpheein structure was altered and had a greater tendency of forming hexamers. Although both residues are polar, arginine is charged and slightly bulkier than cysteine. Analysis of the pH optimum revealed that this mutant had an altered (more basic) pH optimum; while kinetic studies revealed that only 4 % of wild type residual activity was retained. This mutant also disrupted the binding of ZnB in the active site (Jaffe & Stith, 2007).

It appears that the binding of cofactor is critical to the structural integrity and functioning of the ALAD protein. That is to say when different sections of the protein require communication, the cofactor region could be playing a central role in such communication. Ligands involved in cofactor binding can therefore form a communication network that will allow for “opening”, “closing” as well as substrate interaction.

University of Cape Town

A

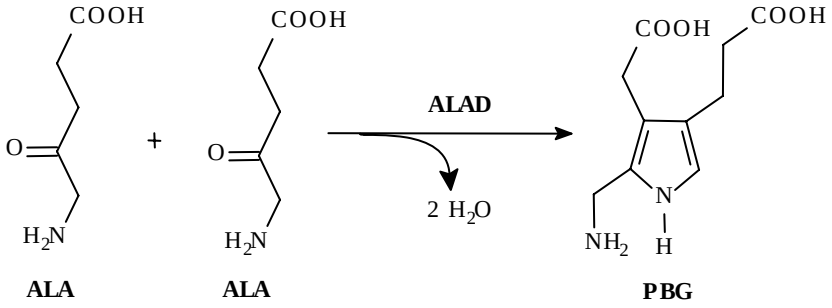

B

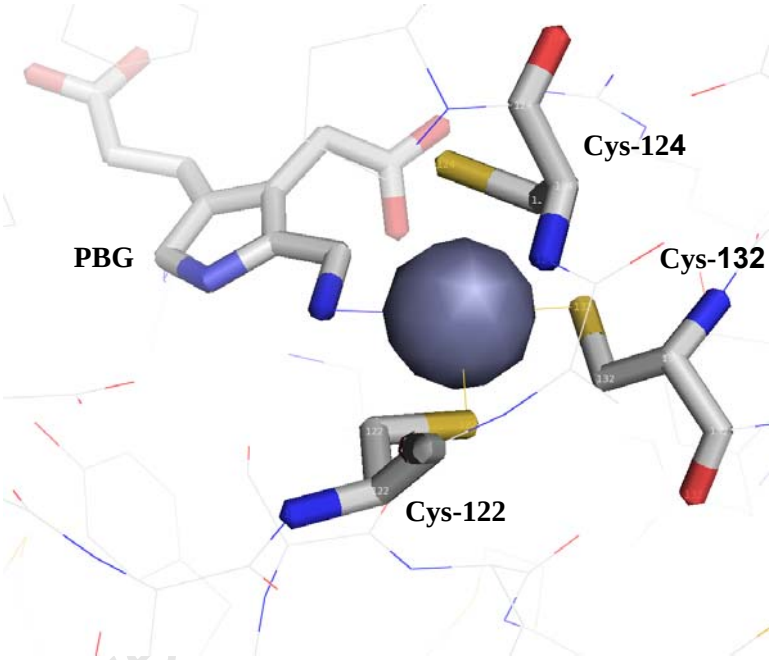

Figure 1.3: A) Chemical schematic of the biosynthesis of PBG from ALA, catalysed by ALAD (Davids, 2003). B) Self-constructed PyMol (Mills-Davies, 2000) image showing the schematic representation of the catalytic Zn binding region in human ALAD protein structure (PDB: 1E51), highlighting the importance of the 3 Cys residues. PBG and cysteine residues are shown in stick format; the Zn ion is shown as a purple sphere; neighbouring protein residues are shown as lines. Blue - nitrogen; red - oxygen; grey - carbon; yellow - sulphur.

Porphobilinogen deaminase

PBGD (E.C. 4.3.4.8), also known as hydroxymethylbilane synthase, preuroporphyrinogen synthase or uroporphyrinogen I synthase, is the third enzyme in the haem biosynthetic pathway. Still in the cytoplasm, PBGD catalyzes the formation of hydroxymethylbilane with the aid of cofactor, dipyrromethane (DPM); which the enzyme is able to generate (Jordan & Warren, 1987; Jordan *et al*., 1988). The proposal and elucidation of the PBGD reaction remains one of the most interesting and seminal biochemical achievements in the haem biosynthetic field.

The biosynthesis of hydroxymethylbilane begins with the binding of cofactor to protein. In this reaction a PBG deaminates to yield a methylene pyroline, it then reacts with the deprotonated sulfydryl group of Cys-216; this then forms DPM. The DPM clearly can be considered a 'cofactor' in that catalysis cannot occur in its absence. DPM now acts as a primer for the addition of the first substrate. Again a PBG substrate deaminates but instead of reacting with a sulfydryl group of a cysteine, it reacts with the free α-position of the DPM ring. The remaining three substrates are added sequentially, forming four intermediates (ES1, ES2, ES3, and ES4 where ES denotes enzyme-substrate complex), fig. 1.4. Once ES4 is produced, the limiting size of the active site prevents further extension. The resulting enzyme-bound hexapyrrole is then hydrolysed releasing the unstable tetrapyrrole product, hydroxymethylbilane (Jordan, 1990; Song *et al*., 2009).

The human structure of PBGD (PDB: 3EQ1 and 3ECR) reveals a monomeric enzyme composed of three domains namely: I (N-terminal), II (central), and III (C-terminal) (Gill *et al*., 2009; Song *et al*., 2009). The active site is located in a cleft between domains I and II; domain I has an extended section made of loops that act as a cap to shield active site from solvent. Domain III is different from domains I and II and comprises an open face, three stranded, antiparallel beta-sheet with three alpha-helical segments covering one of the faces. A conserved residue Cys-261, which covalently links DPM to protein, is located in domain III; and positions DPM to allow for further substrate binding and extension in the active site. The active site pocket is lined with positively charged residues and is large enough to accommodate the cofactor, DPM, and as mentioned, four molecules of PBG molecules. Besides the Cys-261 covalent linkage, DPM also forms several ionic interactions with surrounding positively charged residues. These

University of Cape Town

residues include the conserved Arg-149, Arg-150, Arg-175 and Arg-195 (Gill *et al*., 2009).

The importance of DPM in PBGD is not merely catalytic; DPM has also been reported to enhance stability of the protein. This is achieved through the many interactions with several conserved residues of the protein. Firstly an interaction with a cysteine residue (Cys-261) ensures that DPM is covalently linked to the protein. DPM is further attached to the protein through an invariant lysine and aspartate residue (Lys-98 and Asp-99, respectively). Lys-98 forms a salt bridge with the acetate cofactor side chain while Asp-99 hydrogen-bonds to both pyrrole rings of the DPM cofactor. Both these interactions have been reported to be critical for the integrity of the protein structure. Another important interaction with the protein and DPM involves the carboxylate group of DPM and several invariant residues among these is Arg-149; through mutagenesis studies, its role in DPM function/binding has been determined (Gill *et al*., 2009).

Structural analysis shows that, Arg-149 is directly involved in DPM binding (fig. 1.4). The amide nitrogen of Arg-149 forms a 2.8 Å hydrogen bond with the carboxyl oxygen of the acetic acid side chain. This interaction is said to be critical for the optimal docking of PBG into the active site (Gill *et al*., 2009). Mutant Arg149Gln (alteration from a positive polar to a neutral polar residue) had less than 5 % wild type residual activity. The mutant was also unable to bind either DPM or substrate even though the apoenzyme conformation was similar to wild type (Jordan & Woodcook, 1991; Shoolingin-Jordan *et al*., 2003).

The interaction between DPM and Arg-149 clearly highlights the role that conserved interactions have in optimizing the cofactor's binding and orientation for optimal catalysis. Although, Arg-149 does not form the critical Schiff base interaction which is considered to be an essential stabilizing interaction (Cys-261 is responsible for this interaction, fig. 1.4), removal of its interaction affected the DPM's ability to interact with Cys-261. Since the removal of the Arg-149 inhibited the Cys-261 interaction, it is tempting to speculate that these ligand residues display some sort of "positive co-operative" binding under normal conditions.

University of Cape Town

A

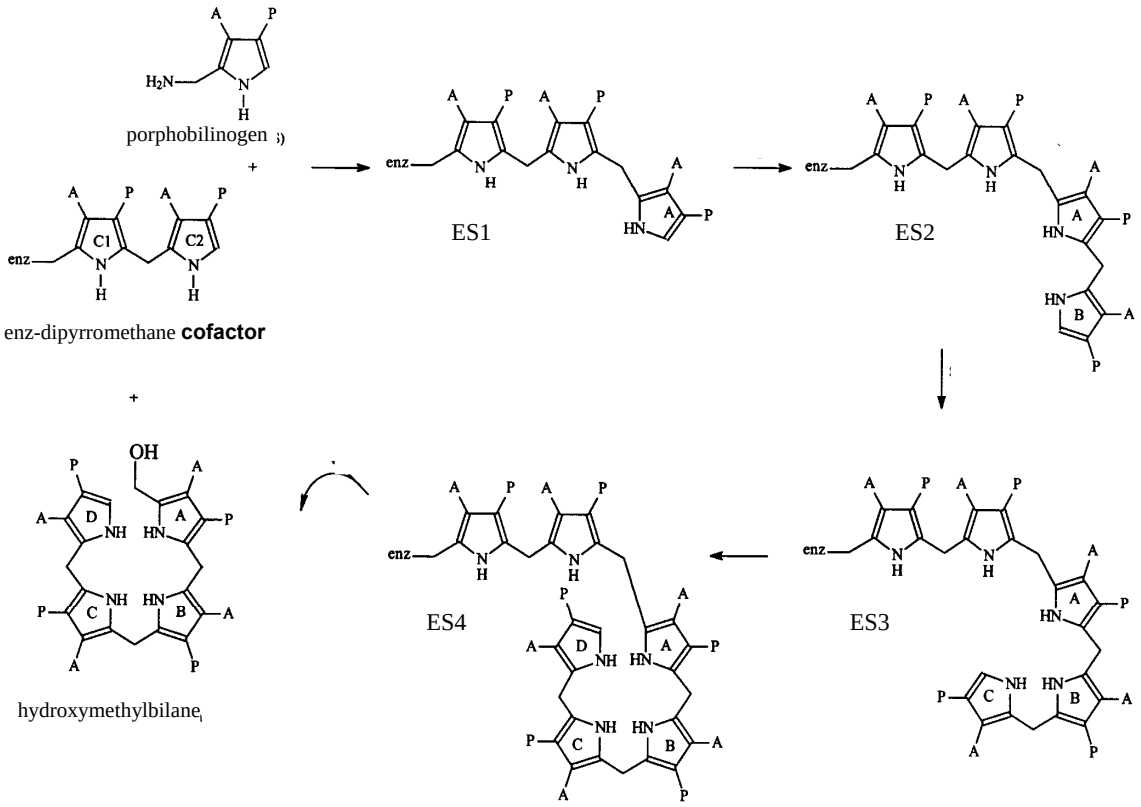

B

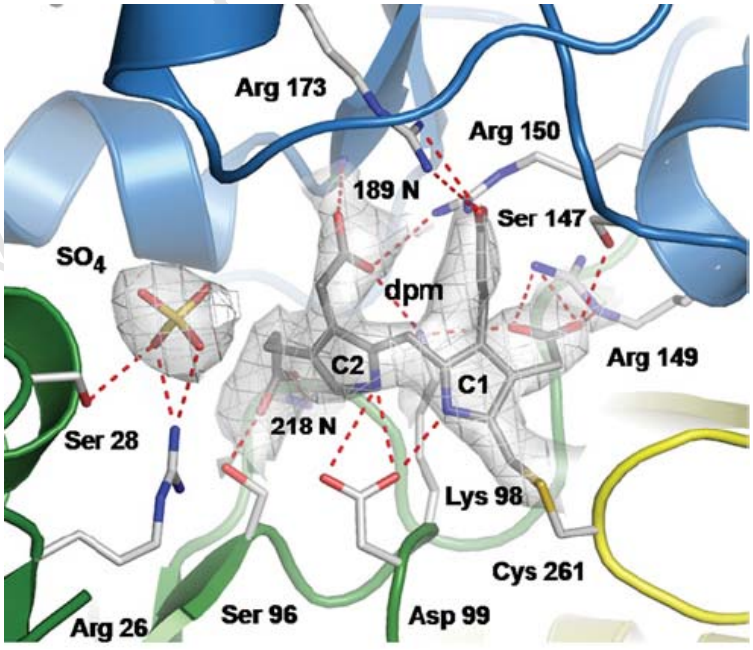

Figure 1.4: A) A chemical schematic view of the biosynthesis of hydroxymethylbilane. B) Image showing the dipyrromethane (DPM) binding region in PBGD. Hydrogen bond interactions are show as dotted lines. Interacting residues and DPM are shown in stick format while surrounding protein is shown as a cartoon (secondary structure) (Gill *et al*., 2009). In the stick structures red = oxygen; yellow = sulphur; blue = nitrogen; grey = carbon.

Uroporphobilinogen III synthase

Once hydroxymethylbilane is formed, cyclisation and ring rearrangement to form the required tetrapyrrolic porphyrin isomer can proceed. The enzyme responsible for this is UROIIIS also known as uroporphyrinogen III cosynthase (E.C.4.2.1.75). It catalyzes the cyclization of hydroxymethylbilane (HMB) to produce uroporphyrinogen III (UROIII) in the cytosol. UROIIIS does not require the aid of a cofactor for catalysis. Interestingly, sequence analysis reveals UROIIIS to belong to the flavodoxin-like fold family - members of this family are known to bind nicotinamide adenine dinucleotide (NAD) (Jordan, 1990; Shoolingin-Jordan, 2003).

HMB can spontaneously cyclize to form UROI, however, this product cannot be converted into haem (fig. 1.5). Rather, HMB is cyclized and ring D rearranged to form UROIII, the required tetrapyrrole, in the cytosol by UROIIIS (fig. 1.5). Arrangement of A-ring results in the loss of the C-20 hydroxyl group to create a carbo-cation at C-20 that performs an electrophilic attack on C-16 to form a spirocyclic pyrrolene intermediate. The intermediate then resolves to generate an azafulvene which then cyclizes to UROIII (Jordan, 1990; Mathews *et al*., 2001).

The structure of UROIIIS (PDB: 1JR2) has a bi-lobed structure comprised of 2 domains (consisting of beta-sheets and alpha-helices); the two domains are linked by two anti-parallel beta-sheets (Mathews *et al*., 2001). The N-terminal (domain I) resembles a flavodoxin fold whereas domain II has similarities to a DNA glycosylase-like fold. Three invariant residues have been identified in UROIIIS; these are serine (Ser-63), tyrosine (Tyr-168) and threonine (Thr-228). UROIIIS exists as a monomer with two domains as previously mentioned. UROIIIS folds in two domains; each domain consists of beta-sheets surrounded by alpha-helices. The two are then connected by two anti-parallel beta-sheets. The active site is speculated to lie between these domains, where a number of conserved residues cluster (Mathews *et al*., 2001; Schubert *et al*., 2008).

Protein side chains form hydrogen bonds with the product namely: Lys-141 (with ring A propionate), His-165 (with ring A acetate) and Gln-194 (ring B acetate). However these residues are nonconserved and are unlikely to play a vital role in the enzymes catalytic mechanism. Furthermore, there are backbone interactions that stabilize

University of Cape Town

substrate/product binding. The product binds between the two domains and is held in place by a network of hydrogen bonds between the product's side chain carboxylates and the protein's main chain amides. Interactions of the ring A and B carboxylate side chains with both structural domains of UROIIIS appear to dictate the relative orientation of the domains in the closed enzyme conformation and likely remain intact during catalysis. The product C and D ring are less constrained in the structure, consistent with the conformational changes required for the catalytic cyclization with inversion of ring D orientation. A conserved tyrosine residue is potentially positioned to facilitate loss of a hydroxyl from the substrate to initiate the catalytic reaction (Mathews *et al*., 2001).

UROIIIS is one of the most highly diverged of the haem biosynthetic enzymes. A structure base sequence alignment revealed only seven residues are conserved among UROIIIS proteins (Schubert *et al*., 2008). Three of the conserved residues are glycine residues (Gly-22, Gly-90, and Gly-212) positioned in tight turn conformation only, optimal for their small structure to fit. A proline (Pro-29) located on a beta-sheet and an alanine (Ala-94) located on a helix are said to contribute to a hydrophobic pocket in the protein, are also among the conserved seven. The sixth conserved residue is a threonine (Thr-217) whose hydroxyl points to bound product. Mutation of threonine to an alanine (nonpolar replacement and removal of the threonine hydroxyl group) in human UROIIIS, lead to 32 % residual activity (Mathews *et al*., 2001). Therefore six of the seven conserved residues have a structural, as opposed to a catalytic role. The final residue, tyrosine (Tyr-155) has been reported to possibly contribute to the deamination of the substrate during catalysis of UROIIIS. Studies in various species showed this residue to have different functions. When tyrosine was mutated to an alanine in *A. nidulans* UROIIIS, no activity was detected. However, when the corresponding residue was mutated to an alanine in human UROIIIS, 50 % residual activity was reported. Interestingly, the structural orientation of this residue near the formed product in different species differs. This could account for the functional difference noted (Mathews *et al*., 2001; Roessner *et al*., 2002; Schubert *et al*., 2008). The point of detailing this here is to show that a conserved residue can perform different functions in a protein, depending on its exact atomic structural location.

University of Cape Town

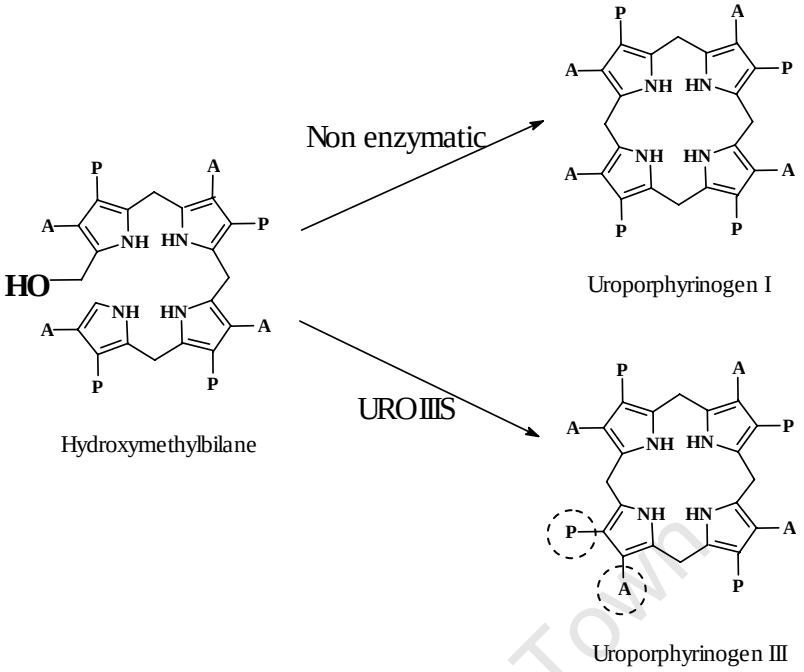

Figure 1.5: A chemical schematic view of the biosynthesis of uroporphyrinogen. Both the non-enzymatic as well as enzymatic (UROIIIS) reaction is shown (Davids, 2003). P = propionate (-CH_2CH_2COOH), and A = acetate (-CH_2COOH).

University of Cape Town

Uroporphyrinogen decarboxylase

Once the octacarboxylic tetrapyrrole (UROIII) has been formed, the fifth enzyme of the haem biosynthetic pathway UROD (EC 4.1.1.37) catalyzes the decarboxylation of four acetate side chains of UROIII to generate CPO in the cytosol. Unlike most decarboxylases, UROD does not require a cofactor to function (Roth *et al*., 1983).

Thus, the catalytic reaction of UROD can be viewed as involving the removal of four carboxylic groups from the acetate side chains of UROIII (fig. 1.6). The first ring to be decarboxylated is ring D, decarboxylation then precedes clockwise (Phillips *et al*., 2003). The decarboxylation begins at the asymmetric ring D and proceeds sequentially to ring A, B, C. The decarboxylation of the first acetic acid side chain is faster than of the next three and a porphyrinogen with seven carboxyl groups accumulates (Jordan, 1990; Phillips *et al*., 2003).

UROD (PDB: 1URO) is a homodimer and each monomer consists of three domains with an active site cleft at the centre of the three domains (Whitby *et al*., 1998). The tetrapyrrolic product adopts a domed conformation that lies against a collar of conserved hydrophobic residues and allows formation of hydrogen-bonding interactions between a carboxylate oxygen atom of an invariant Asp-86 side chain and the four pyrrole NH groups (fig. 1.6). Three pyrrole rings have their NH groups pointing at Asp-86 for optimal hydrogen bonding geometry (Phillips *et al*., 2003).

University of Cape Town

It is clear from structural analysis, and being an invariant residue, that Asp-86 plays a vital function in UROD. It was hypothesized that since Asp-86 is the only negatively charged residue in the active site cleft (there are mostly hydrophobic residues in the active site cleft), that this residue could be coordinating the pyrrole NH groups, through hydrogen bond interactions. Additionally, the negative charge of Asp-86 would stabilize a protonated pyrrole. In a mutagenesis study, Asp-86, a negative, polar residue, was mutated to a glycine (a neutral nonpolar replacement), an asparagine (a neutral polar replacement), and a glutamate (a negative, polar replacement). Asp86Gly was able to bind substrate and intermediates with similar geometry as substrate. In this mutant, the alteration of size, glycine being less bulky than aspartate, resulted in two water molecules accompanying and aiding the binding of the substrate. However, even with “favourable” binding, residual activity was only 0.1 - 2.4 % that of wild type. This shows

that Asp-86 is directly involved in catalysis. Even though asparagine is a polar residue, and has the same size as aspartate, the removal of the negative charge resulted in a mutant that bound substrate poorly and only retained 0.1-0.6 % of wild type activity. Conserved replacement, Asp86Glu, showed similar binding of substrate as wild type when the crystal structure was analysed. However, kinetics showed a reduced substrate affinity and a surprising 5-10 % residual activity. Since no intermediate-enzyme complex has been reported, it is difficult to assess whether this mutant was able to bind intermediates similarly to wild type. One can conclude that an aspartate residue is critical at this position for the optimal function of the enzyme (Phillips *et al*., 2003).

University of Cape Town

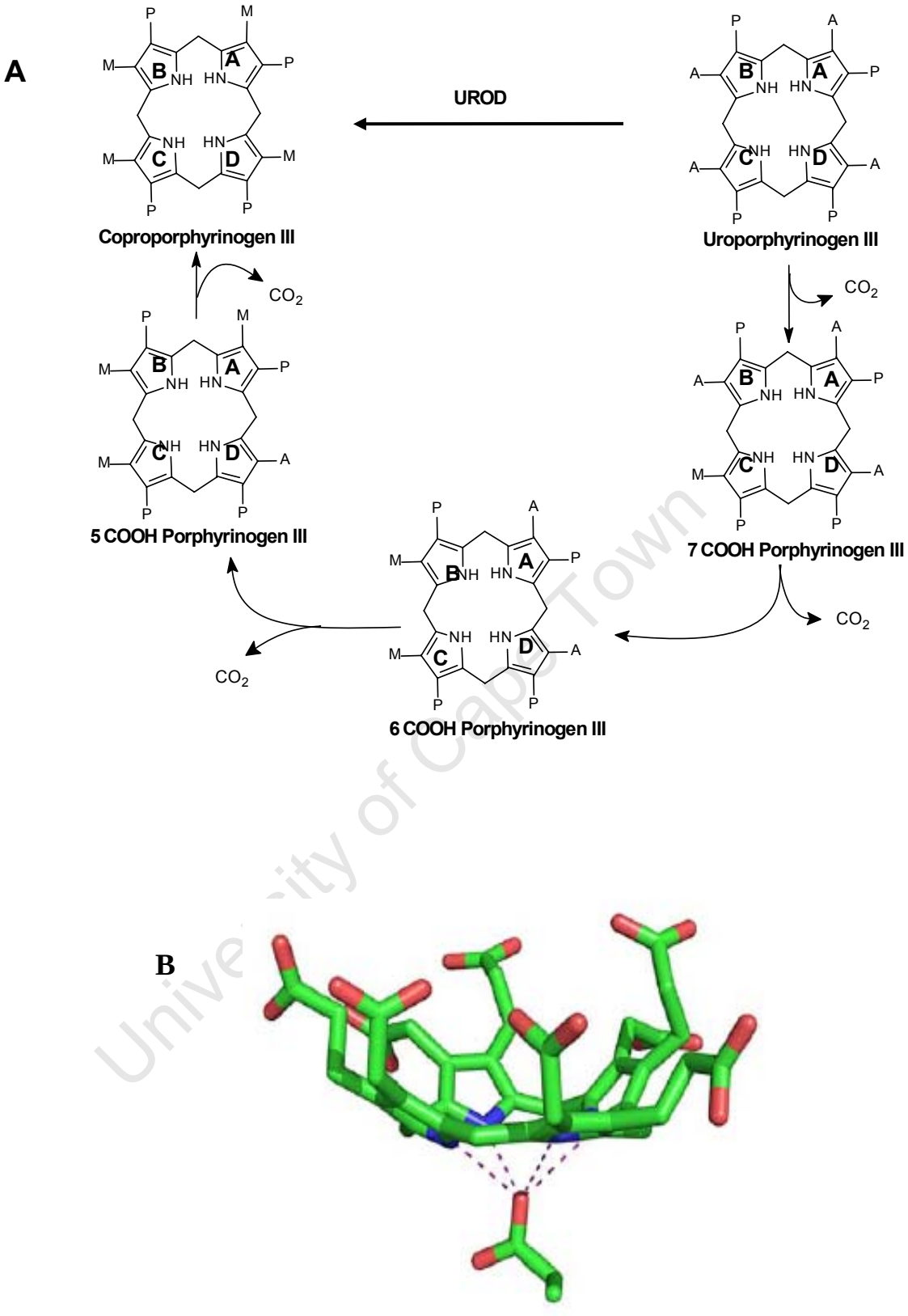

Figure 1.6: A) A chemical schematic view of the decarboxylation of uroporphyrinogen III to form corproporphyrinogen III. Reaction catalysed by uroporphyrinogen decarboxylase (UROD) releasing carbon dioxide (CO_2) as by-product. B) Interaction of asparagine 86 with the porphyrinogen macrocycle (Ajioka *et al*., 2006). Red = oxygen, blue = nitrogen, and green = carbon.

University of Cape Town

Coproporphyrinogen oxidase

The sixth enzyme in the haem biosynthetic pathway is CPOX, (E.C. 1.3.3.3). It catalyzes the oxidative decarboxylation of CPO to protogen, fig. 1.7 (Elder & Evans, 1978; Grandchamp *et al*., 1978; Jordan, 1990). Interestingly, although CPOX is an oxidase, it functions in the absence of cofactor (most oxidases have an electron accepting cofactor) but rather in the 'direct' presence of O_2 (Sano & Granick, 1961; Elder & Evans, 1978; Fetzner, 2002). In oxidases that function without cofactor, substrate forms radicals and/or carbonionic intermediates that react with O_2. This is the first of three terminal steps of haem biosynthesis occurring within the mitochondria.

The detailed catalytic mechanism of CPOX has not yet been elucidated. The proposed sequence of catalysis involves the deprotonation of the NH group of the pyrrole. Thereafter the alpha carbon of the pyrrole reacts with O_2 to form a transient peroxide anion which decarboxylates the propionate moiety (Lee *et al*., 2005).

CPOX (PDB: 2AEX) is a homodimer. It catalyses the oxidative decarboxylation of propionic acid side chains of ring A and B of CPO. CPOX assumes a previously unknown tertiary topology characterized by a large seven-stranded beta-sheet that is flanked on both sides by alpha-helices. The up-and-down beta-sheets are similar to porins but the beta-sheet in CPOX is flat and does not form a barrel (Lee *et al*., 2005).

A sequence analysis of CPOX study revealed three residues completely conserved in the CPOX between species. The residues are Asp-400, Arg-401 and Arg-262. A structure function study was carried out in order to understand their role in CPOX (Lee *et al*., 2005; Stephenson *et al*., 2007). Aspartate, due to its negative charge, is able to play the role of stabilizing a protonated pyrrole (see section on UROD); while arginine has been reported as a candidate for carboxylate recognition (Lee *et al*., 2005). All three residues were mutated to an alanine, a neutral, nonpolar residue. Asp400Ala, had a similar K_M as wild type but a drastically reduced activity. Both arginine mutants bound substrate poorly and had reduced catalytic functioning, proving their role in the activity of UROD (Stephenson *et al*., 2007).

University of Cape Town

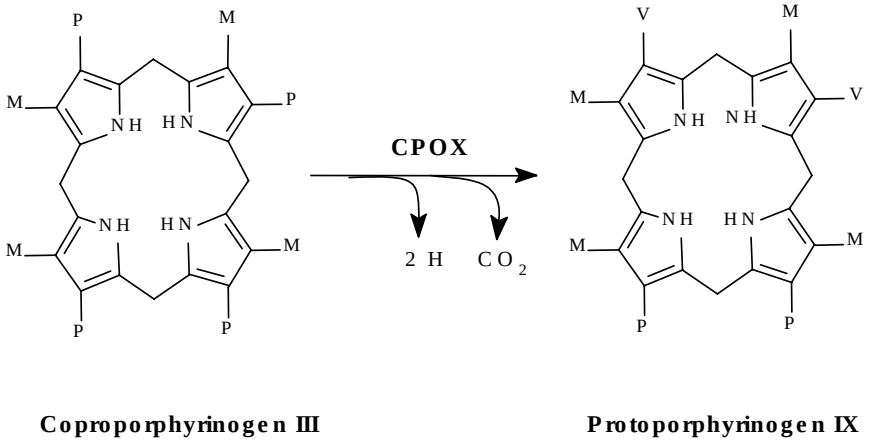

Figure 1.7: A chemical schematic view of the decarboxylation of coproporphyrinogen III to form protogen. Reaction catalysed by coproporphyrinogen oxidase (CPOX) releasing carbon dioxide (CO_2) as by product. P = propionate ($-CH_2CH_2COOH$), M = methyl ($-CH_3$), V = vinyl ($-CH=CH_2$).

University of Cape Town

Protoporphyrinogen oxidase

In the penultimate step of the haem biosynthetic pathway, PPOX (E.C. 1.3.3.4) catalyzes the oxidation of protogen to proto (Poulson & Polglase, 1975; Jordan, 1990). The reaction requires the presence of an electron accepting cofactor, typically flavin adenine dinucleotide (FAD). Indeed, as early as 1987, Siepker *et al*. (1987) identified FAD as the prosthetic group attached to PPOX in purified bovine liver PPOX. PPOX is a homodimer structured protein and is classified as a flavoprotein oxidase. PPOX combines the dehydrogenation of substrate with the reduction of molecular O_2, to form H_2O_2. Thus, in PPOX the FAD molecule is reduced by the substrate which in turn oxidizes the final electron acceptor (O_2) forming H_2O_2 in the process. As PPOX is the topic of this study it is reviewed in necessary detail in chapter 2.

Ferrochelatase

The final enzyme in the biosynthesis of haem is FECH also known as haem synthetase (E.C. 4.99.1.1). It catalyzes the insertion of ferrous iron (Fe^{2+}) into proto to form haem with the aid a cofactor, [2Fe-2S] cluster. It has been shown that Fe^{3+} is reduced to Fe^{2+} inside the inner mitochondrial membrane in proximity to FECH (Wu *et al*., 2001).

The mechanistic insertion of Fe^{2+} into a porphyrin macrocycle in solution chemistry is well understood, however, the catalysed insertion of Fe^{2+} into proto in vivo is not fully elucidated (Clayden *et al*., 2001) . FECH catalysis involves the acquisition and desolvation of Fe^{2+}; this is then followed by the binding of proto to FECH. The bound macrocycle then distorts prior to the removal of two pyrrolic protons. It has been proposed that substrate binding and distortion is mediated by conserved hydrophobic residues. Two protons are then removed from the porphyrin in the so called bi-bi mechanism (fig. 1.8). Lastly the macrocycle is metallated and haem is released (Dailey *et al*., 2000).

The crystal structure of FECH has revealed important characteristics that have helped add to the knowledge of FECH mechanism (Dailey *et al*., 2000; Wu *et al*., 2001). Human FECH is a homodimer with each monomer, elongated in shape. Each monomer has two domains, consisting of a mixture of alpha-helices and beta-sheets. The active site is located between the two domains. The structure also revealed an iron-sulphur ([2Fe-2S]) clusters. These clusters allow iron to clyclize between Fe^{+2} and Fe^{+1} oxidation states. The crystallisation of the human FECH with a bound substrate revealed several differences between bound and unbound FECH. These differences include the opening and closing of the active site “lip”. In the unbound FECH the active site “lip” is in an open confirmation and as expected in the bound FECH the “lip” is closed. Also, the orientations of several residues are altered upon the binding of the substrate molecule.

FECH (PDB: 1HRK) does not function with a cofactor, however, the active site is lined with hydrophobic conserved residues that have been proposed to act as ligands in both the binding of substrate as well as the catalytic insertion of Fe^{2+} (Wu *et al*., 2001).

His-263 (human numbering), is an active site residue that is conserved in all known FECH (Dailey *et al*., 2000). It was initially thought that His-263, was involved in binding

University of Cape Town

of Fe^{2+} (Kohno *et al*., 1994). In a structure-function study when His-263 was mutated to an alanine, it resulted in an increased K_M for Fe^{2+}. Analysis of the resolved structure as well as further characterisation of His263Ala from a purified enzyme (rather than crude cell extracts as was done by Kohno *et al*., (1994)), showed that His-263 was not involved in Fe^{2+} binding (Sellers *et al*., 2001).

Histidine is able to participate in catalysis because of its positively charged imidazole side chain. When protonated the imidazole can act as an acid while in its unprotonated state it acts as a base. This residue has also been reported to stabilize folded protein. Therefore, histidine can have both catalytic and structural roles in protein. Sellers and colleagues used site-directed mutagenesis to mutate histidine to an alanine (nonpolar neutral), a methionine (nonpolar neutral), a cysteine (polar, neutral), and an asparagine (polar, neutral). Although mutants were able to bind substrate (proto) and Fe^{2+}, no activity was detected in any of them.

In 2007 Dailey and colleagues published a structure of ferrochelatase with a mutated His-263 (Dailey *et al*., 2007). Based on orientation and interaction with surrounding residues, they showed that His-263 could be involved in a hydrogen bonding network with surrounding residues (His-341 and Glu-343) and at least one proton group of the substrate ring. These residues (His-263, His-341 and Glu-343), are among the six residues that are reorientated once the substrate binds. When His-341 was mutated to cysteine and crystallized, the structure had similar reorientation of residues as was seen in His263Cys structure. However, this mutant (His341Cys) had little activity while His263Cys had no activity showing that the inactivity was most probably not due to rearrangement alone. LigPlot analysis of the wild type FECH structure reveals a network of water molecules involved in extensive hydrogen bond network with His-263 (fig. 1.8). These water molecules allow His-263 to interact with the “substrate” in the active site. In the mutant His263Cys structure, the water network is disrupted and no water molecule is seen interacting with the His-263 (fig. 1.9). Interestingly, the His314Cys structure, which was reported to have little activity, had one water molecule interacting in the His-263 structure, allowing a water mediated interaction with the bound “substrate” (fig. 1.9). These water molecules could be playing a vital role in the catalytic reaction of FECH, be it in the structural integrity or directly in catalysis.

University of Cape Town

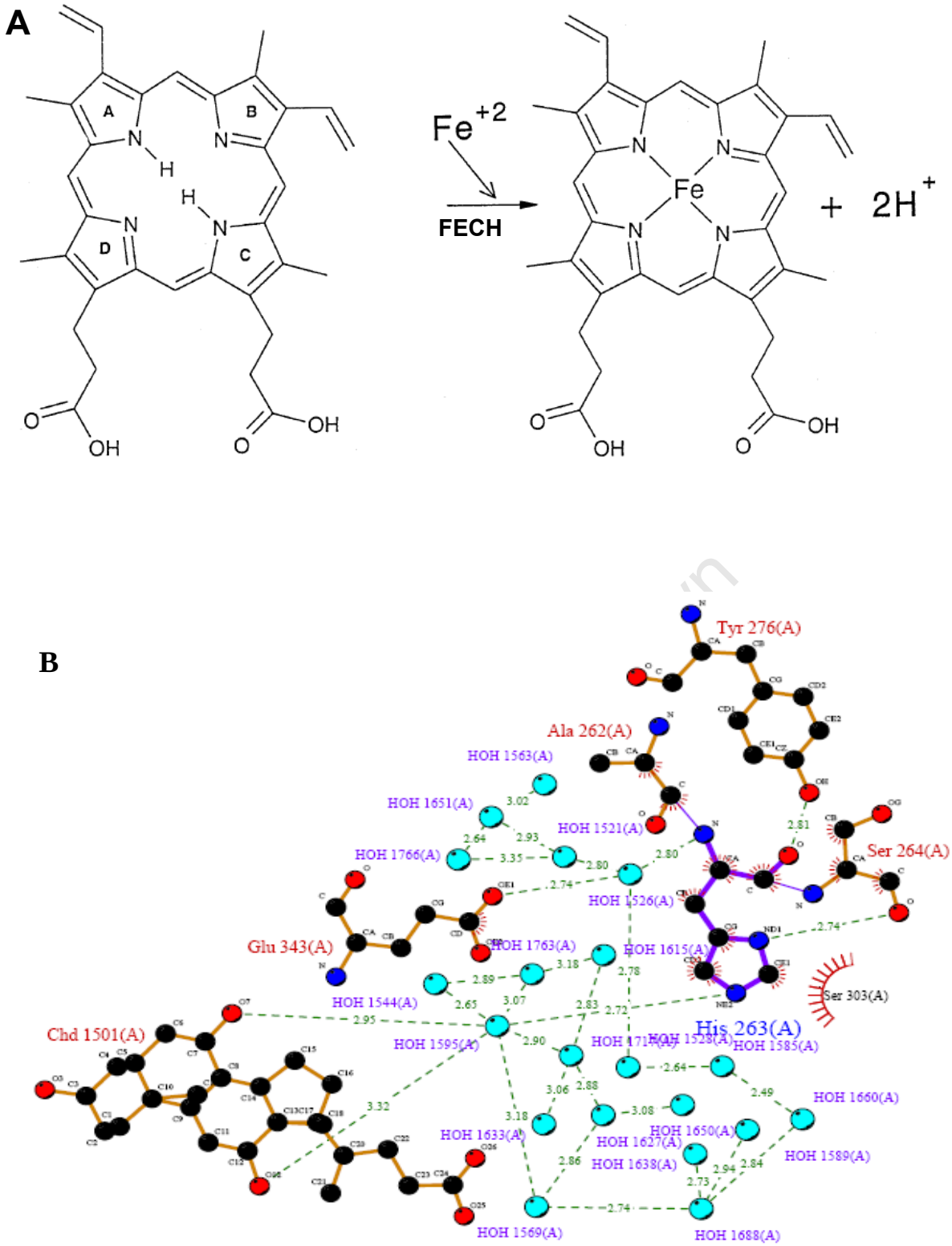

Figure 1.8: A) A chemical schematic view of the insertion of iron (Fe^{2+}) into proto to form haem. Reaction catalysed by ferrochelatase (FECH) (Dailey *et al*., 2000). B) Self-constructed LigPlot showing the hydrogen bond network around His-263 in wild type FECH. Image drawn using subunit A. Black = carbon; blue = nitrogen; red = oxygen; purple = phosphate; yellow = sulphur. Polar interactions are shown as dotted lines and hydrophobic interactions are shown as "eye-lashes".

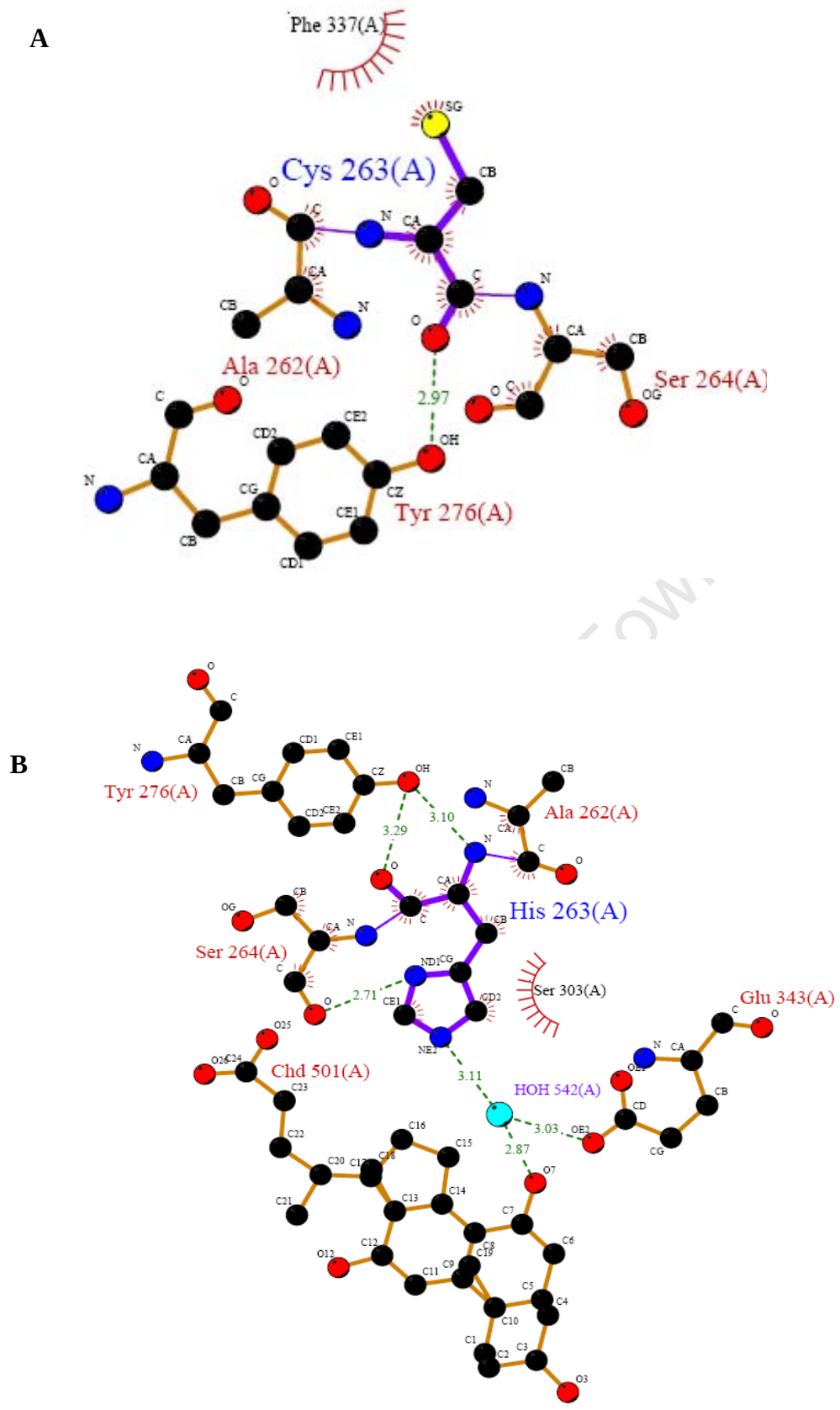

Figure 1.9: Self-constructed LigPlot showing the hydrogen bond network of residue 263. A) His-263 was mutated to a cysteine residue (PDB: 2PO5); no water molecules are seen interacting with the Cys-263. B) The structure of His341Cys (PDB: 2PO7 showing the hydrogen bond network around His-263; one water molecule is seen interacting with His-263. Both images drawn using subunit A. Black = carbon; blue = nitrogen; red = oxygen; purple = phosphate; yellow = sulphur. Polar interactions are shown as dotted lines and hydrophobic interactions are shown as “eye-lashes”.

CHAPTER 2

Protoporphyrinogen oxidase

University of Cape Town

Introduction

Protoporphyrinogen oxidase (PPOX; E.C.1.3.3.4) is the seventh enzyme in the haem biosynthetic pathway (Poulson & Polglase, 1975). Although protogen auto-oxidizes spontaneously to proto *in vitro,* (especially in the presence of light and O_2), i*n vivo,* an enzyme is necessary. Indeed, the relatively anaerobic environment in the mitochondria prevents such auto-oxidation. PPOX is thus required, to catalyze the conversion of protogen to proto in the mitochondria (Jordan, 1990).

Function

What is the role of PPOX as part of the haem biosynthetic pathway? PPOX catalyzes the removal of six electrons from protogen to form proto, with the aid of a flavin adenine dinucleotide (FAD) cofactor (Dailey, 1990; Dailey & Dailey, 1996a; Dailey & Dailey 1996b). This reaction (fig. 2.1; described in the previous chapter and in further sections), is biologically relevant as the oxidized proto molecule is required for the final step in the haem biosynthetic pathway. Iron cannot be chelated into protogen and the oxidised form of the molecule, proto, is the preferred substrate for FECH (Brenner & Bloomer, 1980; Meissner *et al*., 1986; James & Hift, 2000; Thunell, 2006).

University of Cape Town

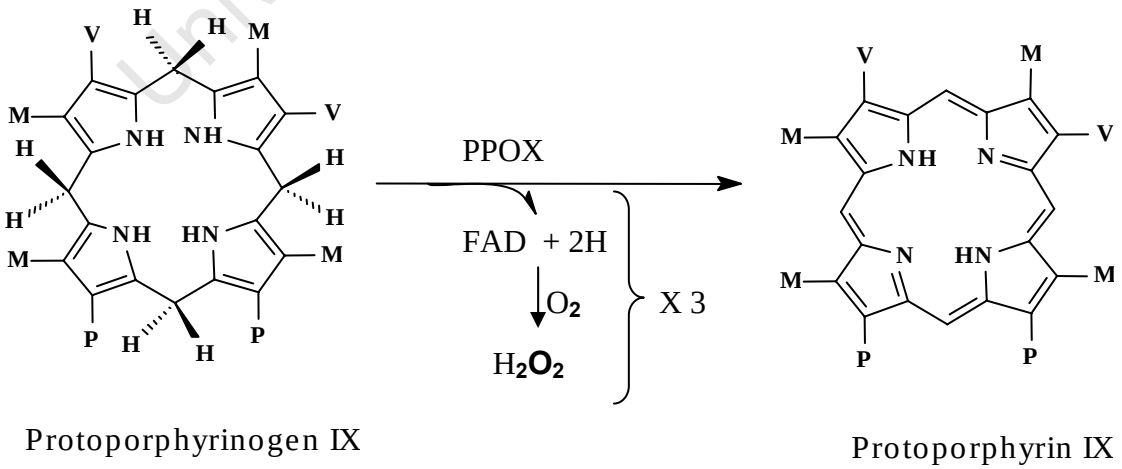

Figure 2.1: A chemical schematic view of the oxidation of protogen. Protogen is oxidised in the presence of O_2 and flavin adenine dinucleotide (FAD) to generate proto and H_2O_2. The reaction is catalysed by protoporphyrinogen oxidase (PPOX).

Structure

PPOX structures from four species have been resolved to date, including the recently resolved human structure (fig. 2.2) (Koch *et al*., 2004; Corradi *et al*., 2006; Qin *et al*., 2010; Qin *et al*., 2011). These structures provide new insight into the structure-function properties of this enzyme. PPOX can either be a monomer or a dimer composed of three binding regions, namely: substrate, membrane and FAD. The cofactor, FAD, is securely, but noncovalently, bound in the FAD binding region.

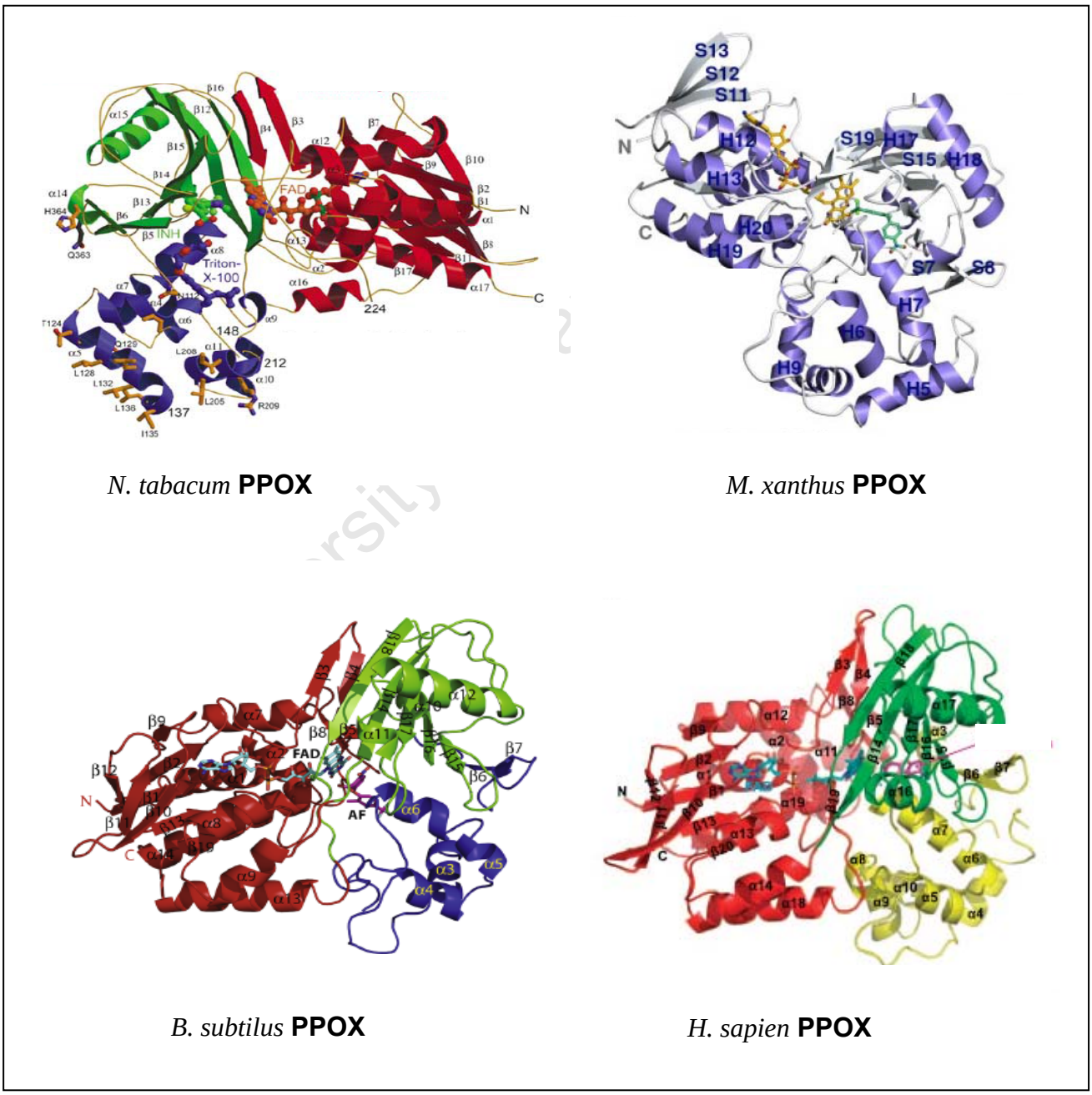

N. tabacum **PPOX**

M. xanthus **PPOX**

B. subtilus **PPOX**

H. sapien **PPOX**

Figure 2.2: Secondary structural images of the four crystallised PPOX proteins as published (Koch *et al*., 2004; Corradi *et al*., 2006; Qin *et al*., 2010; Qin *et al*., 2011).

Functional characterisation

Classification

PPOX is a flavoprotein, which literally means a protein containing a flavin (Birchfield *et al*., 1998). In 1998, through a sequence alignment study, Dailey and Dailey (1998) identified a consensus sequence that allowed for the classification of PPOX in an FAD superfamily. Other proteins found in this superfamily include, Monoamine oxidases, and Phytoene desaturases. Proteins in this superfamily were found to be FAD-containing homodimers, located in the mitochondria (Dailey & Dailey, 1998). Many flavoproteins, like PPOX, are involved in oxidation-reduction reactions, whereby a hydride is transferred from a carbon-nitrogen bond to the flavin cofactor (fig. 2.1) (Massey & Hemmerich, 1980; Ghisla & Massey, 1989).

Flavoproteins partake in a large range of catalytic reactions leading to their functional classification into five distinct, but related, classes (Massey & Hemmerich, 1980): class 1 - transhydrogenases, class 2 - oxidases, class 3 - oxygenases, class 4 - electron-transferases and class 5- pure electron-transferases. In PPOX, FAD reduction is followed by O_2 reduction to form H_2O_2. Thus PPOX, as well as nonrelated proteins, amino oxidase for example, falls under class 2, flavoprotein oxidases (Pollegioni *et al*., 1995). Besides their reactivity with O_2, other properties of flavoprotein oxidases include formation of an anionic flavin semiquinone when reduced with one electron, as well as the ability to form reversible flavin N(5) sulfite adducts (fig. 2.3) (Massey *et al*., 1969). FAD, an essential cofactor in the oxidation of protogen, has multifaceted chemical properties and is discussed next.

University of Cape Town

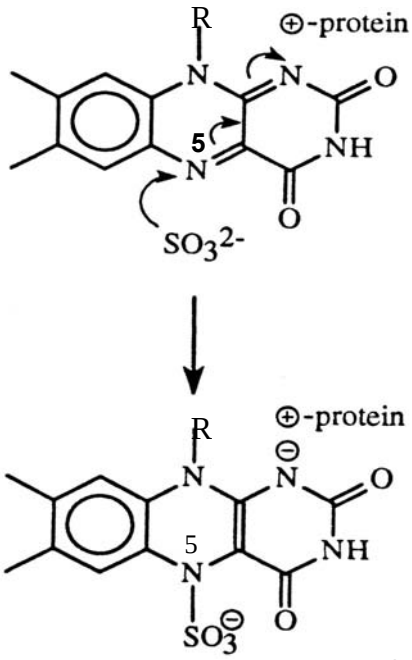

Figure 2.3: An example of sulfite (SO_3) reactivity with FAD-N(5). R denotes the remaining FAD molecule.

University of Cape Town

Flavin adenine dinucleotide

FAD was first isolated from an oxidase in 1938 and yet even today, this complex and versatile molecule has not been fully elucidated (Senda *et al*., 2009). FAD is composed of a flavin mononucleotide (FMN) and an adenosine diphosphate (ADP) moiety (fig. 2.4). FMN is composed of a heterocyclic isoalloxazine, which has both a nonpolar and a polar ring, and a ribityl chain (fig. 2.4). ADP is composed of two phosphate groups, a ribose and an adenine ring. FAD can have three redox states, oxidized, semiquinone and reduced. The semiquinone state can be both neutral and anionic (fig. 2.5). Spectral analysis (used in quantitating FAD content) reveals two bands with peaks at 375 nm and another at 450 nm in the UV/VIS range (Ghisla *et al*., 1972; Massey & Hemmerich, 1980). The reactive part of FAD is the isoalloxazine ring which allows FAD to exist in three redox state: oxidized, semiquinone (one electron-reduced) and fully reduced (two–electron also known as a hydroquinone) states (Ghisla & Massey, 1986; Mushegian & Koonin, 1995; Sampson, 2001; Fitzpatrick, 2011). It is the oxidised state that gives FAD its typical yellow colour while the reduced FAD loses its yellowness and becomes somewhat transparent. The semiquinone form can exist in the neutral, protonated, or anionic form.

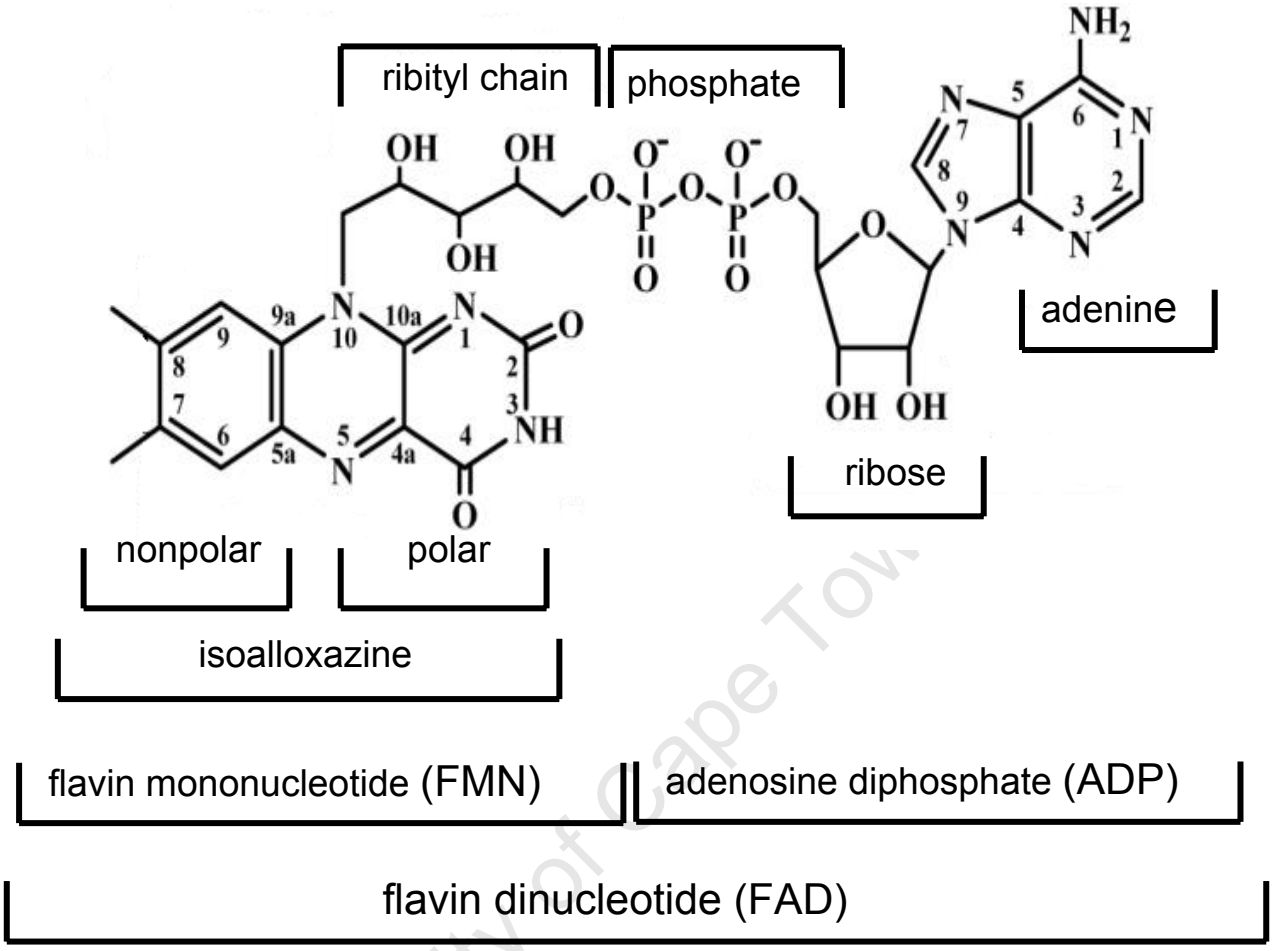

Figure 2.4: A schematic view of flavin adenine dinucleotide (FAD) structural formula in its oxidized state.

University of Cape Town

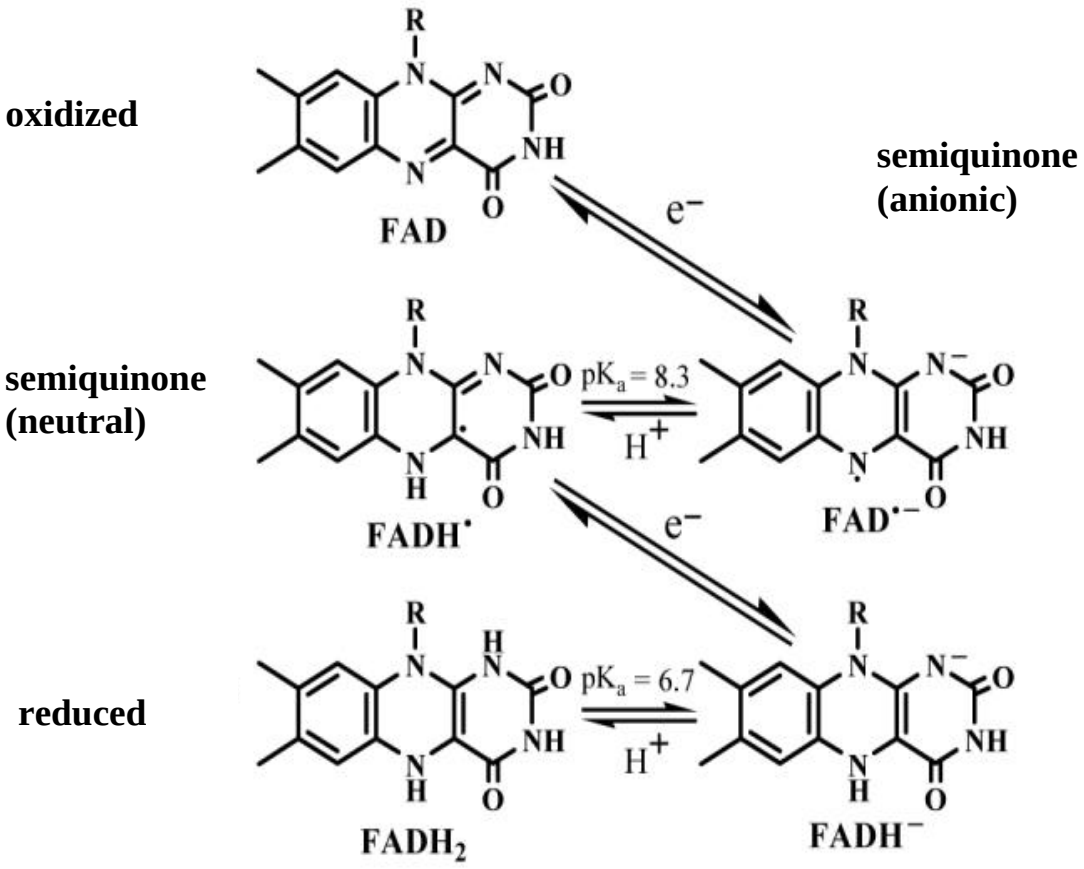

Figure 2.5: Redox states of the flavin adenine dinucleotide (FAD). R denotes the rest of the FAD molecule.

University of Ca

Catalytic reaction

In PPOX, catalysis can be divided into two sections namely: the reductive half and oxidative half. During the reductive half, FAD accepts two electrons from the substrate and is reduced to $FADH_2$. This is then followed by the oxidative half, whereby O_2 oxidizes $FADH_2$ to FAD and O_2 is in turn reduced to H_2O_2. The reduction-oxidation half reaction has been proposed to occur three times (Dailey, 2002). In total six electrons are therefore removed from the methylene bridges and two pyrrollic nitrogens of the substrate (Poulson & Polglase, 1975; Dailey & Dailey, 1996a; Koch *et al*., 2004). A fully conjugated, fluorescent product, proto, is formed.

University of Cape Town

Reductive half

As mentioned above the reductive half involves the extraction of electrons from substrate to FAD. How are these electrons extracted from the substrate, protogen? The exact mechanism of electron extraction is unknown. Based on stereochemical studies, Akhtar *et al*. proposed that there are four *meso* hydrogens in the porphyrin ring, of which three are removed from one face and one from the other face of the ring (Jones *et al*., 1984; Akhtar, 1991). After analysis of the crystalised mtPPOX structure, Koch *et al*. suggested that the electrons are lost from a single point in the macrocycle, due to the lack of space for the substrate to rotate in the active site (Koch *et al*., 2004). This has been verified in mtPPOX, mxPPOX and bsPPOX crystal structures (Koch *et al*., 2004; Corradi *et al*., 2006; Qin *et al*., 2010). Six electrons are removed in total, a reaction that is of biological interest as FAD is only able to accept a maximum of two electrons at a time. Dailey (2002) therefore proposed that the electrons are released in pairs, resulting in the formation of three intermediates ES1, ES2, ES3, before final product, proto is formed.

What is the role of FAD in catalysis? The FAD-N(5) of the isoalloxazine ring, takes part directly in substrate dehydrogenation, and any interaction involving this atom should affect catalysis (Corradi *et al*., 2006). This N(5) is within hydrogen-bonding distance from a hydrogen bond donor, typically a backbone or side chain nitrogen atom (Massey & Hemmerich, 1980). The stereochemistry of this interaction is highly conserved. In mxPPOX the hydrogen bond donor is believed to be an asparagine (Asn-63). However, this residue, which is highly conserved in prokaryotic PPOXs (appendix 21), as well as

other non-related oxidases (monoamine oxidase, MAO; polyamine oxidase, PAO), is not within hydrogen bonding distance from the FAD-N(5) (Edmonson *et al*., 2004). Rather, in mxPPOX it is involved in a water mediated interaction with the N(5) and this water molecule is within hydrogen bond distance from the FAD-N(5) (fig. 2.6). The proximity of a hydrogen-bond is generally expected to increase the oxidative power of the cofactor as well as increase the reactivity of the FAD-C(4) with H_2O_2 (Fraaije & Mattevi, 2000).

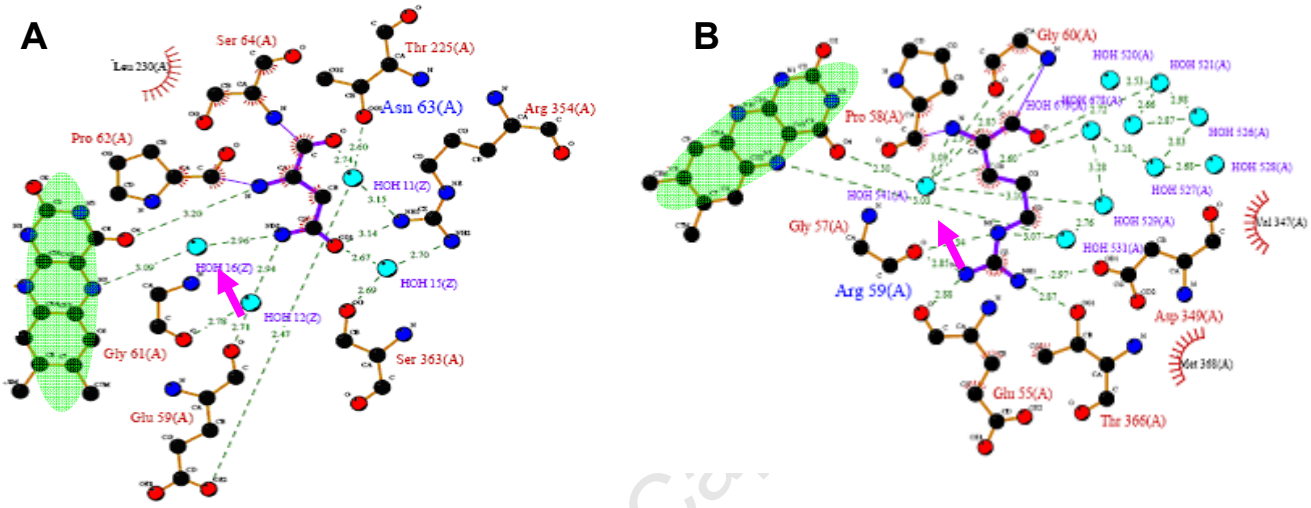

Figure 2.6: Constructed LigPlot of the isoalloxazine ring of FAD (highlighted in green) and the FAD-N(5) conserved water molecule (pink arrow). A) mxPPOX showing four water molecules interacting with the FAD isoalloxazine. B) hPPOX showing ten water molecules interacting with the FAD isoalloxazine. Black – carbon, blue – nitrogen, red – oxygen, cyan – water, dotted line – hydrogen bond, "eye-lashes" – hydrophobic interaction.

Once substrate is bound, two electrons are removed, one at a time. The first electron reduces the FAD forming an anionic semiquinone (Massey & Hemmerich, 1980; Ghisla & Massey, 1989). Upon reduction, the FAD-N(5) becomes protonated so that the hydrogen bond interaction with protein (Asn-63 water mediated) becomes energetically less favourable in the semi-reduced state of FAD (Mattevi *et al*., 1997). This FAD intermediate is also unable to react with O_2. It is only upon the second electron reduction that the fully reduced FAD reacts with O_2, initiating the oxidative half reaction (Birchfield *et al*., 1998; Dailey, 2002; Maneli *et al*., 2003; Qin *et al*., 2010).

Oxidative half

The oxidative half involves the oxidation of the fully reduced FAD, $FADH_2$, by O_2. The reaction of O_2 with the reduced FAD has been the subject of much study and

speculation since 1972 (Ghisla *et al*., 1972). The exact mechanism of O_2's entry into the protein was thought to be through random diffusion (Ghisla *et al*., 1972). The O_2 would then somehow be directed to its point of activation to receive electrons. However, this random movement of O_2 in the protein was assumed, and not proven (Massey, 1994; Riistama *et al*., 1996; Hofacker & Schulten, 1998). Work by Massey *et al*., (1980) suggested otherwise. They showed that the series of co-ordinated steps in the dehydrogenation of substrate could mean that the route of O_2 movement from outside the protein to its final state (e.g. H_2O_2) was through a more co-ordinated route. It has since been illustrated in several enzymes that O_2 does not diffuse freely through these enzymes to its point of activation, but that access is modulated by specific protein-mediated events. Pathways, as well as gated tunnels, have been identified with regards to the movement of O_2 in certain proteins such as cholesterol oxidases, cytochrome c oxidases, and lipooxidases (Riistama *et al*., 1996; Hofacker & Schulten, 1998; Regan *et al*., 1998; Riistama *et al*., 2000; Yue *et al*., 2001; Kuhn *et al*., 2007; Chen *et al*., 2008).

In PPOX, three molecules of O_2 are consumed per substrate oxidized. As previously mentioned, it is likely that these three molecules are consumed in a stepwise fashion – perhaps suggesting a co-ordinated path of O_2 within the molecule. However, little is known of O_2's movement in PPOX or its point of activation. As proposed by Dailey (2002), during catalysis, electrons are released in a stepwise series and are received by FAD. Therefore, a complete cycle would involve the removal of one electron from substrate, which then reduces FAD to produce a semiquinone. The semiquinone is non-reactive to O_2 (Massey, 1994). Assuming that O_2 does not randomly diffuse to its point of activation, a coordinated series of protein movements would then allow the O_2 to be released and activated. This has been shown to be probable, as seen in cholesterol oxidase (Piubelli *et al*., 2008). Once activated, the FADH semiquinone then receives the last electron, forming $FADH_2$. It is in this reduced form, that O_2 is able to react with FAD and H_2O_2 is released. In PPOX this cycle would need to occur three times, resulting in the release of three H_2O_2 molecules.

Previous studies show that in most forms of PPOX O_2 is indeed the final electron acceptor, and the affinity for O_2 in both yeast and mouse has been determined to 0.5 - 1.5 and 125 μM, respectively (Ferreira & Dailey, 1988; Camadros *et al*., 1994). The study in mouse PPOX demonstrated that three moles of O_2 are consumed for every mole of substrate (Ferreira & Dailey, 1988), but, as mentioned, little is known of O_2's movement within PPOX.

University of Cape Town

Reactivity with Sulfite

Another property of flavoprotein oxidases is their ability to react with sulfite. As early as 1966, while studying glucose oxidase from *Aspergillus niger*, a reaction between flavoproteins and sulfite was discovered by Massey and colleagues (Massey *et al*., 1969). The reaction was shown to be independent of the presence of O_2 and was characterised by a reduced absorption spectrum. The term “bleached” was coined for this phenomenon whereby the visible absorption spectrum of the enzyme was similar to, but not identical with, that of a reduced flavoprotein spectrum. This equilibrium reaction was dependent on the concentration of the enzyme, sulfite, and on temperature and pH. Analysis of the spectroscopic shift brought to light the weak covalent interaction occurring at the FAD-N(5) of the isoalloxazine ring. This ability to reversibly bind sulfite and form an N(5) adduct has been used to determine oxidation-reduction potential of many proteins for example cholesterol oxidases (Gadda *et al*., 1997; Motteran *et al*., 2001). Interestingly, a few oxidases have been reported to not interact with sulfite (Massey *et al*., 1969; Edmondson *et al*., 2004).

University of Cape Town

Structural characterisation

Expression and purification properties

Recombinant mxPPOX has been expressed and characterized. Dailey and Dailey (1996a) found it to be a hydrophobic homodimer. Expression of the mxPPOX cloned into the His-Tag pTRC-His vector has been shown to be optimum at 30 °C. The hydrophobic nature of mxPPOX requires that the protein be purified in the presence of a detergent (Dailey and Dailey, 1996a). In mxPPOX, Tween 20 is considered effective as a detergent (Dailey & Dailey, 1996a). The expressed His-tagged hPPOX is readily purifiable by metal-affinity column chromatography (Talon resin). Purification at cold temperatures (4 °C) was reported to be more efficient compared to purification at room temperature (25 °C) (Maneli, 2002). In theory, one FAD binds per monomer and crystal structures of PPOX confirm this. However purified mxPPOX only binds approximately 0.5 per monomer; Dailey *et al*. suggested that flavin could be readily dissociated from the protein (Dailey & Dailey, 1996a), in keeping with the noncovalent nature of its

binding. Dissociation of FAD has been shown to affect the stability of protein, and purified mxPPOX tends to precipitate, even at 4 °C. However, the addition of commercial FAD to the purified protein has been shown to improve the stability the protein (Corradi *et al*., 2006). This suggests that the protein-ligand interaction in PPOX could also be playing a role in maintaining the integrity of the protein structure; similar ligand association is seen in ALAD (see chapter 1).

While mxPPOX has been shown to be a homodimer (Dailey and Daile 1996b), PPOXs from various species have been reported to exist as either a monomer or homodimer (Koch *et al*., 2004; Corradi *et al*., 2006; Qin *et al*., 2010; Qin *et al*., 2011). In keeping with the presence of an oxidized FAD, virtually all forms of purified PPOX proteins have a characteristic yellow colour. Reported size ranges from 50 - 57 000 Da (Camadros *et al*., 1994; Dailey & Dailey, 1996). mxPPOX is 51 kDa in size and is located on the cytosolic side of the inner mitochondrial membrane (Deybach *et al*., 1985; Dailey & Dailey, 1996).

University of Cape Town

Structural properties

At the commencement of this study (2007) the structure of human PPOX (hPPOX, 3NKS) had not been resolved, and has only more recently been resolved (Qin et al., 2011). Previously reported PPOX crystal structures are: *Nicotiana tabacum* (mtPPOX, 1SEZ), *Myxococcus xanthus* (mxPPOX, 2IVE), *Myxococcus xanthus* with inhibitor - acifluorfen (AF-mxPPOX, 2IVD), and *Bacillus subtilis* with AF (bsPPOX, 3I6D) (Koch *et al*., 2004; Corradi *et al*., 2006; Qin *et al*., 2010). The bsPPOX crystal structure confirmed the monomeric form of bsPPOX as reported Corrigall and colleagues (Corrigall *et al*., 1998; Qin *et al*., 2010). The mtPPOX structure also confirmed the dimeric form of mtPPOX as reported ealier (Lermontova *et al*., 1997; Koch *et al*., 2004).

In the case of hPPOX and mxPPOX previous protein studies based on size-exclusion column analysis and gel filtration respectively, showed these PPOXs to be homodimeric (Dailey & Dailey 1996a; Dailey & Dailey 1996b). However, the recently resolved structures showed that the crystal forms resolved appeared monomeric (Corradi et al., 2006; Qin *et al*., 2011). Of the bacterial forms studied to date, that of *M. xanthus* appears most similar to the human form (Dailey & Dailey, 1996b; Qin et al., 2011). It is approximately 51 000 Da, membrane bound and is also well inhibited by the diphenyl

ether herbicide, acifluorfen. In addition, it is easily purified in large amounts in an expressed recombinant form (Dailey & Dailey, 1996a; Dailey & Dailey 1996b).

The resolved structures reveal that PPOX comprises of three binding regions viz. a membrane, a substrate and an FAD binding region. A hydrophobic active site cavity is found at the interface of the FAD and substrate binding region (Corradi *et al*., 2006). Secondary structure analysis reveals the membrane region to consist mainly of helical structures; the substrate to be predominantly beta-sheet while the FAD binding region is a mixture of alpha-helices and beta-sheets (Corradi *et al*., 2006).
A detailed review of the binding region of protogen in mxPPOX has been reported (Koch *et al*., 2004; Corradi *et al*., 2006). An interesting feature about the FAD and substrate binding region in mxPPOX, is the Asn-63 residue. This polar neutral residue is involved in a complex multiple hydrogen bonding network, with H-bonded residues found in both substrate and FAD binding region. This network of interactions has been hypothesized to maintain the integrity of both substrate and FAD binding regions in mxPPOX (Corradi *et al*., 2006). It is therefore tempting to speculate that this residue could facilitate "communication" between the two regions, as seen in ALAS-PLP interaction.

University of Cape Town

The PPOX FAD conserved binding sequence

Using sequence alignment analysis, Dailey and Dailey (1998) identified a group of enzymes that share a conserved FAD-binding domain. These proteins favour noncovalent binding of FAD and are membrane associated. PPOX together with monoamine oxidase (MAO) were among the proteins classified in this superfamily (Dailey & Dailey, 1998). Proteins from this family possess a dinucleotide binding motif (50-residue long) near the amino terminus which commences with the well known GlyXGlyXXGly consensus (where Gly denotes glycine and X denotes any amino acid). The identified consensus sequence for the PPOX superfamily is:
$U_4G(G/A)GUXGL(X_2)(A/S)(X_2)L(X_{6\text{-}12})UX(L/V)UE(X_4)UGG(X_{9\text{-}13})(G/V)(X_3)(D/E)XG$
where X denotes any residue and U any hydrophobic residue (Dailey & Dailey, 1998). This consensus sequence has been described to consist of beta-sheet1-alpha-helix-beta-sheet2 referred to as the Rossman fold; a structural fold responsible for the binding of the adenine moiety of FAD (Bottoms *et al*., 2002). In mxPPOX, the protein of interest in this study, the consensus sequence reads:
VAVVGGGISGLAVAHHLRSRGTDAVLLESSARLGGAVGTHALAGYLVEQG

where underlined residues represent the conserved residues of the consensus and residues not underlined represent X (which, as mentioned previously, denotes any residue).

Across different proteins and species the motif seems to have a low sequence homology, but structural homology is preserved. Two regions of the motif are commonly found interacting directly with FAD in flavoproteins. The first is the common GlyXGlyXXGly region which forms part of a loop. The second is the side chain of a glutamate interacting with the ribose group. Several water molecules have also been identified near the FAD and Rossmann fold with some water mediated interactions being conserved (Bottoms *et al*., 2002).

FAD binding features

The FAD binding region consists of both alpha-helices and beta-sheets. FAD appears to be involved in numerous noncovalent interactions with the surrounding protein through both backbone and side chain interactions. These interactions are considered to securely stabilize and position the flavin in a favourable orientation for catalysis. Structures of PPOX reveal a conserved FAD interaction with protein.

The schematic view of the FAD binding region in mxPPOX (fig. 2.7) shows the binding region – highlighting both hydrophobic and hydrogen bond interactions, either via the side chains or backbone bonds. Side chains are considered more flexible than backbone atoms, therefore interactions with side chain is most likely to allow flexibility in that region (Petsko & Ringe, 2004). The following details the binding region of FAD in mxPPOX (Corradi *et al*., 2006).

University of Cape Town

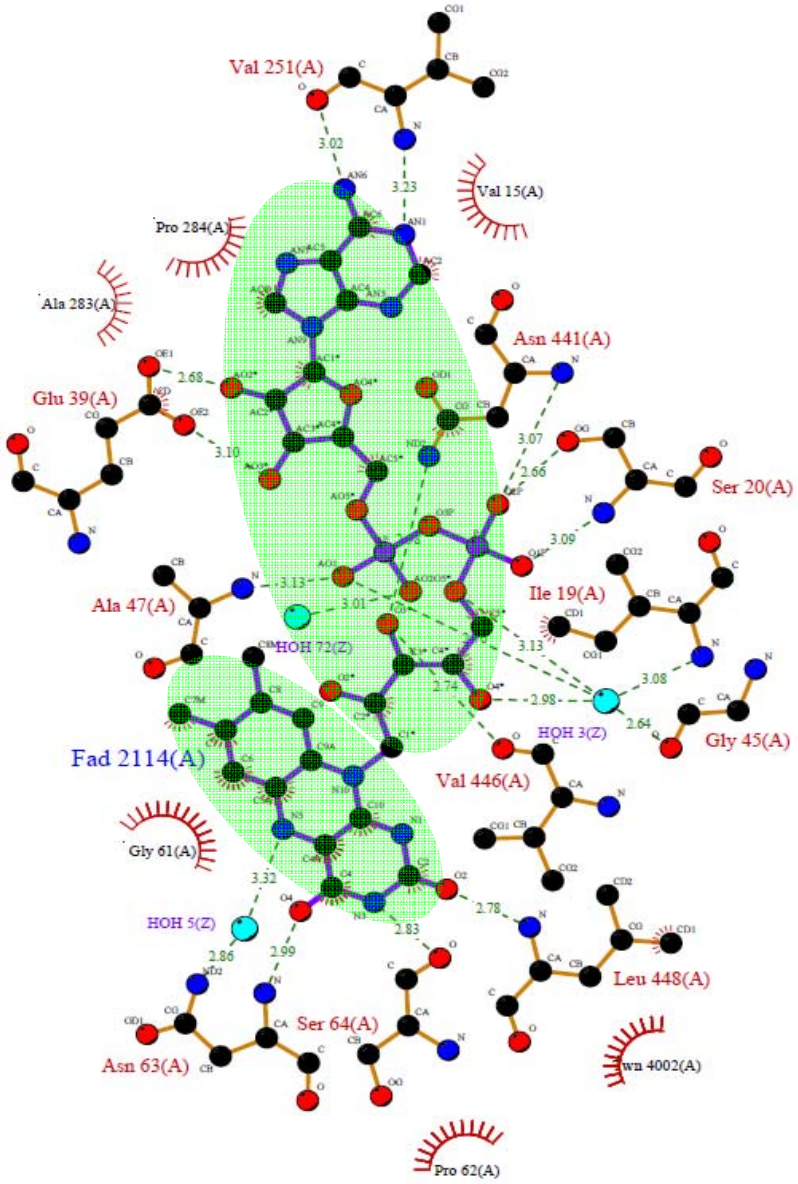

Figure 2.7: Self-constructed LigPLot, representation of the FAD (highlighted in green), binding site in subunit A of mxPPOX (PDB: 2IVE) (Corradi *et al*., 2006). Black = carbon; blue = nitrogen; red = oxygen; purple = phosphate; Cyan = water molecule. Polar interactions are shown as dotted lines and hydrophobic interactions are shown as “eye-lashes”.

Binding features of FAD in mxPPOX (refer to fig. 2.7):

ADP consists of an adenine linked to a ribose linked to two phosphates

a. The backbone COOH and NH group of Val-251 forms a hydrogen bond with the N6 and N1 atoms of the adenine ring respectively. This residue's interaction is reported to stabilize the cofactor binding in other non-related oxidases (Binda *et al*., 1999; Dym *et al*., 2001; Edmondson *et al*., 2004).

b. The following residues: Val-15, Pro-284 and Ala-283, interact hydrophobically with the adenine moiety; further stabilizing the binding of FAD.

c. The side chain of Glu-39 forms two hydrogen interactions with the oxygen groups of the *ribose*. This residue forms part of the 50 residue long conserved FAD binding motif and Glu-39 is equivalent to the glutamate residue that is often seen interacting with the adenine group of FAD.

Phosphate groups and ribityl chain

Interactions between the phosphate and the proteins are conserved and considered vital in stabilizing the cofactor.

d. The backbone of Asn-441 forms a hydrogen bond with the phosphate group.

e. A water molecule near the phosphates (HOH3) has five hydrogen bond interactions. It is securely positioned by Gly-45 and Ile-19; allowing for two water mediated interaction with phosphate and one interaction with the ribityl chain.

f. HOH7 interacts with the phosphate–O2 and the backbone of Ala-47 interacts with phosphate both through hydrogen bond interactions

g. The negative charge of the phosphates may interact with positively charged amino acids, amide protons of the protein main chain or α-helix dipole.

h. Val-446 (backbone), Asn-441 (side chain) and as mentioned, neighbouring water molecule (HOH3), interacts with the ribityl chain through hydrogen bond interactions.

i. Ser-20 forms two hydrogen bond interactions with the ribityl chain with both its backbone and side chain.

Isoalloxazine ring

The literature reveals that this part of the ring (O2, N3 and O4) interacts mainly with the backbone of amino acids (Fraaije & Mattevi, 2000). In mxPPOX the:

j. Leu-448 backbone nitrogen group forms a hydrogen bond with the O2.

k. Ser-64 backbone carbonyl group forms a hydrogen bond interaction with N3.

l. Asn-63 backbone nitrogen group hydrogen bonds with the O4. This residue is also involved in a water mediated interaction with N(5). An interaction that seems positioned to perform the nucleophilic attack on substrate (Yin *et al*., 2001).

University of Cape Town

m. Pro-62 hydrophobic interacts with the (hydrophilic part of the isoalloxazine) and is speculated to stabilize FAD (Qin *et al*., 2010).

n. Gly-61 hydrophobic interacts with the hydrophobic section of the isoalloxazine.

In the mxPPOX structure with bound inhibitor acifluorfen, an interesting conformational change occurs such that more water molecules are occupied in the FAD binding region; instead of three water molecules, a total of nine H_2O molecules are occupied and a potentially tighter network is formed between protein and FAD (fig. 2.8).

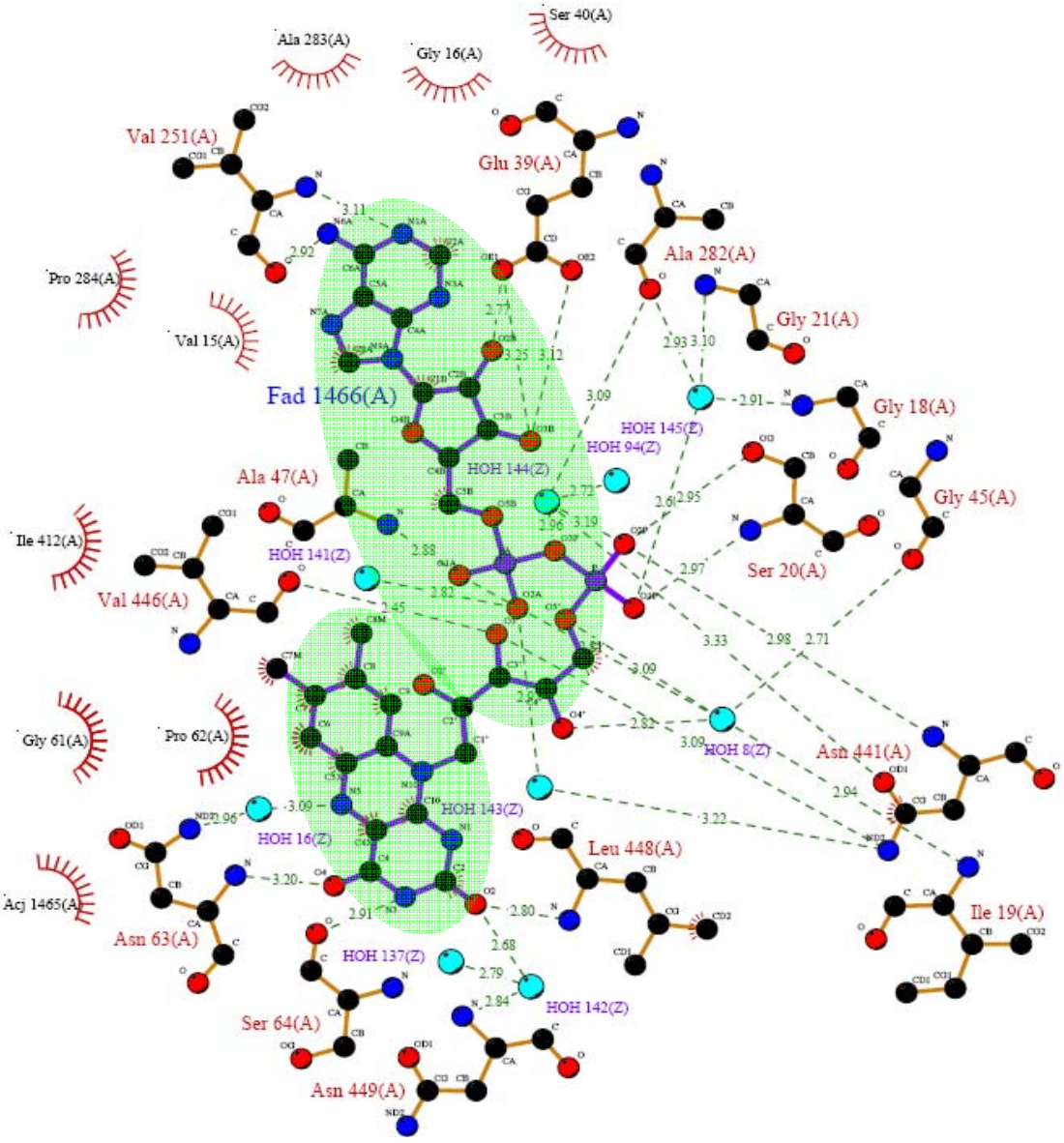

Figure 2.8: Self-constructed LigPlot representation of the FAD (highlighted in green), binding site in an occupied active site, subunit A of mxPPOX with an occupied active site (acifluorfen; PDB: 2IVD) (Corradi *et al*., 2006). Black = carbon; blue = nitrogen; red = oxygen; purple = phosphate; Cyan = water molecule. Polar interactions are shown as dotted lines and hydrophobic interactions are shown as “eye-lashes”.

FAD binding in other PPOX structures

mtPPOX

In plant PPOX two forms of PPOX proteins are found. One located in chloroplast and the other, is found in the mitochondria (mtPPOX). mtPPOX was the first PPOX structure to be resolved (Koch *et al*., 2004). Similar to mxPPOX, mtPPOX makes various interactions with its cofactor, FAD (fig. 2.9). The N-3 of the isoalloxazine ring forms a hydrogen bond with the backbone of threonine (Thr-68). The N(5) of the isoalloxazine ring is not seen forming any hydrogen bond interactions with a nearby water molecule as seen in mxPPOX. Further analysis of Asn-67 (equivalent to the Asn-63 of mxPPOX, which makes a water mediated interaction with the N(5)), shows that its side chain required for positioning the water molecule in front of the N(5) is orientated away from the FAD. In contrast, the Asn-63 side chain in mxPPOX is orientated towards the isoalloxazine ring. Therefore, in mtPPOX, Asn-67 does not appear on the FAD-ligand interaction plot (fig. 2.9). The FAD isoalloxazine ring also makes another hydrogen interaction via its O2 with the backbone of Val-475. Other interactions with the isoalloxazine ring include hydrophobic interactions with Ala-66, Gly-65, Phe-439, Ala-438 and Trp-435 (equivalent to Trp-408 of mxPPOX). The ribityl chain linked to the isoalloxazine ring is stabilized through a water molecule involved in a complex hydrogen bond network with the backbones of Val-23, Lys-51. This water molecule further stabilizes the phosphate groups via two hydrogen bond interactions. Ser-24 (equivalent to mxPPOX Ser-20) and Lys-51 make further interactions with the FAD phosphate group. Glu-43 (equivalent to Glu-39 mxPPOX) stabilizes the ribose ring together with a water molecule. The adenine group is stabilized by hydrophobic (Ala-304, Ile-19, Ala-44) as well as hydrogen bond interactions (Val-264 - equivalent to Val-251 of mxPPOX). The interactions of FAD with protein in PPOX are summarized in the table 2.1.

University of Cape Town

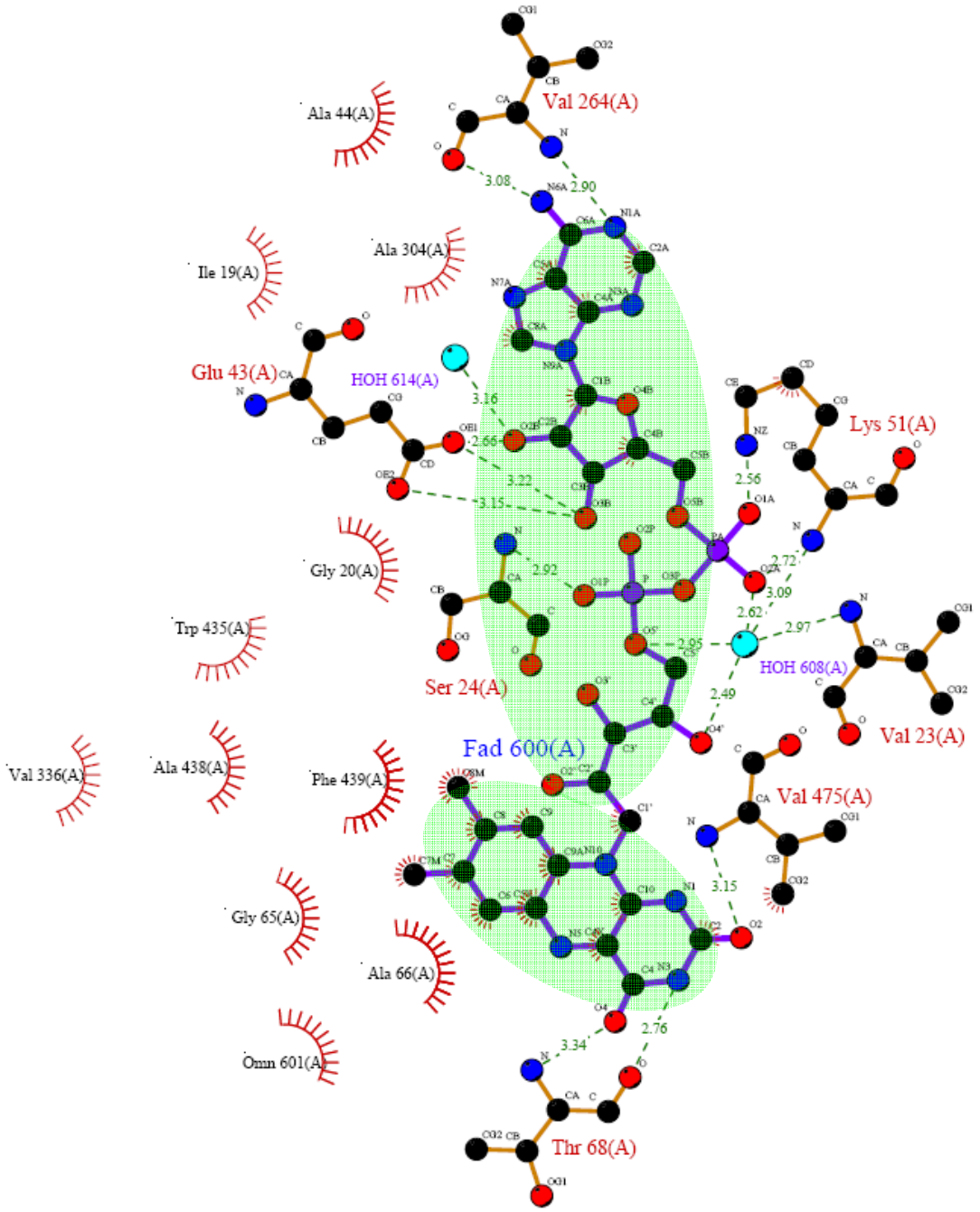

Figure 2.9: Self-constructed LigPlot representation of the FAD binding site in subunit A of mtPPOX (PDB:1SEZ). Black = carbon; blue = nitrogen; red = oxygen; purple = phosphate; Cyan = water molecule. Polar interactions are shown as dotted lines and hydrophobic interactions are shown as “eye-lashes”.

bsPPOX

bsPPOX differs from PPOXs that have been characterized to date. Firstly it is a soluble monomer, and secondly, it is able to oxidize CPO to coproporphyrin III with some efficiency. It is only weakly inhibited by acifluorfen compared to human, plant and *M. xanthus*. The bsPPOX structure reveals that FAD is noncovalently bound to the protein in the FAD binding region as seen in other PPOX structures. However, unlike the mxPPOX-AF structure, the AF in bsPPOX is positioned parallel to the FAD isoalloxazine ring, participating in the so-called aromatic-aromatic interaction with the isoalloxazine ring of FAD. The 2-D representation of the FAD-protein interaction revealed bsPPOX binds FAD without the aid of water molecules which is seen in mxPPOX, mxPPOX-AF, mtPPOX and hPPOX structures (see table 2.1). This structure, although having an occupied active site, has no water molecules participating the binding of FAD to the FAD binding site of the protein (fig. 2.10). Besides these differences the adenine ring of the FAD is seen interacting with a valine (Val-256), while the ribose interacts with a glutamate (Glu-41) as is seen in mxPPOX structure. A threonine (Thr-16) makes a side chain polar interaction with the phosphate group; the nonpolar ring of the isoalloxazine interacts with as tryptophan residue (Trp-409) and lastly an aspartate (Asp-65) interacts with the polar ring of the FAD isoalloxazine ring.

University of Cape Town

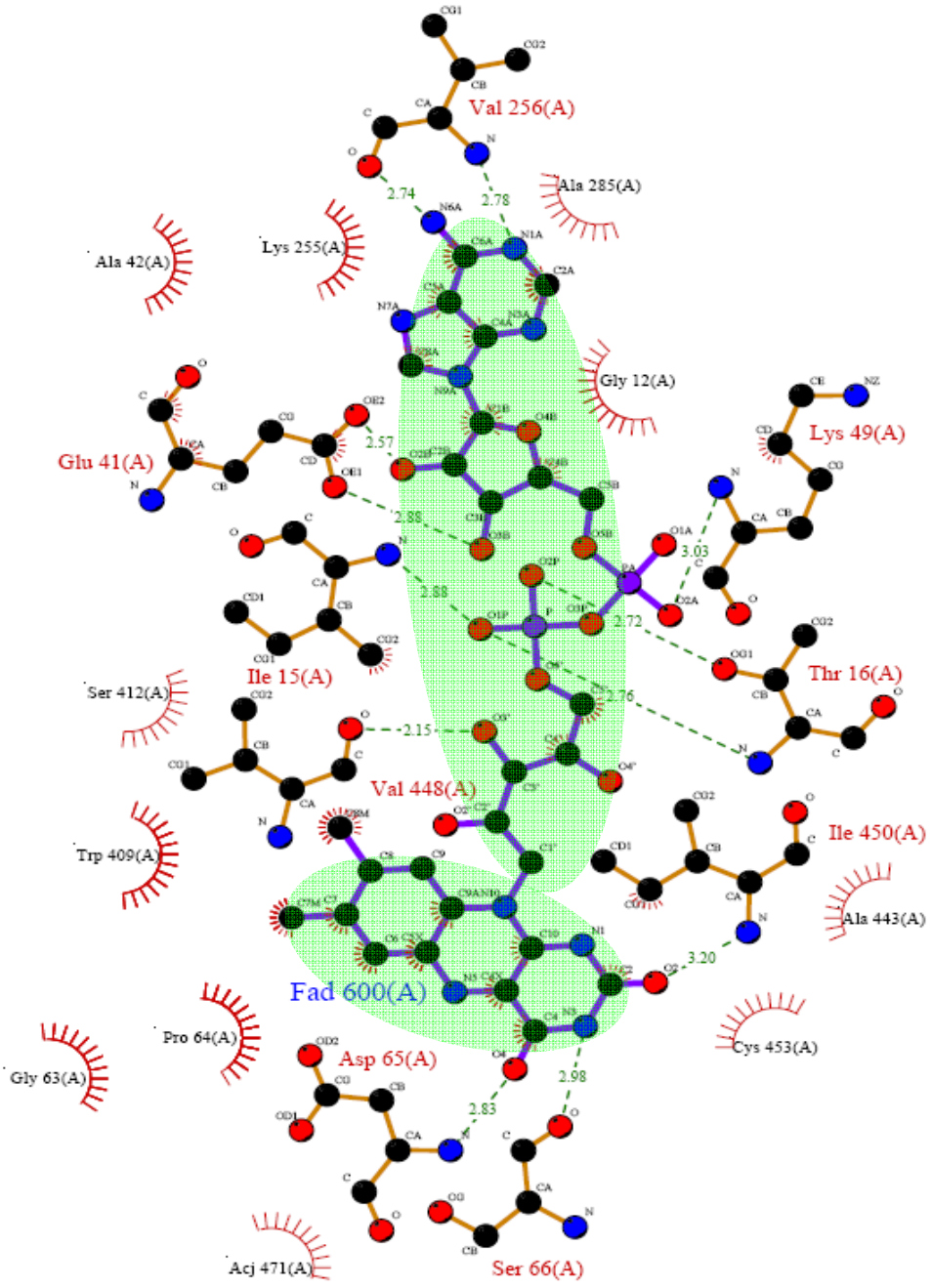

Figure 2.10: Self-constructed LigPlot representation of bsPPOX FAD (highlighted in green) binding region in subunit A. Black = carbon; blue = nitrogen; red = oxygen; purple = phosphate Acj = acifluorfen (AF). Polar interactions are shown as dotted lines and hydrophobic interactions are shown as"eye-lashes".

hPPOX

The recently resolved structure of hPPOX has enabled insight into its structure-function properties. Firstly, although *in vitro* experiments showed this protein to be a homodimer, the resolved structure reveals the hPPOX is a monomer. Secondly, compared to PPOX proteins with resolved structure, hPPOX has an excessive amount of water molecules (42 total) interacting with the FAD to allow for a "secure" fit (fig. 2.11). Among these water molecules is the conserved water mediated interaction seen at FAD-N(5) with Arg-59 (equivalent Asn-63, mxPPOX). Unlike mxPPOX, the ribose of hPPOX is not only stabilized by a glutamate (Glu-34) but a polar interaction with a serine residue (Ser-35) is also seen. Another interesting interaction is the network of nine water molecules that are orderly placed to position Gly-41 which has a water mediated interaction with the ribose. It is tempting to state that water molecules play a vital part in the FAD-hPPOX interaction. As in mxPPOX, mtPPOX and bsPPOX, a valine is seen interacting with the adenine ring of FAD. A glutamate (Glu-34), a serine (Ser-35) and as mentioned a network of water molecules interact with the ribose ring. A tryptophan (Trp-42) is seen near the nonpolar ring of FAD while an arginine (Arg-59) via a water molecule interacts with the FAD-N(5).

University of Cape Town

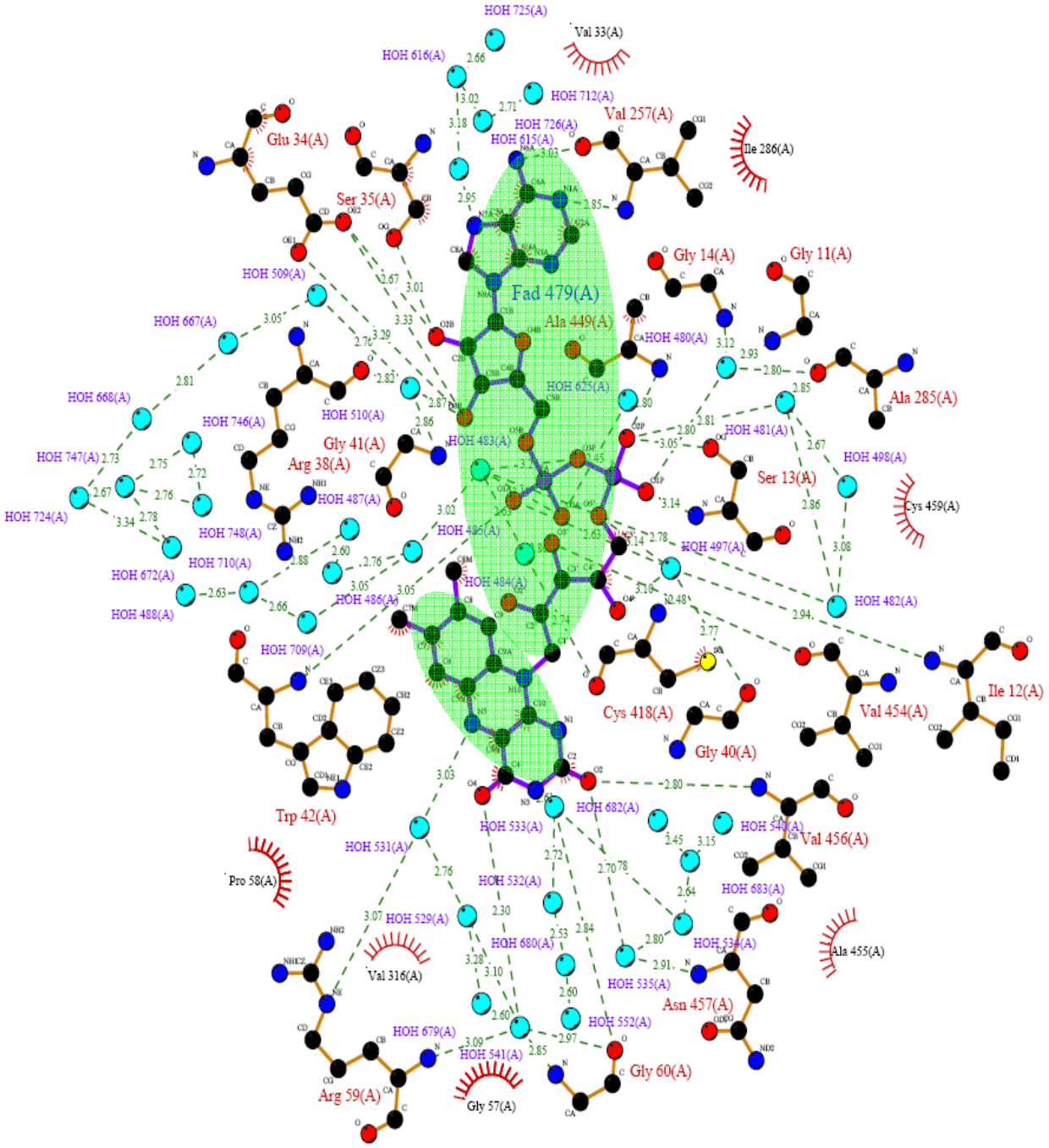

Figure 2.11: Self-constructed LigPlot image of the FAD (highlighted in green) binding region in hPPOX, subunit A. Black = carbon; blue = nitrogen; red = oxygen; purple = phosphate; yellow = sulphur. Polar interactions are shown as dotted lines and hydrophobic interactions are shown as "eye-lashes".

Table 2.1: A summary of FAD - protein interactions in PPOX structures obtained from LigPlots. In the case of mxPPOX and mtPPOX subunit A was analyzed.

	mxPPOX	**mxPPOX-AF**	**mtPPOX**	**bsPPOX**	**hPPOX**
Crystal structure resolution	2.70 Å	2.30 Å	2.90 Å	2.90 Å	1.90 Å
FAD					
Triple ring					
O4	Asn-63	Asn-63	Thr-68	Asp-65	Gly-60 Arg-59 HOH
N3	Ser-64	Ser-64	Thr-68	Ser-66	HOH Gly-60
O2	Leu-448	Leu-448 Asn-449	Val-475	Ile-450	Val-456 HOH
N5	HOH Asn-63	HOH Asn-63	N/A	N/A	Arg-59 Gly-60 HOH
C5-C9	Gly-61	Gly-61 Pro-62	Ala-66 Gly-65 Phe-439 Trp-435	Trp-409 Pro-64 Gly-63	Trp-42
Ribityl chain	Val-446 Asn-441	Val-446 Asn-441	HOH	Val-448	Val-454 HOH
Phosphate group 1	Ser-20	Ser-20	Ser-24	Thr-16 Ile-15	Ala-449 Gly-14 Ala-285 Gly-11 Ser-13 Ile-12 HOH
Phosphate group 2	HOH Ala-47 Asn-441	HOH Ala-47 Asn-441	Lys-551	Lys-49	Trp-42 HOH
Ribose ring	Glu-39	Glu-39	Glu-43	Glu-41	Glu-34 Arg-38 HOH
Adenine moiety	Val-251	Val-251	Val-264	Val-256	Val-257 HOH
Total water per monomer	3	9	2	N/A	42

University of Cape Town

The role of water molecules in FAD binding

Water molecules play several roles in protein binding region. Water molecules have been reported to link the phosphate (or pyrophosphate) group of FAD to the GlyXGlyXXGly loop of the protein (Bottoms *et al*., 2002). The linkage is stereospecific with the stereochemically distinct oxygen molecules of the pyrophosphate. This conserved water molecule makes four hydrogen interactions with either the first or second conserved glycine, the last conserved glycine, a C-terminal of a beta-sheet and the OP1 of the pyrophosphate (fig. 2.12). It has been suggested that this water molecule may be required for dinucleotide recognition – by helping maintain the conformation of the glycine-rich loop during FAD binding (Bottoms *et al*., 2002).

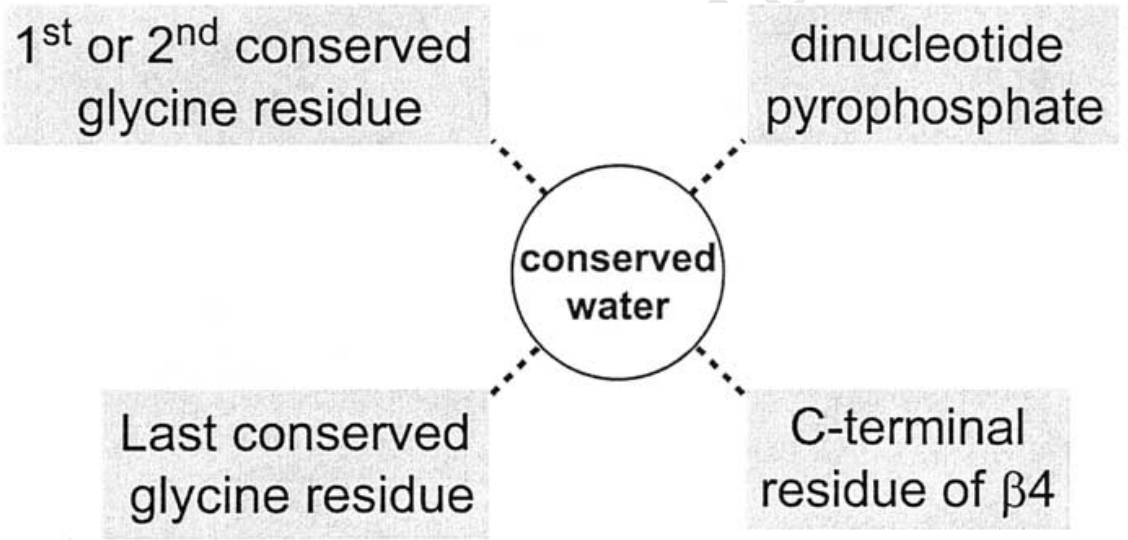

Figure 2.12: Schematic hydrogen bond pattern of conserved water molecule's interaction with the phosphate group of FAD. Dotted line denotes hydrogen bonds (Bottoms *et al*., 2002).

In mxPPOX, as well as human, a similar stereochemical water interaction is seen in the occupied active site structure, mxPPOX-AF. Water molecule, HOH-145, makes hydrogen bond interactions with the second conserved glycine (Gly-18), the last glycine residue (Gly-20), Ala-282 and the OP1 of FAD (fig. 2.13a). This interaction is neither seen in the mxPPOX (structure without acifluorfen), nor in the mtPPOX. Both structures have unoccupied active sites; which suggests some structural manoeuvring occurs upon substrate binding requiring the optimum FAD phosphate-protein association. Other water molecules may aid in maintaining the extended conformation the FAD. A

similar interaction is seen in hPPOX with the conserved water molecule HOH480 (fig. 2.13b).

Another recurrent characteristic of FAD binding is seen at the FAD-N(5). This section of the FAD is normally located within hydrogen bond distance from a hydrogen-bond donor. Both mxPPOX and hPPOX structures have a water molecule interacting at the FAD-N(5). This has also been reported in MAO and PAO (Binda *et al*., 1999). As mentioned earlier the presence of a hydrogen bond increases the oxidative power of FAD.

University of Cape Town

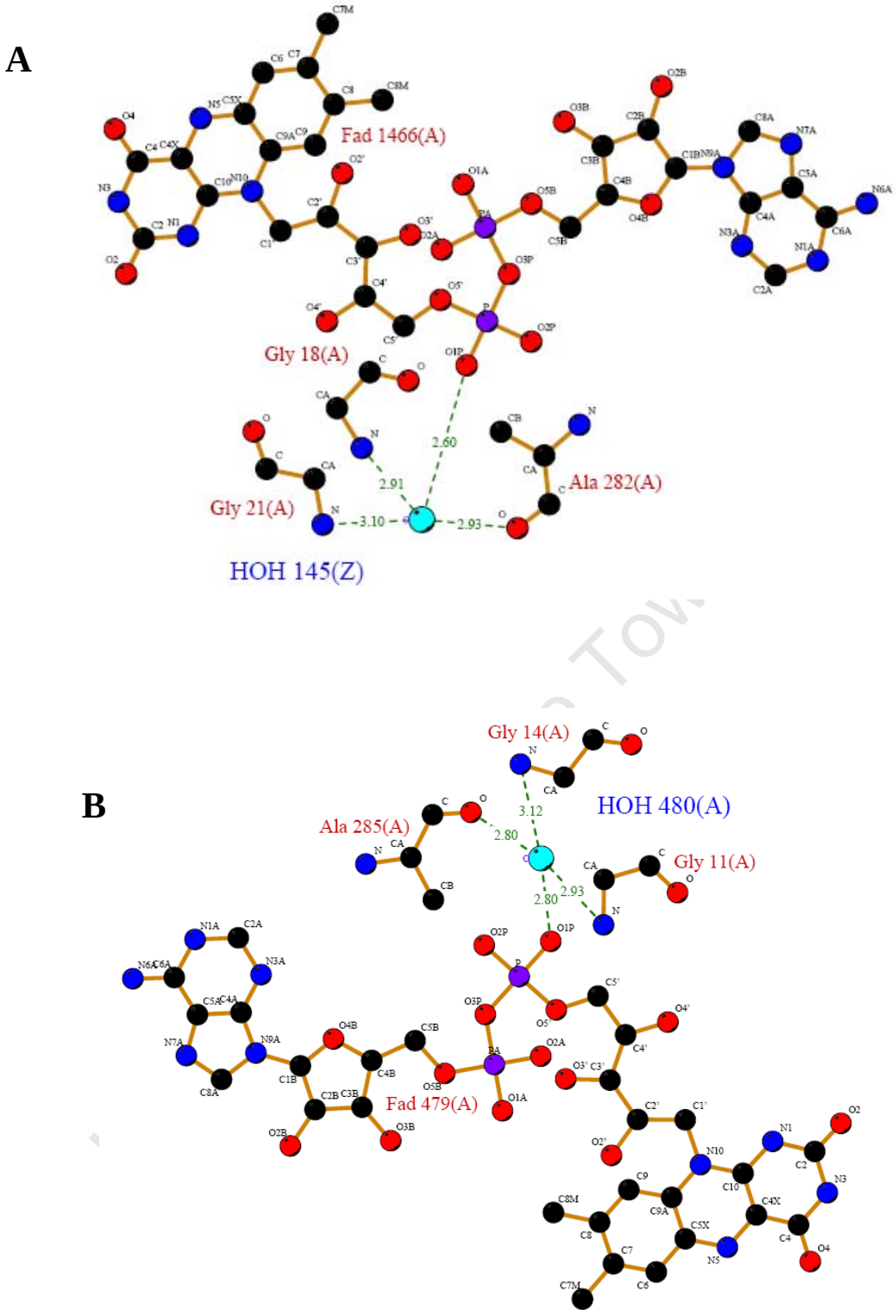

Figure 2.13: Self-constructed LigPlot of the hydrogen bonding pattern of conserved water molecules in PPOX. A) A schematic view of the stereochemical hydrogen bond interaction of the structurally conserved water molecule (HOH145) with conserved residues (Gly-18 and Gly-21) in mxPPOX-AF (PDF: 2IVD). B) A schematic view of the stereochemical hydrogen bond interaction of the structurally conserved water molecule (HOH480) in hPPOX (PDF: 3NKS). Black = carbon; blue = nitrogen; red = oxygen; purple = phosphate; cyan = water molecule. Polar interactions are shown as dotted lines.

Structure function studies

The dominantly inherited disorder, variegate porphyria, results from impaired PPOX activity as a consequence of an amino acid residue exchange. To date well over 100 mutations (mis-sense) have been reported in the human *PPOX* gene as disease causing (Qin *et al*., 2011).

Arginine 59

In 95 % of the VP cases reported in South Africa, Arg-59 is mutated to tryptophan (Meissner *et al*., 1996). Structure function studies have been reported which characterise this mutation in both human and plants (Maneli *et al.,* 2003; Heinemann *et al*., 2007). The corresponding residue to human Arg-59 in mtPPOX and mxPPOX is Asn-67 and Asn-63, respectively (Koch *et al*., 2004; Corradi *et al*., 2006). In mtPPOX, it is positioned on a long loop between the FAD binding and substrate binding sites. Asparagine was mutated to an arginine (human equivalent) which is the replacement of a neutral polar for a positively charged polar residue. It was also mutated to a tryptophan (an aromatic nonpolar), mimicking the naturally occurring Arg59Trp mutation. Both arginine and tryptophan are bulkier than asparagine. The Asn67Arg mutant bound FAD poorly and as a result the overall catalytic efficacy of the enzyme was affected. In the Asn67Trp mutant no activity was detected. Both asparagine mutants bound FAD, although it is not possible to ascertain if the FAD cofactor orientation was affected by these mutants as no FAD UV/VIS spectra were reported for this study (Heinemann *et al*., 2007). In studies on human PPOX it was found that a positive polar residue is favoured in the Arg-59 position. Mutation of this group to an aromatic polar tryptophan resulted in a mutant which bound FAD poorly. The UV/VIS spectra also showed an altered 450 nm spectral shift. Thus both the binding and orientation of the FAD were affected in this mutant (Maneli *et al*., 2003).

GlyXGlyXXGly

Previous studies have been carried out to investigate the importance of the GlyXGlyXXGly in PPOX (Dym *et al*., 1995). In our lab the first, second and the third conserved glycine residues were mutated to an alanine (Maneli *et al*., 2003). The

University of Cape Town

alteration of the first and second glycine residue resulted in the protein's inability to bind FAD. The alteration of the third glycine to an alanine had a less drastic effect. FAD binding was not retarded and the enzyme maintained 42 % of wild type activity. These results show that in the nucleotide binding motif the first two glycine residues are involved in the binding of FAD. Therefore it is tempting to conclude that this region may be required for the initial binding of FAD to the protein, while the remaining interactions are to stabilize and aid in the redox reaction.

VP mutations

A more recently published paper of the human PPOX structure analysed the effect of mutations on PPOX (Qin *et al*., 2011). This paper demonstrated that mutations close to the FAD binding region affects FAD binding or orientation. Residues analysed include Gly11Asp and Gly11Ser, whereby bulky replacements led to restricted conformational movements as well as electrostatic friction between the negative pyrophosphates and negative aspartate replacement. Also note that this residue is involved in the stereochemical interaction with the conserved water molecule, and bulky replacement could possibly alter the positioning of the conserved water molecules (HOH480), fig. 2.13b. Other mutations that affect FAD binding include His20Pro, Gly40Glu, Gly40Ala, Gly232Arg, Gly232Ser, Asp349Ala, Ser350Pro, Gly448Arg, Ser450Pro, Gly453Val and Gly453Arg.

Glu34Val is located in a loop and is said to coordinate the 2-OH and 3-OH groups of the adenosine moiety of the FAD molecule. The hydrophobic replacement led to a severely reduced FAD binding. Lastly, in the Arg59Trp mutation the aromatic, nonpolar replacement causes electrostatic conflict, thereby weakening FAD-protein interaction.

Flavin binding studies in Monoamine oxidase

Study of the FAD-superfamily classified PPOX with MAO (Dailey & Dailey, 1998). MAO catalyzes the oxidative deamination of amines (Edmonson *et al*., 2004). With regards to FAD, MAO and PPOX share conserved residues showing a conserved binding mechanism. In MAO, however, FAD is bound covalently as opposed to the noncovalent binding of FAD in PPOX (Zhou *et al*., 1998).

University of Cape Town

A study to characterize the binding region of FAD in MAO showed that there are various residues that act as ligands in the binding of FAD to protein. A conserved glutamate (mxPPOX, Glu-39) interacts with the hydroxyl group of the ribose moiety of FAD is a good example of residues that act as ligands in FAD binding. Mutation of this glutamate (Glu-34) to an alanine (neutral, nonpolar); aspartate (negative, polar) or glutamine (neutral, polar) resulted in a protein that bound FAD weakly. Therefore in the binding of FAD in MAO, Glu-34 plays a vital role (as a ligand; Zhou *et al*., 1998).

Based on these structural and functional analyses of these proteins in the haem biosynthetic pathway, it is clear that cofactors play a unique and vital role in enzyme activity. Focusing on PPOX, the role of FAD, particularly binding properties that allow for movement and orientation, requires further investigation. Ultimately, further understanding of these interactions may elucidate the precise catalytic mechanism(s) of PPOX. It is hoped that the understanding of PPOX at structural and/or chemical level will shed light on the defects in VP cases. Partial characterisation of potential FAD-PPOX interactions forms the basis of this MSc project, and is developed further in the following chapters.

University of Cape Town

CHAPTER 3

Development of this thesis

University of Cape Town

Introduction

As detailed in chapter 1, partial defects in all eight enzymes of the haem biosynthetic pathway lead to the porphyrias, a group of genetically inherited metabolic disorders. In PPOX, the penultimate enzyme in this pathway, and the enzyme of interest in this study, partial defects lead to VP. A high incidence of VP is seen in South Africa due to founder effect (Arg59Trp) (refer to chapter 2). Consequently, many of the studies undertaken in the Lennox Eales Porphyria Laboratories, both in the past and presently, focus on this disease and PPOX.

Defects in this enzyme result in reduced enzyme activity, leading to the characteristic accumulation of haem precursors as well as porphyrin(ogen)s responsible for VP (Meissner *et al*., 1996; Maneli *et al*., 2003). In some cases, reduced enzyme activity has been attributed to inferior or reduced protein-FAD interaction (Meissner *et al*., 1996; Morgan *et al*., 2002; Maneli *et al*., 2003; Heinemann *et al*., 2007).

At the commencement of this study in 2007, the structure of the hPPOX had not yet been resolved. However, that of mxPPOX had been resolved through collaborative efforts between our laboratory and researchers from the University of Bath (Corradi *et al*., 2006). Of the bacterial forms studied to date, mxPPOX resembles the hPPOX most closely, being membrane bound and sensitive to acifluorfen inhibition (Dailey & Dailey, 1996a & b). Furthermore, a good expressing mxPPOX plasmid (pMx-PPOX) was available in our laboratory, (kindly donated by Prof H. Dailey (University of Georgia, Georgia, USA)). It was therefore decided to investigate and better characterise FAD binding in mxPPOX.

University of Cape Town

Previous studies on PPOX and FAD

Sequence alignment, together with available PPOX crystal structure studies, revealed that the conserved FAD binding properties in flavoproteins in general, were also conserved in PPOX (Dailey & Dailey, 1998; Dym *et al*., 2001; Koch *et al*., 2004; Corradi *et al*., 2006; Qin *et al*., 2010; Qin *et al*., 2011).

mxPPOX protein has been partially characterised by Dailey and Dailey (1996a). They expressed and purified mxPPOX, reported FAD stoichiometry and further analysed mxPPOX activity. While FAD stoichiometry is often reported in PPOX proteins, detailed

FAD binding properties such as FAD spectral analysis are not consistently reported. Furthermore, sulfite FAD-N5 reactivity is considered a characteristic of some flavoprotein oxidases; although reported in other flavoproteins, such studies are lacking for PPOX.

There are some earlier reports on naturally occurring VP mutations which have shed some light on the binding properties of FAD in PPOX (chapter 2) (Morgan *et al*., 2002; Maneli *et al*., 2003; Heinemann *et al*., 2007; Qin *et al*., 2010). Several of these mutants have been engineered and reported to affect FAD (binding and/or change in orientation; Meissner *et al*., 1996; Maneli *et al*., 2003). Earlier work from our laboratory, examined the three glycine residues in the GlyXGlyXXGly FAD binding motif in hPPOX (Maneli *et al*., 2003). It appears that these residues are critical for FAD binding as their mutation in hPPOX resulted in inferior FAD binding; the mutants Gly9Ala and Gly11Ala bound no FAD, whereas Gly14Ala bound FAD poorly (Maneli *et al*., 2003). Studies such as these revealed that PPOX, like other enzymes with a characterised cofactor binding region (as discussed in chapter 2), could have a “sensitive”, co-ordinated interaction with FAD.

All PPOX structures to date clearly show the presence of the FAD cofactor. The recent publication of the hPPOX crystal structure, which includes study of various mutants, reports on several mutations affecting FAD binding in the human *PPOX* gene (Qin *et al*., 2011). One of these is Glu-34. When Glu-34 (equivalent to mxPPOX Glu-39) was mutated to a valine, a hydrophobic neutral residue, the polar interactions of glutamate with the ribose group of FAD were abolished, resulting in weak or compromised FAD interaction in the mutant (Qin *et al*., 2011). This study lends weight to and justifies our decision to study the mxPPOX Glu-39 residue (see below).

University of Cape Town

This Study

In light of the above, we deemed it important to focus this study on PPOX-FAD interaction. We analyzed the FAD binding site in mxPPOX using available structural information in PPOX and non-related proteins such as MAO and PAO. Furthermore, this study utilised insight from previous studies in PPOX, where mutagenesis was employed to characterise potentially vital residues (Koch *et al*., 2004; Corradi *et al*., 2006; Heinemann *et al*., 2007). Lastly, this study drew from previous studies of flavins in flavoproteins in general, in order to shed light on the binding of FAD in mxPPOX. We used several other flavoprotein studies to inform and serve as guidelines and references for this study (Massey *et al*., 1969; Massey & Hemmerich, 1980; Ghisla & Massey, 1986; Ghisla & Massey,1989; Massey, 1994; Mattevi *et al*., 1997; Dailey & Dailey, 1998; Zhou, *et al*., 1998; Sampson, 2001; Ma & Ito, 2002; Edmondson *et al*., 2004; Basran *et al*., 2006; Piubelli *et al*., 2008; Senda *et al*., 2009).

The structures of PPOX reveal a significant level of complexity around FAD positioning and binding in PPOX. This is presented and detailed in chapter 4. In mxPPOX, three residues are seen to interact with FAD via their side chains namely Ser-20, Glu-39, Asn-441. Hence, this study assessed the roles of these residues in FAD binding. We also investigated Trp-408, based on previous reports of a conserved tryptophan aromatic interaction with FAD in flavoproteins. Specifically, we assessed the importance of polarity in the Ser-20 position; of polarity, size and charge in the Glu-39 position; of polarity in the position occupied by Asn-441, and finally Trp-408 was mutated to assess the role of the aromatic ring in this position.

Chapter 5 describes the site-directed mutagenesis employed to generate a series of 10 mutants from the selected four residues. Thereafter, mutant proteins were expressed and purified to allow further characterisation.

Chapter 6 further characterises the FAD-PPOX interaction by determining the UV-VIS spectral properties of FAD in both mutants and wild type mxPPOX.

In chapter 7 some key kinetic parameters of mutant PPOXs were determined and compared to those of wild type PPOX. Structural integrity of these proteins (wild type and mutants) was also analysed by measuring the T½.

University of Cape Town

In chapter 8 PPOX reactivity with sulfite in both mxPPOX and hPPOX was assessed as reactivity with sulfite is a common characteristic of flavoproteins, yet appears not to have been documented in PPOX. Furthermore, the oxygen consumption in mxPPOX was assessed and related to protogen conversion.

Finally, in chapter 9 a cohesive overview is presented and conclusions drawn. In addition, possible future studies are suggested.

University of Cape Town

Primary Aim

To characterise the FAD binding region in mxPPOX.

Secondary aims:

- To visualize FAD-PPOX interactions in order to identify amino acid residues important for FAD binding.
- To engineer, express and purify a selection of mutant PPOXs to allow for the study of FAD binding in PPOX.
- To characterise the FAD-PPOX interaction through analysis of the UV-VIS spectral properties of FAD in both mutants and wild type mxPPOX.
- To assay the kinetic parameters of mxPPOX mutants and compare them to wild type mxPPOX and each other, in order to better interpret their importance in FAD binding.
- To determine the reactivity (or lack thereof) of wild type PPOX with sulfite and to analyze the consumption of O_2 during catalysis in mxPPOX.

The specific objectives to meet the above aims are presented at the beginning of each relevant chapter.

University of Cape Town

CHAPTER 4

Selection of *M. xanthus* PPOX mutant proteins for further study

University of Cape Town

Introduction

With the availability of resolved protein structure and protein visualisation software tools – visualisation of protein environment and interaction with bound cofactor, FAD, is made possible. PyMol is a software tool used to visualize molecules. With regards to protein, PyMol allows for a 3-D view of a protein, as well as its interactions (with substrate, or inhibitor or cofactor). LigPlot is a software tool that allows for a 2-D representation of a protein-ligand complex (for example mxPPOX-FAD complex). BioEdit-ClustalW, a sequence alignment software tool, allows for the identification of conserved/potentially vital residues.

Here we use a combination of these three software packages for selection of residues that could be potentially playing a vital role in the binding of FAD in mxPPOX.

University of Cape Town

Objectives

- To analyze and identify important residues in the PPOX FAD binding region that interact with FAD, using the software packages PyMol (for protein crystal structure visualisation), LigPlot (to generate 2-D diagrams of protein-ligand interactions) and BioEdit-ClustalW (to align multiple protein sequences to help identify conserved residues).
- To simulate possible mutant structures for characterisation of FAD binding, using the PyMol mutagenesis tool.

Method

Mutant selection

Sequence Alignment

The principle of sequence comparison is based on the fact that sequences derived from the same ancestral sequence will have some homology. When homologous sequences are compared, the percentage of similarity is thought to be equivalent to their similarity in function. That is to say, two highly homologous sequences are more likely to have similar functions compared to two sequences with less homology (derived from a distant common ancestor). In this study the alignment software, BioEdit-ClustalW was utilised. ClustalW uses the hidden Markov Model, a statistical model that considers all possible combinations of matches, mismatches to generate the best alignment of two or more sequences (Petsko & Ringe, 2004).

In order to identify residues important in the function of prokaryotic PPOX, the protein sequence of mxPPOX (appendix 1) was 'blasted' against other sequences in the NCBI protein data bank (Altschul *et al*., 1990). Homologous sequences were selected (based on their Expect value (E-value)) and subjected to multiple alignment (Altschul *et al*., 1990). E-value describes the expected similarity between two sequences. An E-value is given to the sequence of interest (the query sequence) and each proposed "similar" sequence. A low E-value, indicates a more significant match.

University of Cape Town

Protein structure analysis

Using sequence alignment alone to identify protein function is inadequate (Petsko & Ringe, 2004). This is because sequences change much more rapidly with evolution than does structure. In nature there are proteins that have no sequence homology but a similar fold and hence a similar function (Petsko & Ringe, 2004). By analysing the mxPPOX structure and comparing it to other PPOX structures, one would be able to identify conserved residues that are critical for binding or catalysis (Dym *et al*., 2001; Zhao *et al*., 2008). Protein data bank (PDB) files of known PPOX structures were retrieved from the protein data bank website (www.pdb.org). Using PyMol (freely available software), structures were analysed for unique properties such as a hydrophobic environment. The location and interactions of conserved residues identified

were analysed with respect to the flavin binding region. In this study, PyMol was also used to generate “virtual mutants”, allowing for the assessment of the possible orientation of the potential mutants. The specific mutants chosen for this study were based on base pair substitution allowing for the alteration of side chain properties e.g. a negative to a positive charge replacement, or an aromatic to a linear replacement etc.

For protein-ligand interactions, LigPlot was used to analyse the 2-D interaction of the cofactor (FAD) and PPOX, see appendix 20 for detailed LigPlot programming instructions (Dym *et al*., 2001). LigPlot shows hydrogen bond interactions between a selected ligand and surrounding protein. A residue’s conservation, as well as mode of interaction, was carefully assessed to allow for a strategic selection of residues for analysis of FAD interaction with mxPPOX.

University of Cape Town

Results

Sequence alignment

An alignment of prokaryotic PPOX protein sequences was successfully performed followed by an alignment of the sequence of mtPPOX, mxPPOX, bsPPOX and hPPOX (PPOXs with resolved structure) – detailed results are given in appendix 21. The latter alignment confirms the alignment done by Dailey and Dailey (1996a).

LigPlot analysis

A 2-D representation of mxPPOX FAD binding region was drawn using LigPlot. Residues involved in a polar interaction with FAD via their side chain are, Ser-20, Glu-39, Asn-441 (chapter 2, fig. 2.7). A tryptophan is seen interacting with the FAD isoalloxazine ring (in mtPPOX and bsPPOX); their tryptophan aligns with Trp-408 in mxPPOX. Other relevant LigPlot images can also be viewed in chapter 2 (fig. 2.6, 2.8).

PyMol analysis

Four residues (which interact with FAD via their side chain), were identified as playing a potentially important role in FAD binding in mxPPOX namely Ser-20, Glu-39, Trp-408 and Asn-441. Table 4.1 below shows the ten mutants that were engineered for further study.

Table 4.1: mxPPOX mutants engineered in this study.

Residue	**Mutant**
Serine 20	Ser20Thr Ser20Ala
Glutamate 39	Glu39Asp Glu39Lys Glu39Gln Glu39Ala
Tryptophan 408	Trp408Leu Trp408Tyr
Asparagine 441	Asn441Ile Asn441Gln

University of Cape Town

Simulation of possible mutants' interaction with FAD using protein visualisation software, PyMol.

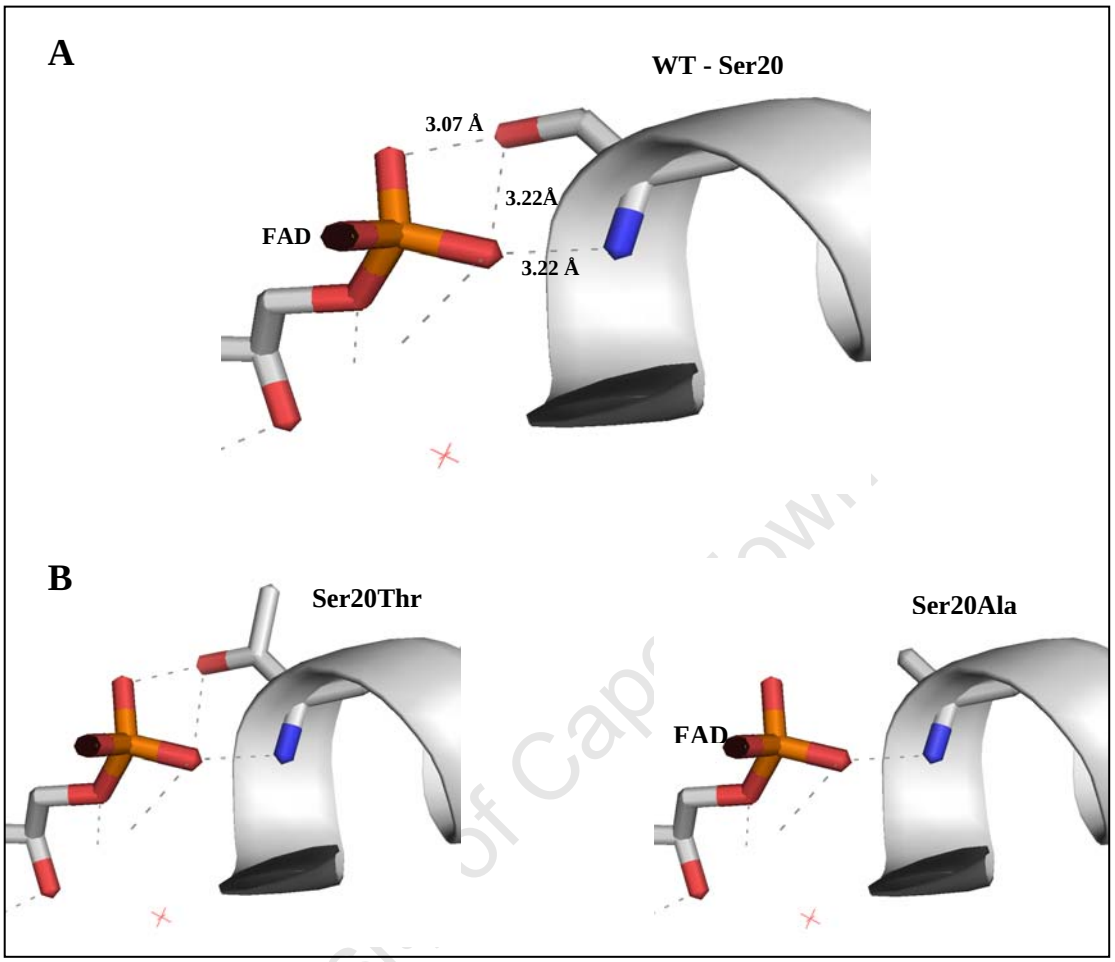

Figure 4.1: A PyMol image of the possible interaction of Ser-20 mutants (shown in stick format within an alpha-helix - grey), with pyrophosphate section of the FAD cofactor (shown in stick format). Red stars - represent surrounding water molecules. A) Wild type Ser-20 interaction with FAD-pyrophosphate. B) Mutants (Ser20Thr and Ser20Ala) possible interaction with FAD. In all cases red - oxygen; blue - nitrogen; grey - carbon, orange - phosphate and red stars - water molecules. Polar interactions are shown as dotted lines.

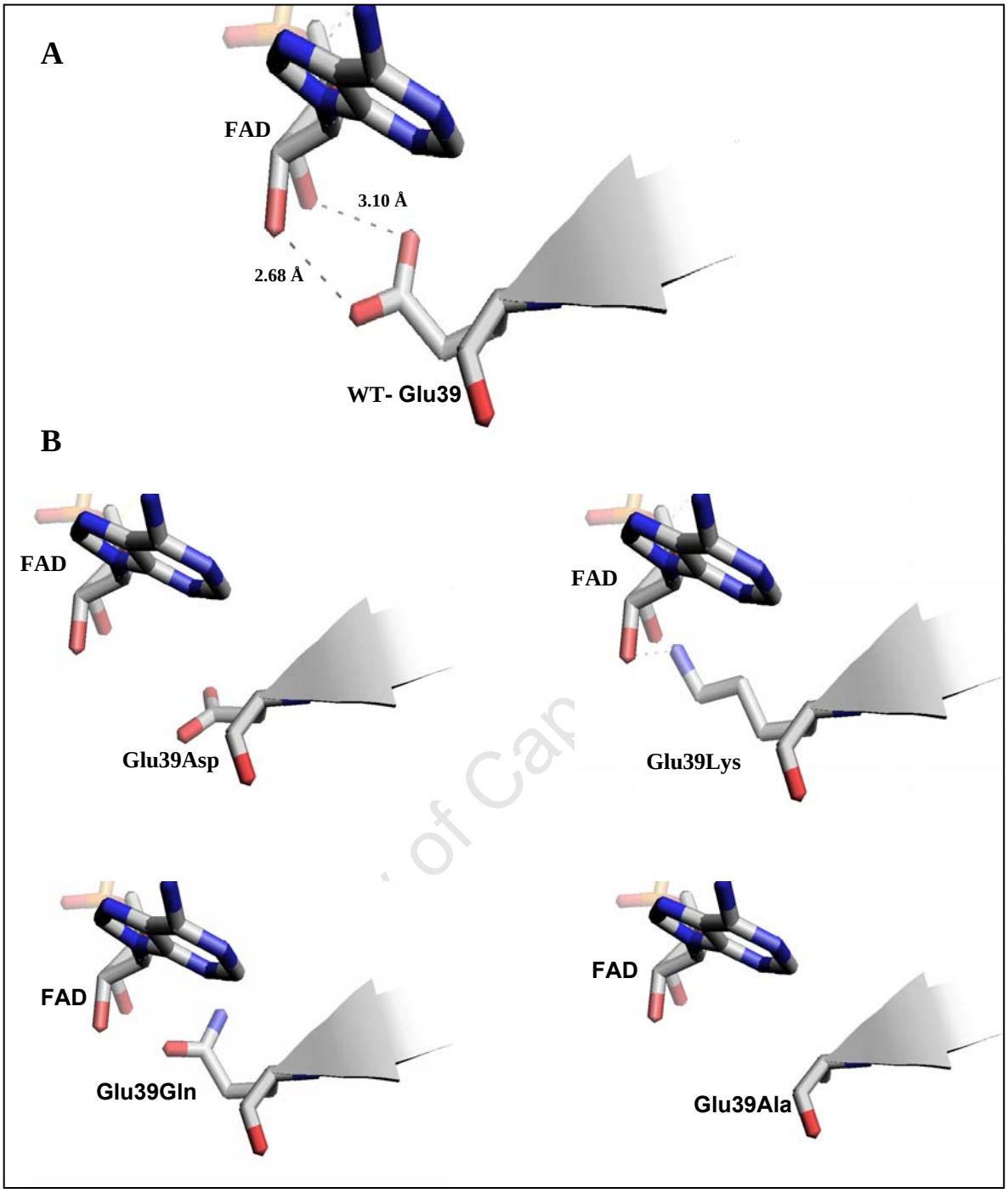

Figure 4.2: A PyMol image showing the possible interaction of Glu-39 mutants with the adenine ring of the FAD cofactor. Glu-39 is shown in stick format at the end of a beta-sheet (grey). A) Wild type Glu39 interaction with FAD-adenine. B) Mutants (Glu39Asp, Glu39Lys, Glu39Gln and Glu39Ala) possible interaction with FAD. In all cases red - oxygen; blue - nitrogen; grey – carbon, and orange - phosphate. Polar interactions are shown as dotted lines.

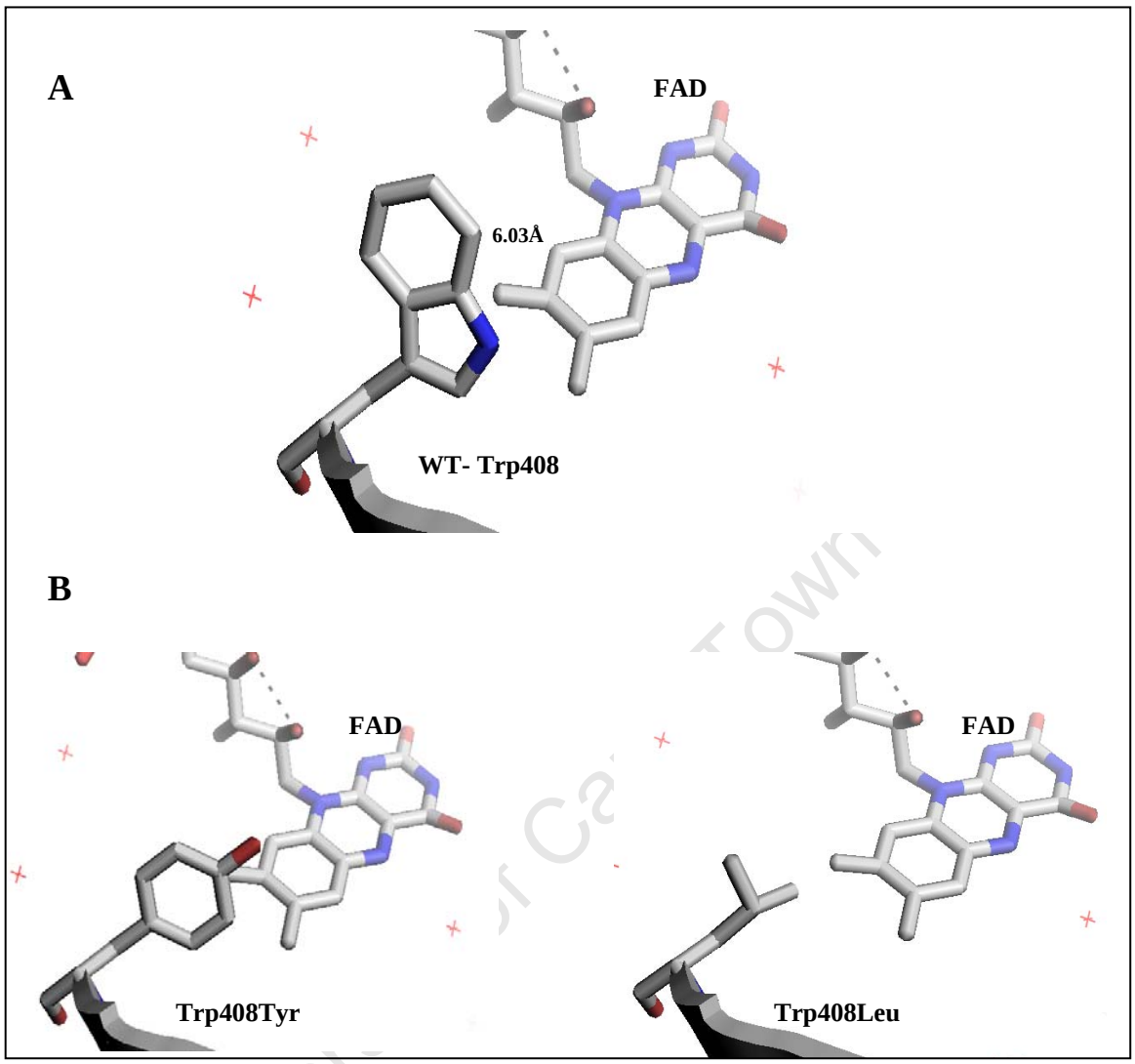

Figure 4.3: A PyMol image showing the possible interaction of Trp-408 mutants with isoalloxazine ring of the FAD cofactor. Trp-408 is shown in stick format at the end of a beta-sheet. A) Wild type Trp-408 interaction with FAD-isoalloxazine. B) Mutants (Trp408Tyr and Trp408Leu) possible interaction with FAD. In all cases red - oxygen; blue - nitrogen; grey - carbon and red stars - water molecules. Polar interactions are shown as dotted lines.

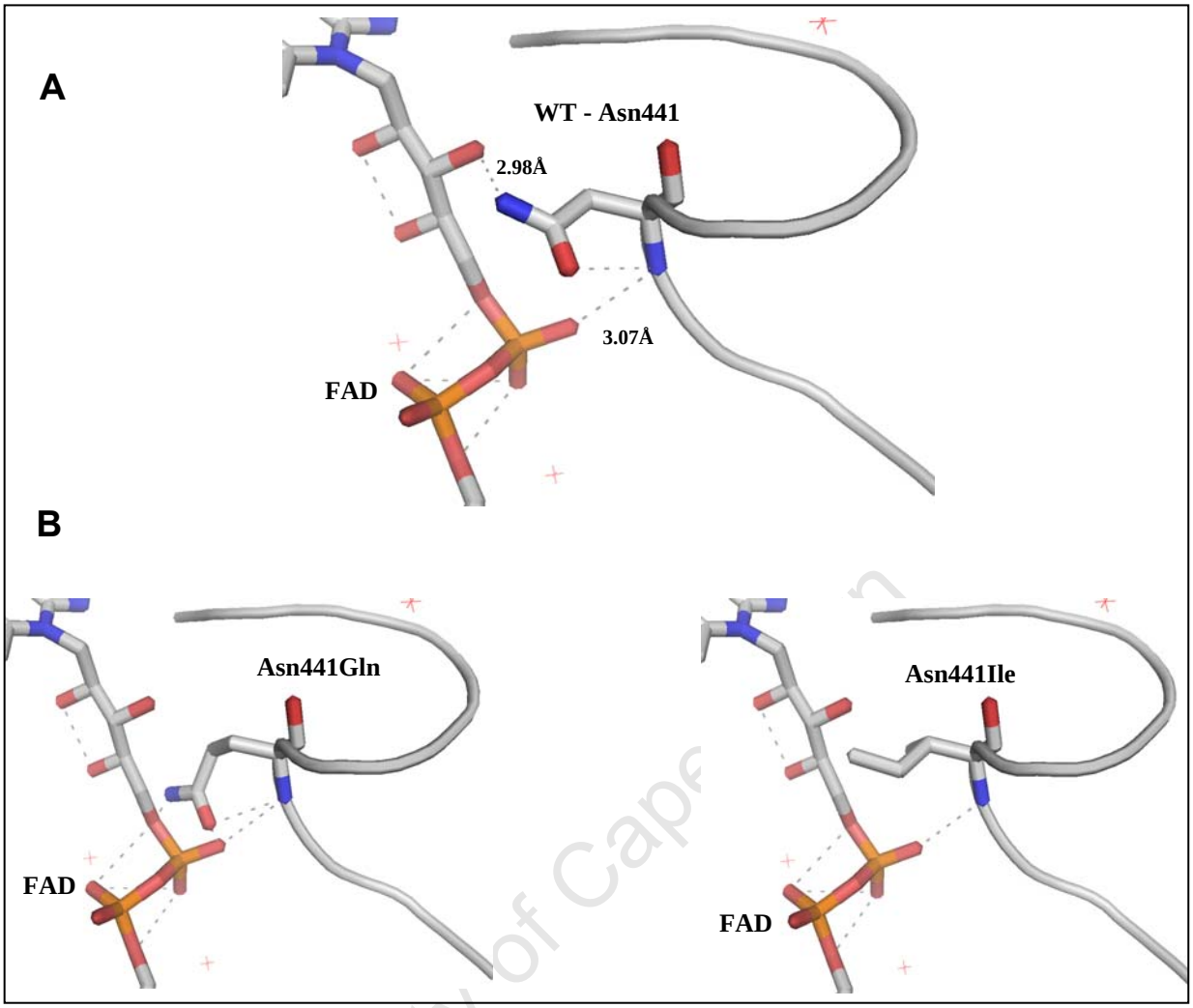

Figure 4.4: PyMol image showing the possible interaction of Asn-441 mutants with both ribityl and pyrophosphate section of the FAD cofactor. Asn-441 is shown in stick format within a turning loop (grey). A) Wild type Asn-441 interaction with FAD. B) Mutants (Asn441Gln and Asn441Ile) possible interaction with FAD. In all cases red - oxygen; blue - nitrogen; grey - carbon, orange - phosphate and red stars - water molecules. Polar interactions are shown as dotted lines.

University of Cape

Discussion

Amino acid Sequence alignment

Alignment of mxPPOX with various prokaryote PPOX protein sequences confirmed the consensus sequence of the FAD superfamily reported by Dailey and Dailey, (1998). Residues Ser-20 and Glu-39 are part of this consensus sequence and are highly conserved; suggesting the importance of their interaction with FAD. Asn-441 is highly conserved among the prokaryotes. This residue is seen interacting with FAD via its side chain and water molecules in the mxPPOX_AF structure (chapter 2, fig. 2.8). An interaction that could possible benefit protein-FAD association by allowing for increased flexibility of the bound FAD.

Furthermore, the tryptophan residue, which is normally seen in proteins of the FAD superfamily interacting with the hydrophobic ring of the FAD isoalloxazine ring, is equivalent to Trp-408 in mxPPOX (Binda *et al*., 1999; Neeli *et al*., 2005). Interestingly, however, this residue is not conserved among the PPOX prokaryotes. Nevertheless, study of the alignment suggests that an aromatic ring is favoured in this position (appendix 21, alignment 1). Interestingly, in hPPOX, although Trp-42 does not align with mxPPOX Trp-408, it is positioned near the nonpolar ring of the FAD isoalloxazine ring and could therefore potentially be stabilizing the isoalloxazine during catalysis.

Although Asn-63 (human equivalent Arg-59) was not analysed in this study it is worth noting that this residue is conserved in prokaryotic PPOX. Asn-63 forms a water mediated interaction with the FAD-N(5) (Corradi *et al*., 2006). It has been hypothesized that the water molecule interacting at this position in oxidases, plays a direct role in the oxidation of the substrate (Binda *et al*., 1999). Studies in other oxidases reveal that either an asparagine or an arginine are commonly favoured at this position (Yin *et al*., 2001; Yue et al., 2001; Piubelli *et al*., 2008). However, due to its involvement in extensive hydrogen bond interactions in the substrate binding region (structural integrity), as well as its interaction (water mediated) with the FAD-N5, it was not considered in this study (refer to chapter 2 for a detailed review).

University of Cape Town

LigPlot analysis

Protein-ligand interaction in mxPPOX structure revealed that three residues interact with FAD via their side chains; hence they could possibly be playing a role in the binding and orientation of FAD. These residues are Ser-20, Glu-39, and Asn-441 (for detailed interactions refer to chapter 2, structural properties). In mtPPOX a lysine interacting with the phosphate group (Lys-51) and glutamate interacting with the ribose ring (Glu-43) interact with the FAD via their side chains; in bsPPOX a threonine (Thr-16) interacting with the phosphate group and glutamate (Glu-41) interacting with the ribose ring are seen interacting with their side chain; lastly in hPPOX a glutamate and serine (Glu-34 and Ser-35, respectively) both interact with the ribose ring via their side chains followed by a serine residue (Ser-13) that interacts with the phosphate group via its side chain. Due to the fact that side chain interactions allow for more movement compared to backbone interactions, it is tempting to speculate that flexibility at both ribose and phosphate region of FAD could be vital. Although *M. xanthus* Trp-408 aligns with bsPPOX and mtPPOX, it is located further away from the FAD isoalloxazine ring. This difference in location suggests that the role of Trp-408 may be different from those of mtPPOX and bsPPOX. In hPPOX, although a histidine aligns with Trp-408, a Trp-42 rather than a histidine is seen near the isoalloxazine ring.

University of Cape Town

PyMol simulation of mutant PPOXs

Serine 20

The wild type Ser-20 side chain makes three interactions with the phosphate group of FAD - two via its carbonyl group and one via its amino group (fig. 4.1). Alteration of serine to a threonine, a conserved polar neutral, retains the carbonyl as well as amino group, resulting in a similar FAD interaction as wild type (fig. 4.1). However, alteration to an alanine, a nonpolar neutral residue, removes the carbonyl group while maintaining the amino group of the serine side chain. Consequently, the two carbonyl interactions found in wild type are missing in this mutant. These simulations suggest Ser20Ala will have inferior interaction with FAD whilst Ser20Thr to bind FAD similarly to wild type.

Glutamate 39

The Glu-39 side chain has two carbonyl groups (fig. 4.2) and these carbonyl groups interact with the hydroxyl group of the ribose ring. In the conservative change (Glu39Asp) one would expect to see an interaction with the FAD. However, the PyMol mutagenesis simulation shows that no interaction is possible between this mutant and FAD. This can be either due to difference in size, or PyMol mutant simulation criteria. With regards to size, aspartate is shorter than glutamate by a methyl group and therefore increasing the distance between the FAD and mutant. This increase in distance could therefore hinder bond formation. Another factor is that PyMol mutagenesis software does not take into account spatial alterations due to change in size, but imposes the same fit as the native residue. Glu39Lys, a positively charged polar residue, has a single polar interaction with the ribose ring and together with neighbouring hydrophobic interactions this mutant should theoretically be able to bind FAD, although not as well as wild type. Both Glu39Gln and Glu39Ala show no interaction with the FAD (fig. 4.2). In the case of glutamine, the distance between FAD and glutamine is optimal for interaction, suggesting that the neutrally charged side chain could be playing a role in preventing FAD-glutamine interaction. With regards to alanine, although its size is small enough to allow for an optimal positioning with the FAD, the PyMol mutant simulation criteria limit this option. It is therefore difficult to say whether distance or side chain properties (neutral) or both play a role in FAD-ribose interaction.

Tryptophan 408

The interactions of FAD with a conserved Trp-408 were investigated by mutating this residue to a polar aromatic, tyrosine and a nonpolar linear, leucine residue. A tryptophan was seen interacting with the nonpolar ring of the isoalloxazine ring in various oxidases as well as PPOXs (Binda *et al*., 1999; Neeli *et al*., 2005). Here we simulated the effect of mutating this residue to a leucine (removal of the aromatic ring) and a tyrosine (polar aromatic residue). Both tyrosine and leucine are optimally positioned to interact with FAD (fig. 4.3). It is difficult to say whether an aromatic ring alone is vital for interaction or whether nonpolarity is a critical factor in stabilizing the bound FAD. However, analysis of the FAD binding region reveals that a nonpolar residue would be more preferable in stabilizing FAD in this region than a polar. Based on previous studies it would be interesting to see if Trp-408 has similar functions to those reported in other oxidases (Binda *et al*., 1999; Neeli *et al*., 2005).

Asparagine 441

University of Cape Town

Asn-441 is located in a long loop that twists perfectly to orientate the Asn-441 residue to interact with the phosphate group of FAD via its side chain and the amino group with the ribityl chain of the FMN group. Asparagine was mutated to a polar neutral, glutamine (Asn441Gln) and nonpolar neutral isoleucine (Asn441Ile). In simulating the asparagine mutants the Asn441Gln mutant side chain position was altered from that of wild type and consequently the ribityl chain interaction was diminished. Interestingly a new interaction with the phosphate group was formed resulting in a total of two pyrophosphate interactions. The nonpolar side chain of isoleucine failed to make an interaction with ribityl chain. However, the backbone interaction was maintained (fig. 4.4). This suggests that polarity could be playing a role at this position. Theoretically the Ans441Gln should have similar interactions with FAD while the isoleucine replacement, should have inferior interaction.

University of Cape Town

Conclusions

Protein crystal structure and sequence analysis allowed us to identify four mxPPOX amino acid residues most likely to be involved in FAD binding in mxPPOX. These were selected for further analysis.

Ten mutants (covering the four amino acid positions) were successfully simulated and visualised using the PyMol mutagenesis software tool, allowing for preliminary mutant/protein interaction assessment.

Based on our analyses and simulations we propose that the highly conserved residues Ser-20, Glu-39 and Asn-441 could be playing an important role in FAD/protein interaction.

The alignment study further suggests that an aromatic ring (Trp-408) is favoured to interact with the FAD isoalloxazine ring and FAD binding region analysis suggests that a nonpolar residue would be more preferable in stabilizing FAD in this region than a polar.

Finally, the analyses suggest that flexibility at both ribose and phosphate region of FAD could be vital.

CHAPTER 5

Engineering, expression, and purification of *M. xanthus* PPOX mutant proteins

University of Cape Town

Introduction

As in other forms of PPOX (Camadros *et al*., 1994; Dailey *et al*., 1994; Dailey & Dailey, 1996a; Dailey & Dailey, 1996b), FAD plays a vital role in the catalytic reaction of mxPPOX; it is the intermediate electron acceptor in the oxidation of protogen (see chapter 2; Dailey & Dailey, 1996a). Generally, in flavoproteins, the biological function of the flavin ring is modulated by its binding to and specific interactions with its protein environment (Petsko & Ringe, 2004). Site directed mutagenesis, followed by expression and analysis of mutant proteins, is a technique which has been used in numerous studies to understand the role of residues that could potentially be vital in the functioning of a protein (Gadda *et al*., 1997; Petsko & Ringe, 2004; Neeli *et al*., 2005). Therefore, in order to shed light on the FAD binding properties in mxPPOX, potential key residues were selected (chapter 4), mutated (this chapter) and subjected to comparative analysis with that of wild type mxPPOX (later chapters).

Objectives

- To generate mutants and screen clones wherever possible by restriction analysis to enable easy identification of desired mutants.
- To sequence the entire *PPOX* gene in these engineered mutants to confirm correct insertion of the desired base alteration, as well as to confirm the absence of any spurious base change.
- To express, purify and quantify mutant mxPPOX proteins to allow for their characterisation.

University of Cape Town

Method

Site-directed mutagenesis

Two site-directed mutagenesis methodologies were used in this study namely: the *GeneEditor™ in vitro Site-Directed Mutagenesis System* and the *QuickChange® Site Directed Mutagenesis system*.

The GeneEditor kit had been successfully utilised in the Lennox Eales Porphyria laboratories for several years prior to the commencement of this study. However, great difficulties were experienced in successfully generating mxPPOX mutants using this kit. After repeated efforts, and many attempts at trouble shooting, the reason for this remains unclear. It was decided to change kits and the QuickChange system was successfully utilised. Thus, all the mutants engineered in this study (apart from Trp408Leu), were generated using this kit, the methodology of which is described below and in appendix 11. The GeneEditor kit methodology is given in appendix 10 and is not detailed here.

University of Cape Town

QuickChange® Site Directed Mutagenesis kit system

Principle

QuickChange utilizes a supercoiled double-stranded plasmid and two synthetic oligos containing the desired mutation to incorporate a mutation through a highly efficient DNA polymerase, *PfuTurbo*. The oligos, each complementary to opposite strands of the plasmid, are extended during temperature cycling by *PfuTurbo* DNA polymerase (high fidelity). Incorporation of the oligos generates a mutated plasmid containing staggered nicks. Products are then treated with *DpnI* endonuclease which recognises sequence 5' -Gm^{6}ATC-3', dam methylation found in DNA isolated from *E. coli*; thus allowing for the selection of the plasmid with the desired mutation. The removal of wild type strands through *DpnI* endonuclease digestion increases efficiency of the technique enabling easy screening for positive clones. DNA is then finally transformed into supercompetent cells.

Oligonucleotide design

Complementary mutagenic oligos were designed according to the manufacturer's parameters and contained the desired mutation approximately positioned in the centre of the oligo, with 10 - 15 bases on either side of the mutation. The 3' end of the oligo should end with a G or C nucleotide to stabilize the oligo during annealing between the oligo and template.

Once parameters such as GC content, melting temperature (Tm), ∆G, hairpin, etc were optimized; the restriction site for screening of mutants was identified using freely available internet software e.g. Webcutter.

Procedure

Plasmid DNA was generated from expressed wild type mxPPOX (appendix 4). To synthesize mutagenic strands, a thermal cycling reaction was set up and included a mixture of dNTPS, *PfuTurbo* polymerase and buffer, mutagenic oligos and plasmid DNA. Once the thermal cycling reaction was complete, *DpnI* and relevant buffer were added to allow for the digestion of the wild type strands. Digested product was then transformed into JM109 competent cells, followed by incubation on shaking incubator at

University of Cape Town

37 °C. Cells were then plated on agar plates containing ampicillin and incubated at 37 °C overnight.

Screening clones

A selection of single colonies from the above agar plates, were inoculated in LB (with ampicillin) and incubated at 37 °C in a shaking incubator O/N.

Thirty % glycerol stocks were made from the overnight cultures and stored at -70 °C.

Plasmid DNA, from a minimum of two overnight cultures (6 ml) of the above expressing JM109 cells, was extracted using the Wizard® Plus SV Minipreps DNA Purification system (appendix 5). Previously designed oligos for wild type mxPPOX were used to prime mxPPOX sequence. PCR was performed, as described in appendix 8, on the fragment containing the introduced base alteration (see appendix 2 for mxPPOX sequence fragments). After checking of the amplified PCR products on 6 % PAGE (appendix 9), relevant restriction analysis was performed if possible (appendix 12). Restriction enzyme digests, were analysed on a 6 % non-denaturing polyacrylamide gel to identify positive clones.

University of Cape Town

Sequence confirmation

For convenience, the *PPOX* gene was divided into 4 fragments and primers were designed to these enabling the entire gene to be sequenced. In positive clones, the PCR product of the relevant fragment covering the section of the gene that contained the mutated bp was sequenced by direct sequencing. Thereafter, the three remaining mxPPOX fragments were also amplified and sequenced, to ensure no other mutations had been spuriously introduced. The PCR products were cleaned using the GFX PCR DNA Purification kit (appendix 13).

In order to screen the entire mxPPOX plasmid a second oligo was designed in the vector to flank over fragment 4 and a small section of the vector sequence (appendix 2, Fragment 4 extended), oligo was named vMxF4R. For oligo design and sequence refer to appendix 7.

Sequencing was by automated direct sequencing using the ABI-3100 Automated Genetic Analyzer and a Big Dye version 3.0 kit (Applied Biosystems, Brachberg, USA) (Core DNA Sequencing Facility, University of Stellenbosch, SA). Sequences were then analysed using BioEdit by aligning wild type mxPPOX sequence with the positive clone sequence.

Expression of wild type and mutant mxPPOX protein

A wild type pMx-PPOX with a 6X His tag in a tac promoter-driven expression plasmid, was kindly donated by Professor Harry Dailey (University of Georgia, Georgia, USA) and was used to express the protein (Dailey & Dailey, 1996a).
The PPOX-containing plasmid was transformed in our laboratory into competent JM109 cells (for growth media refer to appendix 3). One ml glycerol stock of wild type mxPPOX was inoculated in 1 L LB medium containing ampicillin and incubated for 22 hr at 30 °C with shaking (225 rpm). Mutant mxPPOX JM109 cells were expressed under the same conditions as wild type mxPPOX. In the case of low expressing mutants, 2 ml instead of one ml JM109 cells, were inoculated into 1 L of LB medium with 100 µg/ml of ampicillin. The culture was then grown in an incubator with shaking (225 rpm) at 37 °C for 22 hr.

University of Cape Town

Purification of wild type and mutant mxPPOX protein

The TALON metal affinity resin protein purification system was used for the purification of both wild type and mutant proteins (appendix 14). This system has many advantages such as a reduced affinity for non-6X His proteins as well as a high affinity for 6X His proteins. It can be used to purify proteins expressed in both eukaryotic and prokaryotic systems; in small or large scale preparations. Another advantage includes its stability of system under native and denaturing purification conditions.

The principle of purification is based on interaction between cobalt and histidine residues. Cobalt has six available coordination sites arranged in an octahedral configuration - allowing interaction with an electron-rich histidine. mxPPOX having a

previously inserted 6X His tag insertion makes it susceptible to purification via this Talon-His tag chromatography technique.

Briefly, cells from an overnight 1 L culture were harvested and pellet was resuspended in sonication buffer. Cells were then lysed; lysate was centrifuged at 105 000 g. A volume of 600 µl Talon resin was equilibrated 10 ml of equilibration buffer. The supernatant was loaded at a flow rate of 15 ml/hr. The flow through was collected and pooled (void). The column was washed with at least 10 ml of wash buffer prior to elution. A final concentration of 1 µg/ml phenylmethylsulfonylfluoride (PMSF) was added throughout the purification procedure (appendix 14). The different fractions (load, void, wash and eluate) were then quantitated using the Biorad microassay protein quantitation system (appendix 16). Purity of the proteins was assessed on SDS PAGE (appendix 15).

University of Cape Town

Results

Mutational analysis

Restriction analysis was successfully employed to screen for positive clones in seven engineered mutants: Glu39Ala, Glu39Asp, Glu39Gln, Glu39Lys, Trp408Leu, Asn441Gln, and Asn441Ile (fig. 5.1 - 5.5). Digests were visualized on a 6 % SDS polyacrylamide gel. Due to the high success rate of the QuickChange mutagenesis system, the final mutants engineered (Ser20Ala, Ser20Thr, and Trp408Tyr) were simply directly sequenced. Two colonies from clones were randomly selected, cDNA isolated, followed by the amplification and sequencing of the appropriate fragment. In all cases, the correct insertion of the desired base change was identified. Screening of the remaining fragments of the cDNA of one of the positive clones, confirmed that no erroneous mutations had been introduced.

Relevant PCR products of Glu39Ala, Glu39Gln, and Glu39Lys mutant clones were analyzed using *HinfI* restriction enzyme. In all cases a cutting site was abolished creating a three fragment digest as opposed to the four fragment digest seen in the wild type sequence digest (table 5.1). All clones were positive (fig. 5.1). Glu39Asp clones

were screened using the *TfiI* restriction enzyme. The positive clone creates an additional cutting site (two fragments in wild type and three in mutants; see table 5.1 and fig. 5.2). Trp408Leu clones were screened using the *ItaI* restriction enzyme (table 5.1). Both positive and negative clones were identified (fig. 5.3). Asn441Gln clones were digested using the *Hpy188III* which cuts fragment four once (table 5.1). In the mutant clone a cutting site is abolished (fig. 5.4). All clones were positive. Asn441Ile clones were screened using the *BsmI* restriction enzyme (refer to table 5.1). All four clones screened were positive (fig. 5.5). For details of the number of fragments as well as fragment sizes of each digest see table below.

Table 5.1: Restriction analysis and details of fragments produced by restriction enzyme

RE	Clone	Recognition sequence	No. of fragments	Fragment sizes (bp)	comment
HinfI	Glu39Gln	g/antc	3	233, 68, 50	Cutting site abolished in mutant clone
	Glu39Lys	g/antc	3	233, 68, 50	
	Glu39Ala	g/antc	3	233, 68, 50	
	Wild type	g/antc	4	122, 111, 68, 50	
TfiI	Glu39Asp	g/awtc	3	122, 118, 115	Cutting site introduced in mutant clone
	Wild type	g/awtc	2	237, 118	
ItaI	Trp408Leu	gc/ngc	8	133, 123, 113, 73, 33, 12, 5, 3	Cutting site abolished in mutant clone
	Wild type	gc/ngc	9	133, 113, 77, 73, 46, 33, 12, 5, 3	
Hpyl88III	Asn441Gln	tc/nnga	0	559	Cutting site abolished in mutant clone
	Wild type	tc/nnga	2	109, 450	
BsmI	Asn441Ile	gaat/gc	2	124, 371	Cutting site abolished in mutant clone
	Wild type	gaat/gc	3	36, 88, 371	

University of Cape Town

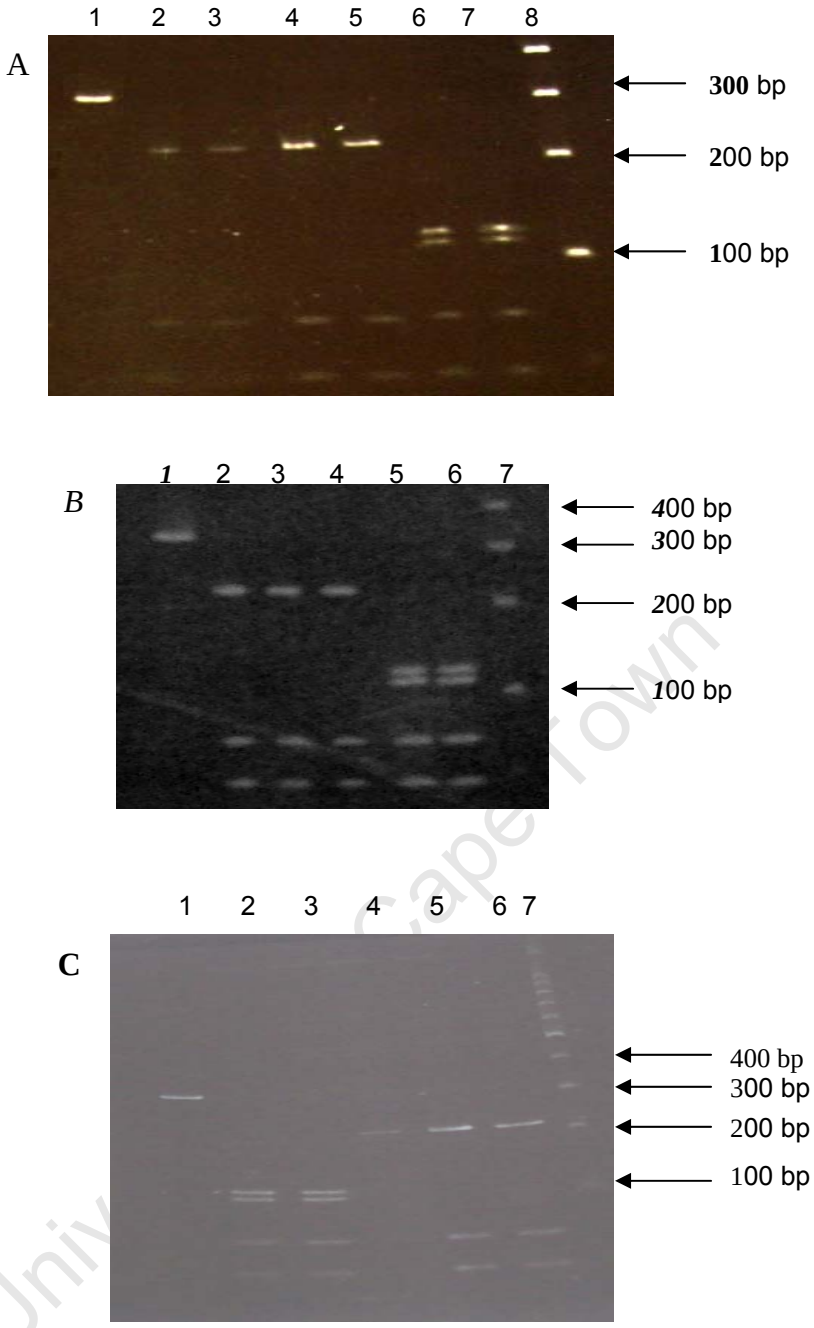

University of Cape Town

Figure 5.1: 6 % SDS PAGE showing *HinfI* restriction digest analysis of the PCR product of fragment 1 of three Glu-39 mutants. The wild type fragment has three cutting sites whilst the incorporation of the single base change results in the abolishment of a cutting site, hence two cutting sites in the mutant. A) Glu39Gln restriction analysis. Lanes 1 = pre-digest; 2-5 =positive clones; lanes 6, 7 wild type negative controls and lane 8 - bp marker. B) Glu39Lys restriction analysis using *HinfI*. Lane 1 - pre-digest; lanes 2-4: positive clones; lanes 5, 6 = wild type, negative controls; lane 7 – bp marker. C) Glu39Ala restriction analysis. Lanes 1 = pre-digest; lane 2-3 = wild type; lanes 4-6 = positive clone; lane 7 =bp marker.

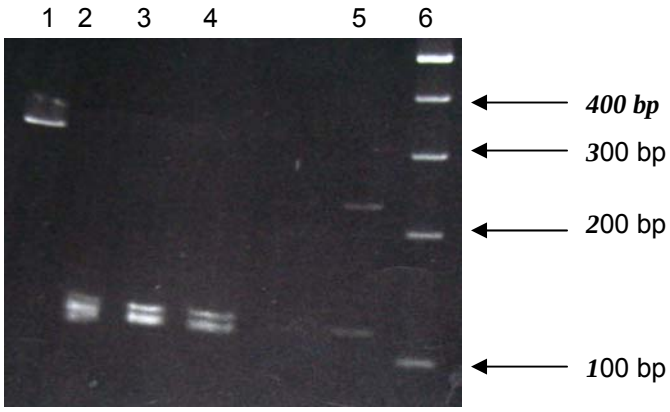

Figure 5.2: 6 % SDS PAGE showing *TfiI* restriction digest analysis of the PCR product of fragment 1 of the Glu39Asp mutant. Lane 1 = pre-digest; lanes 2- 4 = positive clones; lanes 5 = wild type; lane 6 = bp marker. **Note** the 115 and 118 bp fragments are not resolved hence only 2 bands are clearly visible, the lower one being thicker in lanes 2, 3, and 4.

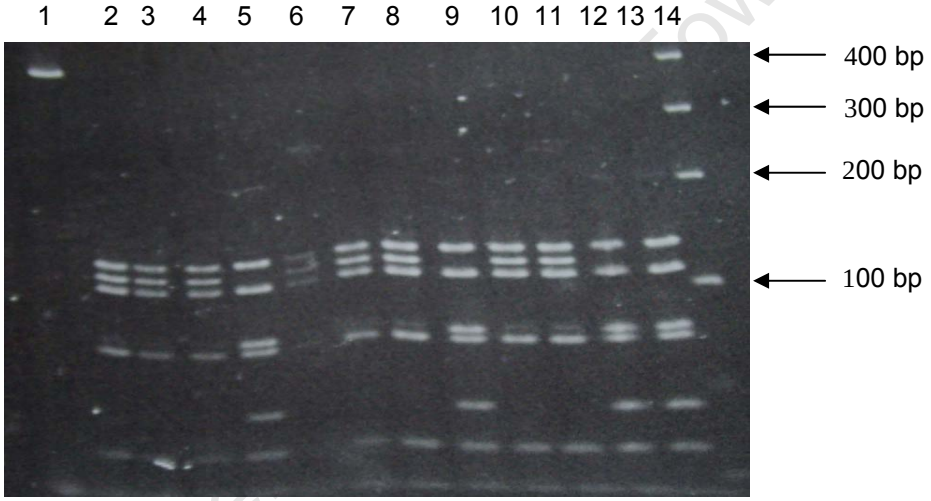

Figure 5.3: 6 % SDS PAGE showing *ItaI* restriction digest analysis of the PCR product of fragment 4 (using the MxF4R oligo) of the Trp408Leu mutant. Lane 1 = pre-digest; lanes 2-4, 6-8, 10-11 = positive clones; lanes 5, 9 = negative clones; lanes 12-13 = wild type; lane 14 = bp maker.

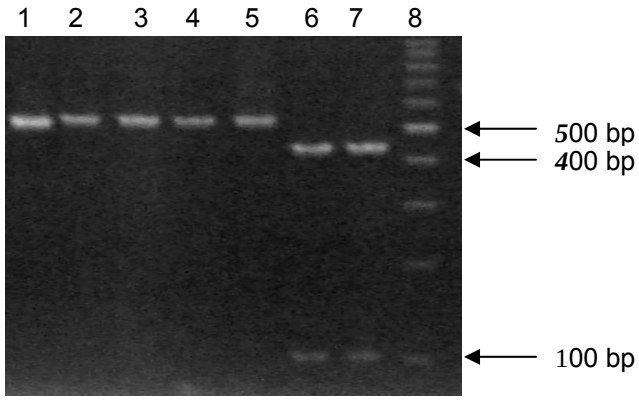

Figure 5.4: 6 % SDS PAGE showing *Hpy188III* restriction digest analysis of the PCR product of fragment 4 (using the vMxF4R oligo) of the Asn441Gln mutant. Lane 1 - pre-digest; lanes 2-4: positive clones; lanes 5, 6 = wild type negative controls; lane 7 - bp marker.

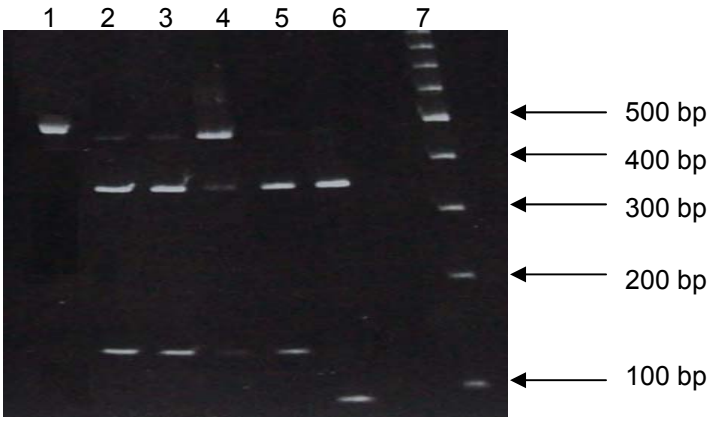

Figure 5.5: 6 % SDS PAGE showing *BsmI* restriction digest analysis of the PCR product of fragment 4 (using the MxF4R oligo) of the Asn441Ile mutant. Lane 1= pre-digest; 2, 3, 5 = positive clones; lane 4 = incomplete digestion; lane 6 = wild type; lane 7 = bp marker.

University of Cape Town

Sequence confirmation

Confirmation of successful engineering of mutants was by sequence analysis; figs 5.6 – 5.9 show partial sequencing for these. In all cases the altered bp(s) is encircled and the wild type sequence is shown above the mutant sequence.

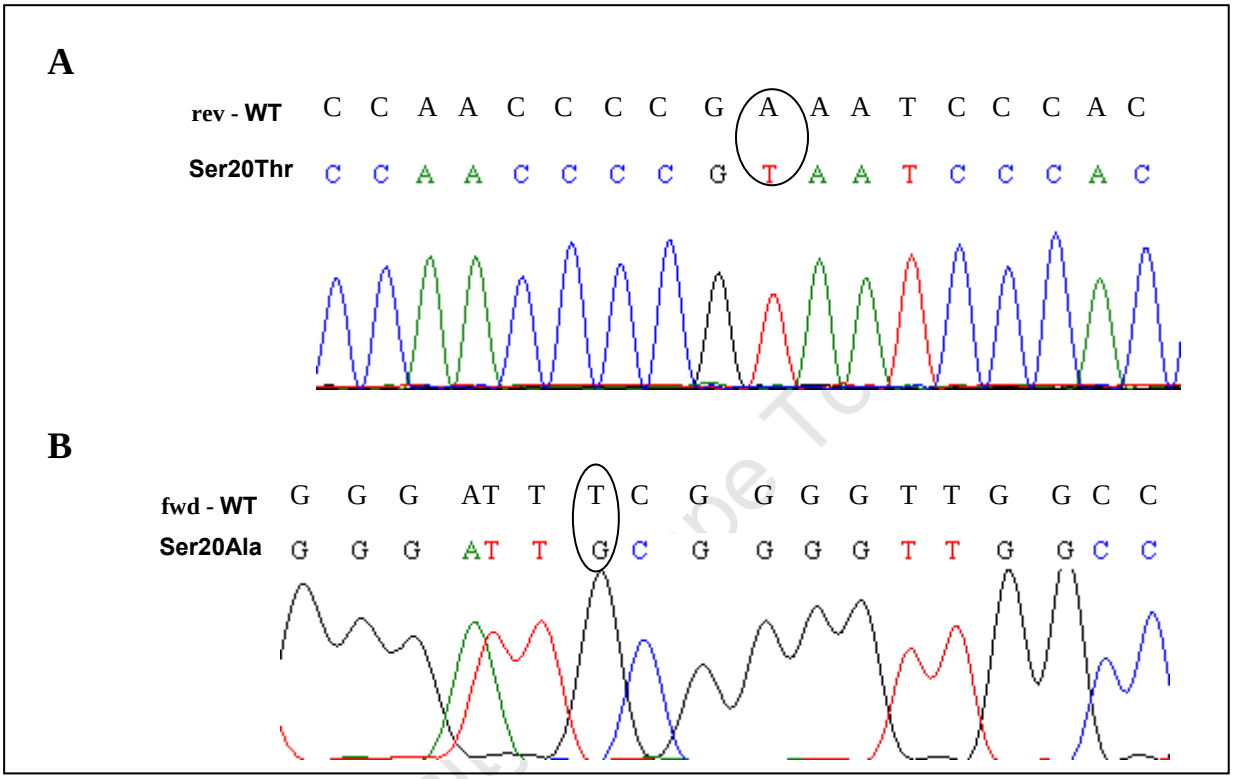

Figure 5.6: Partial direct sequencing of fragment 1 of the Ser-20 mutants: A) Ser20Thr using the reverse primer mxF1R. B) Ser20Ala sequenced using primer mxF1F. The altered bp is encircled.

University of the

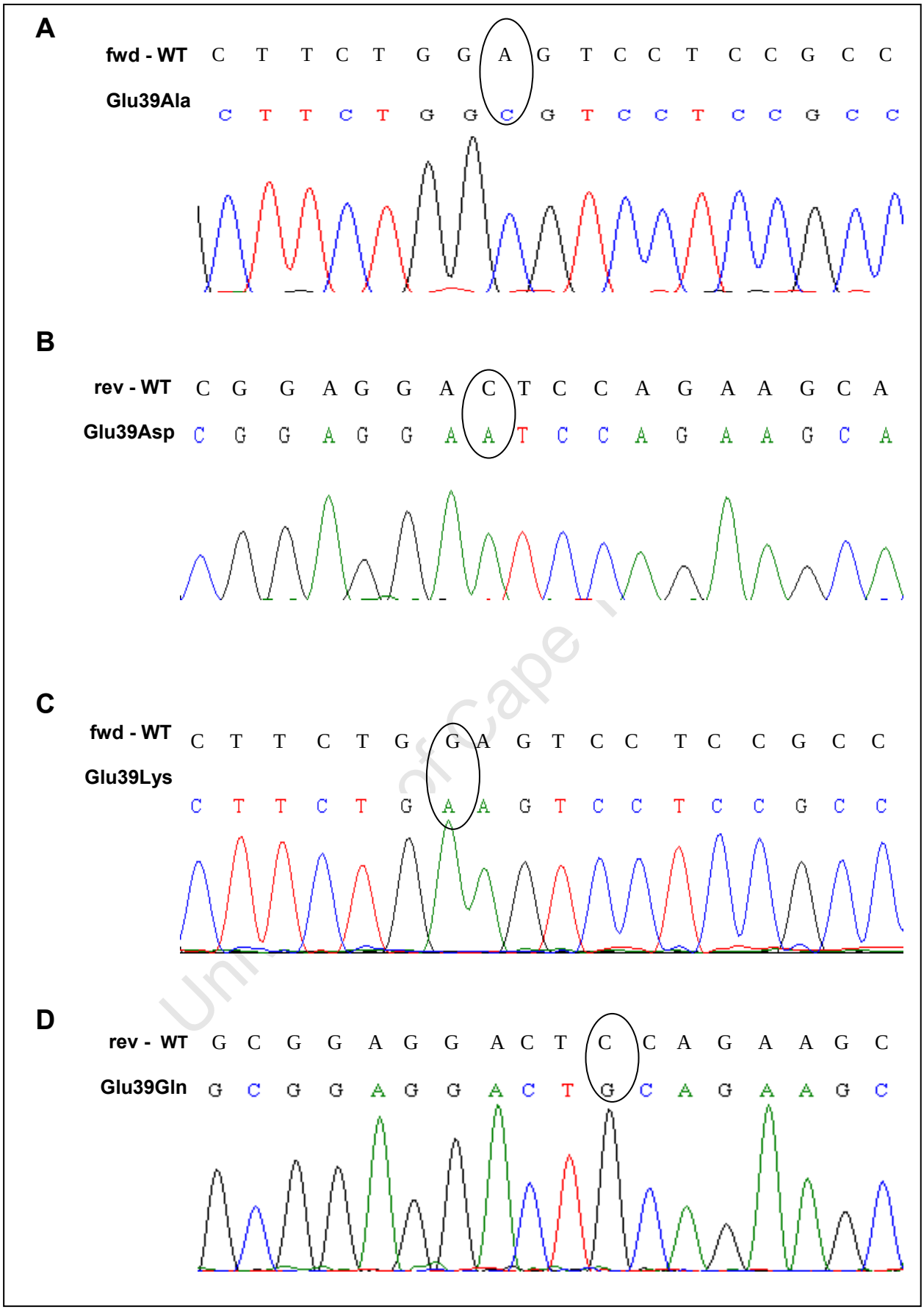

Figure 5.7: Partial direct sequencing of fragment 1 of the Glu-39 mutants: A) Glu39Ala using the forward primer mxF1F; B) Glu39Asp mutant using the reverse primer mxF1R; C) Glu39Lys using primer mxF1F; D) Glu39Gln mutant using primer mxF1R. The altered bp is encircled.

University of Cape Town

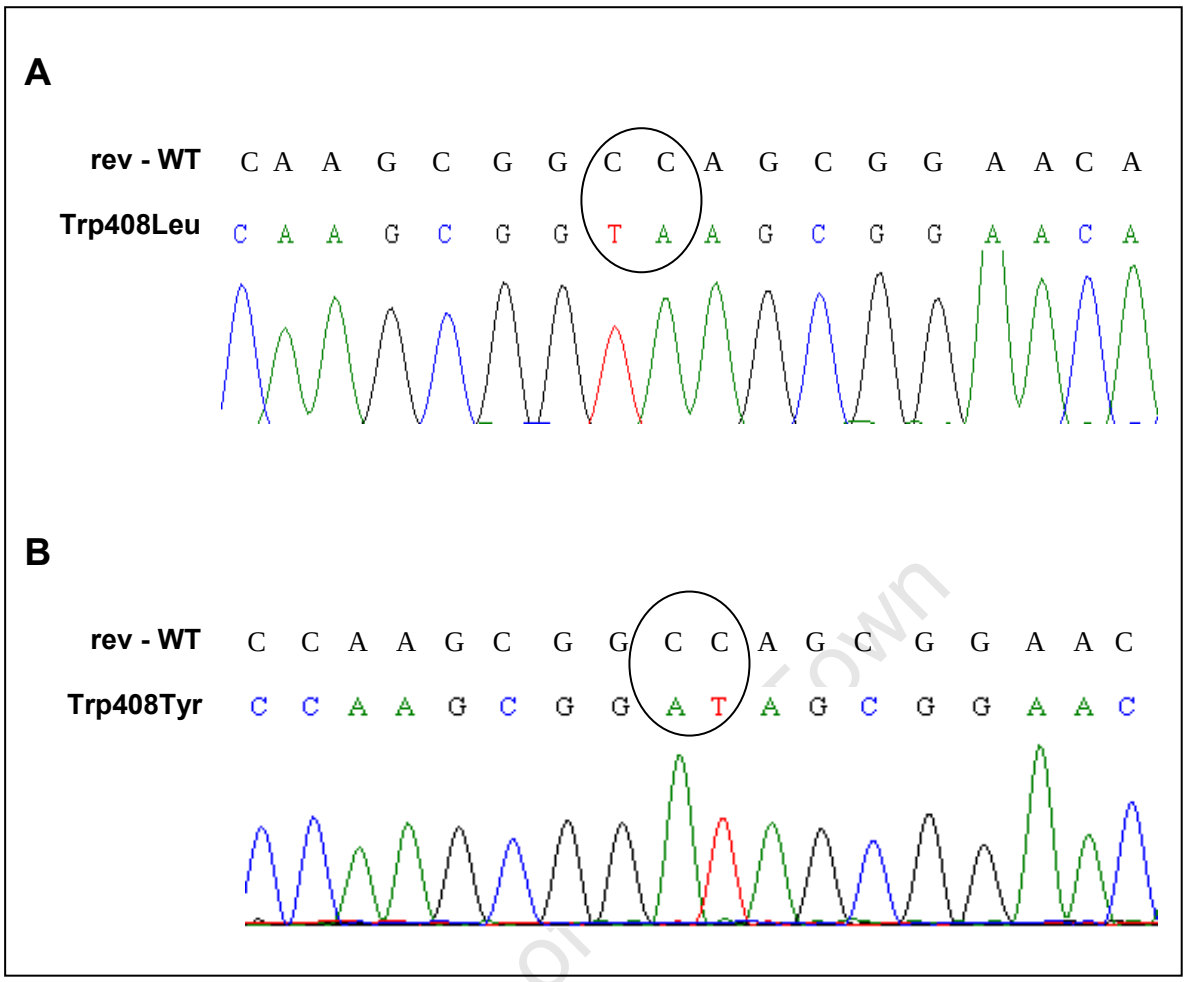

Figure 5.8: Partial direct sequencing of fragment 4 of the Trp-408 mutants: A) Trp408Leu using reverse primer vMxF4R; B) Trp408Tyr using reverse primer, vMxF4R. The altered bps are encircled.

University of Pretoria

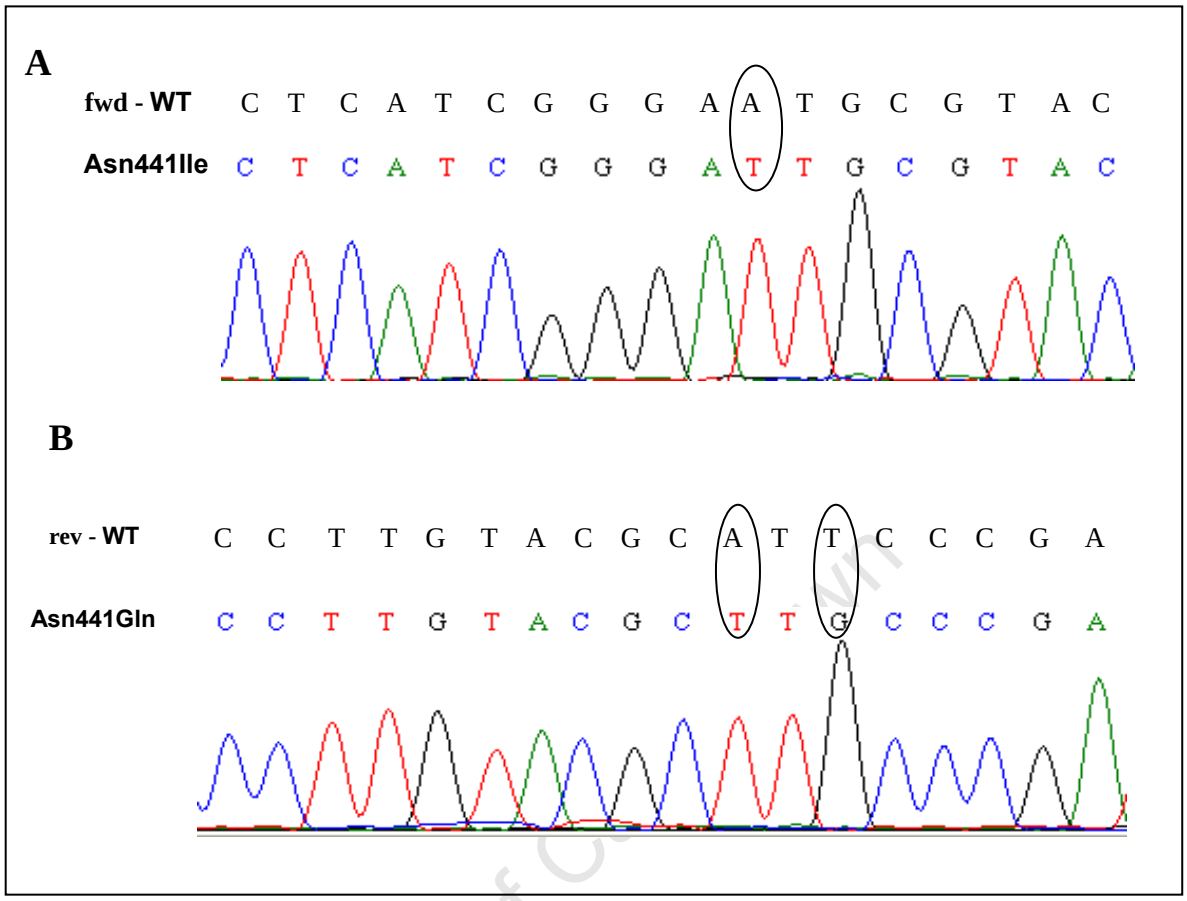

Figure 5.9: Partial direct sequencing of fragment 4 of the Asparagine 441 mutants: A) Asn441Ile mutant using primer vMxF4F; B) Asn441Ile using primer vMxF4R. The altered bps are encircled.

University of Cape Town

Expression and purification

Both WT and all 10 PPOX mutants were successfully expressed and purified by Talon metal affinity chromatography. Gradient SDS-PAGE confirmed a pure enzyme, M_r of 51000 Da as judged against molecular weight markers on SDS-PAGE (fig. 5.10). Table 5.2 shows a purification table for both WT and mutants.

SDS-PAGE

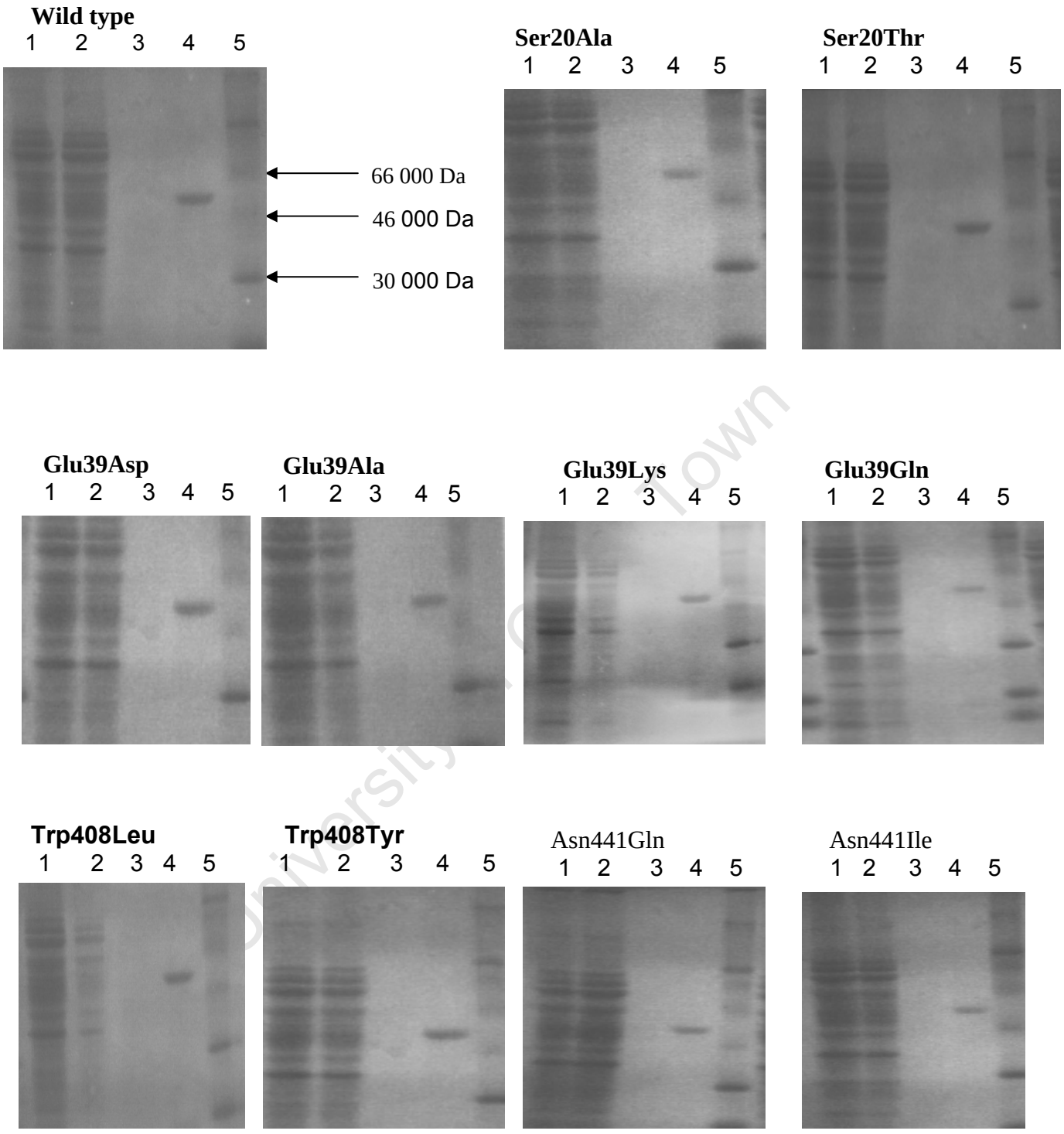

Figure 5.10: 7.5-17 % denaturing SDS-PAGE of the purification of wild type and mutant mxPPOX proteins. Lane 1 – load (5 µl protein) was loaded; lane 2 –void (5 µl) was loaded; lane 3 – wash (50 µl) was loaded; lane 4 – eluate protein (5 µl was loaded except in Glu39Gln and Glu39Ala where 50 µl was loaded); lane 5 – molecular weight marker (6 µl was loaded).

University of Cape Town

Table 5.2: Purification table showing yield, activity and recovery % of WT and mutant mxPPOX protein. Where result = 0, no activity was detected.

	Volume (ml)	Protein Concentration (mg/ml)	Total protein (mg/L)	Activity (nmol/mg/hr)	Total Activity (nmol/hr)	Recovery (%)
Wild type						
Load	28	13.67	383	4572	1749979	100
Void	35	8.26	289	398	115062	7
Wash	20	0.60	12	7320	85644	5
Eluate	2	1.50	3.45	71333	246099	14
Ser20Thr						
Load	30	11.40	342	1081	369750	100
Void	30	11.04	331	242	80025	22
Wash	30	0.71	21	1232	26232	7
Eluate	2	1.27	2.67	7063	18837	5
Ser20Ala						
Load	29	7.93	229.87	866	199085	100
Void	29	7.76	224.91	74	16748	8
Wash	30	0.50	14.88	83	1230	1
Eluate	1	0.59	0.47	4971	2336	1
Glu39Asp						
Load	30	14.50	435	10875	4730625	100
Void	30	13.98	419	9087	3811088	81
Wash	30	1.40	42	190	7997	0
Eluate	2	0.95	2.02	13555	27400	1
Glu39Lys						
Load	30	13.90	417	3	1379	100
Void	30	10.50	315	4	1280	0.48
Wash	22	0.37	7.85	35	274	0.10
Eluate	4	1.30	4.68	13	61	0.02
Glu39Gln						
Load	30	10.52	316	0	0	0
Void	30	10.28	309	0	0	0
Wash	40	0.99	40	0	0	0
Eluate	3	0.24	0.63	0	0	0
Glu39Ala						
Load	30	12.93	388	0	0	0
Void	30	12.83	385	0	0	0
Wash	30	0.47	14	0	0	0
Eluate	2	0.14	0.33	0	0	0
Trp408Leu						
Load	30	8.01	240	339	81450	100

University of Cape Town

	Volume (ml)	Protein Concentration (mg/ml)	Total protein (mg/L)	Activity (nmol/mg/hr)	Total Activity (nmol/hr)	Recovery (%)
Void	30	8.10	243	34	8148	10
Wash	30	1.71	51	79	4028	5
Eluate	2	0.90	1.34	37188	49980	61
Trp408Tyr						
Load	30	20.90	628	10252	6437294	100
Void	30	16.00	481	6583	3165588	49
Wash	30	4.60	59	1206	63857	0.99
Eluate	2	2.60	5.80	12464	71788	1.12
Asn441Ile						
Load	30	12.91	387	30	11580	100
Void	32	10.42	333	10	3392	29
Wash	30	0.62	19	54	998	8.61
Eluate	1	0.40	0.30	11541	3462	30
Asn441Gln						
Load	30	13.32	400	221	88500	100
Void	30	12.97	389	116	45000	51
Wash	30	0.91	27	143	3900	4.41
Eluate	1	1.65	1.90	19272	36524	41

University of Cape Town

Purification of human PPOX

With regards to the FAD-N(5) sulfite reactivity study we set out to purify hPPOX, to allow for comparative analysis. The HPPO-X/pTrcHis vector was kindly donated by Professor HA Dailey, University of Georgia, Athens, Georgia, USA. Previously this vector had been expressed and purification procedure optimized in our laboratory (Maneli *et al*., 2003). These optimized conditions and purification protocol were used in this study. A culture of *E. coli* cells with transfected HPPO-X/pTrcHis vector were expressed as described in appendix 4. This was followed by a 1 ml cell culture in 1 L LB media as previously described for mxPPOX for 22 hr at 30 ºC on shaker (appendix 14). Cells were harvested, lysed and subjected to TALON resin purification system as described above for mxPPOX. The protein was purified using buffers listed in appendix 14.2.

Human PPOX was successfully purified (fig. 5.11). A purification table is show in table 5.3

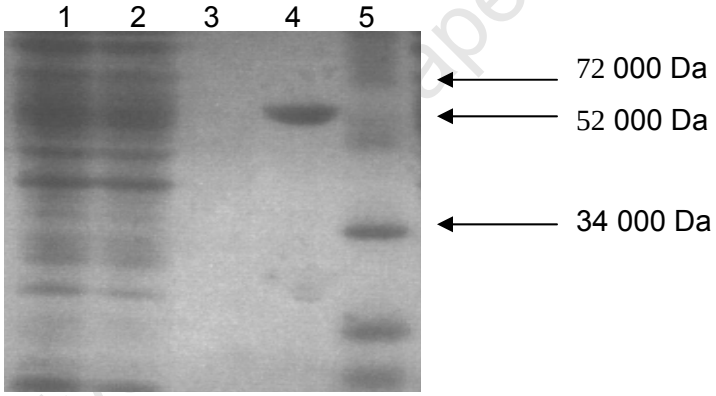

Figure 5.11: 7.5-17.5 % denaturing SDS-PAGE of purified wild type hPPOX protein. Lane 1 – load (5 µl loaded); lane 2 –void (5 µl loaded); lane 3 – wash (50 µl loaded); lane 4 – purified protein (5 µl loaded); lane 5 - molecular weight marker (7 µl loaded).

Table 5.3: Purification table showing yield, activity and recovery WT hPPOX protein

Human PPOX	Volume (ml)	Protein Concentration (mg/ml)	Total protein (mg/L)	Activity (nmol/mg/hr)	Total Activity (nmol/hr)	Recovery (%)
Load	30	5.6	168	4834	812160	100
Void	30	5.3	159	4129	656520	81
Wash	30	0.6	18	1076	19362	2
Eluate	1.04	0.56	0.58	26250	15288	2

Univ of Cape Town

Discussion

Site-directed Mutagenesis

QuickChange and the GeneEditor mutagenesis systems were successfully used to generate 9 and 1 PPOX mutants, respectively. In the GeneEditor, difficulty was experienced in obtaining growth in the overnight culture after the initial transfection. The antibiotic selection mix added to the overnight culture was reduced to 50 % (as was previously done in our laboratory (Maneli, 2002)). However, this still did not result in growth of cells. The steps before the overnight culture were also repeatedly troubleshot without success. Hence, the decision to change the method of site-directed mutagenesis from GeneEditor to QuickChange was made.

In this study, homogeneous, and soluble forms of mxPPOX were required for analysis and characterisation. Several mutants had low expression compared to wild type. IPTG induction had no effect on expression (data not shown). However, growth at 30 °C (rather than at 37 °C) improved expression. Yield was increased by doubling the number of cells inoculated in 1 L growth media. This was effective, and growth time was minimized to prevent the production of insoluble inclusion bodies (Kane & Hartley, 1988). Proteins were purified using metal affinity chromatography at 4 °C. In cases where expression of mutant protein was low, and non-tagged proteins bound to the resin, a 40 ml wash step (as opposed to the 20 ml wash) was included. With the exception of Trp408Leu, during purification, less than 50 % of target protein was recovered in both wild type and mutant proteins (table 5.2). Yields of all proteins purified protein varied considerably (table 5.2). Specific activity of the individual proteins is discussed in chapter 7.

The human PPOX was expressed using a prokaryotic expression system (*E. coli JM109*). Protein was then purified under the same conditions as mxPPOX, i.e. at 4 °C using 600 µl TALON resin. The addition of imidazole to the lysis buffer ensured non-specific binding of non-6X his tag protein, resulting in a low but pure yield of target protein. This resulted in the recovery of only 2 % of protein from the lysed sonicate. Nonetheless, a soluble active protein (M_r ± 52 000 Da) was purified and further analysed.

University of Cape Town

Conclusions

In our hands, the QuickChange mutagenesis system was more effective than the GeneEditor system in generating mxPPOX mutants.

Although, several mutants needed optimisation, both wild type and mutant proteins could be successfully expressed and purified using the Talon resin purification system.

Except in the case of Glu39Lys, acceptable protein yields were obtained, allowing for further analysis and characterisation detailed in the chapters to follow.

Human PPOX protein was expressed and purified and an acceptable yield was obtained, allowing for further analysis which is detailed in chapters 6 and 8.

University of Cape Town

CHAPTER 6

Spectral analysis of the FAD cofactor of *M. xanthus* PPOX

University of Cape Town

Introduction

As mentioned previously (chapter 2), the oxidation of protogen to proto requires the removal of six electrons, with FAD being the intermediate electron acceptor in this reaction. FAD is noncovalently bound to PPOX. In general, flavins can exist in three redox states (oxidised, semiquinone and reduced) as detailed in chapter 2 and the yellow colour, associated with oxidised FAD, is frequently utilised to determine its presence (Gadda *et al*., 1997; Lountos *et al*., 2009). Thus, we investigated the flavin binding in mxPPOX by measuring the UV/VIS spectrum of mutants and wild type. General spectral properties of oxidised FAD include two peaks at 375 nm and 450 nm, and FAD has an extinction coefficient of 11 300 $M^{-1}cm^{-1}$ (Whitby, 1954). Previously, Dailey and Dailey (1996a) reported the spectrum of FAD in mxPPOX wild type. In this chapter the flavin binding integrity in mxPPOX was determined by measuring the UV/VIS spectrum of mutants and compared to that of wild type.

Objectives

- To determine the relative amount of bound FAD in wild type and mutant mxPPOX by measuring absorption at a wavelength of 450nm.
- To investigate the spectral properties of FAD in wild type and mutant mxPPOX by performing a wavelength scan of purified protein.

University of Cape Town

Method

FAD quantitation

FAD was quantitated by measuring absorption at a wavelength of 450 nm in a UV/VIS absorption spectrophotometer. Absorbance at 450 nm was expressed as OD_{450nm}/mg protein/ml as previously reported from our laboratory, as well as Dayan and colleagues (Maneli *et al*., 2003; Dayan *et al*., 2010).

Wavelength scan

To analyse the potential effects of mutation of certain residues on FAD binding to the protein, PPOX UV/VIS spectra were recorded from 550 nm to 250 nm for both purified wild type and mutant PPOX (appendix 18). All spectroscopic readings were performed in 50 mM $NaPO_4$, pH 7.0 in 0.5 % Tween 20 for mxPPOX.

For some later comparative experiments (chapter 8) we required the absorption spectra for hPPOX. The human protein is more stable at pH 8.0 and therefore spectral readings were initially performed at pH 8.0, followed by readings at pH 7.0 to allow for comparative analysis with mxPPOX. Buffer used consisted of 50 mM $NaPO_4$ buffer, in 0.5 % n-octyl-β-D-glucopyranoside. In all cases the peaks and valleys obtained from the UV/VIS scan were noted and plotted using Microsoft Excel graph software.

University of Cape Town

Results

FAD quantitation

All mutants bound FAD to varying degrees (fig. 6.1) with the exception of Glu39Gln and Glu39Ala (no FAD detected).

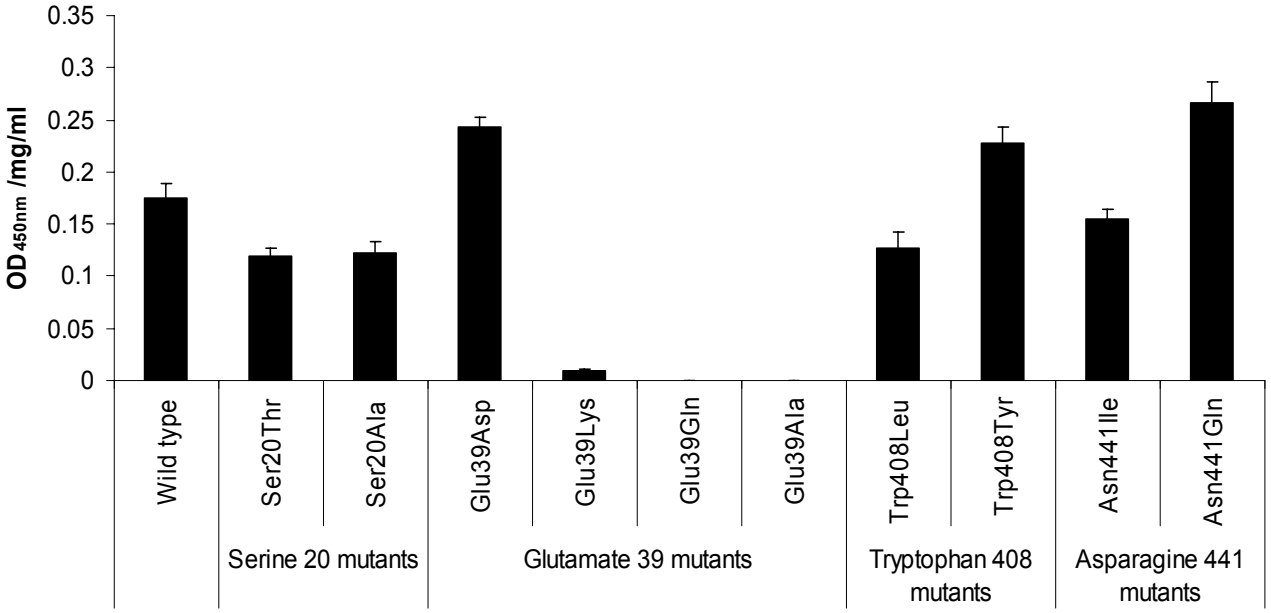

Figure 6.1: FAD quantitation in mxPPOX protein; FAD absorbance at 450 nm was expressed as OD_{450nm}/mg of protein/ml. Data=mean ± SD, n=3.

University

Wavelength scan

Absorption spectra, showing the typical FAD peak, in the cases where FAD bound can be seen in fig. 6.2 - 6.5. The following mutants: Ser20Thr, Glu39Asp, Trp408Leu, Trp408Trp, Asn441Gln, and Asn441Ile displayed a similar spectrum to that of wild type. Interestingly, Ser20Ala showed a spectral shift with a peak at 360 nm rather than the expected 375 nm peak (fig. 6.2). In the case of Glu39Gln and Glu39Ala no peaks were detected at 450 nm or at 375 nm.

Spectral readings for hPPOX were performed at both pH 8.0 (previously optimized condition; Maneli, 2002) and pH 7.0. Both readings showed the typical FAD spectrum displaying a typical peak at 450 nm and 375 nm as previously reported (Maneli *et al*., 2003). hPPOX also bound FAD similarly to mxPPOX (fig. 6.6).

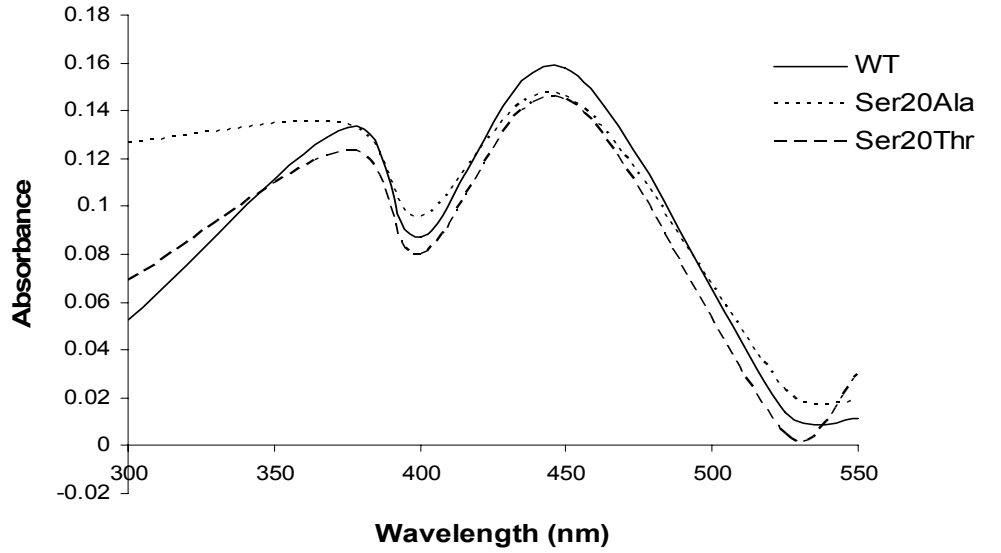

Figure 6.2: UV/VIS spectra (300 - 550 nm) of wild type mxPPOX (solid line), Ser20Thr (dashed lines) and Ser20Ala (dotted lines). Enzymes (~10 µM) were recorded in 50 mM $NaPO_4$ buffer pH 7.0, 0.5 % Tween 20.

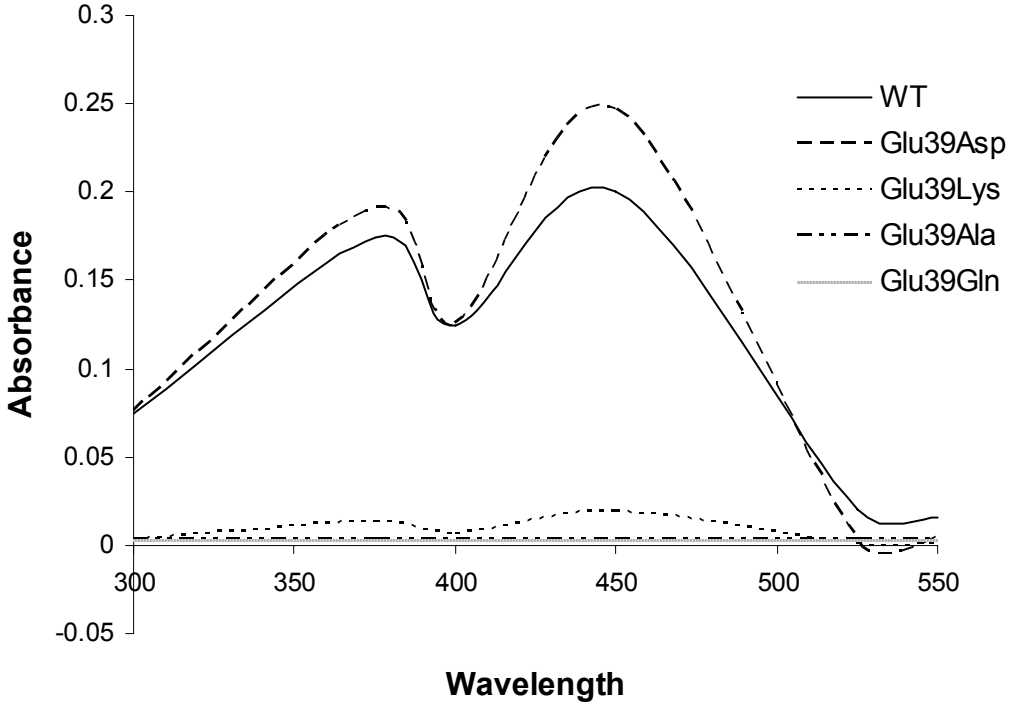

Figure 6.3: UV/VIS spectra (300 – 550 nm) of wild type (solid line), Glu39Asp (dashed line), Glu39Lys (dotted line), Glu39Ala (dotted and dashed line) and Glu39Gln (dotted maze line). Enzymes (~10 µM) were recorded in 50 mM $NaPO_4$ buffer pH 7.0, 0.5 % Tween 20.

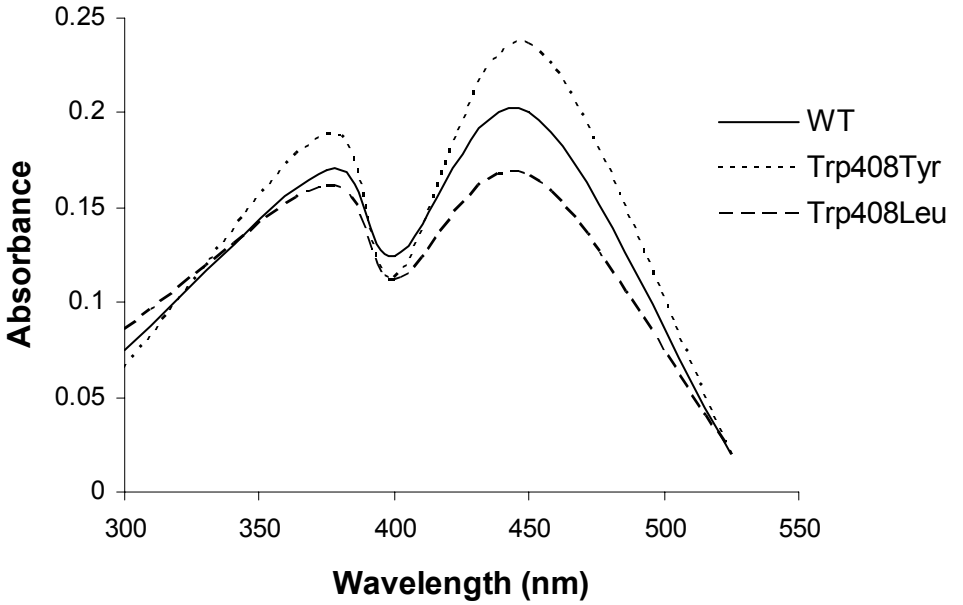

Figure 6.4: UV/VIS spectra (300 - 530 nm) of wild type (solid line), Trp408Tyr (dashed lines) and Trp408Leu (dotted lines). Enzymes (~10 µM) were recorded in 50 mM $NaPO_4$ buffer pH 7.0, 0.5 % Tween 20.

pe Town

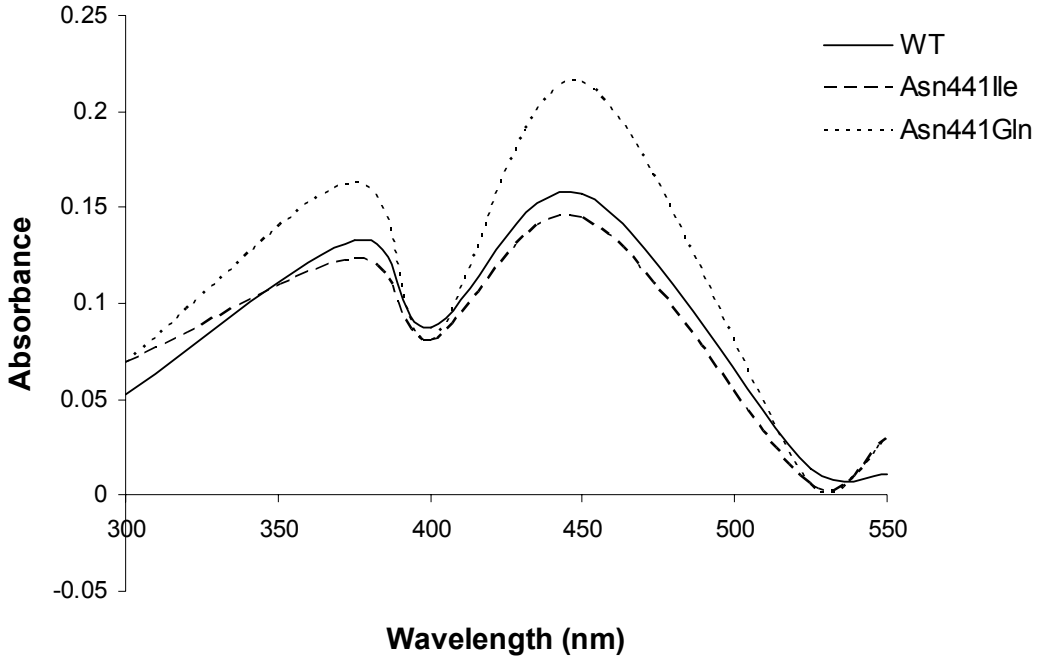

Figure 6.5: UV/VIS spectra (300 - 550 nm) of wild type (solid line), Asn441Gln (dashed lines) and Asn441Ile (dotted lines). Enzymes (~10 µM) were recorded in 50 mM $NaPO_4$ buffer pH 7.0, 0.5 % Tween 20.

Human PPOX FAD analysis

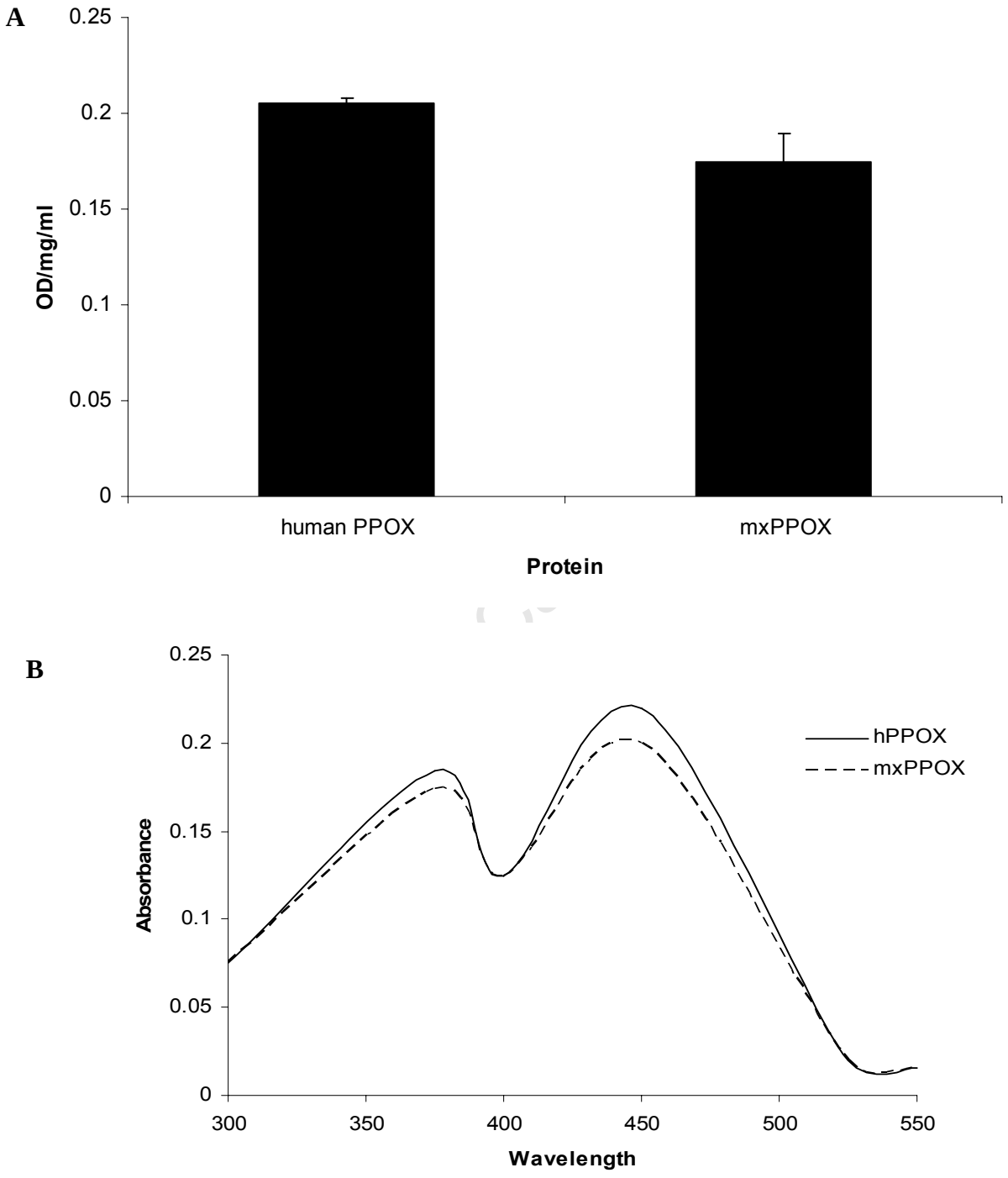

Figure 6.6: A) Bar graph showing FAD quantitation in hPPOX and mxPPOX. Plots are of mean ± S.D (n=3). B) Spectral analysis of hPPOX showing peaks at 450 nm and 375 nm. hPPOX spectrum (~10 μM) was recorded in 50 mM $NaPO_4$ buffer pH 7.0, in 0.5 % n-octyl-β-D-glucopyranoside.

Discussion

Flavoproteins have been studied over many years (Raszka & Kaplan, 1974; Massey & Hemmerich, 1980; Ghisla & Massey, 1989; Edmondson *et al*., 2001; Yin *et al*., 2001; Efimov & McIntire, 2004; Zhao & Jorns, 2006; Dong *et al*., 2008) and previous studies reveal PPOX to be membrane associated and to require a noncovalently bound FAD cofactor for catalysis (Camadros *et al*., 1994; Dailey *et al*., 1994; Dailey & Dailey, 1996a; Dailey & Dailey, 1996b; Maneli, 2002; Heinemann *et al*., 2007). PPOX crystal structures have confirmed this (Koch *et al*., 2004; Corradi *et al*., 2006; Qin *et al*., 2010; Qin *et al*., 2011).

M. xanthus and human PPOX

FAD in solution displays typical UV/VIS spectra with peaks at 450 nm and 375 nm. Both wild type mxPPOX and hPPOX have this typical FAD spectrum. The 450 nm peak is higher than the 375 nm peak indicating an oxidized FAD, and is in agreement with earlier FAD PPOX studies (Dailey & Dailey, 1996; Maneli et al., 2003).

Serine 20

Serine 20 was mutated to a threonine and an alanine. Threonine is a conservative change (polar neutral), and has a similar structure to serine. Alanine, also of similar size, is a nonpolar neutral residue. In Ser20Ala, although this mutant bound FAD (0.7 X that of wild type), the UV/VIS spectrum shows a spectral shift from 375 nm to 360 nm (fig. 6.2); the 450 nm peak is unaltered. This alteration of the peak at 375 nm may be explained by the change in polarity. This alteration could also imply that the integrity of the bound FAD has been altered. The UV/VIS spectrum of Ser20Thr was similar to that of wild type and this mutant was also able to bind FAD (0.7 X that of wild type). Being a conservative change, the polar side chain of threonine is able to form polar interactions with the FAD phosphate groups (as predicted in the PyMol mutagenesis simulation in chapter 4, fig. 4.1). The interaction of serine with FAD is via its polar side chain groups. As discussed in chapter 4, Ser-20 has three hydrogen bond interactions with the phosphate group of FAD. These interactions are maintained in Ser20Thr. However, in Ser20Ala, the replacement of the polar side chain results in an inferior FAD interaction (chapter 4, fig. 4.1). It is important to note that although serine is the only residue to interact via its side chain with the phosphate groups, it is not the only residue interacting with the phosphate group. Therefore, compromising Ser-20 interaction could result in

University of Cape Town

the remaining phosphate-protein interactions compensating for Ser-20's "missing link". Judging from the spectra of these mutants, a polar group is more favourable at this position.

Glutamate 39

Glutamate is a polar negative residue that interacts with the ribose ring of FAD; this conserved residue is the only residue interacting with the FAD ribose ring (hydrogen bond interactions). In this study Glu-39 was mutated to an aspartate (polar negative, conservative change), lysine (polar, positive), glutamine (polar, neutral) and alanine (nonpolar, neutral). Glu39Asp bound FAD (1.4 X that of wild type). Another mutant that bound FAD to some extent was Glu39Lys (0.06 X that of wild type). PyMol simulation in chapter 4, revealed this slightly bulky mutant to have inferior interaction with FAD. In chapter 4 we discussed the interaction of Glu-39 with the ribose ring of FAD. As mentioned, Glu-39 makes two hydrogen bond interactions with the FAD ribose ring. Although the PyMol mutant simulation revealed that Glu39Asp does not interact with FAD this mutant bound FAD 1.4 X more than wild type. This may however, be explained, as aspartate and glutamate, although different in size, have similar chemical properties.

In the case of Glu39Gln and Glu39Ala no FAD bound. This implies that the complete removal of the FAD-ribose ring interaction may compromise the remaining FAD interactions (such as interaction with the adenine ring, ribityl chain, isoalloxazine ring, etc). Another possibility is that the remaining interactions are present, but insufficient to maintain the FAD bound, hence FAD dissociates readily (this phenomenon has previously been proposed (Dailey & Dailey, 1996)).

Tryptophan 408

In various flavin oxidases a tryptophan residue is seen near the FAD isoalloxazine ring (Binda et al., 1999; Neeli et al., 2005). This residue is believed to stabilize the isoalloxazine ring during catalysis. In this study Trp-408 was mutated to a leucine (nonpolar linear) and a tyrosine (polar aromatic). Both mutants bound FAD, (0.7 X and 1.3 X that of wild type for Trp408Leu and Trp408Tyr, respectively), similar spectra to wild type mxPPOX. The 2-D schematic view of mtPPOX and bsPPOX show a tryptophan near the isoalloxazine ring (table 2.1). However, in mxPPOX, although Trp-408's side chain is orientated towards the nonpolar ring of the FAD isoalloxazine ring, Trp-408 is positioned slightly further away from the isoalloxazine ring, and based on the

University of Cape Town

difference in distance/positioning, could have a different role in mxPPOX. Nevertheless, it appears that the polar aromatic group is favoured at this postion with regards to the amount of FAD bound.

Asparagine 441

Asn-441 is a polar neutral residue involved in stabilizing the ribityl chain of FAD. In this study asparagine was mutated to an isoleucine (nonpolar, neutral) and a glutamine (polar, neutral). Asn441Ile bound FAD similarly to wild type (0.9 X that of wild type) while Asn441Gln bound 1.5 X that of wild type. The UV/VIS spectra of both mutants were similar to that of wild type implying that change in polarity at this region does not affect the FAD spectrum. PyMol simulation shows that Asn-441 makes two hydrogen bond interactions with the FAD ribityl group. PyMol mutant simulation revealed that Asn441Gln mutant interacts with the phosphate rather than the ribityl chain. Interestingly, this residue showed superior FAD binding to wild type. PyMol simulation of Asn441Ile showed that isoleucine was unable to make a hydrogen bond via its side chain with the ribityl chain of FAD, suggesting inferior FAD interaction. Since both mutants were able to bind FAD, it is likely that Asn-441 is not involved in FAD binding but rather in stabilizing and orientating FAD.

University of Cape Town

Conclusions

Wild type mxPPOX and hPPOX both have a typical FAD spectrum, confirming all previous studies.

Ser-20 does not affect FAD binding significantly, but could be involved in the integrity of FAD binding.
A polar group is favoured at position 20; compromising Ser-20's interaction with FAD could result in the remaining phosphate-protein interactions compensating for Ser-20's "missing link".

Glu-39's interaction with FAD plays a critical role in the binding of FAD in mxPPOX, as non-conservative replacements resulted in insufficient FAD binding.
A glutamate or an aspartate (polar negative group) residue is favoured in this position.

Although tryptophan is considered vital in stabilizing the FAD isoalloxazine ring, in related and unrelated proteins, based on its position and unaltered FAD spectrum, in mxPPOX Trp-408 appears to have a different role.
The polar aromatic mutant is favoured at this position with regards to the amount of FAD bound.

Asn-441 could be involved in the stabilizing rather than the binding of FAD.

University of Cape Town

CHAPTER 7

Kinetic characterisation of *M. xanthus* PPOX

University of Cape Town

Introduction

In 1996, Dailey and Dailey characterised mxPPOX wild type protein activity and behaviour (Dailey & Dailey, 1996a). The K_M and k_{cat} for protogen was reported to be 1.6 μM and 5.2 min^{-1}, respectively. More recently, studies have characterised naturally occurring VP-causing mutations, including some that may affect FAD binding such as Gly11Asp, Gly11Ser, Glu34Val, Asp349Ala, Ser350Pro, Gly448Arg, Ser450Pro, and Gly453Arg (chapter 2) (Qin et al., 2011). With respect to Glu-34, equivalent to mxPPOX Glu-39, which is analysed in this study, mutation of this polar negative charge to a nonpolar neutral residue (valine) resulted in inferior binding of FAD to protein. In this chapter we analyse the activity of both wild type and mutant mxPPOX in order to assess the effect of mutation on the activity of protein in the case of altered, as well as unaltered, FAD binding capacity.

University of Cape Town

Experimental difficulties in assaying protogen oxidase activity

It is appropriate, at this point, to highlight a primary experimental difficulty when working with PPOX. This limitation has made it difficult to unequivocally elucidate the sequential steps involved in the catalytic reaction. Protogen, the substrate, is highly labile and spontaneously auto-oxidises in vitro. In fact, for many years it was thought that protogen randomly autooxidized to proto in the mitochondria, without the aid of an enzyme (Jordan, 1990).

Thus, in laboratories working on PPOX, including ours, substrate, protogen, has to be freshly generated by reducing commercially available proto (appendix 17), normally using sodium-mercury amalgam. Substrate can therefore not be used over a long time frame, nor stored successfully, nor do workers relish working with mercury. These limitations have not only made the successful assay of PPOX difficult, they have also made it difficult to crystallize enzyme-substrate complex. Detailed knowledge on the precise, likely catalytic reaction of PPOX, is relatively limited, at least compared to our knowledge of the reaction mechanisms of most of the other haem biosynthetic enzymes.

Other reducing agents include palladium and sodium borahydrate. In the case of palladium at ambient temperature and pressure in the dark, palladium is able to

catalyse the reduction of proto, however, it is highly toxic (Phillips et al., 2009). Sodium borahydrate has been used in our laboratory and proved to be less efficient.

In this chapter we establish the kinetic parameters of both wild type and FAD-associated mutants of mxPPOX (described in the previous chapters) in order to determine the effect of mutations on the protein.

Objectives

- To determine activity and kinetic constants of both wild type and mutant mxPPOX proteins
- To determine the effect of temperature on enzyme activity by measuring T½ on wild type and mutant proteins.

University of Cape Town

Method

PPOX activity assay

Activity was assessed by measuring the formation of protoporphyrin IX from protoporphyrinogen IX (appendix 17; Meissner, 1986). This activity was determined by measuring product formation spectrofluorimetrically; at excitation and emission wavelengths of 405 nm and 634 nm, respectively. A reaction comprised of assay buffer, enzyme (with additional FAD), and was initiated by the addition of substrate. A negative control (blank) was prepared for each enzyme reaction by using an equivalent amount of bovine serum albumin (BSA) in place of enzyme. Assays were performed under-dimmed lighting conditions in a circulating water bath at 37 °C. Assays were performed no less than three times on different days using different enzyme preparations. Results are presented as mean ± standard deviation.

University of Cape Town

Derivation of kinetic constants

The constant velocity formation of proto from protogen in the substrate range of 0.1 - 25 µM was measured for a total of 40 min at 10 min intervals. Substrate concentrations were plotted against velocity values. Calculated values were determined using the computerised Gauss-Newton iterative, non-linear curve fitting procedure (appendix 17). Kinetic constants, V_{max}, (maximal velocity), and K_M, (the substrate concentration at which V_{max} is halved), were extrapolated from the graph. The value of k_{cat} (catalytic turnover rate) was calculated from V_{max}.

Determination of T½

Appropriate aliquots of wild type or mutant mxPPOX of relevant concentrations (~10 -20 µM) were incubated at a specific temperature for 5 min, and then placed on ice immediately. Specific activity was then determined (at excess substrate concentration). The temperature range examined was from 30 - 65 °C and T½ calculated graphically. T½ is defined as the temperature that reduces enzyme activity to half its maximal velocity.

pH gradient

In order to further investigate the abnormal spectrum of Ser20Ala (fig. 6.2, chapter 6), a pH gradient assay was performed on both Ser-20 mutants and wild type protein. The effect of pH on activity was determined over the pH range of 6 - 7 using phosphate buffer (pH range 6 -7) and Tris/HCl buffer (pH range 7.2-9) buffers (appendix 17).

Results

Table 7.1 lists PPOX specific activity (wild type and mutants). All mutants with the exception of Trp408Leu, had less than 50 % residual activity. Table 7.2 shows the kinetic constants as well as T½ of both wild type and mutant mxPPOX. All mutants except Ser20Thr and Asn441Gln had a slightly increased T½ to that of wild type. Both wild type and Ser20Thr had pH optimum of 8.1 while Se20Ala has a pH optimum of 7.5 (fig. 7.1).

Effect of FAD on catalytic activity

Addition of exogenous FAD (5 - 50 µM) to the assay did not increase the activity of the WT or any of the mutants (data not shown).

University of Cape Town

Table 7.1: Specific activity of PPOX WT and mutant proteins

Protein	Specific activity	
	(nmol/mg/hr)	(%) of WT
WT	71333	100
Ser20Thr	7063	10
Ser20Ala	4971	7
Glu39Asp	13555	19
Glu39Lys	61	0.1
Glu39Gln	0	0
Glu39Ala	0	0
Trp408Leu	37188	52
Trp408Tyr	12464	18
Asn441Ile	11541	16
Asn441Gln	19272	27

Table 7.2: Kinetic parameters of wild type and mutant mxPPOX proteins. ND – not determined. Results determined as mean ± SD (n=3).

n=3	K_M (µM)	k_{cat} (s^{-1})	k_{cat}/K_M ($µM^{-1}.s^{-1}$)	T½
Wild type	0.38 ± 0.03	0.72 ± 0.06	1.88	50 ± 0.2
Ser20Thr	1.17 ± 0.04	0.78 ± 0.06	0.67	50.5 ± 0.5
Ser20Ala	0.92 ± 0.01	0.41 ± 0.02	0.45	56 ± 0.7
Glu39Gln	ND	ND	ND	ND
Glu39Ala	ND	ND	ND	ND
Glu39Asp	0.59 ± 0.03	1.52 ± 0.08	2.58	55 ± 0.1
Glu39Lys	ND	ND	ND	ND
Trp408Leu	0.51 ± 0.05	0.14 ± 0.01	0.28	52 ± 0.2
Trp408Tyr	1.49 ± 0.09	0.23 ± 0.04	0.15	56 ± 0.01
Asn441Ile	0.51 ± 0.02	0.08 ± 0.001	0.16	56 ± 0.5
Asn441Gln	0.75 ± 0.01	0.32 ± 0.01	0.43	50 ± 0.5

of Cape Town

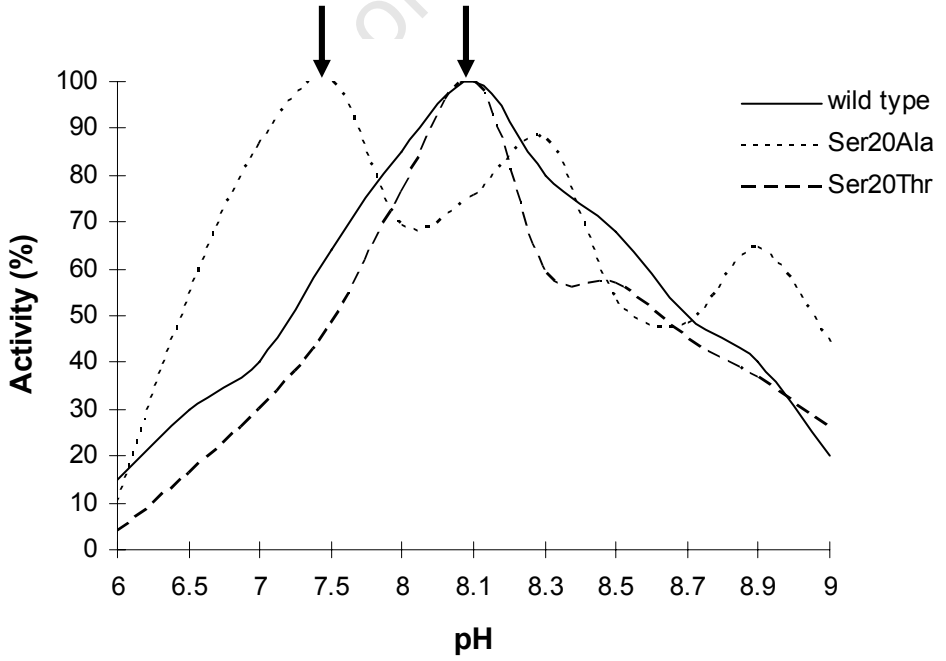

Figure 7.1: A pH versus percentage of activity plot showing the pH optimisation of wild type (solid line), Ser20Ala (dotted line), Ser20Thr (dashed line). Arrows indicate the pH optimum.

Discussion

Serine 20

In this chapter the activity and kinetic parameters of mutants were analysed and compared to wild type activity (table 7.2). Ser20Thr had a similar catalytic turnover rate as wild type. However, it had a weaker substrate affinity; therefore, the overall catalytic efficiency was decreased compared to wild type (table 7.2). Ser20Ala also had an increased K_M compared to wild type, affecting its catalytic efficiency. In addition Ser20Ala had an increased T½ suggesting that this mutant has an influence on the structure of the active site.

Nineteen prokaryotic sequences of PPOX were aligned (appendix 21) using the ClustalW multiple sequence alignment software. The alignment revealed that Ser-20, part of the nucleotide binding motif reported by Dailey and Dailey (1998), is conserved. Analysis revealed that at this position either a serine or an alanine is favoured (Dailey & Dailel, 1998). In this study, Ser-20 was mutated to both an alanine (nonpolar neutral) and a threonine (polar neutral). Surprisingly, Ser20Ala bound FAD (0.7 X that of wild type), even with the removal of the polar side chain which the PyMol simulation suggested to be vital for FAD interaction. However, a spectrophotometric scan from 550 -300 nm showed a shift from the 375 nm peak in the case of Ser20Ala. It is possible that the orientation of the bound FAD is altered in this mutant. This alteration, however, could result in the accommodation of additional water molecules in the FAD binding region to compensate for the lost FAD protein interactions (as seen in UROD, chapter 1). This compensation may also only be triggered upon substrate binding as is seen in the LigPlot diagram of mxPPOX with an occupied active site (fig. 2.8, chapter 2). Hence, the activity of the enzyme is unaffected in Ser20Ala compared to the conservative Ser20Thr.

In order to investigate the spectral shift in Ser20Ala, a pH optimum analysis was performed on wild type mxPPOX and both serine mutants; as change in polarity is frequently associated with spectral shift (Gadda *et al*., 1997). A study of the pH optima revealed both wild type and Ser20Thr to have a pH optimum of 8.1 whilst Ser20Ala, has a lower pH optimum at 7.5 (fig. 7.1), suggesting that the polar groups interaction with FAD-phosphate stabilised the bound FAD. Furthermore, Ser20Ala has a T½ of 56 °C showing that this protein has an influence on the structure of the active site. The

University of Cape Town

increase in T½ could also be attributable to the same properties resulting in the spectral shift. Ser20Thr had a similar T½ to wild type of 50 °C. These results confirm the alignment findings of Dailey and Dailey (1998) which revealed that an alanine is often replaces serine in other species.

Glutamate 39

Interaction of a glutamate with the ribose ring of FAD is conserved in both PPOX as well as other oxidases in the same superfamily as PPOX. The consensus sequence suggests that a glutamate or an aspartate is vital at this position. Interestingly, kinetic analysis of Glu39Asp (negative replacement) shows an increase in both k_{cat} and catalytic efficiency (k_{cat}/K_M). This suggests that a polar negatively charged residue is favoured to interact with the ribose ring. Although the T½ of Glu39Asp revealed an increased T½, (55 °C compared to the wild type's 50 °C), this change, which could be associated with structural change in the active site, did not appear to have any major effect on substrate affinity (table 7.2). As expected, removal of the negative charge resulted in a dramatic reduction in specific activity (hence kinetic parameters not determined) suggesting the importance of the negative group's interaction with the ribose ring of FAD.

Tryptophan 408

A tryptophan residue is frequently seen near the isoalloxazine ring of FAD. This residue, which is near the aromatic nonpolar half of the isoalloxazine ring, has been hypothesized to interact via an aromatic-aromatic interaction to stabilize the bound FAD in other non-related proteins. In mxPPOX, although Trp-408 aligns with the tryptophan residues in bsPPOX and mtPPOX, the positioning of Trp-408 is further away from the isoalloxazine ring, suggesting as mentioned earlier, that in mxPPOX Trp-408 could have an alternative role. Despite the removal of the aromatic ring, Trp408Leu showed a higher specific activity and a better susbtrate affinity (K_M) compared to Trp408Tyr. In Trp408Leu, this linear, nonpolar replacement led to a lower catalytic turnover rate than wild type and slightly increased T½ (table 7.2).

This suggests that the nonpolar property of leucine is favoured at this position with regards to activity of the enzyme; however, the removal of the aromatic group did not result in an optimally functioning enzyme. In the polar replacement (Trp408Tyr) both substrate affinity and enzyme efficiency was dramatically reduced compared to wild-type. Spectral analysis of Trp408Tyr in chapter 6 revealed that this polar aromatic is

University of Cape Town

favoured with regards in the amount of FAD that bound. Kinetic analysis reveals, however, that this mutant does not function as optimally as wild type. The Trp408Tyr mutant had bound substrate less efficiently (~4 fold decrease) than wild type while Trp408Leu bound substrate similarly to wild type. This highlights the importance of a nonpolar residue's interaction with the substrate. Trp-408 could possibly be involved in FAD/substrate stability during substrate binding or catalysis.

Asparagine 441

Asn-441 appears to interact with its side chain to stabilize the ribityl chain of the FAD. In the inhibitor-bound active site, several water molecules are seen interacting with Asn-441 to secure the ribityl chain which is directly linked to the isoalloxazine ring, the active part of the FAD. In this study, Asn-441 was mutated to an isoleucine, a neutral nonpolar residue, and a glutamine, a neutral polar residue. Assessment of the kinetic behaviour revealed that both mutants were less efficient that wild type. The Asn441Ile showed an 11-fold decrease in catalytic efficiency compared to wild type as well as an increase in T½. Asn441Gln, although less efficient than wild type protein, was more catalytically efficient than the Asn441Ile mutant. This highlights the importance of a polar side chain for efficiency and interaction with the ribityl chain of FAD. This conclusion is strengthened by our finding (previous chapter) that Asn-441 is not involved in binding but rather in the alignment of FAD, as both mutants bound.

University of Cape Town

Conclusions

This study confirms the FAD binding consensus sequence alignments which suggest that a serine or an alanine is preferred at position 20. Ser-20's polarity plays a role in orientating FAD and we suggest that water molecules could be aiding the optimal functioning of FAD in mxPPOX.

Interaction of Glu-39 with the FAD-ribose is critical for FAD binding in mxPPOX and we show that a polar negative group is favoured at position 39 to interact with the ribose ring of FAD.

In the case of mxPPOX we propose that Trp-408 has a different positioning (compared to related protein- bsPPOX and mtPPOX - and unrelated protein such as MAO). Results suggest that Trp-408 is involved in substrate stability during catalysis.

Asn-441's polarity appears vital for FAD-ribityl chain stability.

CHAPTER 8

FAD-N(5) sulfite reactivity and the effect of substrate oxidation on oxygen consumption in *M. xanthus* PPOX*

University of Cape Town

* This Chapter is presented as two parts, one dealing with sulfite reactivity and the second with oxygen consumption.

FAD-N(5) sulfite reactivity

Introduction

Several studies to date have shown that many flavoproteins react with sulfite (Massey, 1994; Massey *et al*., 1969). As described in chapter 2, the N5-sulfite formation indicates the ability of the FAD to be stabilized via a positive charge during reduction. There are reports indicating that some flavoproteins show no reactivity with sulfite, even at high sulfite concentrations (Massey *et al*., 1969). Therefore it was suggested that only flavoproteins with high reactivity toward O_2 i.e. the flavoprotein oxidases, react with sulfite. Still yet, some of these oxidases have been shown to lack reactivity with sulfite (Massey *et al*., 1969). This shows that the FAD-sulfite reactivity is a complex reaction that requires much elucidation.

In short, when sulfite reacts with FAD the visible absorption spectrum of the FAD-enzyme complex is “bleached”, similar, but not identical to a reduced flavoprotein (Massey *et al*., 1969). This bleaching phenomenon is used as an indication of oxidation reduction potential. It is considered a helpful technique in structure function studies of flavoproteins, as the redox potential is determined in the absence of substrate.

In a recent study on cholesterol oxidases, the residues interacting with the N(5) of the FAD isoalloxazine ring were shown to play a role in the movement of O_2 from the protein exterior to its point of activation (Kuhn *et al*., 2007; Chen *et al*., 2008). In mxPPOX and hPPOX these residues are likely to be asparagine-63 (a polar neutral) and arginine-59 (polar positive), respectively (chapter 2). Here we assess the reactivity of mxPPOX with sulfite in order to establish whether, like in other oxidases, sulfite reactivity is present or not. We also compared its reactivity with that of hPPOX.

University of Cape Town

Objectives

- To study the reactivity of sulfite with wild type mxPPOX and hPPOX.

Method

Reactivity with sulfite

Reactivity with sulfite was performed using commercial FAD, and recombinant, purified mxPPOX and hPPOX. In order to determine PPOX reactivity with sulfite, a free stock solution of 2 M sodium salt (Na_2SO_3) was used. The sodium salt was dissolved in elution buffer (50 mM NaPO4, 100 mM NaCl, 10 % glycerol). Different detergents were used namely 0.5 % Tween 20 for both commercial FAD and mxPPOX and 0.5 % N-octyl-β-D-glucopyranoside was used for hPPOX. A total of 10 µM protein or commercial FAD was incubated 37 ºC (15 - 30 min). Aliquots of Na_2SO_3 (50 - 300 mM, as typically used in the literature, Gadda et al., 1997) were then added to enzyme (10 µM) and absorbance at 450 nm was determined over time, as reported by Gadda and colleagues (1997). The spectrum of the reaction was then measured from 550 - 300 nm in order to observed the “bleached” FAD band. Reactions were performed at 37 °C over 10 - 120 min (appendix 18.2).

University of Cape Town

Results

When commercially obtained FAD was incubated at varying concentrations of Na_2SO_3, a decrease in absorbance at 450 nm was seen as well as a “bleached” band in the 450 nm range (fig. 8.1). In mxPPOX no “bleaching” phenomenon was observed (see page 56). Indeed, a wavelength scan revealed no “bleaching” of the band even after a 2 hr incubation at a high [Na_2SO_3] (300 mM, fig. 8.2). In hPPOX, after incubating for 30 min, a decrease in absorbance was observed at 450 nm. Absorption spectrum revealed a “bleaching” in the 450 nm range. At high sulfite concentrations (300 mM) an abnormal increase in absorbance was seen at 450 nm (fig. 8.3).

Commercial FAD

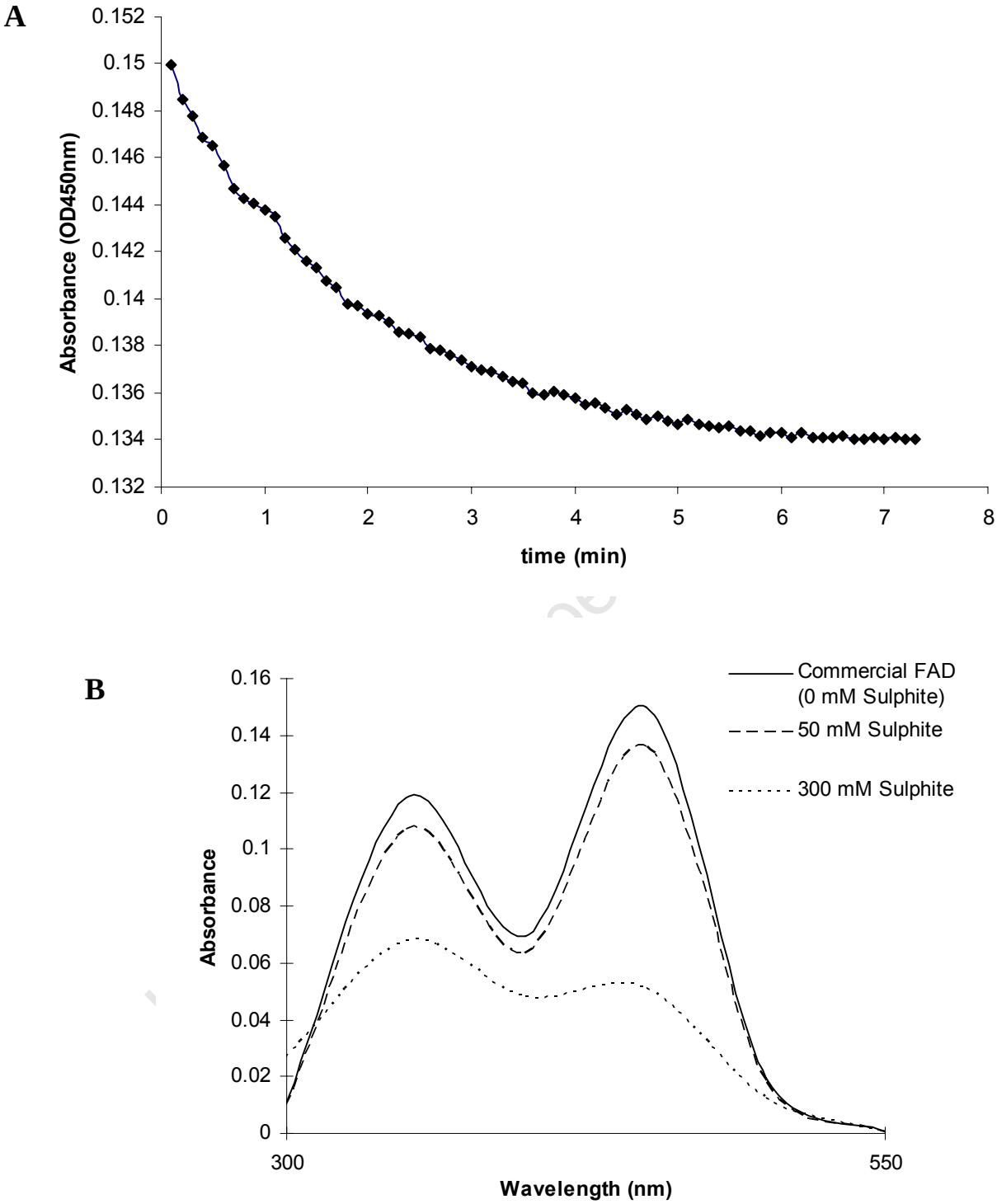

Figure 8.1: A) The spectral measurement of sulfite [50 mM] reactivity with commercial FAD (~10 μM). Absorbance (OD_{450nm}) versus time plot. B) FAD spectra showing a normal (solid line) and two bleached spectra upon addition of 50 mM (dash line) and 300 mM (dotted line) [sulfite].

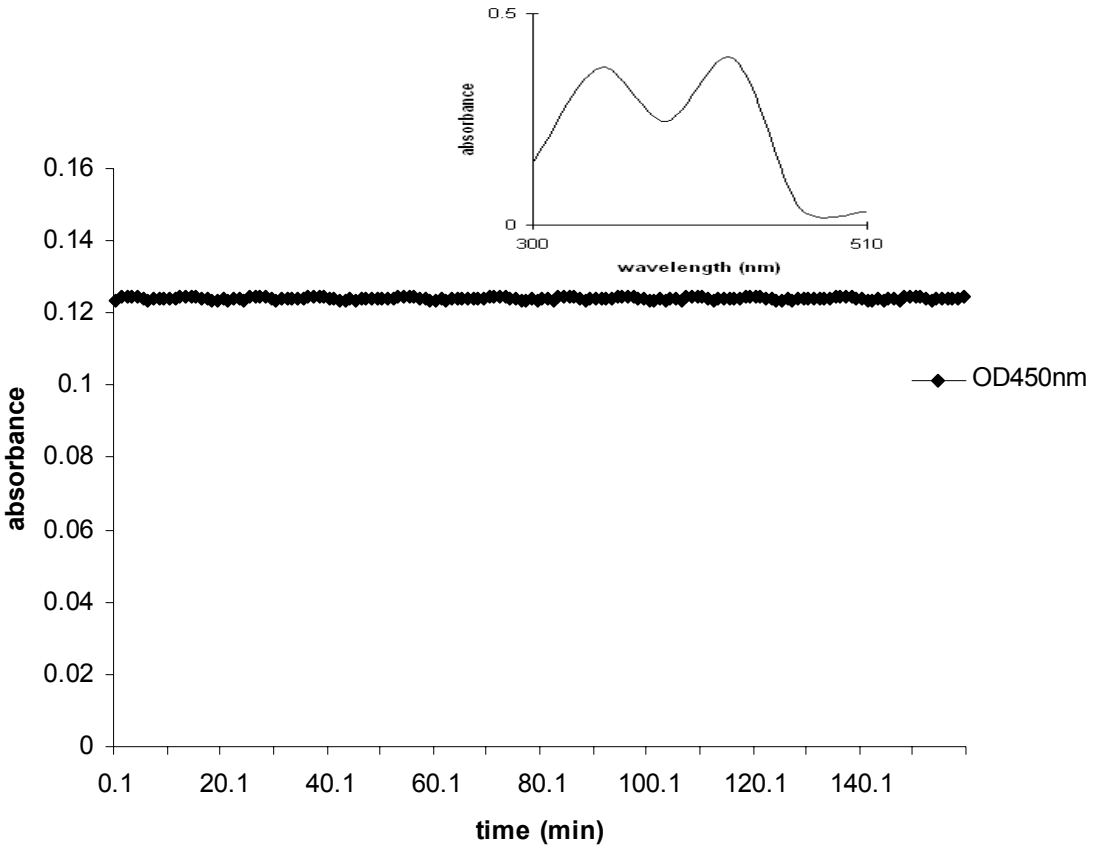

Figure 8.2: Spectral measurement of mxPPOX reactivity with sulfite (300 mM). A final concentration of 10 µM protein was used. Absorbance (OD_{450nm}) versus time plot, showing no increase in absorbance. Insert: FAD spectra showing an "unbleached" (normal) spectrum.

University of

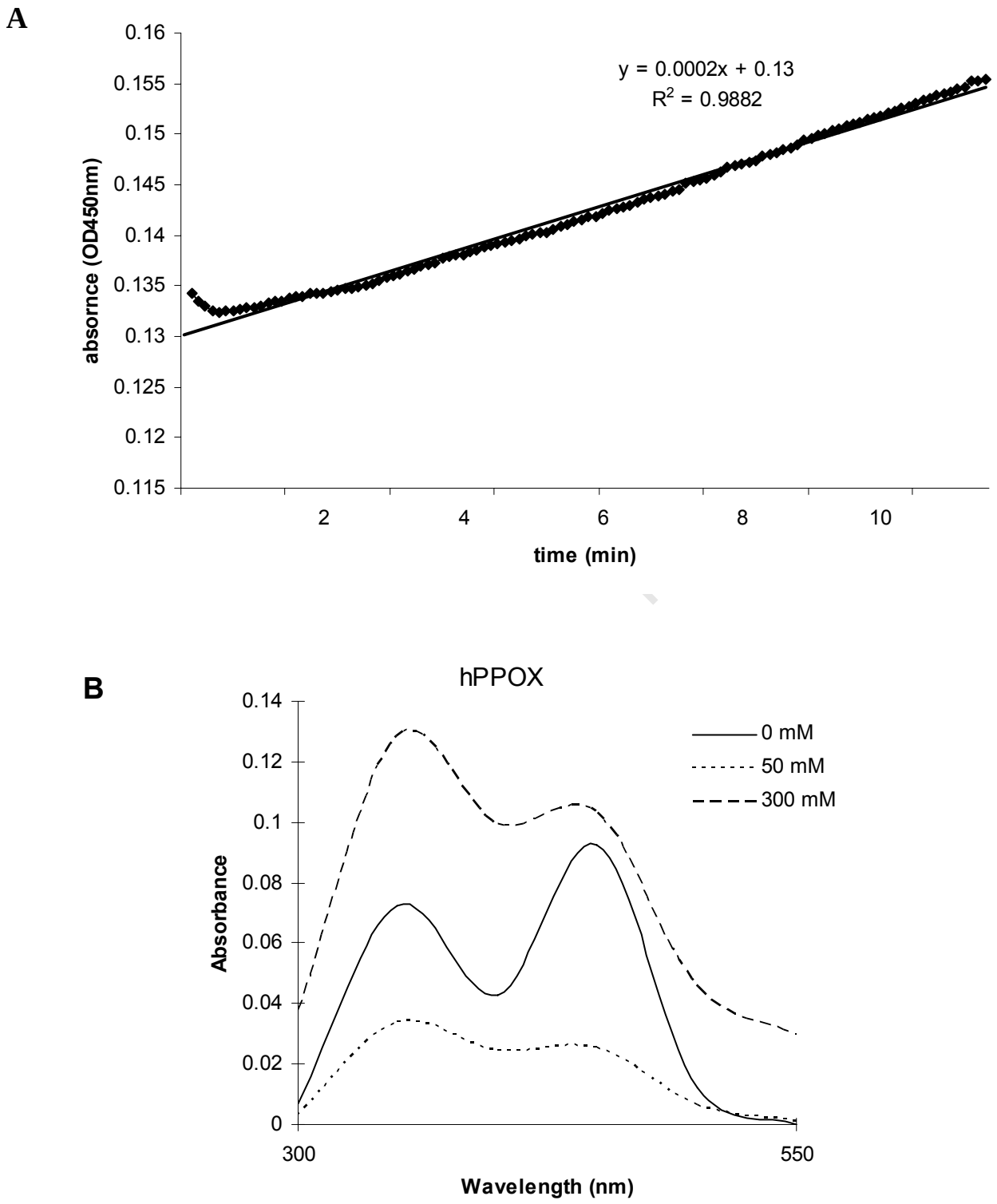

Figure 8.3: Spectral measurement of Na_2SO_3 reactivity with human PPOX (~10 µM). A) Time vs absorbance plot showing an increase in absorbance at OD_{450nm} observed in 300 mM [sulfite]. B) FAD spectra of human PPOX showing a normal spectrum (solid line); 50 mM [sulfite] incubation reaction spectrum (dotted) and a 300 mM [sulfite] reaction (dashed line).

In hPPOX protein, at high concentrations of Na_2SO_3 both bands have increased absorbance, compared to the pre-sulfite FAD spectrum. This bleaching effect is also reversible by the removal of excess sulfite from reaction using a PD-10 buffer exchange column. Reading at OD_{600nm} was unstable; this is used to determine protein stability.

Discussion

A common property of some flavoprotein oxidases is their ability to exhibit a high reactivity with sulfite anion to form an FAD-N(5) sulfite adduct. This characteristic may be used to determine the redox potential of an enzyme in the absence of substrate (Massey & Homeric, 1980; Piubelli *et al*., 2008). The rate of sulfite interaction with the FAD-N5 gives an indication of how the protein receives electrons from its substrate. Here we investigated the reactivity of PPOX with sulfite. As mentioned in chapter 2, the structure of mxPPOX reveals that Asn-63 (human equivalent Arg-59) interacts with the FAD-N(5). This residue has also been reported to be associated with O_2 transport in non-related proteins (such as cholesterol oxidases, chapter 2). Since protein reactivity with O_2 is a pre-requisite for sulfite reactivity, both these proteins, one having an asparagine and the other an arginine, were investigated.

University of Cape Town

Unlike many other flavoprotein oxidases, mxPPOX does not react with sulfite even at high concentrations of sulfite or at increased time incubation (3 hr). A similar sulfite non-reactivity has been reported in MAO (Edmondson *et al*., 2004). A possible explanation, which was also proposed by Edmonson and colleagues (2004) for MAO, is that the hydrophobic environment of the bound FAD makes it energetically unfavourable for a polar anion, such as sulfite, to traverse the hydrophobic path and react with FAD.

hPPOX reacts with sulfite in the range of 50 mM, however, this bleaching phenomena only occurs 30 min after incubation. This suggests that hPPOX reacts slowly with sulfite, as opposed to the rapid interactions reported in other oxidases (Gadda *et al*., 1997). With regards to hPPOX reduction potential this would suggest that hPPOX has a low reduction potential. At 300 mM an abnormal increase in absorbance is observed. This unusual bleaching phenomenon is similar to those reported in other flavoproteins with a “bleached” band in the UV/VIS range although both bands have increased absorbance compared to the pre-sulfite FAD spectrum. This abnormal increase can be attributed to

unfolding of the protein structure as the reading at 600 nm was unstable (personal communication, Professor Loredano Pollegioni, University of Konstanz, Konstanz, Germany). The reactivity with sulphite, seen in hPPOX and lacking in mxPPOX, could be either due to the positively charged polar group's (Arg-59) possible interaction with FAD-N(5) or the highly polar environment of the bound FAD in hPPOX. In mxPPOX the neutral polar Asn-67 may be inhibiting sulphite reactivity. This is highly unlikely, as in other non-related proteins sulphite reactivity has been reported for proteins that have an asparagine interacting with the FAD-N(5) (Piubelli *et al*., 2008). Another possibility is the difference in the binding region of FAD in these two proteins. In hPPOX crystal structure, 42 molecules of water are seen interacting with the bound FAD and protein, however, in mxPPOX, with an inhibitor bound active site, 9 water molecules are seen (table 2.1). This difference in water-mediated polarity suggests it could be energetically more favourable for sulphite to react with the FAD in hPPOX than in mxPPOX. However, caution should be applied in any interpretation due to the differences in resolution of these two structures. Also, because mxPPOX does not react with sulphite, using FAD-N5-sulphite adduct to determine redox potential is accordingly, not an efficient technique in PPOX.

University of Cape Town

Effect of substrate oxidation on oxygen consumption

Introduction

Flavoproteins may also be classified based on their reactivity with O_2, as well as O_2's 'final product' upon its reduction. PPOX falls in the category of flavoprotein oxidases - flavoproteins that react with O_2 to form H_2O_2.

Thus, as has been outlined in chapter 2, PPOX requires the presence of O_2 for catalysis, and O_2 plays the role of final electron acceptor. The catalytic reaction of PPOX involves the oxidation of protogen to form proto. Six electrons are removed in total and three molecules of O_2, the final electron acceptor, is reduced to $3H_2O_2$.

Previously, the effect of substrate oxidation on O_2 consumption was measured in both mouse and yeast PPOX protein (Ferreira & Dailey, 1988; Camadros *et al*., 1994). The K_MO_2 was reported to be 125 µM in mouse and estimated to be between 0.5 -1.5 µM in yeast PPOX. The affinity for O_2 in these two species appears to be dramatically different. Here, we assess O_2 reactivity in mxPPOX.

University of Cape Town

Objectives

- To investigate O_2 consumption and determine K_MO_2 in mxPPOX.

Clarke Electrode

To measure O_2 the Oxygraph system (Hansatech Instruments, UK) was utilized. The Oxygraph is a specialized Clark type polarographic electrode. It consists of a central platinum cathode and a centric silver (Ag) anode. Cathode and anode are connected by an electrolytic bridge and polarized by the O_2 electrode control unit. Polarization ionizes the electrolyte and a current is formed. The current is directly proportional to the amount of dissolved O_2 within the sample held in the vessel.

Electrode preparation

An electrolyte bridge is needed to allow current between the anode and cathode in the presence of O_2. Although different electrolytes can be used in this study, 50 % KCl solution was the recommended electrolyte (as detailed by the manufacturer). A protective membrane is then placed over the electrolyte on the cathode to prevent deposition from reaction mixture from interfering with reading and at the same time allow the diffusion of O_2. The membrane also serves as a wick, providing electrolytes (KCl) during operation. Steps of electrode preparation are detailed in appendix 19.

University of Cape Town

O_2 consumption was measured polarographically using the Clarke oxygen electrode chamber system connected to a circulating water bath at 37 °C (Hansatech Instruments, UK). Prior to experiment the electrode was prepared as described in appendix 19. The limiting factor in using the OxyGraph is the minimal initial substrate concentration; protogen is prepared in micro concentrations (30 to 10 µM). O_2 concentration can range from ~200 – 10 µM total concentration. This leads to early termination of experiments as protogen runs out first at high oxygen concentration. For kinetic analysis low concentrations of oxygen (30 – 20 µM) was therefore used.

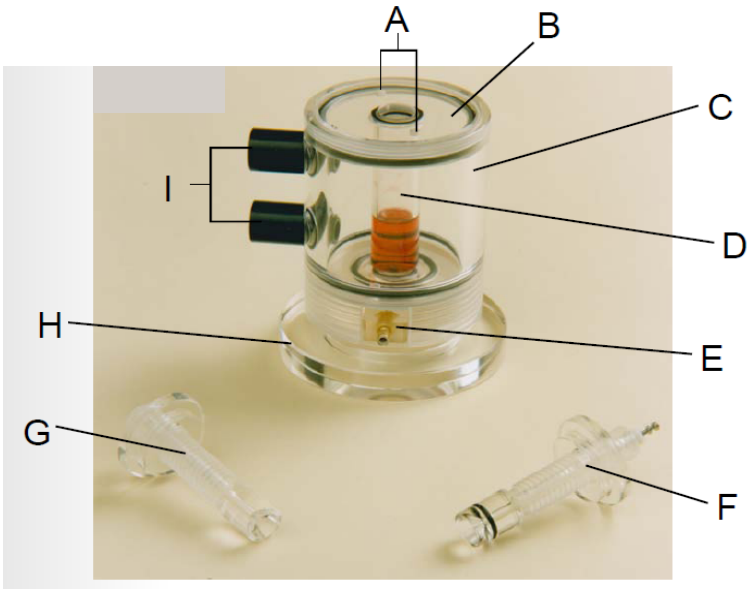

Figure 8.4: Reaction chamber and water jacket the Oxygraph. A) Lugs B) Top plate; C) Water jacket; D) glass reaction vessel; E) Electrode disc; F) Standard plunger (used in this study) G) Non-gas tight plunger assembly; H) Base ring; I) Water jacket.

Reference reaction with BSA – a reference reaction was set up to assess O_2 consumed by auto-oxidation. Another negative control reaction was set up with 1,4-dithiol - DL - threitol (DTT). DTT is used in normal kinetic assays to reduce autooxidation by quenching some O_2 in the reaction. In an open reaction where consumed O_2 is constantly being replaced, the effect of DTT on O_2 is negligible. In a sealed system, however, consumed O_2 is not replaced, and hence the presence of DTT could affect O_2 concentration. The effect of DTT on O_2 consumption was determined by running an assay with and without DTT.

Assay buffer, 100 mM Tris, pH 8.1, was mixed with an appropriate enzyme concentration (range 0.01 - 0.2 µM). The buffer was left to equilibrate at 37 °C and the plunger was used to seal entrance of chamber. An appropriate volume of substrate (~ 25 µM) was injected into the chamber through the plunger using a Hamilton syringe. The lid of plunger was then further sealed to eliminate any entrance of O_2. O_2 consumption was measured until substrate was consumed.

The OxyGraph electrode was connected to a computer to allow for the efficient reading of oxygen over intervals as short as 0.1 sec. Readings for mxPPOX were done at 10 sec intervals until the reaction was complete (as judged by the unchanging oxygen concentration). The oxygen concentration was varied using nitrogen gas which was used to degas buffer in the OxyGraph chamber to the desired oxygen concentration.

University of Cape Town

Buffer was then left to stabilize at that oxygen concentration in a sealed chamber 1 hr before reaction commenced at 37 ºC with continuous stirring.

During measurement, the O_2 signal was continuously plotted using the Oxygraph software for the rate of change in O_2. The rate was calculated by performing a least squares regression over 10 sec (user defined) time line. Rate was continuously re-calculated over 10 sec and displayed in the data bar in nmol/min. O_2 concentrations at a calculated rate were plotted against rates. Furthermore, for the overall rate of the reaction, the line of best fit is calculated over a defined area, and the rate of reaction determined.

For stoichiometric analysis a simliar reaction was set up as described in the Oxygraph chamber, and another in an assay glass tube sealed with mineral oil to mimic the Oxygraph chamber. Product formation (determined by reading the sample fluorimetrically) and oxygen comsumption (Oxygraph continuous reading) was determined every 10 min.

Results

Reading of oxygen concentration was electronically captured and a graph was plotted by OxyGraph software (fig. 8.5). The [O_2] was plotted versus time. Rate of O_2 consumption was derived from this data using a Microsoft Excel spreadsheet. The spreadsheet allowed a double-reciprocal plot to determine the Michaelis constant for oxygen (fig. 8.6). The K_MO_2 for mxPPOX was 0.90 ± 0.012 µM (n = 8). The stoichiometry of the reaction showed 3.2 ± 0.1 (n=4) moles of O_2 were consumed per mole of substrate oxidized. This was calculated using different protein concentrations (table 8.1).

University of Cape Town

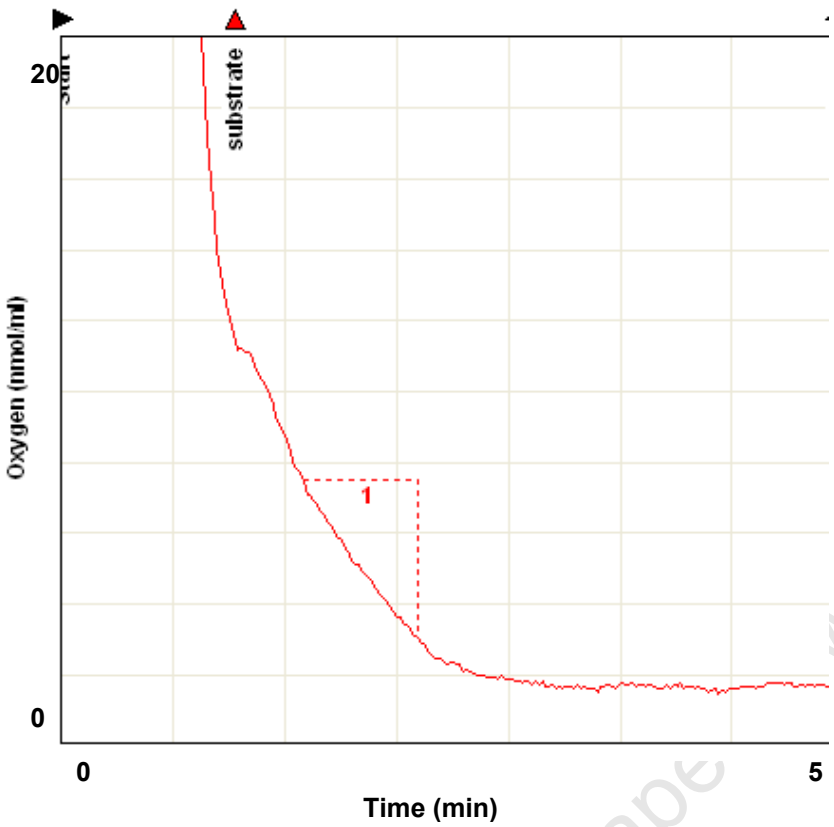

Figure 8.5: Graph showing the continuous measurement of O_2 consumption during the consumption of protogen. Approximately 25 µM substrate was used and 0.04 µM protein.

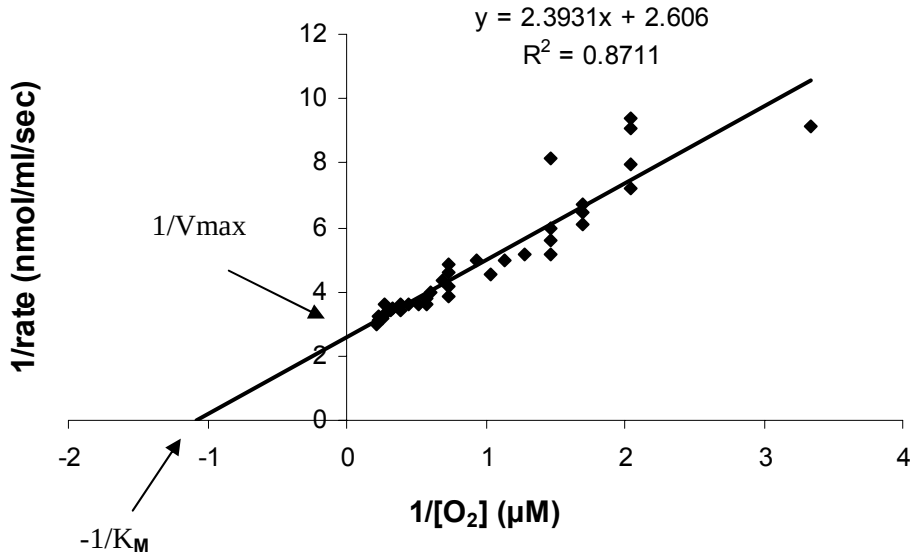

Figure 8.6: Double reciprocal plot, showing O_2 consumption in mxPPOX. V_{max} and K_M were extrapolated from the graph. Graph plotted using Microsoft-Excel.

Table 8.1: The stoichiometry of O_2 consumed per product (proto) formed in mxPPOX catalytic reaction for different protein concentrations.

mxPPOX (μM)	A O_2 consumption (nmol/hr)	B Proto production (nmol/hr)	ratio A/B
0.206	1187	366.5	3.238745
0.105	517.86	153.9	3.364912
0.071	352	112	3.142857
0.013	115	37.7	3.050398

Discussion

In this study the K_MO_2 in mxPPOX was determined using a Clarke cell oxygen electrode ("OxyGraph") and found to be 0.90 μM.

Previously other workers determined the apparent K_M for O_2 in mouse and yeast PPOX (Ferreira and Dailey, 1988; Camadros *et al*., 1994). K_M was calculated using different O_2 concentrations and measuring proto production by withdrawing from the reaction tube and measuring proto production during O_2 consumption. In the mouse study O_2 and protogen consumptions were monitored simultaneously. O_2 uptake was measured using a Clark-cell oxygen electrode while proto production was monitored by withdrawing 0.1 ml samples from the Clark cell every 10 min. K_MO_2 was found to be 125 μM (Ferreira and Dailey, 1988). In yeast, oxygen consumption was determined using the "oxygen-depleted assay medium" method. Nitrogen was used to degas buffer prior to reaction and then sealing degassed buffer with mineral oil. Oxygen was then measured using a Clarke electrode. The K_MO_2 for oxygen was determined to be 0.5-1.5 μM (Camadros *et al*., 1994).

The above findings indicate that the affinity for O_2 differs across species in PPOX. Interestingly, the affinity for oxygen in mxPPOX was similar to the affinity reported for yeast. However, it may be unwise to infer too much into these differences as we note that different experimental methods were used to measure O_2 in mouse, yeast and *M. xanthus* PPOX respectively (Ferreira and Dailey, 1988; Camadros *et al*., 1994).

University of Cape Town

Repeating the experiments on mouse and yeast PPOX in the system we used to measure mxPPOX O_2 consumption was deemed beyond the scope of this particular study, but probably should be done in the future.

The stoichiometric study of mxPPOX reaction, as expected, showed ~3 moles of oxygen consumed per substrate consumed. Previous, stoichiometric studies (Ferreira and Dailey, 1988) on mouse PPOX also reported the 3 mole ratio, confirming that the PPOX reaction formula holds true across species, or at least between mouse and *M. xanthus* PPOX. This three moles of oxygen consumed for every protogen consumed, lends weight to H_2O_2 being the by-product formed rather than H_2O.

Conclusions

mxPPOX does not react with sulfite whereas hPPOX reacts slowly with sulfite.
Water-mediated polarity around the FAD binding region could be playing a key factor in the difference in sulfite reactivity in mxPPOX and hPPOX.
In PPOX the use of sulfite reactivity as an indication of redox potential is not a useful technique.

mxPPOX has a binding affinity of 0.9 μM for oxygen.

Three moles of oxygen is consumed for every product (proto) produced.

University of Cape Town

CHAPTER 9

Overview, Final Conclusions, and Future Work

Overview, and Final Conclusions

PPOX, the penultimate enzyme in the haem biosynthetic pathway, catalyzes the oxidation of protogen to proto and requires the presence of FAD, as an intermediate electron acceptor, and oxygen, as the final electron acceptor. PPOX combines the dehydrogenation of substrate with the reduction of three molecules of O_2, to form product and three molecules of H_2O_2. In human, partial defects in PPOX lead to VP, an autosomal, dominantly inherited disorder.

Previously Dailey and Dailey (1998), using sequence alignment, identified an FAD superfamily of which PPOX is a member. In PPOX, FAD is located in a distinct binding region, the so called FAD binding domain. FAD can be viewed as consisting of two chemical entities – FMN and ADP (fig. 2.4, chapter 2). It is the ADP that interacts with the highly conserved sequence in the FAD binging domain, suggesting that the ADP is important in the binding of FAD to protein. Previous studies of FAD/PPOX interaction reveal that PPOX could have a “sensitive”, co-ordinated interaction with FAD. FAD’s interaction with PPOX involves water molecules that are seen forming polar bonds between the protein and FAD in what seems like an effort to stabilize the bound FAD.

In this study we investigated the FAD binding domain in mxPPOX by engineering various relevant mutants using site directed mutagenesis. The binding, orientation and stabilization of FAD were analysed by focusing particularly on highly conserved residues that most likely interact with FAD via their side chains.

University of Cape Town

Protein structure

Four crystal structures of PPOX have been resolved to date; including the recently resolved hPPOX. Sequence analysis, as has previously been shown (Dailey and Dailey, 1998), revealed that the FAD binding region is highly conserved amongst flavoproteins. Structure analysis further confirmed that most of the conserved residues are located in similar positions relative to FAD and therefore are likely to interact similarly with FAD in different species of PPOX, as well as non-related flavoprotein oxidases. These residues include a glutamate that interacts with the ribose of FAD, and a serine that interacts with one of the phosphate groups of FAD.

Serine 20

Ser-20 is a highly conserved residue which forms part of the FAD consensus sequence. It interacts with one of the phosphate groups of FAD. In this study the role of Ser-20 with regard to FAD's interaction with mxPPOX was assessed. It was determined that Ser-20 does not affect FAD binding significantly but that polarity in this position is important for the integrity of FAD binding.

The Ser20Ala mutant (removal of the polar side chain) revealed that compromising Ser-20 interaction with FAD could result in the remaining phosphate-protein interactions compensating for Ser-20's missing link. This lends weight to our earlier rationale that PPOX could have a sensitive, co-ordinated interaction with FAD.

Glutamate 39

Glu-39 also falls within the highly conserved FAD consensus sequence and interacts with the ADP section of FAD. It has been proposed in other oxidase that this region is involved in the binding of FAD. This study showed that a negative charge at this position is critical for FAD binding as all non-conservative replacements bound insufficient FAD. It is attractive to speculate that it is the ADP section of the FAD that binds first in mxPPOX to the FAD binding domain, as mutation of the Glu-39 residue resulted in lack of FAD binding, unlike the other residues studied. Based on sequence alignment a similar binding mechanism could be applied in other PPOX proteins.

Tryptophan 408

A tryptophan is commonly seen interacting with the nonpolar section of the isoalloxazine ring of FAD. Alignment study suggests that an aromatic ring (Trp-408) is favoured to interact with the nonpolar ring of the FAD isoalloxazine. Furthermore, analysis of the FAD binding regions suggests that a nonpolar residue would be more preferable in stabilizing FAD in this region than a polar residue. In mxPPOX it appears that aromaticity is vital with regards to the total amount of FAD that bound to the protein. However, crystal structure reveals that in mxPPOX Trp-408, although orientated towards the nonpolar ring of the FAD-isoalloxazine ring, is position further away from FAD compared to other PPOXs (as well as non-related oxidases) with resolved structures. Here it was shown that Trp-408 could be involved in orientating or stabilizing the bound substrate during catalysis.

University of Cape Town

Asparagine 441

Asn-441 interacts with the ribityl chain which is part of the FMN section of FAD, therefore this residue could be playing a role in orientating and stabilizing the isoalloxazine ring of FAD. Alignment studies revealed that although this residue is not grouped with the FAD consensus sequence, it is highly conserved in prokaryotes. This suggests that Asn-441 could be playing a vital role in FAD's interaction with mxPPOX. Our studies confirm that indeed Asn-441 is not involved in the binding of FAD, but in the stabilizing the bound FAD. Furthermore, the polarity of Asn-441 appears vital for stability.

FAD-N5-Sulfite

Analysis of sulfite reactivity in mxPPOX and hPPOX revealed that mxPPOX does not react with sulfite, while hPPOX reacts slowly. Water-mediated polarity could possible be playing a major role in the difference in sulfite reactivity as mxPPOX has fewer water molecules interacting with the FAD/protein; hPPOX has a large number (42) of water molecules. Sulfites reactivity with hPPOX and not with mxPPOX indicates that the use of sulfite to analyse redox potential in PPOX proteins is not a reliable tool. Nevertheless, studying sulfite reactivity may be valuable in shedding light on structural differences amongst PPOX proteins.

University of Cape Town

Oxygen

The reactivity of mxPPOX with oxygen was analysed in this study. mxPPOX has a high affinity (0.9 μM) for oxygen and 3 moles of molecular oxygen is consumed for every mole of proto formed. This confirms that 3 moles of molecular oxygen are consumed for every product formed, and is consistent with H_2O_2 being the by-product formed rather than H_2O. mxPPOX has a high affinity for oxygen although it does not react with sulfite, suggesting that polarity around the FAD binding domain may be a prerequisite for FAD-N5 sulfite reactivity.

FAD

This study demonstrates that the different sections of FAD play different roles in FAD/protein interaction. The ADP which consists of adenine, ribose and a phosphate

group is involved in the binding of FAD. We propose that this region binds first to the protein. Binding of the ADP is followed by FMN's interaction with the protein. FMN consists of the isoalloxazine ring, ribityl chain and a phosphate group. The ribityl group could be aligning the isoalloxazine ring of the FAD. Isoalloxazine is the reactive part of the FAD (the part to receive electrons from substrate) and hence its correct orientation and alignment is vital in mxPPOX for catalysis.

VP

This study has shown (at least indirectly) how mutations that affect FAD's interaction with PPOX may result in decreased functioning of this step in haem biosynthesis, leading to VP. By studying potentially vital residues in mxPPOX we have shown that certain residues are intimately involved in the binding of FAD. Therefore, their mutation may affect the binding of FAD. In such a scenario the enzyme becomes non-functional, leading to the build up of porphyrin(ogen)s. The naturally occurring mutant Glu34Val was previously characterized in human PPOX and results showed that FAD binding was comprised in this mutant (Qin et al., 2011).

Mutation of residues responsible for orientation and alignment of the FAD isoalloxazine ring may similarly result in a decrease in activity of the enzyme, which, *in vivo* could lead to the build up of porphyrin(ogen)s resulting in VP.

University of Cape Town

Future Work

PPOX plays a role in the biosynthesis of haem. It catalyzes the oxidation of protogen by removing six electrons to form proto. Due to the unstable nature of protogen (as mentioned in chapter 7) there is a void in our knowledge of the sequential chemical formation of proto in the enzyme-catalyzed reaction.

mxPPOX does not react with sulfite (a method used in many but not all flavoproteins to determine reduction potential of a protein). The investigation of PPOX reactivity with sulfite in other PPOX species could help shed light on the difference in structure as well as inhibitor binding differences found in the different PPOXs. In this regard bsPPOX could prove especially useful as this PPOX can utilise a much wider range of substrates and is not inhibited by acifluorfen. Characterisation of mxPPOX activity with regard to O_2 was analysed in this study. The transportation of O_2 to its point of activation, the interaction of O_2 with FAD as well as the location of H_2O_2 formation and its transportation is a much debated topic in flavoproteins; little work has been done on PPOX regarding O_2 and H_2O_2. Thus, studies aimed at elucidating the mechanism of function of O_2 in PPOX will help in the overall characterisation of PPOX and contribute to the biochemistry of flavoproteins.

This study focuses only on characterising PPOX from *M. xanthus.* This has allowed us to extrapolate information that can be indirectly applied to the human PPOX. Indeed, with the publication of the recently resolved human structure, and in order to understand mutant/disease function in variegate porphyric patients, study of the human PPOX FAD binding interactions may well shed further light in this regard.

University of Cape Town

References

Ajioka R, Phillips J, Kushner J. Biosynthesis of heme in mammals. Synthesis. 2006; 1763723 - 736.

Akhtar M. Mechanism and stereochemistry of the enzymes involved in the conversion of uroporphyrinogen III into haem. In: Jordan PM, editor(s). Biosynthesis of Tetrapyrroles. Amsterdam: Elsevier; 1991. p. 67-99.

Altschul S, Gish W, Miller W, Myers E, Lipman D. BLAST: Basic Local Alignment Search Tool [Internet]. Journal of Molecular Biology. 1990; 403-410.Available from: www.ncbi.nlm.nih.gov/BLAST/

Astner I, Jahn D, Schubert W-dieter, Heinz DW. Crystal structure of 5-aminolevulinate synthase, the first enzyme of heme biosynthesis, and its link to XLSA in humans. EMBO Journal. 2005; 24(18):3166-177.

Basran J, Fullerton S, Leys D, Scrutton NS. Mechanism of FAD reduction and role of active site residues His-225 and Tyr-259 in Arthrobacter globiformis Dimethylglycine oxidase: Analysis of mutant structure and catalytic function. Biochemistry. 2006; 4511151-161.

Bergonia HA, Phillips JD, & Kushner JP. Reduction of porphyrins to porphyrinogens with palladium on carbon. 2009; 384: 74-78.

Binda C, Coda A, Angelini R, Federico R, Ascenzi P, Mattevi A. A 30 A long U-shaped catalytic tunnel in the crystal structure of polyamine oxidase. Structure. 1999; 7(3):265-275.

Birchfield NB, Latli B, Casida JE. Human Protoporphyrinogen Oxidase: Relation between the herbicide binding site and the Flavin cofactor. Biochemistry. 1998; 376905-910.

Bottoms CA, Smith PE, Tanner JJ. A structurally conserved water molecule in Rossmann dinucleotide-binding domains. Protein Science. 2002; 112125-137.

University of Cape Town

Breinig S, Kervinen J, Stith L, Wasson AS, Fairman R, Wlodawer A, *et al*. Control of tetrapyrrole biosynthesis by alternate quaternary forms of porphobilinogen synthase. Nature Structural Biology. 2003; 10(9):757-764.

Brenner DA, Bloomer JR. The Enzymatic Defect in Variegate Porphyria — Studies with Human Cultured Skin Fibroblasts. New England Journal of Medicine. 1980; 302765-769.

Brenner S, Hay S, Munro AW, Scrutton NS, No H, Our R. Inter- flavin electron transfer in cytochrome P450 reductase – effects of solvent and pH identify hidden complexity in mechanism. FEBS Journal. 2008; 2754540-557.

Camadros J-M, Thome F, Brouillet N, Labbe P. Purification and Properties of Protoporphyrinogen Oxidase from the Yeast Saccharomyces cerevisiae. Biochemistry. 1994; 269(51):32085-091.

Chen L, Lyubimov AY, Brammer L, Vrielink A, Sampson NS, About M, *et al*. The Binding and Release of Oxygen and Hydrogen Peroxide Are Directed by a Hydrophobic Tunnel in Cholesterol Oxidase. Biochemistry. 2008; 475368-377.

Clayden J, Greeves N, Warren S, Wothers P. Organic Chemistry: Saturated heterocycles and stereoelectronics. Oxford.University Press. 2001; 42: 1177-179.

Corradi HR, Corrigall AV, Boix E, Mohan CG, Sturrock ED, Meissner PN, *et al*. Crystal Structure of Protoporphyrinogen Oxidase from Myxococcus xanthus and Its Complex with the Inhibitor Acifluorfen. Journal of Biological Chemistry. 2006; 281(50):38625-633.

Corrigall AV, Siziba KB, Maneli MH, Shephard EG, Ziman M, Dailey TA, *et al*. Purification of and kinetic studies on a cloned protoporphyrinogen oxidase from the aerobic bacterium Bacillus subtilis. Archive Biochemistry and Biophysics. 1998; 358:251-256.

Dailey HA. Conversion of coproporphyrinogen to protoheme in higher synthesis of heme and chlorophylls. New York: McGraw Hill. Terminal three enzymes. In: Dailey HA, ed. 1990; pp 123-161.

Dailey HA. Terminal steps of haem biosynthesis. Biochemical Society Transactions. 2002; 30(4):590-595.

University of Cape Town

Dailey HA & Dailey TA. Protoporphyrinogen Oxidase of *Myxococcus xanthus*: expression, purification and characterisation of the cloned enzyme. Biochemistry. 1996a; 271(15):8714-718.

Dailey TA & Dailey HA. Human protoporphyrinogen oxidase: Expression, purification, and characterization of the cloned enzyme. Protein Science. 1996b; 598-105.

Dailey TA & Dailey HA. Identification of an FAD superfamily containing protoporphyrinogen oxidases, monoamine oxidases and phytoene desaturase. Journal of Biological Chemistry. 1998; 273(22):13658-662.

Dailey TA, Meissner PN, Dailey HA. Expression of a Cloned Protoporphyrinogen oxidase. New York. 1994; 269813-815.

Dailey HA, Dailey TA, Wu C, Medlock AE, Wang K, Rose JP, *et al*. Ferrochelatase at the millennium : structures , mechanisms and [2Fe-2S] clusters. Cellular and Molecular Life Sciences. 2000; 571909-926.

Dailey HA, Wu CK, Horanyi P, Medlock AE, Najah-Missaoui W, Burden AE, et al. Altered orientation of active site residues in variants of human ferrochelatase. Evidence for a hydrogen bond network involved in catalysis. Biochemistry. 2007; 46(27) 7973-979.

Danishefsky A, Onnufer J, Petsko G, Dagmar R. Activity and Structure of the Active-Site Mutants R386Y and R386F of *Escherichia coli* Aspartate Aminotransferase. Biochemistry. 1991; 301980-985.

Davids LM. Mitochondrial targeting of wild-type and mutant human Protoporphyrinogen oxidase (PPOX). PhD thesis. 2003; 11-29.

Davydov R, Osborne RL, Kim SH, Dawson JH, Hoffman BM. EPR and ENDOR Studies of Cryoreduced Compounds II of Peroxidases and Myoglobin . Proton-Coupled Electron Transfer and Protonation Status of Ferryl. Simulation. 2008; 5147-155.

Dayan F, Daga P, Duke S, Lee R, Tranel P, Doerksen R. Biochemical and structural consequences of a glycine deletion in the alpha-8 helix of protoporphyrinogen oxidase. Biochimica et Biophysica Acta. 2010; 18041548-556.

Deybach JC, Da Silva V, Grandchamp B, Nordmann Y. The mitochondrial location of protoporphyrinogen oxidase. European Journal of Biochemistry. 1985; 431 - 435

University of Cape Town

Dong C, Dong C, Flecks S, Unversucht S. Tryptophan 7-Halogenase (PrnA) Structure Suggests a Mechanism for Regioselective Chlorination. Science. 2008; 2216

Dym O, Eisenberg D, Dym O, Eisenberg D. Sequence-structure analysis of FAD-containing proteins. Protein Science. 2001; 1712-728.

Edmondson DE, & Newton-vinson P. Flavins in biological systems. Antioxidants & redox signaling. 2001;(5):789-806.

Edmondson DE, Binda C, & Mattevi A. The FAD binding sites of human monoamine oxidases A and B. Neurotoxicology. 2004; 2563-572.

Efimov I, & Mcintire WS. Relationship between Charge-Transfer Interactions , Redox Potentials , and Catalysis for Different Forms of the Flavoprotein Component of p-Cresol Methylhydroxylase. Biochemistry. 2004; (3):964-967.

Elder GH, & Evans OJ. Evidence that the Coproporphyrinogen oxidase activity of rat liver is situated in the intermembrane space of mitochondria. Biochemistry. 1978; 178345-347.

Erskine PT, Newbold R, Roper J, Coker A, Warren MJ, Shoolingin-jordan PM, *et al*. The Schiff base complex of yeast 5-aminolaevulinic acid dehydratase with laevulinic acid. Protein Science. 1999; 81250-256.

Falk, JE, Porphyrins and metalloporphyrins. Elsevier, New York. 1964

Ferreira GC, Dailey HA. Mouse protoporphyrinogen oxidase Kinetic parameters and demonstration of inhibition by bilirubin. Journal of Biochemistry. 1988; 250597-603.

Fetzner S. Oxygenases without requirement for cofactors or metal ions. Applied Microbiology Biotechnology. 2002; 60243-257.

Fitzpatrick PF. Oxidation of amines by flavoproteins. Archive Biochemistry and Biophysics. 2011; 493(1):13-25.

Fraaije MW, Mattevi A. Flavoenzymes: diverse catalysts with recurrent features. TIBS. 2000; 25126-132.

Fraser DJ, Podvinec M, Kaufmann MR, & Meyer UA. Drugs Mediate the Transcriptional Activation of the 5-Aminolevulinic Acid Synthase (ALAS1) Gene via the Chicken

University of Cape Town

Xenobiotic-sensing Nuclear Receptor (CXR). The Journal of Biological Chemistry. 2002; 277(38):34717-726.

Gadda G, Wels G, Pollegioni L, Zucchelli S, Ambrosius D, Pilone MS, *et al*. Characterization of cholesterol oxidase from Streptomyces hygroscopicus and Brevibacterium sterolicum. European Journal of Biochemistry. 1997; 250369-376.

Ghisla S, & Massey V. New flavins for old: artificial flavins as active site probes of flavoproteins. 1986; 2391-412.

Ghisla S, & Massey V. Mechanisms of flavoprotien-catalyzed reactions. European Journal of Biochemistry. 1989; 1811-817.

Ghisla S, Massey V, Lhoste J-marc, & Mayhew SG. Fluorescence and Optical Characteris tics of Reduced Flavines and Flavoproteins. Biochemistry. 1972; 13(3):589-597.

Gill R, Kolstoe SE, Mohammed F, D-bass AAL, Mosely JE, Sarwar M, *et al*. Structure of human porphobilinogen deaminase at 2.8 A the molecular basis of acute intermittent porphyria. Biochemistry. 2009; 42017-025.

Gong J, Kay CJ, Barber MJ, & Ferreira GC. Mutations at a Glycine Loop in Aminolevulinate Synthase Affect Pyridoxal Phosphate Cofactor Binding and Catalysis. Biochemistry. 1996; 3514109-117.

Gong J, Hunter GA, & Ferreira GC. Aspartate-279 in Aminolevulinate Synthase Affects Enzyme Catalysis through Enhancing the Function of the Pyridoxal 5 ′ -Phosphate Cofactor †. Biochemistry. 1998; 37(10):3509-517.

Grandchamp BB, Phung NHU, Nordmann Y, Biochimie LD, Medecine FD, Bichat X, *et al*. The Mitochondrial Localization of Coproporphyrinogen III Oxidase. Biochemistry. 1978; 17697-102.

Harvey JD, & Ziegler CJ. The metal complexes of N-confused porphyrin as heme model compounds. Journal of Inorganic Biochemistry. 2006; 100869-880.

Heinemann IU, Diekmann N, Masoumi A, Koch M, Messerschmidt A, Jahn M, *et al*. Functional definition of the tobacco protoporphyrinogen IX oxidase substrate binding site. Biochemical Journal. 2007; 402575-580.

University of Cape Town

Heuts DPHM, Hellemond EWV, Janssen DB, & Fraaije MW. Discovery, Characterization, and Kinetic Analysis of an Alditol Oxidase from Streptomyces coelicolor. Journal of Biological Chemistry. 2007; 282(28):20283-291.

Hofacker I, & Schulten K. Oxygen and Proton Pathways in Cytochrome c Oxidase. Proteins. 1998; 107:100-107.

Hunter GA, & Ferreira GC. Lysine-313 of 5-Aminolevulinate Synthase Acts as a General Base during Formation of the Quinonoid Reaction Intermediates. Biochemistry. 1999a; 383711-718.

Hunter GA, & Ferreira GC. Pre-steady-state Reaction of 5-Aminolevulinate Synthase. The Journal of Biological Chemistry. 1999b; 274(18):12222-228.

Jaffe EK. The porphobilinogen synthase catalyzed reaction mechanism. Bioorganic Chemistry. 2004; 32316-325.

Jaffe EK, & Hanesg D. Dissection of the Early Steps in the Porphobilinogen Synthase Catalyzed Reaction. The Journal of Biological Chemistry. 1986; 261(20):9348-353.

Jaffe EK, & Stith L. ALAD Porphyria Is a Conformational Disease. Journal of Human Genetics. 2007; 80329-337.

Jaffe EK, Martins J, Li J, Kervinen J, & Dunbrack RL. The Molecular Mechanism of Lead Inhibition of Human Porphobilinogen Synthase. The Journal of Biological Chemistry. 2001; 276(2):1531-537.

James MFM, & Hift RJ. Porphyrias. British Journal of Anaesthesia. 2000; 85(1):143-153.

Jones C, Jordan PM, & Akhtar M. Mechanism and stereochemistry of the porphobilinogen deaminase and protoporphyrinogen IX oxidase reaction: stereospecific manipulation of hydrogen atoms at the four methylene bridges during the biosynthesis of haem. Journal of Chemical Sociology Perkin Translation. 1984; 12625-633.

Jordan PM. Biosynthesis of Heme and Chlorophylls. McGraw-Hill, New York; 1990.

Jordan PM, & Warren MJ. Evidence for a dipyrromethane cofactor at the catalytic of E . coli porphobilinogen deaminase. FEBS Letters. 1987; 225(1):87-92.

University of Cape Town

Jordan PM, & Woodcook SC. Mutagenesis of arginie residues in the catalytic cleft of Escherichia coli porphobilinogen deaminase that affects dipyrromethane cofactor assembly and tetrapyrrole chain initiation and elongation. Biochemistry. 1991; 280445-449.

Jordan PM, Warren MJ, Williams HJ, Stolowich NJ, Roessner CA, Grant SK, *et al*. Identification of a cysteine residue as the binding site for the dipyrromethane cofactor at the active site of Escherichia coli porphobilinogen deaminase. FEBS Letters. 1988; 235(1):189-193.

Kane J, & Hartley D. Properties of inclusion bodies from recombinant Escherichia coli. Biochemical Society Transactions. 1988; 16(2):101-102.

Koch M, Breithaupt C, Kiefersauer R, Huber R, & Messerschmidt A. Crystal structure of protoporphyrinogen IX oxidase: a key enzyme in haem and chlorophyll biosynthesis. The EMBO Journal. 2004; 231720-728.

Kohno H, Okuda M, Furukawa T, Tokunaga R, & Taketani S. Site-directed mutagenesis of human ferrochelatase: Identification of histidine-263 as a binding site for metal ions. Biochimica et Biophysica Acta. 1994; 1209(1):95-100.

Kuhn H, Saam J, Ivanov I, Walther M, & Holzhu H-G. Molecular dioxygen enters the active site of 12 / 15-lipoxygenase via dynamic oxygen access channels. Distribution. 2007; 104(33):13319-324.

Lee D-S, Flachsova E, Bodna M, Demeler B, Marta P, Raman CS, *et al*. Structural basis of hereditary coproporphyria. Proceedings of the National Academy of Sciences. 2005; 10214232 - 237.

Lermontova I, Kruse E, Mock HP, & Grimm B. Cloning and characterisation of a plastidal and a mitochondrial isoform of tobacco protoporphyrinogen IX oxidase. PNAS. 1997; 94:8895-900.

Ma J, & Ito A. Tyrosine residues near the FAD binding site are critical for FAD binding and for the maintenance of the stable and active conformation of rat monoamine oxidase A. Journal of Biochemistry. 2002; 131107-111.

Maneli MH. Studies on human Protoporphyrinogen oxidase. PhD thesis. Cape Town, South Africa: University of Cape Town; 2002.

University of Cape Town

Maneli MH, Corrigall AV, Klump HH, Davids LM, Kirsch RE, & Meissner PN. Kinetic and physical characterisation of recombinant wild-type and mutant human protoporphyrinogen oxidases. Biochimica et Biophysica Acta. 2003; 165010 - 021.

Massey V. Activation of Molecular Oxygen by Flavins and Flavoproteins. The Journal of Biological Chemistry. 1994; 269(36):22459-462.

Massey V, & Hemmerich P. Active-site probes of flavoproteins. Biochemical Society Transactions. 1980; 8(3):246-257.

Massey V, Muller F, Feildberg R, Schuman M, Sullivan PA, Howell LG, *et al*. The Reactivity of flavoproteins with Sulfite. The Journal of Biological Chemistry. 1969; 244(15):3999-4006.

Mathews MAA, Schubert HL, Whitby FG, Alexander KJ, Schadick K, Bergonia HA, *et al*. Crystal structure of human uroporphyrinogen III synthase. EMBO Journal. 2001; 20(21):5832-839.

Mattevi A, Vanoni MA, & Curti B. Structure of D-amino acid oxidase: new insights from an old enzyme. Current Opinion in Structural Biology. 1997; 7804-810.

Max Heiman. WebCutter [Internet]. 1997; available from: http://bio.lundberg.gu.se/cutter2/

McCall KA, Huang C-chin, & Fierke CA. Function and mechanism of Zinc Metalloenzymes. The Journal of Nutrition. 2000; 1301437 - 446.

Mehta PK, Hale TI, & Christen P. Aminotransferases: demonstration of homology and division into evolutionary subgroups. European Journal of Biochemistry. 1993; 214549-561.

Meissner PN, Day R, Moore M, Disler P, & Harley E. Protoporphyrinogen oxidase and porphobilinogen deaminase in variegate porphyria. European Journal of Clinical Investigation. 1986; 16(3):257-261.

Meissner PN, Dailey TA, Hift RJ, Ziman M, & Corrigall AV, Roberts AG, *et al*. A R59W mutation in human protoporphyrinogen oxidase results in decreased enzyme activity and is prevalent in South Africans with variegate porphyria. Nature Genetics. 1996; 1395-397.

University of Cape Town

Mills-Davies NL. Structure of human erythrocyte 5-aminolaevulinic acid dehydratase, the second enzyme in the biosynthesis pathway of haem. PhD Thesis. Southampton, UK: University of Southampton; 2000.

Morgan R, Silva V da, Puy H, Deybach J, & Elder G. Functional studies of mutations in the human protoporphyrinogen oxidase gene in variegate porphyria. Cell Molecular Biology (noisy-le-grand). 2002; 4879-882.

Motteran L, Pilone MS, Molla G, & Ghisla S. Cholesterol Oxidase from Brevibacterium sterolicum. The Journal of Biological Chemistry. 2001; 276(21):18024 -030.

Mushegian AR, & Koonin EV. A putative FAD-binding domain in a distinct group of oxidases including a protein involved in plant development. Annual Review of Nutrition. 1995; 41243-244.

Neeli R, Roitel O, Scrutton NS, & Munro AW. Switching Pyridine Nucleotide Specificity in P450 BM3. The Journal of Biological Chemistry. 2005; 280(18):17634 -644.

Orville AM, Lountos GT, Finnegan S, Gadda G, & Prabhakar R. Crystallographic, Spectroscopic, and Computational Analysis of a Flavin C4a-Oxygen Adduct in Choline Oxidase. Biochemistry. 2009; 48(4):720-728.

Petsko G, & Ringe D. Protein structure and function: From sequence to consequence. Brandies University: New Science Press Ltd; 2004.

Phillips JD, Whitby FG, Kushner JP, & Hill CP. Structural basis for tetrapyrrole coordination by uroporphyrinogen decarboxylase. EMBO Journal. 2003; 22(23):6225-233.

Piubelli L, Pedotti M, Molla G, Feindler-Boeckh S, Ghisla S, Pilone MS, *et al*. On the oxygen reactivity of flavoprotein oxidases: an oxygen access tunnel and gate in Brevibacterium Sterolicum. The Journal of Biological Chemistry. 2008; 283(36):24738-747.

Pollegioni L, Ceciliani F, Curti B, Ronchit S, & Pilone MS. Studies on the structural and functional aspects of Rhodotorula gracilis D-amino acid oxidase by limited trypsinolysis. Biochemistry. 1995; 310:577-583.

University of Cape Town

Poulson R, & Polglase J. The Enzymic Conversion of Protoporphyrinogen IX to Protoporphyrin IX. Protoporphyrinogen oxidase activity in mitochondrial extracts of Saccaromyces Cerecisiae. The Journal of Biological Chemistry. 1975; 250(4):1269-274.

Puy H, Gouya L, & Deybach J-C. Porphyrias. The Lancet. 2010; 375924-937.

Qin X, Sun L, Wen X, Yang X, Tan Y, Jin H, *et al*. Structural insight into unique properties of protoporphyrinogen oxidase from Bacillus subtilis [Internet]. Journal of Structural Biology. 2010; 170(1):76-82.

Qin X, Tan Y, Wang L, Wang Z, Wang B, Wen X, *et al*. Structural insight into human variegate porphyria disease. The FASEB Journal. 2011; 25653-664.

Raszka M, & Kaplan N. Intramolecular Hydrogen Bonding in Flavin Adenine Dinucleotide. 1974; 71(11):4546-550.

Regan JJ, Ramirez BE, Winkler JR, Gray HB, & Malmstrom BG. Pathways for Electron Tunneling in Cytochrome c Oxidase. Journal of Bioenergetics. 1998; 30(1):35-39.

Riistama S, Puustinen A, Garcla-horsman A, Iwata S, Michel H, & Wikstro M. Channelling of dioxygen into the respiratory enzyme. Biochimica et Biophysica Actami. 1996; 12751-754.

Riistama S, Puustinen A, Verkhovsky MI, Morgan JE, & Wikstrom M. Binding of O2 and Its Reduction Are Both Retarded by Replacement of Valine 279 by Isoleucine in Cytochrome c Oxidase from Paracoccus denitrificans. Biochemistry. 2000; 396365-372.

Rivera M, & Walker AF. Biosynthesis preparation of isotopically labeled heme. Analytical Biochemistry. 1995; 230295-302.

Roessner CA, Ponnamperuma K, & Scott AI. Mutagenesis identifies a conserved tyrosine residue important for the activity of uroporphyrinogen III synthase from Anacystis nidulans. FEBS Letters. 2002; 52525-528.

Roth GJ, Machuga ET, & Ozols J. Isolation and Covalent Structure of the Aspirin-Modified, Active-Site Region of Prostaglandin Synthetase. Biochemistry. 1983; 4675(1976):4672-675.

Sampson NS. Dissection of a Flavoenzyme Active Site: The Reaction Catalyzed by Cholesterol Oxidase. Antioxidants and Redox signaling. 2001; 3(5):839-846.

University of Cape Town

Sano S, & Granick S. Mitochondrial Coproporphyrinogen Protoporphyrin Formation. The Journal of Biological Chemistry. 1961; 236(4):1173-180.

Sawada N, Nagahara F, Arisaka F, Mitsuoka K, & Minami M. Redox and metal-regulated oligomeric state for human porphobilinogen synthase activation. Journal of Biological Chemistry. 2010; Epub ahead of print.

Schubert HL, Phillips JD, Heroux A, & Hill CP. Structure and Mechanistic Implications of a Uroporphyrinogen III Synthase-Product Complex. Biochemistry. 2008; 47(33):8648-655.

Sellers VM, Wu C-kuei, Dailey TA, & Dailey HA. Human Ferrochelatase : Characterization of Substrate-Iron Binding and Proton-Abstracting Residues. Biochemistry. 2001; 409821-827.

Senda T, Senda M, Kimura S, & Ishida T. Redox control of protein conformation in flavoproteins. Antioxidants and Redox signaling. 2009; 11(7):1741-766.

Shemin D, & Kikuchi G. Enzymatic synthesis of Aminolevulinic Acid. Annals New York Academy of Sciences. 1958; 75(1):122-128.

Shoolingin-Jordan PM. The Iron and Cobalt Pigments: Biosynthesis, Structure and degradation. 12th ed. California, USA: Academic Press; 2003.

Shoolingin-Jordan PM, Mcneill LA, Sarwar M, & Butler D. Human porphobilinogen deaminase mutations in the investigation of the mechanism of dipyrromethane cofactor assembly and tetrapyrrole formation. Biochemical Society Transactions. 2003; 31(3):731-735.

Siepker LJ, Ford M, de Kock R & Kramer S. Purification of bovine protoporphyrinogen oxidase: immunological cross-reactivity and structural relationship of ferrochelatase. Biochimica et Biophysica Acta. 1987; 913:349-358.

Song G, Li Y, Cheng C, Zhao Y, Gao A, Zhang R, *et al*. Structural insight into acute intermittent porphyria. The FASEB Journal. 2009; 23(2):396-404.

Stephenson JR, Stacey JA, Morgenthaler JB, Friesen J, Lash TD, & Jones MA. Role of aspartate 400, arginine 262, and arginine 401 in the catalytic mechanism of human coproporphyrinogen oxidase. Protein Science. 2007; 16(309):401-410.

University of Cape Town

Tan D, Harrison T, Hunter GA, & Ferreira GC. Role of Arginine 439 in Substrate Binding of 5-Aminolevulinate Synthase. Biochemistry. 1998; 371478-484.

Tang L, Breinig S, Stith L, Mischel A, Tannir J, Kokona B, *et al*. Single Amino Acid Mutations Alter the Distribution of Human Porphobilinogen Synthase Quaternary Structure Isoforms (Morpheeins). Journal of Biological Chemistry. 2006; 281(10):6682-690.

Thunell S. Genomic Approach to Acute Porphyria. Physiological Respiratory. 2006; 55(2):43-66.

Tsiftsoglou AS, Tsamadou AI, & Papadopoulou LC. Heme as key regulator of major mammalian cellular functions : Molecular , cellular , and pharmacological aspects. Pharmacology & Therapeutics. 2006; 111327 - 345.

Vincze T, Posfai J, & Roberts RJ. NEBcutter [Internet]. Nucleic Acids Res. 2003; 313688-691.Available from: http://tools.neb.com/NEBcutter2/help/cite.html

Whatley SD, Ducamp S, Gouya L, Grandchamp B, Beaumont C, Badminton MN, *et al*. C-Terminal Deletions in the ALAS2 Gene Lead to Gain of Function and Cause X-linked Dominant Protoporphyria without Anemia or Iron Overload. The American Journal of Human Genetics. 2008; 83408-414.

Whitby L. Preparation of flavinadenine dinucleotide (FAD). Biochimica et Biophysica Acta. 1954; 15(1):148-149.

Whitby FG, Phillips JD, Kushner JP, & Hill CP. Crystal structure of human uroporphyrinogen decarboxylase. The EMBO Journal. 1998; 17(9):2463-471.

Wu C-K, Dailey HA, Rose JP, Burden A, Sellers VM, & Wang B-C. The 2 . 0 Å structure of human ferrochelatase , the terminal enzyme of heme biosynthesis. Nature Structural Biology. 2001; 423156-160.

Yin Y, Sampson NS, Vrielink A, & Lario PI. The Presence of a Hydrogen Bond between Asparagine 485 and the pi System of FAD Modulates the Redox Potential in the Reaction Catalyzed by Cholesterol Oxidase. Biochemistry. 2001; 4013779-787.

Yue KQ, Ghisla S, & Vrielink A. Oxygen Access to the Active Site of Cholesterol Oxidase through a Narrow Channel Is Gated by an Arg-Glu Pair. Journal of Biological Chemistry. 2001; 276(32):30435-441.

University of Cape Town

Zappa S, Li K, & Bauer C. The tetrapyrrole biosynthetic pathway and its regulation in Rhodobacter capsulatus. 2010; 675229-250.

Zhao G, & Jorns MS. Spectral and Kinetic Characterization of the Michaelis Charge Transfer Complex in Monomeric Sarcosine Oxidase. Biochemistry. 2006; 45(19):5985-992.

Zhao G, Bruckner RC, & Jorns MS. Identification of the Oxygen Activation Site in Monomeric Sarcosine Oxidase : Role of Lys265 in Catalysis. Mutagenesis. 2008; (19):9124-135.

Zhou B, Wu B, Kwan S, & Abell CW. Characterization of a Highly Conserved FAD-binding Site in Human Monoamine Oxidase B. The Journal of Biological Chemistry. 1998; 273(24):14862-868.

University of Cape Town

Appendices

Appendix 1 - M. xanthus PPOX sequences (GeneBank ID: 4106756)

1.1 cDNA sequence

CAACTGGAATGA**ATG**TCGCCGTCGTGGGAGGTGGGATTTCGGGGTTGGCCGTCGCGC
ATCATTTGCGCTCGCGCGGTACGGATGCCGTGCTTCTGGAGTCCTCCGCCCGACTTG
GCGGCGCGGTGGGCACGCATGCGCTCGCCGGCTACCTGGTGGAGCAGGGGCCCAA
CAGCTTCCTGGACCGCGAGCCCGCAACGCGGGCGCTCGCGGCGGCGCTGAATCTGG
AGGGGCGAATTCGCGCCGCGGACCCGGCGGCGAAGCGTCGCTATGTCTACACGCGG
GGCAGACTCCGGTCGGTACCGGCCTCGCCGCCCGCGTTTCTCGCATCGGACATTCTG
CCGCTCGGCGCGCGGTTGCGCGTCGCTGGCGAACTGTTCTCCCGCCGCGCGCCGGA
GGGTGTGGACGAATCGCTGGCCGCCTTCGGCCGCCGCCACCTGGGACACAGGGCGA
CGCAGGTGCTGCTCGACGCGGTGCAGACGGGCATCTACGCGGGCGACGTGGAGCAG
CTCAGCGTCGCGGCCACCTTCCCCATGCTGGTGAAGATGGAGCGCGAGCACCGCAG
CCTCATCCTGGGCGCCATCCGCGCGCAGAAGGCTCAGCGCCAGGCGGCGCTCCCCG
CGGGAACGGCGCCGAAGTTGAGCGGCGCGCTGAGCACGTTCGACGGCGGATTGCAG
GTGCTCATCGACGCGCTCGCCGCATCGTTGGGTGACGCGGCGCACGTGGGCGCGCG
CGTGGAGGGGCTGGCGCGCGAGGACGGCGGTTGGAGGCTCATCATCGAGGAGCACG
GACGCCGCGCGGAACTGTCCGTGGCCCAGGTGGTACTGGCGGCGCCCGCGCATGCC
ACCGCGAAATTGCTACGCCCACTGGATGACGCGCTCGCCGCCCTGGTGGCGGGTATC
GCCTATGCGCCCATCGCGGTGGTGCACCTGGGCTTCGACGCGGGGACACTTCCGGC
GCCGGATGGCTTTGGGTTCCTGGTGCCAGCGGAGGAGCAGCGGCGGATGCTGGGCG
CCATCCACGCGTCCACCACCTTTCCCTTCCGGGCCGAGGGCGGACGCGTGCTCTATT
CCTGCATGGTGGGGGGCGCGCGTCAGCCAGGGCTGGTGGAACAGGACGAGGATGCA
TTGGCGGCGCTGGCGCGCGAGGAACTGAAGGCGCTGGCAGGCGTGACGGCGCGCC
CCTCCTTCACGCGGGTGTTCCGCTGGCCGCTTGGCATTCCCCAGTACAACCTGGGAC
ACCTGGAGCGCGTGGCCGCTATCGACGCGGCGCTGCAACGCTTGCCCGGCCTGCAC
CTCATCGGGAATGCGTACAAGGGCGTGGGCCTCAACGACTGCATCCGCAACGCGGCG
CAACTCGCGGACGCCCTGGTCGCGGGGAACACCTCCCACGCCCCG**TAG**TGAAGCTT
GCTTG

University of Cape Town

1.2 Amino acid sequence

MHHMPRTTGMNVAVVGGGISGLAVAHHLRSRGTDAVLLESSARLGGAVGTHALAGYLVE
QGPNSFLDREPATRALAAALNLEGRIRAADPAAKRRYVYTRGRLRSVPASPPAFLASDILPL
GARLRVAGELFSRRAPEGVDESLAAFGRRHLGHRATQVLLDAVQTGIYAGDVEQLSVAAT
FPMLVKMEREHRSLILGAIRAQKAQRQAALPAGTAPKLSGALSTFDGGLQVLIDALAASLG
DAAHVGARVEGLAREDGGWRLIIEEHGRRAELSVAQVVLAAPAHATAKLLRPLDDALAALV
AGIAYAPIAVVHLGFDAGTLPAPDGFGFLVPAEEQRRMLGAIHASTTFPFRAEGGRVLYSC
MVGGARQPGLVEQDEDALAALAREELKALAGVTARPSFTRVFRWPLGIPQYNLGHLERVA
AIDAALQRLPGLHLIGNAYKGVGLNDCIRNAAQLADALVAGNTSHAP

University of Cape Town

Appendix 2 - Sequence of designed fragments of M. xanthus PPOX cDNA

For convenience, and in order to sequence the entire *PPOX* gene, the cDNA sequence was divided into 4 fragments. The reverse oligo of fragment 4 (extended) was designed to include part of the plasmid vector to enable sequencing the 3' end of PPOX.

Fragment 1

ACCACATGCCGAGGACAACTGGAATGAATGTCGCCGTCGTGGGAGGTGGGATTTCGG
GGTTGGCCGTCGCGCATCATTTGCGCTCGCGCGGTACGGATGCCGTGCTTCTGGAGT
CCTCCGCCCGACTTGGCGGCGCGGTGGGCACGCATGCGCTCGCCGGCTACCTGGTG
GAGCAGGGGCCCAACAGCTTCCTGGACCGCGAGCCCGCAACGCGGGCGCTCGCGGC
GGCGCTGAATCTGGAGGGGCGAATTCGCGCCGCGGACCCGGCGGCGAAGCGTCGCT
ATGTCTACACGCGGGGCAGACTCCGGTCGGTACCGGCCTCGCCGCCCGCGTTTCTCG
CATCGGACATTC

Fragment 2

GAAGCGTCGCTATGTCTACACGCGGGGCAGACTCCGGTCGGTACCGGCCTCGCCGC
CCGCGTTTCTCGCATCGGACATTCTGCCGCTCGGCGCGCGGTTGCGCGTCGCTGGCG
AACTGTTCTCCCGCCGCGCGCCGGAGGGTGTGGACGAATCGCTGGCCGCCTTCGGC
CGCCGCCACCTGGGACACAGGGCGACGCAGGTGCTGCTCGACGCGGTGCAGACGGG
C

Fragment 3

CTCATCATCGAGGAGCACGGACGCCGCGCGGAACTGTCCGTGGCCCAGGTGGTACT
GGCGGCGCCCGCGCATGCCACCGCGAAATTGCTACGCCCACTGGATGACGCGCTCG
CCGCCCTGGTGGCGGGTATCGCCTATGCGCCCATCGCGGTGGTGCACCTGGGCTTC
GACGCGGGGACACTTCCGGCGCCGGATGGCTTTGGGTTCCTGGTGCCAGCGGAGGA
GCAGCGGCGGATGCTGGGCGCCATCCACGCGTCCACCACCTTTCCCTTCCGGGCCG
AGGGCGGACGCGTGCTCTATTCCTGCATGGTGG

University of Cape Town

Fragment 4

GAAATTGCTACGCCCACTGGATGACGCGCTCGCCGCCCTGGTGGCGGGTATCGCCTA
TGCGCCCATCGCGGTGGTGCACCTGGGCTTCGACGCGGGGACACTTCCGGCGCCGG
ATGGCTTTGGGTTCCTGGTGCCAGCGGAGGAGCAGCGGCGGATGCTGGGCGCCATC
CACGCGTCCACCACCTTTCCCTTCCGGGCCGAGGGCGGACGCGTGCTCTATTCCTGC
ATGGTGGGGGGCGCGCGTCAGCCAGGGCTGGTGGAACAGGACGAGGATGCATTGGC
GGCGCTGGCGCGCGAGGAACTGAAGGCGCTGGCAGGCGTGACGGCGCGCCCCTCC
TTCACGCGGGTGTTCCGCTGGCCGCTTGGCATTCCCCAGTACAACCTGGGACACCTG
GAGCGCGTGGCCGCTATCGACGCGGCGCTGCAACGCTTGCCCGGCCTGCACCTCAT
CGGGAATGCGTACAAGGGCGTGGGCCTCAACGACTGCATCCGCAA

Fragment 4 - extended

GAAATTGCTACGCCCACTGGATGACGCGCTCGCCGCCCTGGTGGCGGGTATCGCCTA
TGCGCCCATCGCGGTGGTGCACCTGGGCTTCGACGCGGGGACACTTCCGGCGCCGG
ATGGCTTTGGGTTCCTGGTGCCAGCGGAGGAGCAGCGGCGGATGCTGGGCGCCATC
CACGCGTCCACCACCTTTCCCTTCCGGGCCGAGGGCGGACGCGTGCTCTATTCCTGC
ATGGTGGGGGGCGCGCGTCAGCCAGGGCTGGTGGAACAGGACGAGGATGCATTGGC
GGCGCTGGCGCGCGAGGAACTGAAGGCGCTGGCAGGCGTGACGGCGCGCCCCTCC
TTCACGCGGGTGTTCCGCTGGCCGCTTGGCATTCCCCAGTACAACCTGGGACACCTG
GAGCGCGTGGCCGCTATCGACGCGGCGCTGCAACGCTTGCCCGGCCTGCACCTCAT
CGGGAATGCGTACAAGGGCGTGGGCCTCAACGACTGCATCCGCAACGCGGCGCAAC
TCGCGGACGCCCTGGTCGCGGGGAACACCTCCCACGCCCCGTAGTGAAGCTTG

University of Cape Town

Appendix 3 - Media

Equipment

- Autoclave Huxley, Speedy (Laboratory and Scientific Equipment Co. (Pty) Ltd., Cape Town, South Africa (RSA)

Reagents

- Agar Noble (Biolab Diagnostics, Gauteng, RSA)
- Bacto®- Yeast extract
- Bacto® - Tryptone
- KCl
- Mg^{2+}
- Glucose
- NaCl
- Ampicillin (Bodene (Pty) Ltd., Port Elizabeth, RSA)

Methodology

3.1 Luria-Bertani medium 1 L pH 7.5

Weigh out the following:

- NaCl 5 g
- Bacto®- Yeast extract 5 g
- Bacto® - Tryptone 10 g

- Add water to dissolve
- Adjust pH to 7.5
- Add H_2O to final volume of 1000 ml
- Sterilize by autoclaving

Store at 4°C

University of Cape Town

3.2 LB Agar plates 200 ml pH 7.5

Weigh out the following:

- NaCl 1 g
- Bacto- Yeast extract 1 g
- Bacto - Tryptone 2 g
- Agar 3 g

- Add H_2O to dissolve
- adjust pH to 7.5

- Add H_2O to final volume of 200 ml
- Sterilize by autoclaving
- Allow to cool (between 35-45 °C)
- Add 0.25 ml ampicillin (100 mg/ml stock)
- Aliquot 20 ml into petri dishes
- Allow to set
- Seal dish with parafilm

Store inverted at 4 °C in sealed plastic bag

3.3 SOC medium pH 7.0

Prepare the following:

- Bacto-tryptone 2 g
- Bacto-yeast extract 0.5 g
- NaCl (1 M) 1 ml
- KCl (1 M) 0.25 ml

- Add H_2O to a final volume of 100 ml
- Adjust pH to 7.0
- Autoclave and allow to cool to RT
- Add 1 ml filter sterilized Mg^{2+} (2 M) and 1ml filter-sterilized glucose (2 M)

Store at 4 °C

University of Cape Town

Appendix 4 - Generation and Storage of M. xanthus PPOX stocks (Dailey & Dailey, 1996a)

Equipment

- Orbital shaker incubator (Yidher LM-510, Taiwan)
- Thin-walled, sterile falcon tube (15 ml)
- Cryo storage tubes (2 ml)

Reagents

- 100 mg/ml Ampicillin (Bodene (Pty) Ltd., Port Elizabeth, RSA)
- 30 % Glycerol stock of pMx-PPOX plasmid DNA
- 6 ml LB medium
- 100 % sterile Glycerol

Methodology

- Inoculate 6 ml LB medium containing ampicillin (0.1 mg/ml) with 6 µl E. coli JM109 mxPPOX plasmid (already available and stored as stock in laboratory at -80 °C)
- Incubate at 37 °C on shaking incubator (225 rmp) overnight (14-18 hr)
- Pipette 300 µl of glycerol and 700 µl of culture into 2 ml cryo storage tubes
- Mix by inverting 4-6 times

Store stocks at -70 °C

University of Cape Town

Appendix 5 - Plasmid DNA extraction

Equipment

- Hermle Z400 centrifuge (Laboratory and Scientific Equipment Co. (Pty) Ltd., Cape Town, RSA)
- Labnet Spectrafuge 24D (Labnet International, Inc., Edison NJ, USA)
- 1.5 ml Sterile microcentrifuge tubes (Axygen Scientific Inc., Union City, CA, USA)

Reagents

- Wizard Plus SV Minipreps DNA purification kit (Promega Corporation, Madison, W1, USA)
    - Cell resuspension solution
    - Cell Lysis solution
    - Alkaline Protease solution
    - Neutralisation solution
    - Wash solution (with 95 % ethanol (Sigma-Aldrich, Buchs, Switzerland))
    - Nuclease-Free water (Elution solution)
    - Collection tube and column

Methodology

- Spin down 6 ml overnight culture (appendix 4) - 10 min at 10 000 xg
- Discard supernatant; resuspend pellet with 250 µl *Cell Resuspension solution*
- Transfer to a 1.5 ml microcentrifuge tube
- Add 250 µl *Cell Lysis Solution* to sample; mix by inverting 4-6 times
- Leave at RT till solution begins to clear(4-5 min)
- Add 10 µl *Alkaline Protease solution*; mix by inverting 4-6 times
- Leave at RT for exactly 5 min
- Add 300 µl of *Neutralising Solution*; mix by inverting 4-6 times
- Centrifuge at 14 000 xg for 15 min at RT
- Place column in *collection tube*
- Remove approximately 850 µl of supernatant (leave a small amount behind above the precipitate) and place in column. Spin at 14 000 xg for 1 min
- Discard flow through in collection tube
- Add 750 µl *Wash solution* to column ; spin at 14 000 xg for 1 min
- Discard flow through in collection tube
- Again, add 750 µl of *Wash Solution* and spin at 14 000 xg for 1 min

University of Cape Town

- Discard flow through; and respin empty column at 14 000 xg for 0.5 min to ensure all liquid is removed.
- Transfer the column to a 1.5 ml microcentrifuge tube; add 50 µl *Elution solution* directly onto the column
- Leave at RT for 2 min
- Elute DNA by spinning at 14 000 xg for 1.5 min

Store DNA at -20 °C

University of Cape Town

Appendix 6 - DNA Quantitation

Equipment

- GeneQuant Spectrophotometer (Pharmacia Biotech, Cambridge, UK)
- Glass capillaries (Separation Scientific, Honeydew, RSA)

Reagents

- Extracted mxPPOX plasmid DNA (appendix 5)
- Reference (nuclease free water used to elute the purified DNA - appendix 5)

Methodology

- Set GeneQuant for double stranded DNA:
  Path length = 0.5
  Factor = dsDNA

Tare Genequant:

- Dip capillary into reference solution till the solution reaches ¾ of capillary
- Prevent solution from leaking out by sealing the top end of the capillary with small ball of presstick. Remove any excess solution on the outside of the capillary using a clean paper towel
- Blank using reference

Quantitating DNA:

- Insert sample into a new capillary as described above
- Read O.D. of DNA and note the % purity and 260/280 ratio

University of Cape Town

Appendix 7 - Oligonucleotides design and preparation for use

Equipment

- Vortex-2 Genie (Scientific Industries Inc., Bohemia, NY, USA)

Internet

- Oligo parameter analyzer: http://eu.idtdna.com/analyzer/Applications/OligoAnalyzer/
- Oligos (Integrated DNA Technologies Inc., Coralville, IA, USA)

Methodology

- For 4 fragments covering *PPOX* gene, design oligo to flank desired region within insert using Primer designer (Software Packaging version 2, Scientific and Education Software)
- An additional oligo was designed for fragment 4, which extended into the vector to allow for complete screening of the *PPOX* gene
- Using oligo parameter analyzer (see material section) analyse oligo parameter: GC content, melting temperature (Tm), ΔG, Hairpin, self-dimer and hetero-dimer (see table below)

Parameter	Min.	Max.	Optimum
GC (%)	50	60	55
Tm (ºC)	70	80	74
polyX	2	3	2

- Oligos were manufactured by Integrated DNA Technologies (see table below)

- Resuspend oligos in 1 ml sterile dH_2O
- Incubate at RT for 30 min (vortexing every 10 min interval) to ensure oligo is completely dissolved
- Use a working stock concentration of 25 µM

Stored in aliquots at -20 ºC

University of Cape Town

mxPPOX oligos covering the *PPOX* gene

Oligo name	Sequence 5'----------3'	GC (%)	Tm (ºC)	Fragment size (bp)
MxF1F	ACC ACA TGC CGA GGA CAA	57.8	57.9	351
MxF1R	GAA TGT CCG ATG CGA GAA AC	50.0	54.0	
MxF2F	GAA GCG TCG CTA TGT CTA CAC	52.3	55.4	519
MxF2R	GAT GAT GAG CCT CCA ACC	55.5	52.8	
MxF3F	CTC ATC ATC GAG GAG CAC	55.5	52.4	313
MxF3R	CCA CCA TGC AGG AAT AGA G	52.6	52.7	
MxF4F	GAA ATT GCT ACG CCC ACT	50.0	52.9	495
MxF4R	TTG CGG ATG CAG TCG TTG	55.5	56.2	
vMxF4R	CTT CAC TAC GGG GCG TGG GAG	66.7	62.1	559

Mx = *M. xanthus*

F = Fragment

F/R = Forward/Reverse

v=vector

1-4 = Fragment number

University of Cape Town

Appendix 8 - Polymerase Chain Reaction

Equipment

- Robocycler Gradient 40 Temperature cycler (Stratagene Cloning Systems, CA, USA)
- Labnet Spectrafuge 24D (Labnet International, Inc., Edison NJ, USA)
- Vortex-2 Genie (Scientific Industries Inc., Bohemia, NY, USA)
- Microcentrifuge tubes 1.5 ml and 0.5 ml (Axygen Scientific Inc., Union City, CA, USA)

Reagents

- Go Taq flexi (Promega Corporation, Madison, W1, USA)
- Magnesium-free DNA polymerase 5 x buffer (Promega Corporation, Madison, W1, USA)
- 25 mM $MgCl_2$ (Promega Corporation, Madison, W1, USA)
- Deoxynucleotide triphosphate (dNTPs) (Promega Corporation, Madison, W1, USA)
    - dATP, dCTP, dGTP, dTTP and dUTP
    - 100 mM stock concentration
- Oligo (forward and reverse) (appendix 7)
- Sterile H_2O (Adcock Ingram Critical Care, Johannesburg, RSA)
- Mineral Oil (Promega Corporation, Madison, W1, USA)

Methodology

- Set up PCR reaction (master mix) in a 1.5 ml micro centrifuge tube on ice for the number of reactions required (see below)

	Final concentration	**Volume (µl)**
H_2O	N/A	32.8
5 X Buffer	1 X	10
25 mM $MgCl_2$	1.5 mM	3
25 µM F/R *	0.5 µM	1 each
2.5 mM dNTPs	100 µM	1
***Taq* polymerase**	1 U	0.2

* F – Forward oligo; R – Reverse oligo

- Aliquot 49 µl of master mix into 0.5 ml micro centrifuge tubes

University of Cape Town

- Add 1 µl DNA (100 -200 ng)
- Add 1 µl H_2O to blank
- Mix and spin down briefly and add a drop of oil before placing in thermo cycler

Polymerase chain reaction programme on Robocycler gradient 40 temperature cycler			
Step	Temperature (°C)	Time (min)	No. of Cycles
Initial Denaturation	95	1	1
Denaturation	95	0.5	
Annealing *	50-65	0.5	35
Extension	72	0.5	
Final Extension	72	7	1

*Determined using temperature gradient programme

University of Cape Town

Appendix 9 - DNA separation and visualization

9.1 6 % Non-Denaturing Polyacrylamide Gel Electrophoresis (PAGE)

Equipment

- 50 ml Measuring cylinder
- 100 ml Beaker
- Glass gel plates
- Hoefer vertical slab gel electrophoresis unit, SE600 series (Hoefer Scientific Instruments, San Francisco, USA)
    - Glass gel plates
    - Spacer comb (1.5 mm)
    - Clamps
    - Cams and spacers (1.5 mm)
    - Casting stand
    - Upper and lower buffer chambers
- Hamilton syringe (The Hamilton Company, Nevada, USA)
- PS1500 DC power supply (Hoefer Scientific Instruments, San Francisco, USA)
- UVItec gel documentation system (UVItech Limited, Cambridge, UK)

Reagents

- 10x TBE buffer pH 8.0
    - Tris/HCl 890 mM
    - Boric acid 890 mM
    - EDTA 20 mM

- 30 % acrylamide, 0.8 % bis-acylamide (A-Bis-A)
- 10 % ammonium persulphate (Promega Corporation, Madison, W1, USA)
- TEMED (N,N,N', N', - Tetramethyl-ethelenediamine)
  Store at 4 °C

- Sucrose sample solution (loading dye)
    - 30 g Sucrose
    - 10 mg Bromophenol blue
    - 5 ml Na_2EDTA (0.5 M), pH 8
    - In final volume 50 ml dH_2O (store in aliquots at -20 °C)

University of Cape Town

- Ethidium bromide - 100 µl of 1 mg/ml stock solution in 200 ml dH_2O (Sigma-Aldrich, St Louis, MO, USA)

Methodology

- Assemble glass plates (using 1.5 mm spacers) with clamps; mount plates on casting stand
- Gel solution – add the following in a 50 ml measuring cylinder:

TBE (10 X)	4 ml
A Bis A	8 ml
Add water to a final volume of	40 ml
TEMED	40 µl
Amps	400 µl

- Mix solution
- Pour solution into the space between 2 clamped plates assembled in the gel casting stand
- Insert 20 bay sample comb
- Allow gel to set at RT – 30 min
- Assemble upper chamber buffer on top of gel plates and fill with 500 ml 1xTBE
- Fill lower chamber with 1L 1XTBE
- Prepare samples and molecular bp marker (1:1 with sucrose sample solution)
- Loading gel – load DNA samples into gel sample wells using a Hamilton syringe
- Run gel at 250 V for 1.5 hr
- Remove gel from between glass plates and allow to stain in a solution of ethidium bromide (200 µl of 1 mg/ml stock solution to 200 ml dH_2O) for 10 min
- Rinse in dH_2O
- Visualize gel on UVItec documentation system and photograph

9.2 Agarose Gel Electrophoresis

Equipment

- Mgu-202T horizontal mini-gel system (CBS Scientific Co. Inc., Del Mar, USA)
- PS-1500 DC power supply (Hoefer Scientific Instruments, San Francisco, USA)
- UVItec gel documentation system (UVItech Limited, Cambrigde, UK)

University of Cape Town

Reagents

- MS-8 Agarose (Whitehead Scientific, Cape Town, RSA)
- 10 x TBE buffer pH 8.0 (see appendix 9.1)
- 1 mg/ml ethidium bromide (Sigma-Aldrich, St. Loius, MO, USA)
- Sucrose sample solution

Methodology

- Set up gel apparatus
- Weigh out agarose (for 1 % gel = 0.5 g in 50 ml 1x TBE) in 250 ml flask and add TBE
- Microwave agarose and cool briefly
- Add 10 µl of 1 mg/ml ethidium bromide, mix and pour into gel tray
- Insert spacer
- Allow gel to set
- Remove spacer
- Pour 1x TBE buffer to cover gel in gel tank
- Load samples (samples prepared in a 2:1 ratio with sucrose sample solution)
- Run gel at 100 V for 1.5 hr
- Visualise gel using the UVItec documentation system

University of Cape Town

Appendix 10 - GeneEditor Site Directed Mutagenesis

Principle

In vitro site-directed mutagenesis using the GeneEditor kit involves the use of antibiotic selection to obtain mutants.

Manually designed mutagenic oligos, as well as the provided selection oligos, are annealed to ssDNA (derived from alkaline denatured dsDNA). The selection oligos encode mutations that alter the ampicillin resistance gene, creating constructs that are resistant to the GeneEditor antibiotics selection mix. The constructs are then transformed into repair minus *E. coli* cells, thereby enhancing efficiency. Finally a second transformation into JM109 ensures proper segregation of mutant and wild type plasmids, increasing the number of mutants.

University of Cape Town

Equipment

- 0.5 ml PCR sterile microcentrifuge tubes (Axygen Scientific Inc., Union City, CA, USA)
- Labnet Spectrafuge 24D (Labnet International, Inc., Edison NJ, USA)
- GeneQuant spectrophotometer (Pharmacia Biotech, Cambridge, UK)
- Hybaid Omnigene thermal cycler (The Scientific Group, Cape Town, RSA)
- Sterile 17 x 100 mm polypropylene tubes (Laboratory and Scientific Equipment Co. (Pty) Ltd., Cape Town, RSA)
- Water bath (Memmert, Laboratory and Scientific Equipment Co. (Pty) Ltd., Cape Town, RSA)
- Orbital shaker incubator (Yidher LM-510, Taiwan)
- SI-18 incubator (Stuart Scientific, Laboratory and Scientific Equipment Co. (Pty) Ltd., Cape Town, RSA)

Reagents

- GeneEditor in vitro site-directed mutagenesis system kit (Promega Corporation Madison, W1, USA)
- Mutagenic oligos (Intergrated DNA Technologies Inc., Coralville, IA, USA)
- 2 M NaOH
- 2 mM EDTA
- 2 M ammonium acetate pH 4.6 (pH with glacial acetic acid)

- 70 % and 100 % ethanol (Sigma-Aldrich, Buchs, Switzerland)
- SABAX sterile, dH_2O (Adcock Ingram Critical Care, Johannesburg, RSA)
- LB broth (Pronadisa, Whitehead Scientific, Brackenfell, RSA)

10.1 Mutagenic Oligonucleotide design and preparation for use

Equipment

- Vortex-2 Genie (Scientific Industries Inc., Bohemia, NY, USA)

Internet

- Oligonucletide parameter analyzer: http://eu.idtdna.com/analyzer/Applications/OligoAnalyzer/
- Webcutter: http://users.unimi.it/~camelot/tools/cut2.html
- NEBcutter: http://tools.neb.com/NEBcutter2/index.php

Reagents

- Mutagenic oligos (Intergrated DNA Technologies Inc., Coralville, IA, USA)

Methodology

- Step 1

Design an oligo manually with the desired base change.

A single oligo is needed annealing to one strand of the DNA. Oligo should contain the desired mutation positioned approximately in the middle of the oligo sequence with 10 - 15 bases on either side of the base change.

- Step 2

Using The Oligonucletide parameter analyzer (see material section), analyse oligo parameters: GC content; melting temperature (Tm); ΔG; Hairpin; self-dimer; and hetero-dimer. The mutagenic oligo 3' end should end with a G or C nucleotide to stabilize the oligo during annealing between the oligo and template. Oligos were 5' phosphorylated to increase number of correctly engineered mutants (prerequisite for Gene-Editor mutagenesis (see table below).

Parameter	Min.	Max.	Optimum
GC (%)	50	60	55
Tm (°C)	70	80	74
polyX	2	3	2

University of Cape Town

- Step 3

Restriction site analysis

Webcutter (Heiman, 1997)	NEBcutter (Vincze *et al*., 2003)

Websites for both Webcutter and NEBcutter include certain additional enzymes absent in the other thereby allowing search of a larger database of restriction enzymes.

M. xanthus mutant oligos

Name	Sequence	Length
W408L	CGG GTG TTC CGC TTA CCG CTT GGC ATT C	28

- Step 4

Resuspend oligo in 1 ml dH_2O

Incubate at RT for 30 min to ensure oligo is completely in solution by vortexing every 10 min interval

Stored oligo concentrate at -20 ºC

10.2 Oligonucleotide T_M optimization

- **Set up PCR (appendix 8)**

- **Polymerase chain reaction programme:**

Step	Temperature (°C)	Time (min)	No. of Cycles
Initial Denaturation	95	1	1
Denaturation	95	0.5	
Annealing *	50-65	0.5	35
Extension	72	0.5	
Final Extension	72	7	1

*Gradient to determine optimum Annealing temperature

10.3 Plasmid DNA extraction (appendix 5)

10.4 Alkaline denaturation of dsDNA

Day1

Equipment

University of Cape Town

- Labnet Spectrafuge 24D (Labnet International, Inc., Edison NJ, USA)

Reagents

- 2 M NaOH
- 2 mM EDTA
- Deionized H_2O
- 2 M ammonium acetate (pH 4.6)
- 70 % and 100 % Alcohol

Methodology

- Set up a reaction with 2000 ng of DNA, 2 µl 2 M NaOH, 2 mM EDTA and dH_2O to make up a final volume of 20 µl
- Incubate at RT for 5 min
- Add 2 µl of 2 M ammonium acetate (pH 4.6) and 75 µl of 100 % ethanol (4 °C)
- Mix briefly before placing at -70 °C overnight

Day 2

Equipment

- Labnet Spectrafuge 24D (Labnet International, Inc., Edison NJ, USA)
- Hybaid Omnigene Thermal cycler (The Scientific Group, Cape Town, RSA)
- 17 x 100 mm polypropylene round-bottom falcon tubes

Reagents

- 70 % ethanol (Sigma-Aldrich, Buches, Switzerland)
- ssDNA (200 ng)
- Mutagenic oligo (1.25 pmol)
- GeneEditor™ system (Promega Corporation Madison, W1, USA)
    - Selection oligo
    - Annealing 10 X buffer
    - Synthesis 10 X buffer
    - T4 DNA Polymerase
    - T4 DNA Ligase
- SABAX sterile, dH_2O (Adcock Ingram Critical Care, Johannesburg, RSA)

Methodology

- Remove overnight reaction mixture from -70 °C

University of Cape Town

- Centrifuge at 14 000 g for 15 min at 4 °C
- Discard supernatant and wash pellet with 200 µl of 70 % ethanol
- Centrifuge at 14 000 g for 15 min at 4 °C
- Discard supernatant
- Air dry and then resuspend pellet in 50 µl nuclease free H_2O

- Quantify DNA using GeneQuant spectrophotometer (appendix 6)

10.5 Hybridization Reactions

- Set up a mutagenesis reaction as follows:

• ssDNA template	200 ng
• *Selection oligo	1 µl (from Gene Editor kit)
• Mutagenic oligo (1.25 pmol)	2 µl
• Annealing 10X buffer	2 µl (from Gene Editor kit)
• Add dH_2O to make up a final volume of	20 µl

* - use top selection oligonucleutide if using a FORWARD mutagenic oligo or bottom if using a REVERSE mutagenic oligo (see table below).

	Oligo	**Annealing temperature**
W408L	Forward	55 ºC

Place reaction tube in Hybaid Omnigene thermal cycler using the following conditions: heat reaction for 5 min at appropriate annealing temperature followed by a stepwise 1 ºC per min gradient cooling to 37 ºC

University of Cape Town

10.6 Mutant strand synthesis and ligation

- Once the hybridisation reaction is complete, spin down reaction and add the following reagent in the order below:

dH_2O	5 µl
Synthesis 10X Buffer	3 µl (from Gene-Editor kit)
T4 DNA Polymerase	1 µl (from Gene-Editor kit)
T4 DNA Ligase	1 µl (from Gene-Editor kit)

- Mix briefly and spin down before incubating at 37 °C (Hybaid Omnigene) for 90 min
- After incubation spin reaction at 14000 xg in microfuge

10.7 - Transformation

Equipment

- Sterile 17 x 100 mm polypropylene tubes
- Water bath
- Orbital shaker incubator
- SI-18 incubator

Reagents

- SOC medium (appendix 3)
- LB broth (appendix 3)
- Agar plates (appendix 3)
- BMH 71-18 mutS competent cells
- JM109 competent cells

Methodology

Transformation into BMH 71-18 mutS Competent Cells

- Pre-chill two 17 x 100 mm polypropylene falcon tubes on ice
- Remove frozen competent cells (at -70 °C) and leave until just thawed
- Flick cells and aliquot 100 µl of the cells into each polypropylene tube
- Add 1.5 µl of the mutagenesis reaction to the competent cells flicking tube 4-6 times and incubate on ice immediately for 10 min
- Heat shock the cells for 45-50 sec in a water bath at 42 °C then place on ice for 2 min

University of Cape Town

- Add 900 µl RT LB broth to the reaction and incubate on shaker at 37 °C for 60 min
- Add 4 ml of LB containing 50 µl of GeneEditor™ Antibiotic Selection Mix to the transformation reaction
- Place reaction back in shaking incubator at 37 °C and incubate for 16-18 hr
- Extract plasmid DNA from culture (appendix 5) and quantify DNA (appendix 6)

Transformation into JM109 competent cells

- Remove JM109 cells from storage (-70 °C) and leave till just thawed
- In pre-chilled polypropylene tubes, add plasmid DNA (5 – 10 ng) to 100 µl of JM109 cells
- Incubate tubes on ice for 30 min
- Heat shock the reaction for 47 sec in a water bath at 42 °C
- Immediately place on ice for 2 min, add 900 µl of RT SOC (appendix 3) medium then incubate at 37 °C for 1 hr in shaking incubator
- Spread previously prepared agar plates (appendix 3) with 100 µl of Gene Editor Antibiotic Mix using a sterile glass hockey stick (1/2-2 hr before spreading transformed JM109 cells)
- Spread 100 µl of cells onto the agar plates
- Leave to air dry for ±30 min
- Invert plates and incubate at 37 °C over night
- Visible single clones can be isolated and inoculated for expression and storage (appendix 4)

University of Cape Town

Appendix 11 - QuickChange Site directed mutagenesis

Equipment

- 0.6 ml PCR sterile microcentrifuge tubes (Axygen Scientific Inc., Union City, CA, USA)
- Labnet Spectrafuge 24D (Labnet International, Inc., Edison NJ, USA)
- GeneQuant spectrophotometer (Pharmacia Biotech, Cambridge, UK)
- Hybaid Omnigene thermal cycler (The Scientific Group, Cape Town, RSA)
- Sterile 17 x 100 mm polypropylene tubes (Laboratory and Scientific Equipment Co. (Pty) Ltd., Cape Town, RSA)
- Water bath (Memmert, Laboratory and Scientific Equipment Co. (Pty) Ltd., Cape Town, RSA)
- Orbital shaker incubator (Yidher LM-510, Taiwan)
- SI-18 incubator (Stuart Scientific, Laboratory and Scientific Equipment Co. (Pty) Ltd., Cape Town, RSA)

Reagents

- *PfuTurbo*® DNA polymerase (Promega Corporation, Madison, W1, USA)
- *Pfu Turbo* ® buffer (Promega Corporation, Madison, W1, USA)
- *DpnI* endonuclease (Fermentas, Life Sciences, Inqaba Biotech, RSA)
- Mutagenic oligos (Intergrated DNA Technologies Inc., Coralville, IA, USA)
- SABAX sterile, dH_2O (Adcock Ingram Critical Care, Johannesburg, RSA)
- Agar plates (appendix 3)

Methodology

11.1 Mutagenic Oligonucleotide design

Step 1

Design two complementary mutagenic oligos with the desired base change. The desired mutation should be in the middle of the oligo with 10-15 bases of the correct sequence on both sides. It is recommended that the oligo ends with a G/C base to stabilize the oligo during annealing between the oligo and template.

University of Cape Town

Step 2

Using Oligonucletide parameter analyzer (see material section) analyse oligo parameters: GC content; melting temperature (Tm); ΔG; Hairpin; self-dimer; and hetero-dimer. No 5' phosphorylation is required.

Parameter	Minimum	Maximum	Optimum
GC %	40	60	55
polyX	2	3	2
length (bp)	25	45	25

Tm of hairpin as well as oligo hetero-dimer should be lower than reaction annealing temperature

Step 3

Where possible select restriction enzyme from provided websites (Webcutter or NEBcutter) below. Select an enzyme that cuts fragment the least amount of times and ensure the altered base/s fall within the recogition sequence

Webcutter - http://users.unimi.it/~camelot/tools/cut2.html

NEBcutter – http://tools.neb.com/NEBcutter2/index.php

University of Cape Town

M. xanthus mutant oligos

Mutant	Sequence	Length (bp)
S20Aforw	5' – CGTGGGAGGTGGGATTGCGGGGTTGGC-3'	27
S20Arev	5'–GCCAACCCCGCAATCCCACCTCCCACG-3'	
S20Tforw	5' - CGTGGGAGGTGGGATTACGGGGTTGGC -3'	27
S20Trev	5' - GCCAACCCCGTAATCCCACCTCCCACG -3'	
E39Qforw	5'-GCCGTGCTTCTGCAGTCCTCCGCCCG-3'	26
E39Qrev	5'-CGGGCGGAGGACTGCAGAAGCACGGC-3'	
E39Dforw	5'- GCCGTGCTTCTGGATTCCTCCGCCCG-3'	26
E39Drev	5'- CGGGCGGAGGAATCCAGAAGCACGG-3'	
E39Aforw	5'–GCCGTGCTTCTGGCGTCCTCCGCCCG -3'	26
E39Arev	5'–CGGGCGGAGGACGCCAGAAGCACGGC -3'	
E39Kforw	5'- GCCGTGCTTCTGAAGTCCTCCGCCCG-3'	26
E39Krev	5'- CGGGCGGAGGACTTCAGAAGCACGG-3'	
W408Yforw	5'–CGGGTGTTCCGCTACCCGCTTGGCATTC -3'	28
W408Yrev	5'–GAATGCCAAGCGGGTAGCGGAACACCCG -3'	
N441Iforw	5'-CACCTCATCGGGATTGCGTACAAGGGC-3'	27
N441Irev	5'-GCCCTTGTACGCAATCCCGATGAGGTG-3'	
N441Qforw	5'–CTGCACCTCATCGGGCAAGCGTACAAGGGCGTG3'	33
N441Qrev	5'–CACGCCCTTGTACGCTTGCCCGATGAGGTGCAG3'	

For oligo preparation see appendix 7

11.2 DNA extraction (appendix 5)

11.3 Mutant Strand Synthesis Reaction

Day 1

Polymerase Chain Reaction

Reagents

- dNTPs 20 mM (stock)
- *PfuTurbo*® polymerase 100 U
- reaction buffer 10 X
- mutagenic oligos 10 µM

University of Cape Town

- dsDNA 10 ng/µl
- H_2O

Methodology

Setup PCR reaction as follows:

Reagent	Volume (µl)
dNTP	1
PfuTurbo® Buffer	5
Oligo Forward	2
Oligo Reverse	2
PfuTurbo® Polymerase (added last)	0.5
H_2O	34.5
DNA	5

University of Cape Town

Flick tube to mix, spin briefly then and place in Omigene Hybaid thermal cycler using the following program:

- **Hybaid Omnigene program cycle for one base change**

	Temp. (°C)	Time (min)	No. of Cycles
Initial Denaturation	94	5	1
Denaturation Annealing Elongation	94 *55 72	0.5 0.5 #12	 12

*-standard annealing temperature used and can be altered for optimization

- 2 min/1kb. *M. xanthus* vector + insert = ±6 kb

- **Hybaid Omnigene program cycle for two or more base change**

	Temp. (°C)	Time (min)	No. of Cycles
Initial Denaturation	94	5	1
Denaturation Annealing Elongation	94 *55 72	0.5 0.5 12	 16

*-standard annealing temperature used and can be altered for optimization

- Place on ice to cool
- To confirm PCR product run a 0.8 % agarose gel (appendix 9) (with 8 µl ethidium bromide (1mg/ml) added to gel). Load 5 µl of product + 5 µl H_2O with 1.5 µl of loading dye. Run gel at 80 mV

- ***DpnI* digest of 45 µl PCR product:**
    - 45 µl PCR product
    - 2 µl *Dpn*I
    - 4.7 µl *DpnI* buffer added directly to the PCR product (10 X)
    - Incubate 1 hr at 37 °C

University of Cape Town

11.4 Transformation

- Pre-chill 17 x 100 mm polypropylene falcon tubes on ice
- Remove frozen JM109 cells (stored at-70 °C)and allow to thaw
- Aliquot 100 µl of JM109 cells into pre-chilled falcon tubes
- Add 5-10 µl of digested product, ensuring no oil is included, to the 100µl of JM109 cells, flick 4-6 times whilst adding
- Incubate on ice for 30 min
- Heat shock the reaction by placing the falcon tubes into a 42 °C water bath for 45 sec
- Immediately place on ice for 2 min
- Add 900 µl LB medium, and incubate in shaking incubator at 37 °C for 1 hr
- Transfer reaction to a 1.5 ml microfuge
- Spin down cells at 14 000 xg for 2 min
- Discard 900 µl of supernatant and resuspend cells with remaining supernatant
- Spread previously prepared agar plate (appendix 3) with 50 µl transformed JM109
- Leave to air dry - 30 min
- Invert plates and incubate in incubator at 37 °C over night
- Visible single clones can then be isolated and inoculated for expression (appendix 4)

University of Cape Town

Appendix 12 - Restriction analysis

Equipment

- 0.6 ml sterile microcentrifuge tubes (Axygen Scientific Inc., Union City, CA, USA)
- Labnet Spectrafuge 24D (Labnet International, Inc., Edison NJ, USA)
- Techni Dri-Block® DB-2D (Laboratory and Scientific Equipment Co. (Pty) Ltd., Cape Town, RSA)

Reagents

- Restriction endonuclease
- Sucrose sample solution
- Mineral oil (Promega Corporation, Madison, W1, USA)

Methodology

- Make up a master mix for the required number of DNA samples and blank using the relevant enzyme and buffer (15 µL used per reaction digest)

	Final Conc.	*HinfI* (µl)	*ItaI* (µl)	*Hpy188III* (µl)	*BsmI* (µl)	*TfiI* (µl)
Enzyme	2 units	0.2	0.2	0.4	0.2	0.4
Buffer	1 X	2	2	2	2	2
*BSA	0.2 mg/ml	0.2	-	0.2	-	-
dH_2O		12.6	12.8	12.4	12.8	12.6
Total vol.		15	15	15	15	15

*Bovine serum albumin

- Add 5 µl of PCR product
- Mix briefly, spin down
- Finally add a drop of mineral oil
- Place on heating block (at relevant optimum temperature: see table below)
- Incubate as seen in table below.
- Visualise digested samples on a 6 % non-denaturing PAGE;
- Load the entire digest product (20 µl digest + 3 µl loading dye).
- Load 100 bp marker using the following dilution (8 µl marker 1:1 with sucrose sample solution)

University of Cape Town

- For sucrose sample solution see appendix 9.1

RE Name	**Recognition sequence 5'……3'**	**Optimum temp. (°C)**	**Incubation Time (hr)**	**Clones**	**Source**
HinfI	GANTC	37	3	Glu39Gln; Glu39Lys; Glu39Ala	Promega Corporation, Madison, USA
ItaI	GCNGC	37	3	Trp408Leu	Roche Diagnostics Pty Ltd, Randburg, SA
BsmI	GAATGC	65	O/N	Asn441Ile	New England Biolabs Inc., Laboratory Specialist Services, Cape Town, RSA
TfiI	GAWTC	65	O/N	Glu39Asp	New England Biolabs Inc., Laboratory Specialist Services, Cape Town, RSA
Hpy188III	TCNNGA	37	3	Asn441Gln	New England Biolabs Inc., Laboratory Specialist Services, Cape Town, RSA

University of Cape Town

Appendix 13 - Direct Sequencing

Equipment

- 1.5 ml sterile microcentrifuge tube (Axygen Scientific Inc., Union City, CA, USA)

Reagents

- Illustra GFX PCR DNA and Gel Band Purification kit (Amersham Biosciences, UK)

Methods

PCR performed as per appendix 8

PCR product clean-up

- Transfer PCR product (without any trace of oil) into a 1.5 ml microcentrifuge tube
- Add 500 µl Capture buffer type 2
- Mix solution thoroughly by pipetting the sample up and down using a 1000 ml pipette
- Spin down briefly
- Place GFX column into a collection tube
- Transfer the capture buffer 2 and sample mixture into the GFX column
- Spin at 16 000 xg for 30 sec
- Discard flow through in the collection tube. Place GFX column back inside the collection tube
- Add 500 µl of wash buffer type 1 to the GFX column
- Centrifuge at 16 000 xg for 30 sec; discard flow through in the collection tube
- Repeat the wash by adding 500 µl of wash buffer type 1 to the GFX column
- Centrifuge at 16 000 xg for 30 sec; discard flow through in the collection tube
- Place GFX column into a sterile 1.5 microcentrifuge tube
- Add 50 µl elution buffer (type 6) directly onto the membrane in the GFX column
- Leave at RT for 2 min
- Centrifuge at 16 000 xg for 1 min
- Quantitate cleaned PCR product
- Store at -20 °C till use

University of Cape Town

Sequencing

- Direct sequencing was done by the Core DNA sequencing facility of the University of Stellenbosch using the ABI-3100 Automated Genetic Analyzer and a Big Dye version 3.0 kit (Applied Biosystems, Brachberg, USA).

- Each fragment was sequenced in both a forward and reverse direction to ensure the entire PPOX gene was covered. A volume of 5 µl (8 ng/µl) was sent for sequencing plus 5 µl of 1.1 pmol/µl oligo (either forward or reverse).

University of Cape Town

Appendix 14 - Protein Purification

Equipment

- Gilson pump
- Oribital shaker incubator (Yidher LM-510, Taiwan)
- Refrigerated centrifuge (Centrikon T-324, Kontron Instruments, Italy)
- Misonix Sonicator 300 (Laboratory and Scientific Equipment Co. (Pty) Ltd., Cape Town, RSA)
- Source 15Q Glass column (6 mm x 300 mm) (Amicon Ltd, Stonehouse, UK)
- Gilson Minipuls 3 pump (Laboratory and Scientific Equipment Co. (Pty) Ltd, Cape Town, RSA)

14.1 *M. xanthus* PPOX purification

Reagents

- TALON metal affinity resin (Clonetech Laboratories, Palo Alto, CA, USA)
- Phenyl-methy-sulfonyl fluoride (PMSF (10 mg/ml) (Sigma-Aldrich, St. Loius, MO, USA)
    - Isopropanol 10 ml
    - PMSF 100 mg

- SONICATION BUFFER pH 8.0
    - Tris-HCl 20 mM
    - NaCl 100 mM
    - Tween 20 1 %

- EQUILIBRATION BUFFER pH 8.0
    - Tris-HCl 20 mM
    - NaCl 100 mM
    - Tween 20 0.5 %

- WASH BUFFER pH 6.3
    - $NaH_2PO_4.2H_2O$ 50 mM
    - NaCl 100 mM
    - Tween 20 0.5 %
    - Glycerol 10 %
    - Imidazole 25 mM

University of Cape Town

- ELUTION BUFFER pH 7.0
  - $NaH_2PO_4.2H_2O$ 50 mM
  - NaCl 100 mM
  - Tween 20 0.5 %
  - Glycerol 10 %
  - Imidazole 150 mM

Methodology

- Inoculate 1 ml of stock cells (pMx-PPOX) and 1 ml ampicillin (100 mg/ml) into 1 LB media (appendix 4)
- Incubate on shaker (225 rpm) at 37°C for 22 hr
- Aliquot culture into 4 centrifuge bottles (250 ml); centrifuge for 30 min
- Discard supernatant; resuspend pellets in 30ml sonication buffer + 30 µl PMSF with the use of a golf-stick shaped glass rod
- Note: Avoid frothing during resuspension

Sonication

- In a plastic beaker, sonicate solution using the macro-probe of the ultra-sonicator
- Sonicate at 60 Watts for 30 sec X 4
- After every 30 sec sonication place beaker on ice to cool reaction (this will prevent solution from overheating resulting in denatured protein)
- Centrifuge sonicate for 40 min at 105 000 xg in ultracentrifuge (4 °C)
- Collect supernatant for column (LOAD)

Column preparation

- Set up column on a retort stand
- Connect column to pump by connecting to plastic tubing
- Add 600 µl mixed Talon resin slurry into the column and allow to settle
- Equilibrate column with 10 ml of equilibrium buffer (containing 10 µl of PMSF) ensuring that the resin bed is not disrupted
- Note final volume of centrifuged sonicate (LOAD)

University of Cape Town

Protein binding and elution

- Load the supernatant of the sonicate onto column (15 ml/hr)
- Collect flow-through (VOID) in fractions
- Pool fractions (note final volume)
- Wash column with column wash buffer (30 ml with 30 µl PMSF) at 16-18 ml/hr
- Collect flow through (WASH) in fractions (bound protein is visible on column – yellow colour)
- Pool fractions (note final volume)
- To elute protein: add Elution buffer (15 ml with 15 µl PMSF) to column
- Remove tubing from the pump
- Collect free-flow eluate in fractions of about 5 drops/tube in glass 5 ml test tubes
- Pool yellow eluate (PPOX) and note final volume

Note: All purification was done at 4 °C to reduce precipitation of PPOX after elution and to avoid non-specific binding of protein to Talon resin. Add 1.5 equivalent commercial FAD cofactor to the purified PPOX protein (improves protein stability).

.

14.2 Human PPOX purification

Reagents

- TALON metal affinity resin (Clonetech Laboratories, Palo Alto, CA, USA)
- Phenyl-methy-sulfonyl fluoride (PMSF (10 mg/ml) (Sigma-Aldrich, St. Loius, MO, USA)
    - Isopropanol 10 ml
    - PMSF 100 mg

- SONICATION BUFFER pH 8.0
    - Tris-HCl 20 mM
    - NaCl 300 mM
    - Imidazole 10 mM
    - N-octyl-β-D-glucopyranoside 1 %

- EQUILIBRATION BUFFER pH 8.0
    - Tris-HCl 20 mM
    - NaCl 300 mM
    - Imidazole 10 mM

University of Cape Town

- N-octyl-β-D-glucopyranoside 0.5 %

- WASH BUFFER pH 7.0
  - Tris-HCl 20 mM
  - NaCl 300 mM
  - Imidazole 20 mM
  - N-octyl-β-D-glucopyranoside 0.5 %

- ELUTION BUFFER pH 7.0
  - Tris-HCl 20 mM
  - NaCl 300 mM
  - Imidazole 200 mM
  - N-octyl-β-D-glucopyranoside 0.5 %

Methodology

Purification was carried out as for mxPPOX purification at 4 °C (appendix 14.1). Add 1.5 equivalent commercial FAD cofactor to the purified PPOX protein (improves protein stability).

University of Cape Town

Appendix 15 - Protein separation and visualisation

Denaturing Sodium Dodecyl Sulphate Polyacrylamide gel electrophoresis (7.5 - 17.5 % gradient SDS-PAGE)

Equipment

- Glass gel plates (Hoefer Scientific Instruments, San Francisco, USA)
- SE600 series vertical slab gel electrophoresis unit (Hoefer Scientific Instruments, San Francisco, USA)
- PS1500 DC power supply (Hoefer Scientific Instruments, San Francisco, USA)
- UVItec gel documentation system (UVItech Limited, Cambridge, UK)
- 0.5 ml Microcentrifuge tubes (Axygen Scientific Inc., Union City, CA, USA)
- Hamilton syringe (The Hamilton Company, Nevada, USA)
- Gilson Minipuls 3 pump (Laboratory and Scientific Equipment Co. (Pty) Ltd., Cape Town, RSA)
- SG Series Gradient Maker (Hoefer Scientific Instruments, San Francisco, CA, USA)

Reagents

- Spacer buffer pH 6.8
  - Tris-HCl 0.125 M

- "Low" glycerol concentration buffer pH 8.8
  - Tris-HCl 1 M
  - Glycerol 7.5 %

- "High" glycerol concentration buffer pH 8.8
  - Tris-HCl 1 M
  - Glycerol 30 %

- A-Bis-A solution
  - Acrylamide 30 g
  - Bisacrylamide 0.8g
    in 100ml

- Loading Dye
  - Glycerol 20 %

University of Cape Town

- SDS 2 %
- Tris-HCl (pH 6.8) 0.125 M
- Bromophenol blue 0.25 % w/v
- β-mercaptoethanol 0.2 %

- RainbowTM colour protein molecular weight marker (Amersham, Pharmacia Biotech, Southampton, UK)
- Spectra^{TM} multicolour broad range protein ladder (Fermentas, Life Sciences, Inqaba Biotech, RSA)
- Ammonium persulphate
- N,N,N',N'-Tetramethyl-ethelendiamine (TEMED)
- Tank Buffer pH 8.8
  - Tris-HCl 0.025 M
  - Glycine 0.2 M
  - SDS 0.1 %
- Coomassie Stain
  - Coomassie Brilliant Blue R250 (w/v) 0.1 %
  - Methanol (w/v) 30 %
  - Trichloroacetic acid (v/v) 10 %

- Destain
  - Methanol (v/v) 20 %
  - Glacial acetic acid (v/v) 20 %

Methodology

- Assemble glass plates (including 1.5 mm spacers) with clamps; mount plates on casting stand

7.5% resolving solution

- To a 25 ml cylinder add:

  - "Low" glycerol concentration buffer 7 ml
  - A-Bis-A solution 5 ml
  - SDS (10 %) 0.3 ml
  - H_2O 7.7 ml

- Mix by covering with parafilm and inverting
- 100 µl ammonium persulphate (50 mg/ml)

University of Cape Town

- 10 µl TEMED
- Mix by covering with parafilm and inverting

17.5 % resolution solution

- To a 25 ml cylinder add:

o "High" glycerol concentration buffer	7 ml
o A-Bis-A solution	12 ml
o SDS (10 %)	0.3 ml
o H_2O	0.7 ml

- Mix solution
- Add 100 µl ammonium persulphate (50 mg/ml)
- Add 10 µl TEMED
- Mix solution
- Ensure taps in gradient maker are both closed
- Pour 15ml of 7.5 % solution into the left chamber of the gradient mixture and 15 ml of 17.5 % solution into right hand chamber
- Turn on magnetic stirrer to mix right chamber solution
- Simultaneously open tap between the two chambers and turn on the pump to allow solution to pump into space between assembled plates in gel casting stand
- Stop the pump when the solution is approximately 2 cm from top of the plate
- Layer water on top of the gel and allow to set for 1 hr

Spacer Solution

- In a 25 ml cylinder add:

o A-Bis-A solution	1.2 ml
o Spacer buffer	8.6 ml
o SDS (10 %)	0.1 ml

- Mix solution
- Add 100 µl ammonium persulphate (150 mg/ml)
- Add 10 µl TEMED
- Remove water from top of set gel as prepared above
- Insert comb (for well formation) in between glass plates
- Add spacer solution to cover the teeth of the comb and allow to set (15 min)

University of Cape Town

- To prepare samples (or molecular weight marker) add an equal volume to loading dye
- Boil molecular weight marker and samples for 3 min
- Assemble upper buffer chamber on top of gel plate and fill with 500ml Tank buffer
- Fill lower chamber with 1 L tank buffer
- Load samples into the wells using a Hamilton syringe
- Run gel at 70 V for 16 hr (use bromophenol blue movement to assess gel front - it should be ±1.5 cm from the bottom of the plates)
- Remove gel from between the plates and stain with constant shaking for 2 h
- Destain by placing gel in destaining solution on shaker
- Visualise using the UVItec documentation system

University of Cape Town

Appendix 16 - BSA microassay protein quantitation

- 12 x 75 mm plastic tubes
- Hitachi U-1100 UV/VIS spectrophotometer (Koki Co. Ltd., Tokyo, Japan)
- Cuvette (plastic)

Reagents

- 1 mg/ml Bovine serum albumin (BSA) (Sigma-Aldrich, St. Louis, MO, USA)
- Bio-Rad Protein Assay Dye Reagent Concentrate (Bio-Rad Laboratories, Munich, Germany)

Methodology

- Make a 1/10 dilution of 1 mg/ml BSA
- Prepare 6 linear dilutions of the 0.1 mg/ml BSA (20-80 µl in a final volume of 800 µl)
- Prepare relevant dilutions of the sample and include a relevant blank
- Add 200 µl Bio-Rad dye reagent to each tube and vortex
- Allow to stand at RT for 5 min minimum and 1 hr maximum for colour development.
- Set the spectrophotometer (595 nm VIS) and read samples against relevant blank
- Plot BSA concentration versus its reading at 595nm (use Microsoft Excel)
- Insert a trendline (for best fit by linear regression)
- Extrapolate concentrations of PPOXs from standard curve

University of Cape Town

Appendix 17 - Protoporphyrinogen oxidase assay (Meissner et al., 1986)

17.1 Preparation of substrate (Protogen)

Equipment

- Magnetic stirrer (Fried Electric, Laboratory and Scientific Equipment Co. (Pty) Ltd., Cape Town, SA)
- 0.45 µM Biological filter (Millex-HV Millipore, Millipore Corporation, Bedford, MA, USA)
- 50 ml Glass Boiling tube with stopper
- Hitachi U-1100 UV/VIS spectrophotometer (Koki Co. Ltd., Tokyo, Japan)

Reagents

- Proto (Porphyrin products, Logan UT, USA)
- KOH
- Ethanol (Sigma-Aldrich, Buchs, Switzerland)
- HCl
- 1.4-Dithio-DL-threitol (DTT) (Fluka Biochemika, Sigma-Aldrich, Switzerland)

Methodology

- In a flask covered with tin foil, dissolve 12 mg proto in 30 ml freshly prepared 10 mM KOH in 20 % ethanol
- Mix on a magnetic stirrer at RT O/N
- Add 5 ml of the dissolved, filtered (0.45 µM) proto stock into a boiling tube (covered in tin foil)
- Add 10 ml of 10 mM KOH
- Make a 1/100 dilution of proto/KOH solution in 2.7 N HCl
- Measure absorption of diluted mix at 408 nm
- Reading should be 0.6-0.8
- Determine concentration of proto
- Proto concentration determine - E_{408nm} = 262 $mM^{-1}.cm^{-1}$ (Falk, 1964)

University of Cape Town

17.2 Na-Hg amalgam

SAFETY PRECAUTIONS WHEN WORKING WITH MERCURY

- EXTRACTOR FAN IN FUME HOOD SHOULD BE TURNED ON FOR 10 MIN PRIOR TO USE AND ENTIRE PROCEDURE PERFORMED IN FUME HOOD
- KEEP EXTRACTOR FAN AND GLASS SHIELD PULLED DOWN TO RECOMMENDED LEVEL
- VACATE ROOM - ONLY EXPERIMENTER SHOULD BE IN THE ROOM
- WEAR DOUBLE GLOVES (VINYL)
- WEAR A RESPIRATOR MASK WITH MERCURY VAPOUR FILTERS (TO PREVENT INHALATION OF MERCURY FUMES)
- CHANGE GLOVES IMMEDIATELY AFER MAKING AMALGAM AND BEFORE PROCEEDING TO NEXT STEP

Equipment

- M-120 weighing balance
- Round bottomed glass flask with side arm
- Bunsen burner
- Mortar and pestle

Reagents

- 1.6 g Sodium metal
- 43.2 g Mercury

Methodology

Reaction to be done in a laminar hood

- Weigh out 1.6 g Na and place in paraffin oil
- Weigh out 43.2 g Hg
- Connect round bottomed flask with side arm to nitrogen gas tube and turn on nitrogen gas
- Turn on Bunsen burner
- Pour the Hg into the round bottomed flask
- Heat Hg for approximately 30 sec over an open flame
- Move flask from flame
- Add sodium metal pieces (one at a time) after blotting to remove oil, shaking briskly while adding
- Once all the Na is added bring flask back to flame and shake over flame

University of Cape Town

- Pour solution into Mortar
- Use pestle to gently break and grind the amalgam into small pieces

17.3 Reduction of proto to protogen (substrate)

- Add the amalgam in 3 additions to the proto in the boiling tube
- Seal with stopper and shake vigorously in the dark under a fumehood
- Release the pressure periodically by removing the stopper to allow gas to escape (ONLY RELEASE GAS IN FUME HOOD BEHIND GLASS SHIELD)
- Keep on shaking until reduction is complete (check under UV light (light pink colour indicates reduction)
- Filter through a 0.45 µM filter into a small beaker
- Use 1M MOPS to reduce the pH of the filtrate to 8.1
- KEEP EXTRACTOR FAN OF FUME HOOD RUNNING AND PULL DOWN GLASS SCREEN TO RECOMMENDED LEVEL. DISPOSE OF GLOVES IN BIOHAZARDOUS BOX, AND PUT ON NEW GLOVES BEFORE PROCEEDING TO NEXT STEP

- Note – protogen autooxidises in the presence of O_2 and light so perform procedure in darkened room and use substrate as soon as possible to minimize background autoreduction

17.4 PPOX assay

Equipment

- Water bath (Memmert, Laboratory and Scientific Equipment Co. (Pty) Ltd., Cape Town, SA)
- Hitachi 650-10S Fluorescence Spectrophotometer (Koki Co. Ltd, Tokyo, Japan)
- 12 x 75 mm Glass tubes
- 12 x 75 mm Plastic tubes
- Lotus 123

Reagents

- Assay buffer pH 8.1
  - Tris/HCl 100 mM
  - EDTA 1 mM
  - DTT 3 mM
  - Tween 20 0.1 %

University of Cape Town

- Cuvette buffer pH 8.1
    - Tris/HCl 100 mM
    - EDTA 1 mM
    - DTT 3 mM

Methodology

- Calibration of the Fluorimeter
- Fluorimeter settings
    - Excitation - 405 nm
    - Emission - 634 nm
    - Sensitivity - 1 X

- Make up a 1/10 dilution of filtered proto in boiling tube
- Add 250 µl of the 1/10 dilution to 6 ml cuvette buffer
- Mix briefly
- Make up the following dilutions with cuvette buffer

Proto 1/250 dilution (µl)	cuvette buffer (µl)
1000	0
800	200
600	400
400	600
200	800

- Calibrate fluorimeter by setting the 1000 µl proto reading at 1000 relative fluorescence units (RFU)

- Cuvette tubes
- Add 1 ml of cuvette buffer to plastic assay tubes

- Assay tube reaction
- To glass assay tubes add 880 µl assay buffer, 20 µl PPOX sample or blank, mix and place in water bath for at least 30 min

See table below:

University of Cape Town

PPOX Assays					
	Enzyme conc optimisation	Purification activity	pH gradient	Temp gradient	kinetic activity
enzyme (µl)	20	20	20	20	20
Assay buffer (µl)	880	880	880	880	#
substrate (µl)	100	100	100	100	#

= varying substrate concentration are used for kinetic determinations (e.g. K_M); therefore different volumes of substrate and assay buffer are added to achieve desired substrate concentration.

- Before adding the substrate to assay glass tube, mix briefly and incubate tubes at 37 °C for 30 min
- Add substrate to assay tubes and continue incubation at 37 °C for 10 min
- At 10 min transfer 100 µl assay reaction into cuvette tube (see above) and read the fluorescence
- Repeat this at 3 further time intervals (e.g. 20, 30 and 40 min)

Calculations

- Use Lotus 123 (spread sheet customized to calculate activity of PPOX)
- Auto-oxidation rate is subtracted
- Activity is expressed as nmol/ml/hr

University of Cape Town

17.5 pH gradient assay

Reagents

- Phosphate buffer (pH 6 - 7)
  - $NaPO_4$ 100 mM
  - EDTA 1 mM
  - Tween 20 0.1 %

- Tris buffer (pH 7.2 - 9)
  - Tris/HCl 100 mM
  - EDTA 1 mM
  - Tween 20 0.1 %

- DTT (Fluka Biochemica, Sigma-Aldrich, Switzerland)

Methodology

- Measure out 10 ml of each buffer and dissolve 3 mM DTT
- Reaction tubes set up for pH 6 - 7 (Phosphate buffer)
- Reaction tubes set up for pH 7.2 - 9.0 (Tris buffer)
- A blank reaction was set up for the respective pH reaction
- Assay performed as in section 17.4
- Obtain activity at respective pH
- Convert activity to percentage of activity
- Plot pH versus percentage of activity using Microsoft Excel. Highest peak is equivalent to pH optimum

University of Cape Town

Appendix 18 - Flavin Cofactor Analysis

18.1 Spectral analysis

Equipment

- Hitachi U-3200 UV/VIS Spectrophotometer (Koki Co. Ltd., Tokyo, Japan)
- Quartz cuvette

Method

- Measure optical density of purified PPOX at a wavelength of 450 nm using elution buffer as a reference solution
- Determine the protein concentration of PPOX
- Express the absorption as 450 nm per mg protein per ml
- Read UV/VIS spectrum 550 - 300 nm of purified wild type and mutants (speed: 120 nm/min)

18 .2 Sulfite-PPOX reactivity

Equipment

- Hitachi U-3200 UV/VIS Spectrophotometer (Koki Co. Ltd., Tokyo, Japan)
- Quartz cuvette

Reagents

- Na_2SO_3 (2 M)
- $NaPO_4$ buffer (50 mM, pH 7.0) (see elution buffer, appendix 14)
- Protein ~10 -20 µM protein

Method

- Prepare 2 M stock solution of Na_2SO_3 in 50 mM phosphate buffer (pH 7.0)
- Set temperature of waterbath attached to spectrophotometer to desired temperature (25 °C or 37 °C)
- For blank reaction add aliquots of sulfite (see table below) to buffer to make up to total reaction volume of 1 ml
- For reaction add aliquots of sulfite to ~10 µM protein/FAD
- For 450 nm bleaching - read absorbance at 450 nm to observe decrease in absorbance.
- Thereafter scan wavelength spectrum.

University of Cape Town

Appendix 19 - OxyGraph: Oxygen consumption

Equipment

- DW1 Oxygraph chamber (Hansatech Instruments Ltd., Norfolk, England)
- Membrane applicator shaft
- O-ring
- Circulating water bath (Memmert, Laboratory and Scientific Equipment Co. (Pty) Ltd., Cape Town, SA)
- Tweezer

Reagents

- DW1 oxygen electrode chamber kit (Hansatech Instruments Ltd., Norfolk, England)
- paper spacer
- membrane
- 50 % saturated KCl solution
- Nitrogen gas

University of Cape Town

<u>Oxygraph Electrode preparation</u>

- Place a drop of KCl electrolyte on top of the dome of the sensor unit (see diagram below)

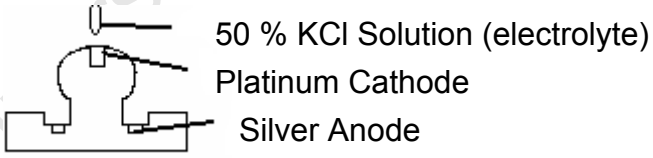

- Place three drops at equal intervals in the electrode well containing the silver anode
- With tweezers, place a 1.5 cm x 1.5 cm paper spacer over the electrode (This acts as a wick to continuously provide an electrolyte layer to the electrode)
- Again place a 2.5 x 2.5 cm area of PTFE membrane over the electrode (Note: membrane is easily damaged and finger marks will reduce the sensitivity of the electrode) (see diagram below)

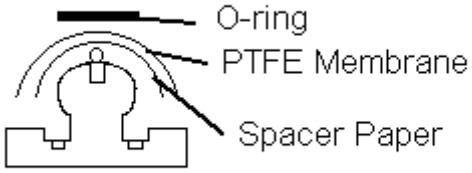

- Using the A2 membrane applicator firmly place an O-ring over the membrane/spacer combination by sliding down the shaft until the O-ring slips off the applicator and over the dome of the electrode disc
- Snip off any excess spacer/membrane protruding from the electrode
- Add a few drops of KCl to provide a reservoir of electrolyte during operation
- Place outer O-ring
- Place electrode back into the oxygen electrode chamber

Chamber preparation

- Switch on circulating water bath
- Set temperature to 37 °C
- Determine temperature of water jacket by placing 1 ml H_2O; turn on stirrer and read temperature with thermometer

Liquid phase Calibration with H_2O

- Turn on stirrer
- Using the OxyGraph software program select “Liquid phase calibration”
- Set temperature to 37 °C
- Set the stirrer to 100 rpm and atmospheric pressure (ATP) to 101 ATP
- Wait for reading to plateau
- “Establish zero O_2 in the chamber”
- Add a few granules of sodium dithionite
- Wait for reading to plateau
- Save calibration factor nmol/ml
- Once plateau is reached wash chamber five times or more times with H_2O (to ensure complete removal of sodium dithionite)

PPOX readings

- Set up a reaction similar to kinetic activity assay (mxPPOX assay; see appendix 17)
- Place buffer and enzyme mix into chamber and allow to equilibrate to 37 °C
- Start reaction by adding appropriate substrate volume and sealing chamber with plunger and prestick

University of Cape Town

Degassing

- Place appropriate buffer into chamber
- Degas buffer
- Monitor [O_2]
- When [O_2] reaches desired concentration seal chamber with stopper and allow to settle. Note if after 10 min the [O_2] is high to too low the sample can be nitrogen can inserted through the sealed chamber and a syringe
- Allow stirring sample to equilibrate 30 min before beginning reaction

University of Cape Town

Appendix - 20 LigPlot analysis (Dym et al., 2001)

- **Installation of LigPlot**

Start - program - accessories - command prompt

Add LigPlot to system's path by typing: path=%path%;C:\ligplot (if LigPlot files are saved on C:\ drive

Test LigPlot command by typing ligplot - this should be followed by LigPlot software information

- **Running LigPLot**

To run LigPlot

Save pdb in C:\ (for easy access)

mxPPOX pdb - 2ive or 2ivd (with acifluorfen)

Draw LigPlot diagrams with know molecule number type: LigPlot 2ive.pdb 2114 2114 A -w

where 2114 is the molecule number

A is the protein subunit of interest

-w is analysis of water molecules

Drawing LigPlot diagrams with molecule number type in: LigPlot 2ive.pdb FAD FAD A -w

where FAD is the molecule name
A the subunit of interest
-w analysis of water molecules

Drawing LigPlot diagrams unknown molecule name or number: LigPlot 2ive.pdb. This lists number and name of molecules available of analysis

To view LigPlot diagram - access image from LigPlot postscript folder (C:\ drive) in pdf format

University of Cape Town

Appendix - 21 Sequence alignment

Alignment 1 - Prokaryote PPOX sequence blast

CLUSTAL-W alignment of PPOX protein sequences from various species. The *M. xanthus* protein sequence was blasted using the NCBI blast application. Sequences were then selected according to their E-score. This was then followed by alignment of sequences from various species. Highlighted in red are the residues analysed in this study; in green is asparagine 63 which is discussed in the chapter 2.

```
Myxoccus_xanthus                -------MHHMPRTTG-----------MNVAVVGGGISGLAVAHHLR--- 29
Stigmatella_aurantiaca          ---------------M-----------AVIAVVGGGITGLALAHRLR--- 21
Gemmata_obscuriglobus           ---------------M-----------PHVVVVGGGLSGLTVALRLKQF- 23
Gloeobacter_violaceus           ------MN--TAEEL-----------LDVLVVGAGLSGLALAWKLKR-- 28
Synechococcus                   ------MNPATPEPLN----------AEVVVIGAGISGLTLAWRLQQGL 33
Chloroflexus_aurantiacus        -----------MMAGYDS-----------VVIGGGIAGLAAAYTLHK-- 25
Chloroflexus_aggregans          ----------MMMANYDS-----------VVIGGGIGGLAAAYTLYK-- 26
Opitutus_terrae                 ----------MSTSPFNPSATASGRPPKTFAVLGAGITGLTAAHRLTQ-- 38
Magnetococcus                   ----------MT--KNPI-----------LIIGGGISGLSTAWFLHK-- 24
Acidithiobacillus_ferrooxidans  -------------MEEV-----------IIIGGGISGLATAYFLRK-- 22
Leptospirillum                  ----------MAGFDCDT-----------LVVGGGISGLAAALTLKN-- 26
Geobacter_metallireducens       MFTFLTAAHAGSINDQSAFIERRGAGMKKVIVVGGGISGLATAFELRNKG 50
Geobacter_sulfurreducens        ------------------------MKKAIVAGGGISGLATAYLLKTRA 24
Pelobacter_propionicus          ------------------------MKRAIIVGGGISGLATAWLLREKA 24
Geobacter_lovleyi               ------------------------MKKVLVIGGGISGLSTAWLLNKRA 24
Desulfuromonas_acetoxidans      ------------------------MTRVAIIGAGVSGLATAYALEKGA 24
Pelobacter_carbinolicus         ------------------------MNISVVGAGISGLATAFAIQQQA 23
Thermodesulfovibrio_yellowston  ----------------------MGSAEIVIVGGGISGLSLAYFLIQK- 25
Roseiflexus_castenholzii        ----------MTAMHSTSAATLFPGGQPHIVVVGGGISGMSAAYELGRAT 40
                                                       : *.*: *:: *  :
```

University of Cape Town

```
Myxoccus_xanthus                ----SRGTDAVLLESSARLGGAVG-THALAGYLVEQGPNSFLDRE----P 70
Stigmatella_aurantiaca          ----SRGKDAVVLEAGAHLGGVIQ-TRQRDGFSTETGPNSFLDRE----P 62
Gemmata_obscuriglobus           ----SPGTAVTVLEPRDRPGGNIH-TESDRGFRVEHGPNGYLDRT----P 64
Gloeobacter_violaceus           -----AGCTFLVCQAGERVGGAIT-TAIADGFVCEGGPNSFQE-S----P 67
Synechococcus                   SARGGSPQAVLLAEASSRVGGCIS-TQSKDGYRWEEGPNSFTP-T----P 77
Chloroflexus_aurantiacus        -----RGYRVLVIESTNRVGGVIQTITTPEGYILDCGPNTVGTGD----A 66
Chloroflexus_aggregans          -----RGYRVLVIEAANRVGGVIHSITTPEGFTLDCGPNTIGTND----V 67
Opitutus_terrae                 -----LGHKVRVFEQSDRVGGSIKTEEV-DGWLIEGGPNTLLSGE----L 78
Magnetococcus                   -----KGEKVILLESRDRVGGNIRTSRNPEGYLIEHGPNSTLQKPGDEED 69
Acidithiobacillus_ferrooxidans  -----RGWSPLLLEAGAAPGGNLQ-SRQEEGYLRDMGPNSLMLKG----R 62
Leptospirillum                  -----RGVDVRLLESRGYLGGAVR-TVREEGYLLEFGPNSLMVRP---DD 67
Geobacter_metallireducens       AEA-GIELDVTLLEKEERVGGKIW-SIKEEGYLCEWGPNGFLDSK----P 94
Geobacter_sulfurreducens        AEE-GLELDVTLVEREERLGGKIW-SIKEEGYLCEWGPNGFLDSK----P 68
Pelobacter_propionicus          LAC-GIQLELVLLEKDQRPGGKIR-SIHEGGYVCEWGPNGFLDSK----P 68
Geobacter_lovleyi               GEA-GISLDLCLLEQEQQPGGKIK-SVREDGFLCEWGPNGFLDSK----P 68
Desulfuromonas_acetoxidans      QAQ-NIDVQITVIEKQPRSGGKIW-SRQEEGYLCEWGPNGFLDNK----P 68
Pelobacter_carbinolicus         RRL-GLEWTLDIFEKEDCSGGKIR-SEKVDGYLCEWGPNGFLDSK----P 67
Thermodesulfovibrio_yellowston  ----NSQLNIKIVEAEKRAGGKII-TENISGFLCEGGVNGFLSNK----P 66
Roseiflexus_castenholzii        RDG-APPVMVTLIEREARLGGKVV-TERNGPFVIEGGPDSFMAQK----P 84
                                          : :    ** :     :  : * :

Myxoccus_xanthus                ATRALAAALNLEGR-IRAADPAAKRRYVYTRGRLRSVPA--------SPP 111
Stigmatella_aurantiaca          ATRELAASLGIEER-IRMADPSAKSRSLYTRGQLRPVPA--------SPP 103
Gemmata_obscuriglobus           ALPNLVRDLGLADQEIAASDGSRKNRYVFLRNKLRKLPG--------GPL 106
Gloeobacter_violaceus           PLIELLTQLQLEDQ-IVTADP-RLARFVWWENRLRSVPL--------TPA 107
Synechococcus                   ALLNLIAEVGLTDQ-LVLADA-KLPRYIYWEGALLPVPL--------SPA 117
Chloroflexus_aurantiacus        RLWQELIDLGLRER-ITPAAPCSKRRFILINGTPVEIPT--------SPV 107
Chloroflexus_aggregans          RLWQELIDLGLRDR-IRPAARCGRRRYILINGTPIEIPS--------SPV 108
Opitutus_terrae                 AVDKLIDELGLNGE-RIAADPAAKNRYIVRRGRALAAPM--------SPP 119
Magnetococcus                   ALGRIITDMALESE-LQEANPLAARRFVMKGGQLHVLPT--------SPP 110
Acidithiobacillus_ferrooxidans  IVPEWLRELQLEGD-IVEANPLAGRRYVLN-RHRQPVAL--------GPG 102
Leptospirillum                  AIDAVLGDPELRAR-IVAASGLSKNRYVVKSGNLYPVPL--------SPW 108
Geobacter_metallireducens       QTLDLCRDLGASER-LLRSNDNARKRFIYTGGVLNRLPE--------NGP 135
Geobacter_sulfurreducens        QTLDLCRELGASDL-LLRSNDNARKRFIYTGGALNRLPE--------NGP 109
Pelobacter_propionicus          QTLELCDAVGVSSD-LLRSNDNARKRFIYSDGELHRLPE--------GGG 109
Geobacter_lovleyi               QTLELCATLGITDR-LHRSNDNARKRYIFTGGELHRLPE--------NGP 109
Desulfuromonas_acetoxidans      ATLDLCKALAIDDT-LLRSNDNARKRFIFSDNMLHRLPE--------NGP 109
Pelobacter_carbinolicus         MTLDLCREAGLAEQ-LLRSNDAARKRFIFSGGRLQRVPE--------SAA 108
Thermodesulfovibrio_yellowston  STISLAKELNIEP---LRGSESSKIRYILIDGKLIRVPE--------NPI 105
Roseiflexus_castenholzii        WAAELAREIGLGDE-LMVASPMRRTTWVLIRGRPQPLPEGMLLIVPTRIA 133
                                              .       :        .

Myxoccus_xanthus                AFLASDILPLGARLRVAGELFS-RRAPEG-VDESLAAFGRRHLGHRATQV 159
Stigmatella_aurantiaca          AFLKSDLLPLGTRLRVLAELFT-GRAPPG-QDESLGDFGRRHVGARATSV 151
Gemmata_obscuriglobus           GLLTTSLLSLRGKWQLLAEPWR-KTPPPK-HEETIQEFVTRRAGSEAANV 154
```

```
Gloeobacter_violaceus              QLVRSDLLSWSGKARLLWELFVPALGEP--REETVAEFVLRRFGEEVLSR 155
Synechococcus                      AALGSRLLSVGGKLRALQGLLGFVPPPPG-HEETVRQFFRRQLGSEVAER 166
Chloroflexus_aurantiacus           GLITTRLLSWRGKLRVLAEPFINRG-STD-PDESVAAFFTRRIGAEATAH 155
Chloroflexus_aggregans             GLITTRLLSWRGKLRVLGEPFVNIG-TPT-GEESVAAFFSRRIGHEAVAH 156
Opitutus_terrae                    SFFASSLFSPVAKFKLLAELFARRR-VRT-TDVSLAEFVESHFGREFVDY 167
Magnetococcus                      GFIKTPLFSLSAKLRLCLEPFIG---KSE-QEESIAQFVIRRLGQEFLDY 156
Acidithiobacillus_ferrooxidans     VLFGGGLLSIRGRLRLLGEPFQPPHPTPD-GEESIADFVRRRLGDEALTW 151
Leptospirillum                     AFIRTPLLSWRGRRDILSEWKVPPR-TGG-PEETLSHFVRRRLGEEALDY 156
Geobacter_metallireducens          TFLKSSLISWPGKLRLAMEP--FISKRTDGTDETLASFGRRRLGEEALQK 183
Geobacter_sulfurreducens           MFLKSGLISWPGKLRLAMEP--FIPKKAGDEDETLAAFGRRRLGDEALRK 157
Pelobacter_propionicus             TFLKSRLISWPGKLRLALEPTPFIARTPAGVDESLADFARRRLGGEALDK 159
Geobacter_lovleyi                  SFLKSRLLSWPGKLRLLGEP---FAANPPGSDESLAAFGRRRLGAEALQK 156
Desulfuromonas_acetoxidans         MFLGSKLISWPGKFRLAGEM--FVPAKRDERDETLAEFGRRRLGAEALDK 157
Pelobacter_carbinolicus            DFFRSSLVSWPGKLRLAAEL--LVPRRKDLTDETLADFVRRRLGREALDQ 156
Thermodesulfovibrio_yellowston     KFFLTPLLSFSGKIRMLREY--FTPPLKEEIDETVESFVSRRVGKEFYEK 153
Roseiflexus_castenholzii           PFAFSPLISPLGKLRMALDL--FVPARRDDGDETLADFIRRRLGNEALDR 181
                                         :..   :                : ::  *   : * .

Myxoccus_xanthus                   LLDAVQTGIYAGDVEQLSVAATFPMLVKMEREHRSLILGAIRAQKAQRQA 209
Stigmatella_aurantiaca             LLDAMQTGTYAGDVEALSAEAAFPTLKQLEREHRSLLLGAVRTQGRQR-A 200
Gemmata_obscuriglobus              FADALVTGIHGGDPAMLSVSAAFPRLPVMERDAGSIVRGFMRAAKKRKED 204
Gloeobacter_violaceus              LVDPLVSGMCAGDVGQLSIEATFERLVDLERRHGGVLRGLWRTARTR--- 202
Synechococcus                      LVEPFTSGVYAGDPDQLSAVAAFPRVAGLEERYGSLFAGALQALRQRPQP 216
Chloroflexus_aurantiacus           LLDPFVAGVYAGDPQRLSTAAVFPSLWEAAQRSGSIVRGMLSKPKPKTQ- 204
Chloroflexus_aggregans             LLDPFVAGVYAGDPNQLSAAAVFPSLWEAVQRGGSIVRGMLRRPKQKTL- 205
Opitutus_terrae                    ALNPFVGGVYAGDPEKLSARQSFPKLWEIEQTHGSLIRGQIAAAKARKA- 216
Magnetococcus                      AIEPFVSGVYAGDPKQLSVRAAVAKIYALEAKYGSLIKGAIA--LGKIR- 203
Acidithiobacillus_ferrooxidans     LVDPFVSGVFAGNPARLSVQATLPRLAALEQDGGSLLRGALR--ARKK-- 197
Leptospirillum                     FVDPFVKGVYASHPDLLSVEAAFPLLVRLEREHGGLLRGALKTFLKRRK- 205
Geobacter_metallireducens          LISPMVSGIFAGDPETMSLRSCFPRIAELEDEYGSLIKAMIKLAKKKKQE 233
Geobacter_sulfurreducens           LIAPMVSGIFAGNPETMSLRSCFPRIAELEDEYGSLVRAMIRLAKKKKQE 207
Pelobacter_propionicus             LISPMVSGIFAGDPETMSLVSCFPRIAQLEREYGGLIRAMVRLARQKKRE 209
Geobacter_lovleyi                  LIAPMASGIFAGDPETMSLVSCFPRIAELEREYGGLFVAMLALAKKKKQE 206
Desulfuromonas_acetoxidans         LIAPMAGGIFAGDPETMSLKSCFPRIAQLEQEYGGLLKAMIKLARKKKAE 207
Pelobacter_carbinolicus            MVGPMAAGIFAGDPETMSLRSCFPRIHELEQQYGGLIRALLLLARKKRAE 206
Thermodesulfovibrio_yellowston     LIDAMSTGIYAGDPSKMSMKSCFPKVYWLEKRHGGLLKGLIALKKEKKDT 203
Roseiflexus_castenholzii           LAEPILSGIHSAECERQSILATFPRFRELEKRHGSLIRGMLAARRTAS-- 229
                                      ..  *  ...    *    .  .        .:. .

Myxoccus_xanthus                   ALPA---GTAPKLSGALSTFDGGLQVLIDALAASLGDAAHVGARVEGLAR 256
Stigmatella_aurantiaca             PAPA---GT--KLKGAMCTFEGGLGTLVEALARALGPAARTGAAVEGLAR 245
Gemmata_obscuriglobus              AKAN---NQPPPGPMRMWSFRDGLQVLVDALAAQVGGGLHCGTRVEAVSE 251
Gloeobacter_violaceus              ---------PPFKR--LCTLRGGLEQLPQALAQRLQPQILLSHRLEALEH 241
Synechococcus                      SPAA---IQPPPKRGQLGNLRQGLQQLPEALAQKLGDSLRLGWRALQLKR 263
Chloroflexus_aurantiacus           -------VSEPKMRSRTFTFRGGLAEWPRALAQALGAGNVWTERRVVKLQ 247
```

Uncorrected Proof

```
Chloroflexus_aggregans              -------ISEPKMRSRTFSFQGGLADWPRAIARALGTGNVWTGRRAVGLR 248
Opitutus_terrae                     -------RGEP--RPGIFSFKHGLHVLPEALAARLPAGAITLGASLDAIV 257
Magnetococcus                       -------KAAGMPRGRMISFETGMETLPATIANRLPHQSIHTNAQVTALC 246
Acidithiobacillus_ferrooxidans      -------KLPGTPKTRLVSFREGLQVLPLRVANTLG-DTLRCDTPVDQLA 239
Leptospirillum                      -------RPSGSAPRGIFSFTGGMGDLVEAMGKRLG-EDVGTNVDVIKYT 247
Geobacter_metallireducens           AAQGKAVSSAAGPGGVLTSFRWGIQELTDILAEQLGSATVVTGQPVTGLT 283
Geobacter_sulfurreducens            VAQGKAVASAAGPGGVLTSFRDGIQALTDILAERLGPDTIVSGQEVLEVS 257
Pelobacter_propionicus              RAAGKAVSSAAGPGGVLTSFRPGIQYLTDSLAASLG-GIVMADREVSWVR 258
Geobacter_lovleyi                   RKEGKISSSAAGPGGTLTSFKEGIQFLTDTLAAQLG-EQVRTGVAVASVT 255
Desulfuromonas_acetoxidans          RKAGKQVASAAGPGGVLTSFNGGIQELTDALQESLS-ATLRFGVAVESME 256
Pelobacter_carbinolicus             RRAGKAVAGAAGPGGILTSFGGGIQELTDGLSRLLA-PNLHLGDAVAAIT 255
Thermodesulfovibrio_yellowston      KAQ---------PSGVLMSFKGGMSELIQSLERHLS-SRILKGKKVLSID 243
Roseiflexus_castenholzii            --------PSSAHQSPFMTLRGGMGTLVERLEQRLT-ARILTNRRVMALT 270
                                                    .:  *:     :   :

Myxoccus_xanthus                    EDGGWRLIIEEHGRR-----AELSVAQVVLAAPAHATAKLLRPLDDALAA 301
Stigmatella_aurantiaca              SQNGWRLSVRERGQQ-----AELEASQVVLTSPAHVSAELLAPLDPSLAG 290
Gemmata_obscuriglobus               AAGVAPWTVHGQSG------YTWSADAVVLACPSYEQAGIVSDISPELSA 295
Gloeobacter_violaceus               LAGDRWRAVVAGPQGE---PVAIAARTVILSGSAHAMASVLRPLDAGLGR 288
Synechococcus                       -AGELYWVGFETPEG----SRWVAARQVVLALPAYEAAALLQELNPPASQ 308
Chloroflexus_aurantiacus            PRDSWWEVTIDG----VNGPETLISRSLIIATPAFTAADLIESVDQRAAG 293
Chloroflexus_aggregans              DLGTYWEVTVDG----TGRLETITTRSVIIATPAYVAAELVEALDPAAAS 294
Opitutus_terrae                     PGDKWNVVWHDD----VATHTQSFDSVVVALPAPALARLQIGTLGEKPLA 303
Magnetococcus                       QHGAAWQVSWQQGGQHGGEPHSIIASQVVLATPASVSAQLLRPLSPQAAD 296
Acidithiobacillus_ferrooxidans      YSGDMWQV--------GSGNQTWQSKRLVLALPAGAAARLLAQTDATLAR 281
Leptospirillum                      RLEEGFRVALMY----DETEYYMTSRRLILATSAPQAAELLEGDPEGPSG 293
Geobacter_metallireducens           RGSSVP--WRLKTP-----TVDIDADVVILASPAHATAGIVSGVDAAMAQ 326
Geobacter_sulfurreducens            RGGSLP--WRVRTG-----SIDMDADLVILATPAYATASIIQGVDSDMAG 300
Pelobacter_propionicus              RGKSAA--WRVGCRD----GGEYDADLVIVASPAHAASAILHDCDAGIAS 302
Geobacter_lovleyi                   RSGDG---WEVRTTG----GETLQADLVISAAPAFAAAGMLEGVDTALVD 298
Desulfuromonas_acetoxidans          YFDNYI--LGLSDG------SQLDADVVISAAPAHALSGMLKKMNGEAAK 298
Pelobacter_carbinolicus             PLKEG---FSLRTHK----GRVHETDIVVAAVPAMALATQVEGFSAPMAA 298
Thermodesulfovibrio_yellowston      RKNTY---YTVHLDD----GNFIEAEKVILACPAHESAEILKELSSELSD 286
Roseiflexus_castenholzii            CDTTAARPYRLWLDD----GATLDADAVILATPSYAAADLVGASFPALAD 316
                                                          ::   ..     :

Myxoccus_xanthus                    LVAGIAYAPIAVVHLGFDAGTLP-APDGFGFLVPAEEQRRMLGAIHASTT 350
Stigmatella_aurantiaca              HLKGIPYAPIAVVHLGFAPGKTP-PPDGFGFLVPGQEQRQLLGVIHVSTV 339
Gemmata_obscuriglobus               EMAAIPYNRIAVVALGYRAEHCPGKHDGFGYIAPQNTRRDLLGVQWCSSI 345
Gloeobacter_violaceus               ALESIYYPPVVSISLAYSKSQVPNAPEGFGHLIPRNQTLRSLGVIWNSSL 338
Synechococcus                       LLAEILYPPVAVVALAYPQEALPQPLRGFGHLIPRSQGLRTLGTIWASCL 358
Chloroflexus_aurantiacus            ALRGIPYAPVAVVHLGFRRDQISQELSGFGVLAPSSEQRQFLGILWTSSI 343
Chloroflexus_aggregans              ALRSIPYAPVSVVHLGFRRDQLSHELNGFGVLAPSSERRQFLGILWASSL 344
Opitutus_terrae                     ALALIEHPPVSSLFLGFRREQVAHPLDGFGVLVPAVEKRSVLGVLFSSSL 353
Magnetococcus                       LLESIRYAPVDSVALGYAKQDINHSLDGFGFLIPRKEQVTTLGGLFSTTL 346
```

University of Cape Town

```
Acidithiobacillus_ferrooxidans      ELDAIPYPAVGSLSIGFRRPQVEHPLDGFGMLIPRVMGLETLGVLFSSTL 331
Leptospirillum                      ELKAIPYAPVTIAYAGFLREQITHPLDGFGLLCPTAENRKVLGVIFSSSL 343
Geobacter_metallireducens           VLGEIPYASMTVVCFGFERERIAYDLNGFGYLIPKDEGMNTLGTLWDSSI 376
Geobacter_sulfurreducens            ILRQIPYATMTVVCFGYDRERIAHDLNGFGYLIPKEEGMNTLGTLWDSSI 350
Pelobacter_propionicus              ILESIPYASMTVVCLGYERELVSHPLDGFGYLIPKKEGRSILGTLWDSSM 352
Geobacter_lovleyi                   TLRQILYSTLNVVCCGFKTEGLGHPLDGFGYLVPKEEGRTVLGTLWDSSM 348
Desulfuromonas_acetoxidans          LLNQIPYAPMNVACFGFNRADLQCDLNGFGYLIPKKEGCSVLGTLWDSSI 348
Pelobacter_carbinolicus             QLRQIPYAPLQIACFGYRREALPLSLDGFGYLAARRSGMHSLGTLWSSSI 348
Thermodesulfovibrio_yellowston      ILKTIPYPPLSVVAFGFKKEQIGFGTSLYGFLIPYREQRKILGTLFDSSI 336
Roseiflexus_castenholzii            ALRAIRYVSTATVSLVYRRSEVGTPLDGYGLVIPRSEQTWINACTLSSVK 366
                                     :  * :         :           :* : .       .    :

Myxoccus_xanthus                    FPFRAEGGRVLYSCMVGGARQ---------PGLVEQDEDALAALAREEL- 390
Stigmatella_aurantiaca              FPFRAEGGRVLYTCLMGGARR---------PDLVGLNEEALAALAQQEL- 379
Gemmata_obscuriglobus               FPDRAPQGFVLWRALCGGVHR---------AEQIDWPDEQLVKAVHAEI- 385
Gloeobacter_violaceus               FPHTAPPNWRLYTCFVGGTTD---------PATPNLSDTELASLAHREL- 378
Synechococcus                       FPERAPQGYHSFLSFLGGATDAALARRRGIPPIPALSPEERAQIAHAELS 408
Chloroflexus_aurantiacus            FPHVAPHDHVLTTTLSGGAIRP---------ELAERSDETLIEAAIRDH- 383
Chloroflexus_aggregans              FPHVAPPDRVLTITLSGGAIRP---------EVAEQSEEALIESAIRDN- 384
Opitutus_terrae                     FPGRAPLGHVALTVMVGGTRQP---------QLASLPADQLLAAVRPDL- 393
Magnetococcus                       FPGRAPQDKALLTCFIGGMTNP---------SITQWSEEKVVTQVDQDM- 386
Acidithiobacillus_ferrooxidans      FPGRAPAGQVLLTAFIGGSQN----------VLAGRDDDDLLATVLREI- 370
Leptospirillum                      FPGRAPDGKVLLTVFVGGMTGQ---------KLAQTFDEDLERIVLREL- 383
Geobacter_metallireducens           FENRAPEGKVLLRSMLGGACFP---------EYVKLSDAEVMQRVKADL- 416
Geobacter_sulfurreducens            FENRAPEGQVLLRSMMGGACFP---------EYVNLTDEEVTGRVKNDL- 390
Pelobacter_propionicus              FENRAPTGKVLLRSMVGGACFP---------DYVHMGDDELLGRVRGDM- 392
Geobacter_lovleyi                   FEERAPDGMALLRSMAGGACRP---------ELMELPESELLQRVRDDL- 388
Desulfuromonas_acetoxidans          FPHRAPKDKVLLRSMMGGATRP---------QAIDLTDDQVLALVQADL- 388
Pelobacter_carbinolicus             FPGRAPAGYVLLRTMFGGATRP---------DAAQLSADEVQQRVEEDL- 388
Thermodesulfovibrio_yellowston      FPNRAPESYVLLRSMIGGRRAP---------ELAMLPDEKLIDTALSEL- 376
Roseiflexus_castenholzii            FRHRAPDEYLLLRCFVGGSRRP---------ELLARDDDDLVRMAQSDL- 406
                                    *   *        : **                          .  :
```

University of Cape Town

```
Myxoccus_xanthus                KALAGVTARPSFTRVFRWPLGIPQYNLGHLERVAAIDAALQR-LPGLHLI 439
Stigmatella_aurantiaca          REMAGVTASPDFTEAVRWPRGIPQYTVGHLERLSAIDSALAR-LPGLHLA 428
Gemmata_obscuriglobus           TLAMGVTGAPVFKKVVRWPNAIPQYVLGHLDRVARIDELASR-HPGLFLT 434
Gloeobacter_violaceus           QTVLGFQAGYQLLRVTRWPQAIPQYALGHPSKQERVERALLG-LPGLFLV 427
Synechococcus                   QVLLTRRAEPVYLGERLWPRAIPQYTLGHRQRIAQVQAHLASQTPGIWVC 458
Chloroflexus_aurantiacus        HQLLGIRGQPIFTHVTRWRTAIAQYTFGHRERIATLVQLEQR-LPTIQFA 432
Chloroflexus_aggregans          QEVLGIRGQPLLTHVTRWHHAIAQYTLGHRERIATLERLEQR-RPTLQLT 433
Opitutus_terrae                 TQLLGVSGDPVFVRHNFWPRAIPQYNLGHEHFIAALAAGERF-HPGLFMG 442
Magnetococcus                   MAALGIQHGAEYVHLTRYTHAIAQYEQGHLQRVGDIDRALAG-YKGLHLR 435
Acidithiobacillus_ferrooxidans  GPLLGISGDPVFSRCRVWPKAIPQYEIGHLDRMKRIDTLSAG-HPGLHFR 419
Leptospirillum                  TELLGVKGAPAFFRIHRWEKAIPQFILGHGETVRTIRKKLP---SGLRLA 430
Geobacter_metallireducens       KATMGITADPSFIRIFRHPQAIPQYTVGHGKRLAALQERSSA-LPGLFLT 465
Geobacter_sulfurreducens        ATIMGITAPPSFVRIFRHHQAIPQYTVGHSTRVAALEQRAAS-LPGLFLT 439
Pelobacter_propionicus          KDVMGIVAEPSFIRIFRHPQAIPQYTVGHGERLKHLEERLAC-HPGLILT 441
Geobacter_lovleyi               QAAMGISQPPCFSRIIRHQQAIPQYTIGHGKRLEAIEGRLSS-LPGLLLT 437
Desulfuromonas_acetoxidans      ERIMGIKATPEMVRIFRHQQAIPQYVSGHASLVAQIRQELSA-CKGFYLT 437
Pelobacter_carbinolicus         SRSMGIKQAPDFVRIIRHTAAIPQYVSGHGARLKVLEDKAAA-YPGLFLV 437
Thermodesulfovibrio_yellowston  KPLLNIKGDPEFIKIFRWEKAIPQYELGHEDKLNRIEQILSE-FSGLYLT 425
Roseiflexus_castenholzii        RAVLGITAVPLLTRVYRWHNGNPQYDVGHLERIAALEALCP---AGLLLA 453
                                                 . .*:  **     :         : .

Myxoccus_xanthus                GNAYKGVGLNDCIRNAAQLADALVAGNTSHAP---------- 471
Stigmatella_aurantiaca          GNAYKGVGLNDCIRNAAALAETLASR---------------- 454
Gemmata_obscuriglobus           GNSYRGVAMADCVEQGEAVAAKVALHLQQAKPR--------- 467
Gloeobacter_violaceus           GNYFGGISLGDCVRHSGAVASRVLQFLTTVASNGSLRPA--- 466
Synechococcus                   ANYLDGVALGDCVRRAEALAQ---QLLSQV------------ 485
Chloroflexus_aurantiacus        GSYRDGVGVPKTWASGVQAGERIAAALAAHGTTAVSTETASG 474
Chloroflexus_aggregans          GSYRGGIGIPKTWASGVGAGERIAAALDAQGTTADTLEQARG 475
Opitutus_terrae                 GQARDGIAVPACIAAGEKLAERAGQ----------------- 467
Magnetococcus                   ANWRDGVSVSDCVLNGEKSAQKILAGVS-------------- 463
Acidithiobacillus_ferrooxidans  ANWQGGVALGDCIEQAWEFSQTADWQH--------------- 446
Leptospirillum                  GNYLDGISIARAFGSGVRAAEELLSEDGGTPG---------- 462
Geobacter_metallireducens       GNSYRGIGLNDCATAANRTTDEVVAYLKGR------------ 495
Geobacter_sulfurreducens        GNSYRGIGLNDCVAAANRTAGEAIAQLTSR------------ 469
Pelobacter_propionicus          GNSYRGIGLNDCVAAAQRASDQALELLR-------------- 469
Geobacter_lovleyi               GNAFKGVGLNDCVAASQATVERAMAYLERV------------ 467
Desulfuromonas_acetoxidans      GNAFEGIGLNDCVANANKTAAEVLAAL--------------- 464
Pelobacter_carbinolicus         GNAFYGVGLNDCVAAADRVASRVLTLMQQRQQA--------- 470
Thermodesulfovibrio_yellowston  GNAYRGVSVNDCIENSLKLAEGIMV----------------- 450
Roseiflexus_castenholzii        GAAYRGVGVPDCIKQGREAARRALDVVATARYPVMEK----- 490
                                .    *:.:      .
```

Alignment 2 - Alignment of PPOX protein with resolved protein structure

ClustalW multiple alignment of protein sequences of resolved protein crystal structures. Highlighted in red are the residues analysed in this study (a similar alignment was done by Dailey and Dailey, 1996a).

```
mxPPOX          ----MHHMPRTTGMNVAVVGGGISGLAVAHHLRSR------GTDAVLLESSARLGGAVG- 49
hPPOX           -----------MGRTVVVLGGGISGLAASYHLSRAP----CPPKVVLVESSERLGGWIRS 45
bsPPOX          --------MSDGKKHVVIIGGGITGLAAAFYMEKEIKEKNLPLELTLVEASPRVGGKIQ- 51
mtPPOX          MAPSAGEDKHSSAKRVAVIGAGVSGLAAAYKLKIHG------LNVTVFEAEGKAGGKLR- 53
                              *.::*.*::***.:. :          . .:.*:. : ** :

mxPPOX          THALAGYLVEQGPNSFLDR---EPATRALAAALNLEGR----IRAADPAAKRRYVYTR-- 100
hPPOX           VRGPNGAIFELGPRGIRPAGALGARTLLLVSELGLDSEVLP-VRGDHPAAQNRFLYVG-- 102
bsPPOX          TVKKDGYIIERGPDSFLER---KKSAPQLVKDLGLEHLLVNNATGQSYVLVNRTLHPMPK 108
mtPPOX          SVSQDGLIWDEGANTMTES---EGDVTFLIDSLGLREK-----QQFPLSQNKRYIARN-- 103
                     * : : *.  :         .  *   *.*               .* :

mxPPOX          GRLRSVPASPPAFLASDILPLGARLRVAGELFSRRAP-----EGVDESLAAFGRRHLGHR 155
hPPOX           GALHALPTGLRGLLRPSPPFSKPLFWAGLRELTKPRG-----KEPDETVHSFAQRRLGPE 157
bsPPOX          GAVMGIPTKIAPFVSTGLFSLSGKARAAMDFILPASK-----TKDDQSLGEFFRRRVGDE 163
mtPPOX          GTPVLLPSNPIDLIKSNFLSTGSKLQMLLEPILWKNKKLSQVSDSHESVSGFFQRHFGKE 163
                *    :*:    :: ..             :          .:::  * :*:.* .

mxPPOX          ATQVLLDAVQTGIYAGDVEQLSVAATFPMLVKMEREHRSLILGAIR----AQKAQRQAAL 211
hPPOX           VASLAMDSLCRGVFAGNSRELSIRSCFPSLFQAEQTHRSILLGLLLG---AGRTPQPDSA 214
bsPPOX          VVENLIEPLLSGIYAGDIDKLSLMSTFPQFYQTEQKHRSLILGMKK--------TRPQGS 215
mtPPOX          VVDYLIDPFVAGTCGGDPDSLSMHHSFPELWNLEKRFGSVILGAIRSKLSPKNEKKQGPP 223
                ...  ::..  *  .*:  .**:   **. : *: . *::**           :

mxPPOX          PAGTAPKLSGALSTFDGGLQVLIDALAASLGDAAH----------VGARVEGLAREDGG 260
hPPOX           LIRQALAERWSQWSLRGGLEMLPQALETHLTSRGV----------SVLRGQPVCGLSLQ 263
bsPPOX          GQQLTAKKQGQFQTLSTGLQTLVEEIEKQLKLT------------KVYKGTKVTKLSHS 262
mtPPOX          KTSANKKRQRGSFSFLGGMQTLTDAICKDLREDELRLNSRVLELSCSCTEDSAIDSWSII 283
                            ::  *:: * : :   *                 .   :   .

mxPPOX          WRLIIEEHGRRAELSVAQVVLAAPAHATAKLLRPLDDALAALVAGIAYAPIAVVHLGFDA 320
hPPOX           AEGRWKVSLRDSSLEADHVISAIPASVLSELLPAEAAPLARALSAITAVSVAVVNLQYQG 323
bsPPOX          GSCYSLELDNGVTLDADSVIVTAPHKAAAGMLS--ELPAISHLKNMHSTSVANVALGFPE 320
mtPPOX          SASPHKRQSEEESFDAVIMTAPLCDVKSMKIAKRGNPFLLNFIPEVDYVPLSVVITTFKR 343
                         .   :..  :  .        :          :  :  ..:: *   :

mxPPOX          GTLPAPDG-FGFLVPAEEQRR---MLGAIHASTTFPFRAEGGR-VLYSCMVGGARQPGLV 375
hPPOX           AHLPVQG--FGHLVPSSEDPG---VLGIVYDSVAFPEQDGSPPGLRVTVMLGGSWLQTLE 378
bsPPOX          GSVQMEHEGTGFVISRNSDFA---ITACTWTNKKWPHAAPEGK-TLLRAYVGKAGDESIV 376
```

University of Cape Town

```
mtPPOX          ENVKYPLEGFGVLVPSKEQQHGLKTLGTLFSSMMFPDRAPNNV-YLYTTFVGGSRNRELA 402
                  :       * ::. ..:       .    .  :*             :* :    :

mxPPOX          EQ----DEDALAALAREELKALAGVTARPSFTRVFRWPLGIPQYNLGHLERVAAIDAALQ 431
hPPOX           ASGCVLSQELFQQRAQEAAATQLGLKEMPSHCLVHLHKNCIPQYTLGHWQKLESARQFLT 438
bsPPOX          DLS----DNDIINIVLEDLKKVMNINGEPEMTCVTRWHESMPQYHVGHKQRIKELREALA 432
mtPPOX          KAS----RTELKEIVTSDLKQLLGAEGEPTYVNHLYWSKAFPLYGHNYDSVLDAIDKMEK 458
                          :   . .      .    *          :* *  .: . :

mxPPOX          RLPG-LHLIGNAYKGVGLNDCIRNAAQLADALVAGNTSHAP------ 471
hPPOX           AHRLPLTLAGASYEGVAVNDCIESGRQAAVSVLGTEPNS-------- 477
bsPPOX          SAYPGVYMTGASFEGVGIPDCIDQGKAAVSDALTYLFS--------- 470
mtPPOX          NLPG-LFYAGNHRGGLSVGKALSSGCNAADLVISYLESVSTDSKRHC 504
                     :   *    *:.: ..: ..   .   :    .
```

University of Cape Town